Investigations into Asphaltenes Destabilization, Aggregation and Deposition

Mohamed Saidoun

UNIVERSITÉ DE PAU ET DES PAYS DE L'ADOUR

DOCTORAL THESIS

Investigations into Asphaltenes Destabilization, Aggregation and Deposition

by

Mohamed SAIDOUN

A thesis submitted in fulfillment of the requirements
for the degree of Doctor of Philosophy (Petroleum Engineering)

in the Université de Pau et de Pays de l'Adour (UPPA)

Laboratoire des fluides complexes et leurs réservoirs (LFCR) - UMR5150
École doctorale des sciences exactes et leurs applications

Dissertation defended on March 26, 2020 to the doctoral committee:

Prof. H. Scott FOGLER	University of Michigan	Committee Chair
Prof. Lamia GOUAL	University of Wyoming	Examiner
M. Loïc BARRÉ	IFP Energies Nouvelles	Examiner
Dr. Thierry PALERMO	Total SA	Industrial advisor
Dr. Nicolas PASSADE-BOUPAT	Total SA	Industrial advisor
Prof. Jean-Luc DARIDON	UPPA	PhD Advisor
Prof. Hervé CARRIER	UPPA	PhD Advisor

Declaration of Authorship

I, Mohamed SAIDOUN, declare that this thesis titled, "Investigations into Asphaltenes Destabilization, Aggregation and Deposition" and the work presented in it are my own. I confirm that:

- This work was done wholly or mainly while in candidature for a research degree at this University.
- Where any part of this thesis has previously been submitted for a degree or any other qualification at this University or any other institution, this has been clearly stated.
- Where I have consulted the published work of others, this is always clearly attributed.
- Where I have quoted from the work of others, the source is always given. With the exception of such quotations, this thesis is entirely my own work.
- I have acknowledged all main sources of help.
- Where the thesis is based on work done by myself jointly with others, I have made clear exactly what was done by others and what I have contributed myself.

Signed: _____

Date: _____

"No amount of experimentation can ever prove me right but a single experiment can prove me wrong."

Albert Einstein

Abstract

Investigations into Asphaltenes Destabilization, Aggregation and Deposition

by

Mohamed SAIDOUN

[ENGLISH VERSION]

Asphaltenes have been known, since decades, to occasionally cause severe industrial problems during crude oil extraction and during its transport. Petroleum fields are apprehensively developed with oversized and costly prevention approaches due to the limited understanding on asphaltenes deposition in conditions of oil production.
Previous fundamental researches provided extensive descriptions of asphaltenes properties in good solvents, such as aromatic solvents. The incompatibility of asphaltenes with alkanes induces their destabilization, their aggregation and their deposition. The aggregation and the mass transfer behavior of asphatenes have been explained by theoretical concepts for oil + liquid alkane systems. The amount of destabilized asphaltenes and their aggregation rate both increase as the volume fraction of the anti-solvent increases. Quantitative laboratory measurements have been accordingly developed for liquid systems at atmospheric pressure. However, risks related to the instability of asphaltenes are only qualitatively understood during the primary production of crude oils. In the oil fields, the pressure decrease of the oil causes the light constituents, such as methane or carbon dioxide, to increase their volume fraction in the liquid phase.
Based on experimental observations, the first part of this dissertation addresses the understanding of bulk behavior (destabilization and aggregation) related to asphaltenes in oil-heptane systems. Analytical equations are proposed to distinctly model both phenomena. Numerical results obtained by combining both equations with time discretization provide good agreements compared to experimental measurements. The study reconciles the continuum consideration of asphaltene molecules in crude oils with the notion of flocculation "onset" by distinguishing the destabilization and the aggregation kinetics. A reasonable match is found between the transition of the theoretical and the adjusted colloidal stability ratio, indicating that underlying physics are captured by considering simultaneous destabilization and aggregation kinetics.
Fully immersed quartz crystal resonators are used to record the mass of deposit on solid surfaces in contact with varying liquid solutions. The deposition rate of asphaltenes is studied during continuous addition of heptane a several conditions. The proposed diffusion-limited model, designed for studied geometry, can explain experimental results and is in agreement with previous research on different apparatus. The mass transfer relationship reveals that primary unstable aggregates of asphaltenes mainly contribute to the deposition process and have an average hydrodynamic radius of 7 nanometers ($\pm$ 50%). A linear relationship is found between the generation rate and the deposition rate of unstable asphaltenes in the investigated conditions. However, the initial presence of large suspending unstable aggregates slows down the asphaltenes deposition process.
In the last phase of this work, the validity of defined concepts for the destabilization, the aggregation and the deposition induced by heptane additions is verified for oil-methane systems. The rate of change of solution properties is found to be the predominant variable affecting the deposition of asphaltenes. The effect of methane is significantly more pronounced than liquid alkanes on the asphaltene deposition.
For the first time, the bulk concentration of unstable asphaltenes and their deposition rate can be quantitatively measured during the depressurization of live oils (light constituent dissolved). Although first tendencies are derived from this work, the effect of the anti-solvent nature still needs further research with the identified variables in order to fully elucidate the thermodynamic driving quantity which controls the amount of destabilized asphaltenes.

[VERSION FRANCAISE]

Du fait des problèmes industriels reliés aux aphaltènes lors de l'extraction, du traitement et du transport des hydrocarbures, les champs pétrolifères sont développés de manière conservative avec des moyens de prévention de risques de dépôts surdimensionnées lors de la mise en production des installations. Les répercussions économiques sur les architectures et les opérations se quantifient en centaines de millions de dollars par an autour du globe terrestre.
De nombreuses études fondamentales menées sur les asphaltènes dans des solvants dispersants, tels que les solvants aromatiques, ont permis une description extensive des propriétés et structures moléculaires des asphaltènes durant les 20 dernières années. Malgré la connaissance accrue sur les dispersions d'asphaltènes en solution colloidales, leur incompatibilité avec certains composés plus légers, tels que les alcanes, demeure quantitativement mal comprise. En effet, la présence d'alcanes ou d'autres constituants légers comme le CO_2 induit une déstabilisation des asphaltènes, sous ces conditions ceux-ci tendent à s'aggréger et/ou à se déposer. De nombreuses précédents études ont montré que des concepts théoriques de transferts de masse peuvent expliquer ces phénomènes dans des solution de pétrole + alcanes liquides au laboratoire. Plus la concentration volumique de mauvais solvants est grande dans la solution, plus la quantité d'asphaltènes instables et leur vitesse d'aggrégation sont grandes. Une bonne représentation de ces tendances par des notions théoriques nécessite des ajustements de paramètres pour ces solutions liquides à conditions atmosphériques. Des expériences ont donc précédemment été conçues en ce sens afin d'établir les paramètres nécessaires aux modélisations tels que la constante d'aggrégation des asphaltènes instables, leur nombre ou leur diffusivité. En revanche, certains de ces coefficients sont inconnus dans les conditions de déstabilisation industrielles en raison de la difficulté à les déterminer expérimentalement, ce qui limite la prédiction quantitative des risques de dépôts d'asphaltènes. En réalité, c'est la décroissance de la pression dans les conduites pétrolière pendant l'écoulement du fluide qui induit une augmentation significative du volume des composés dissouts les plus sensibles à la pression, c'est à dire le methane ou le CO_2. Ainsi, avec l'allègement du solvant certaines fractions d'asphaltènes peuvent être déstabilisées et causer des problèmes.
Ce travail s'inscrit dans une volonté de prédire le comportement des asphaltènes dans les conditions d'opérations de l'amont de l'industrie pétrolière. Son objectif est d'abord de développer la compréhension des systèmes liquides aux conditions atmosphériques afin d'en extraire les mécanismes dominants et limitants. Dans un premier temps, les observations expérimentales sont donc menées sur des mélange de pétrole et d'heptane. Une fois les mécanismes bien compris, un parallèle est réalisé avec d'autres alcanes, dont le methane.
La première partie de cette dissertation est une investigation des deux phénomènes qui ont lieu dans la phase continue pendant l'ajout ininterrompu d'heptane: la déstabilisation et l'aggrégation des asphaltènes. Ces derniers sont d'abord décrits de manière distincte par deux équations analytiques en fonction du temps et de la qualité du solvant. La combinaison de la déstabilisation et de l'aggrégation des asphaltènes est ensuite numériquement résolue en discrétisant le temps. Les résultats de calculs, en accord avec les expériences réalisées, montrent que ces deux processus ont lieu simultanément. L'aggrégation étant plus rapide que la déstabilisation, elle en devient naturellement dépendante car seuls les "clusters" d'asphaltènes instables contribuent à l'agglomération pour former des objets de tailles supérieures aux nanomètres. La notion de seuil ou "onset" de flocculation est alors réintroduite de

manière compréhensive tout en considérant une distribution continue de molécules d'asphaltènes.
Dans une seconde partie, l'utilisation d'un résonateur en cristal de quartz, immergé dans le fluide d'étude, a permis pour la première fois de mesurer la quantité de dépôt d'asphaltènes pendant le changement continu des propriétés du solvant. Un modèle physique est proposé pour résoudre le transfert de masse des asphaltènes dans le fluide vers la surface solide. En accord avec de précédentes recherches, les simulations montrent que le mécanisme d'accumulation est controlé par la diffusion des espèces en question. Ce modèle permet d'identifier les particules primaires d'asphaltènes instables commme contributeurs principales du processus de déposition. Ceci est notamment mis en évidence à travers la taille des objets qui diffusent puisqu'une moyenne de rayon hydrodynamique de 7 nanomètres permet d'expliquer la majorité des résultats expérimentaux. La relation linéaire entre le taux de déstabilisation et le taux de déposition est aussi parlante sur le processus. Par ailleurs, la vitesse de déposition tend à décroître en présence initiale d'asphaltènes instables (grandes particules en suspensions) dans la solution de pétrole et d'heptane.
Dans la dernière partie de ce travail, les concepts définis sur la déstabilisation, l'aggrégation et le dépôt des asphaltènes pendant l'ajout d'heptane sont expérimentalement vérifiés pour des systèmes à gaz dissouts (methane) avec un appareil analogue à capteurs immergés sous haute pression (1000 bars). Pour la première fois, le taux de déposition et la concentration en asphaltènes instables peuvent être quantifiées, en laboratoire, au cours d'une opération de dépressurisation d'un pétrole qui contient des éléments légers. Le taux de changement de paramètre de solublité de la solution liquide est un facteur dominant sur le processus de dépôt. Le methane dissout montre un effet plus sévère que les alcanes plus lourds sur l'instabilité des asphaltènes. Les méthodes empiriques de prédiction ne suffisent pas à expliquer les tendances observées sur cet effet de la nature (ou volume molaire) de l'agent déstabilisant.
Il est important de noter que ce travail doit servir de base pour effectuer des recherches plus fondamentales, dans des conditions désormais dont les effets sont controllés, afin d'élucider les lois thermodynamiques qui gouvernent la déstabilisation des asphaltènes par différents composés.

Acknowledgements

This dissertation is the fruit of a work that would not have been possible without the contribution of many individuals whose support, encouragement and confidence have made huge impact on my life. I am thankful for the intellectual brilliance of people I have professionally been exposed to and for the high quality of personal life I was fortunate to have throughout my doctoral studies. It is with a lot of honour that I am completing this dissertation, and I must acknowledge that beyond the reward of this achievement, the conclusion of my doctoral studies is immensely frustrating for having to end my daily collaboration with tens of exceptional persons. I am very grateful for having been given the opportunity to acquire skills that extensively contribute to my personal development.

I would first like to genuinely acknowledge and thank my academic advisors Prof. Hervé Carrier and Prof. Jean-Luc Daridon for giving me this wonderful opportunity to do my doctoral studies under their supervision. Their respective presence have been complementary and gave me the luxury of interacting with different ingenious perspectives. Both have been exceptional in providing their physical and intellectual guidance to perform experiments at challenging conditions. They have always been very supportive of new ideas and creative thinking. Their accompaniment has always extended to enjoyable interactions that go beyond research topics.

My deep gratitude also go to my advisor in the industry Dr. Thierry Palermo from whom I have always been appreciative of receiving the best mentorship I could ask for. He has been supportive of developing my problem solving skills using physics. He undoubtedly had a great influence in my life by trusting me and giving me opportunities to work for TOTAL along my career, I cannot thank Thierry enough for all the opportunities he has provided to me these years.

I would like to express my gratefulness to my superior in the company Dr. Nicolas Passade-Boupat who did not only provide an appropriate management to my presence in his department with a lot of trust but with whom technical discussions have always been very constructive.

My special thanks go to Prof. H. Scott Fogler, who is chairing my PhD thesis committee, for letting me have the opportunity to join his group of research at the University of Michigan during 10 months long. His outstanding and unique ability to promote the growth of his students have changed my way of working. From preparing experiments to interpreting data, the critical and theoretical thinking he taught me have changed my approach to problems. Beyond Chemical Engineering, I will always remember one of his first lesson which helped me understand the rules of baseball.

I would like to thank Dr. Lamia Goual and M. Loïc Barré for accepting to serve as my doctoral committee members, it is an honour for me to have the opportunity to improve the quality of my work thanks to insightful questions from such renowned researchers.

I had the chance to interact and work with a number of colleagues from the LFCR and more generally from UPPA. I am thankful to Djamel Nasri and Jean-Patrick Bazile who helped me enhancing specific skills related to laboratories or to computing, they have been helping me on various subjects. I thank Eddy Lasseur who was amazing at providing every single glass equipment that I needed in the laboratory by hand manufacturing them. Similarly, I appreciated collaborating with Laurent Marlin and his team who were able to deliver many specific pieces from their mechanical workshop. Catherine Urrea, Patricia Lafont, Véronique Giancola, Sophie Lebatteux and Blandine Gaio have been extremely helpful with their administrative

and IT support. I give thanks to the following individuals for the interesting discussions both related and unrelated to my research topic during the so important coffee time everyday: Jerôme Pauly, François Montel, Guillaume Galliero, Romain Vermorel, Amael Obliger, Abdoul Saley Hamani, Ezequiel Orlandi, Bich Ngoc Ho, Deneb Peredo Mancilla, Daoud El Kadiri, Brice Bouyssières and Abdelhafid Touil.
I feel indebted with a number of persons from the Department of Chemical Engineering at University of Michigan who did not only contribute to my work but also made my life easy and enjoyable during my short stay in Ann Arbor. I thank Cláudio Vilas Boas Fávero for sharing his immense comprehension on the subject. Discussions with Cláudio have been crucial during the major turn I took to relate my research to theories. Jeremy Kach was a graduate student who has not only been very helpful at introducing me to laboratory techniques and to its management, Jeremy has been personally involved at showing me many aspects of students life in Michigan. I appreciated and enjoyed discovering Michigan thanks to his presence. Yi Dai has been a great undergraduate intern who came all the way from China to make a tremendous work in the laboratory during 4 months. I must also thank Luqman Mahir who was conducting his PhD thesis research on paraffins and with whom I enjoyed interacting on several technical subjects. The friendly interactions I had with most of the above mentioned people in Ann Arbor was an important factor that maintained my wish to spend time in the Fogler group at that time. The administrative help of the staff, especially of Laura Bracken and Shelley Fellers, has been invaluably important before, during and after my stay in Ann Arbor.
Number of my colleagues at TOTAL E&P have been directly or indirectly contributing to my research with providing support and with following up on my results. For those reasons my thanks go to Honggang Zhou, Khalid Mateen, Laurent Avaullée, Jean-Philippes Gingras, Roel Belt, Leticia Ligiero, Stephane Jouenne, Laurent Lescoute and Marianna Rondon. I would like to specially praise Carole Desplobins and Marianne Pedelabat Lartigau for their help in performing laboratory studies and for always being present when I needed them to give me a hand. Not to forgot Gabrielle Virenque who has been an outstanding administrative assistant at preparing my travels.
I would like to express my grace to my colleagues from TOTAL ACS based in Givors, Fréderic Tort and Olivier Langlois, without whom I would not have been involved in operational projects. Their presence was extraordinarily helpful for boosting my motivation in the final year of my thesis.
My regards and thanks go to my colleagues from each institution who I did not personally mention but who certainly contributed to the good balance I benefited from during this amazing and interesting period of my life.

I would like to extend my thanks to my supportive friends in Angoulême, Pau and Ann Arbor who have been contributory of my happiness by providing a fun environment to my life and by being present whenever I needed help. My special blessings go to Thomas Elan, Nelson Fleury, William Gairin, Tiphaine Milin, Benoît Tanguy, Edward Pugnet, Benjamin Pignot Loïc Largeron and Cécile Bordenave, with whom I have spent the most part of my fun time those years and with whom I developed a solid friendship for life.
I want to express my deepest gratitude to my family. My first thoughts go to my parents: Djemal and Fatiha for their unconditional love, their support and their sacrifice abilities to raise their children in good conditions. I also have profound and equal recognition toward both of my brothers Amine and Samir who showed a lot of compassion to me and felt honoured during those years. I would like to express

my adoration to my nephew Aden and to my niece Lila for the amount of love they brought to me and for bringing me smiles and for spreading laughs across all my family. I thank my sister-in-law Caroline who has made possible to spend family time all together especially at Christmas time. I want to thank my family in Algeria, in France and in Germany for their support and to apologize for my absence during many years.

My final thanks go to my company *TOTAL* and to institutions which have financially supported my research. Among those institutions, I would like to mention the group of research *Laboratoire des fluides complexes et leurs réservoirs* (LFCR-UMR5150) at the *Université de Pau et des Pays de l'Adour* (UPPA), the consortium *Energy Environment Solutions* (E2S), the Department of Chemical Engineering at the University of Michigan and the *Association Nationale Recherche et Technologie* (ANRT).

Contents

List of Figures

List of Tables

List of Abbreviations

AC	Alternating Current
AFM	Atomic Force Microscopy
AOP	Asphaltene Onset Pressure
ASCI	Asphaltene Stability Class Index
CCC	Critical Coagulation Concentration
CNAC	Critical Nano Aggregate Concentration
CMC	Critical Micelle Concentration
CME	Constant Mass Expansion
DBE	Double Bond Equivalent
EOS	Equation Of State
FHZ	Flory-Huggins-Zuo
FT-ICR	Fourrier Transform Ion Cyclotron Resonance
MD	Molecular Dynamics
MS	Mass Spectrometry
NIST	National Institute of Standards and Technology (U.S. Department of Commerce)
NMR	Nuclear Magnetic Resonance
ODE	Ordinary Differential Equation
PAH	Poly Aromatic Hydrocarbon
QCM-D	Quartz Crystal Microbalance with Dissipation monitoring
QCR	Quartz Crystal Resonator
SANS	Small Angle Neutron Scattering
SARA	Saturates Aromatics Resins Asphaltenes
SAXS	Small Angle X-ray Scattering
VdW	Van der Waals
WAXS	Wide Angle X-ray Scattering

Physical Constants

Avogadro constant	$\mathcal{N}_{\mathcal{A}} = 6.022\,14\,\mathrm{mol}^{-1}$
Boltzmann constant	$k_B = 1.3806 \text{ x } 10^{-23}\ \mathrm{m}^2.\mathrm{kg}.\mathrm{s}^{-2}.\mathrm{K}^{-1}$
Gas constant	$\mathrm{R}_g = 8.314\ \mathrm{J}.\mathrm{K}^{-1}.\mathrm{mol}^{-1}$
Vacuum Permittivity	$\epsilon_0 = 8.85\,\mathrm{F/m} \times$

List of Symbols

Roman alphabet

A	asphaltenes	-
A_c	cross-sectional area of empty packed-bed column	m^2
a	Distance	m
a_s	QCR surface area	m^2
a_1	slope of linear interpolation of C_A vs volume frac. C_7	$kg.m^{-3}$
B	First temperature dependent parameter of Tait EOS	-
C	Second temperature dependent parameter of Tait EOS	-
C_i	Concentration of i component	$kg.m^{-3}$
C_m	Sauerbrey coefficient	$m^2.kg^{-1}.s^{-1}$
C_7	Heptane	-
C_8	Octane	-
C_{10}	Decane	-
C_{11}	Undecane	-
C_{15}	Pentadecane	-
CH_4	Methane	-
D_A	Diffusion coefficient of depositing asphaltenes	$m^2.s^{-1}$
D_f	Fractal dimension	-
f	Resonance frequency	Hz
f_0	Fundamental resonance frequency	Hz
G	Adjusted parameter of the Grunberg-Nissan equation	-
H	Enthalpy	J
K_{ij}	Aggregation Kernel or Aggregation rate constant	s^{-1}
k_c	Convective mass transfer coefficient	$m.s^{-1}$
k_{dep}	Deposition rate constant	s^{-1}
k_N	Generation rate constante of unstable asphaltenes	s^{-1}
k_r	Reaction rate constant	s^{-1}
L	characteristic length	m
J	Scaled deposition rate	$m^{2/3}.s^{1/3}$
m	mass	kg
M_w	Molecular Weight	$g.mol^{-}1$
m/z	FT-ICR MS mass to charge ratio	-
N	Nitrogen	-
N_{agg}	number of asphaltene molecules in an aggregate	-
n	Overtone number of resonance	-
n_D	Refractive index	-
O	Oxygen	-
P	Pressure	bar
Re	Reynolds dimensionless number	-
R_A	Hydrodynamic radius of unstable asphaltenes	nm
$R_{interface}$	Empirical term in the Sauerbrey equation	-
R_m	Molar refractivity	mol^{-1}

R_p	Hydrodynamic radius of primary particles	nm
r_1	Destabilization rate of asphaltenes	$kg.m^{-3}.s^{-1}$
S	Sulfur	-
Sc	Schmidt dimensionless number	-
Sh	Sherwood dimensionless number	-
t	time	s
T	Temperature	K
$t_{detection}$	Detection-time of asphaltenes by microscopy	h
U_0	Fluid superficial velocity	$m.s^{-1}$
V_i	total volume of component i	m^3
v	Molar volume	$cm^3.mol^{-1}$
W	Colloidal stability ratio	-
x	Mass fraction	-

Greek alphabet

α_i	Electronic polarizability of component i	-
β_{ij}	Aggregation collision efficiency between i and j particles	-
δ	Solubility parameter	$MPa^{1/2}$
Δ	Difference	-
ϵ_{10}	Binary operator equal to 0 or to 1	-
Γ	Resonance dissipation	Hz
μ	Dynamic viscosity	mPa.s
ω	Angular speed	$rad\,s^{-1}$
ϕ	Volume fraction	-
ψ	Correction factor of trapped liquid in asphaltenes deposit	-
ρ	Density	$kg.m^{-3}$
τ	Characteristic time to reach equilibrium	h
ζ	Fitting parameter to the size of depositing aggregates	$m^3.kg^{-1}$

Subscripts

X_0	Property at the reference conditions
X_∞	Property at equilibrium
X_A	Property of unstable asphaltenes aggregates
$X_{A,d}$	Property of contributing asphaltenes to deposition
X_{agg}	Property of asphaltenes aggregates
X_{asph}	Property of the asphaltenes
X_{dep}	Property of the deposit
X_{eff}	Effective property
X_f	Final property
X_{gas}	Property of the dissolved gas in solutions
X_i	Initial property
X_k	Property of the k^{th} number
X_{liq}	Property of the liquid solvent
X_{oil}	Property of the oil
X_q	Property of the quartz crystal
X_{vap}	Property of vaporization

Superscripts

X^P	Property at constant pressure
X^T	Property at constant temperature

To my lovely parents and siblings who support me in all circumstances

Chapter 1

Introduction

1.1 Background & Industrial Problems

After the invention of the kerosene lamp in the mid-19th century, large quantities of liquid petroleum have been extracted from geological formations as the demand of fuel for lighting was growing. The standardization of drilling instead of digging to encounter natural resources provoked a major turn in the industrial revolution. In the ensuing years, the world industrial machine of fossil fluid fuels was born. Refineries have been able to deliver highly energetic fluids from extracted crude oils and their development was motivated by continuous discoveries of immense reserves on earth. At that time, the convenient transport properties of liquids compared to the solid coal alternative, along with the high energy density of crude oil products lead the world to abandon steam engines. Instead, the invented combustion piston engines have been extensively used up to nowadays. Relying on this dark raw material, the developed downstream industries modified many aspects of the daily life and made standards of living of the western general population consistently increase. In recent history, the geopolitical, economical and environmental instabilities that the world is facing make us realize how dependent are our societies on hydrocarbon supplies. Meanwhile the current research for substituting energies and for more reasonable lifestyles, the transition period to a low-carbon economy still puts crude oil in a central position of the global energy mix according to forecasts of the international energy agency (see example in Figure 2.1). Within the current situation, the present work finds its interest in the need for better efficiency of the petroleum extraction methods in short terms.
In 1837, the French chemist Boussingault [10] separated for the first time volatile constituents from a natural bitumen sample. The author [10] could not know that the residue of his experiment would become such an internationally known fraction for causing industrial problems in the next centuries. He first named the solid black and heavy material "*asphaltène*" because of its visual similarity to "*asphalt*", a synonym word for bitumen, in contrast with the yellow oily liquid product of his experiment that he had given the name of "*petrolene*" [58]. The term "*asphaltum*" was derived from ancient greek "*ásphaltos*" which means bitumen. At this period of time, worldwide civilizations would use the adhesive and/or water-repealing properties of the naturally-occurring sticky substance for convenient utilization like caulking, cementing parts of constructions or even embalming mummies [1]. In the modern time, it is referred to as a technology after some transformations [67] but the vast majority of asphalt is still used for its same properties. Industrialization has gradually promoted it to a refined product with intended specifications mainly guided by the requirements of paving and roofing applications. However the industry frequently suffers from asphaltic fraction properties and behavior during the transportation, the treatment or the processing of petroleum fluids. Asphaltenes have been known

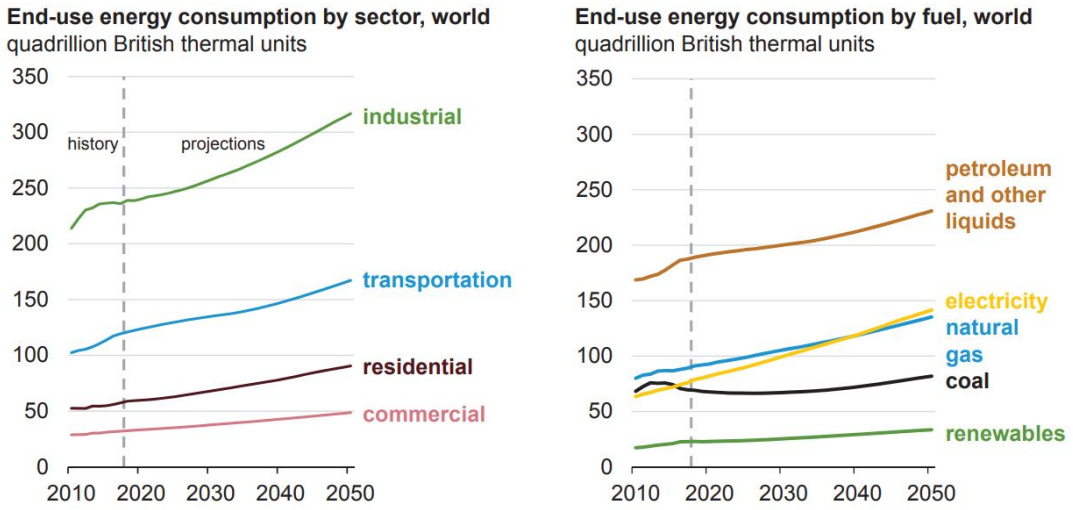

FIGURE 1.1: Projections of the future world energy consumption by sector (left) and by type of fuel (right) according to the reference case of the international energy outlook from the U.S. Energy Information Administration

to stabilize water-in-oil emulsions[40] causing difficulties in phase separation steps. Fouling and deactivation of catalysts in the hydro-conversion processes of heavy fractions is another issue reported in the downstream industry[6]. Blending of incompatible asphaltenic crude oils during upstream transportation[49] or in the refineries[79] is known to cause deposition or sedimentation troubles.

Katz and Beu[38] first reported wellbore deposition issues due to the expansion of volatile hydrocarbons in californian wells. Haskett and Tartera[25] later published an alarming case where algerian wells of Hassi Messaoud field were clogged by asphaltenes within weeks. Figure 1.2 illustrates typical asphaltene deposits found in oil & gas conduits.

FIGURE 1.2: Picture of asphaltenes deposits in tubings (reprinted from www.cere.dtu.dk)

Since then, very few cases of wellbore deposition were publicly reported to cause significant losses of production. In fact, the main related issue is economical because of oversized means of prevention and of remediation. The associated costs are estimated in billions of dollars per year spent worldwide by the upstream petroleum industry[72].
The need for more cost-effective strategies highlights the importance to understand mechanisms by which asphaltenes destabilize and deposit.

1.2 Petroleum fluids and Asphaltene properties

1.2.1 Petroleum composition

Petroleum fluids are mixtures composed of thousands of unique components. Their composition do not only depend on the region where they come from but also depend from which well the sample is collected in a single reservoir of oil. Four subfraction families of components are defined to simplify such complex mixtures: saturates, aromatics, resins and asphaltenes (SARA). The SARA fractionation enables to compare crude oils using a standardized separation technique based on the solubility of components in well-defined conditions[22]. Note that when saturates, aromatics and resins are not individually separated, they are usually regrouped and referred to as maltenes.

In this dissertation, good solvents refer to solvents that are able to disperse asphaltenes in their stable colloidal form, i.e. suspensions of nanoaggregates or clusters of nanoaggregates in the liquid solution, such as aromatic solvents. Contrarily, anti-solvent or destabilizing agents refer to bad solvents for asphaltenes, which tend to induce the coagulation of asphaltenes, such as alkanes. Depending on the solvent and conditions for the extraction of asphaltenes, the total mass of asphaltenes might vary. Therefore asphaltenes are named after the anti-solvent that served to measure their quantity in crude oils; most commonly *n*-pentane or *n*-heptane (e.g. *n*-C_5 or *n*-C_7 asphaltenes)[83].

1.2.2 Molecular structure of asphaltenes

Asphaltenes are defined as a class of relatively heavy, highly aromatic and polar molecules present in native crude oils at concentrations naturally ranging from units of g/L to hundreds of g/L depending on the oil origin[43;5] and on the procedure used for their recovery[51;44;3]. The quantity of heteroatoms (N, O, S) in asphaltene molecules is also variable[13] and their influence on the solubility of asphaltenes has been related to the polarity induced by their presence[37]. Asphaltenes are also richer than other hydrocarbon components in heavy metals like Nickel or Vanadium that can be found at the level of traces (parts per million) in crude oils[4].
Despite tremendous research efforts on the topic, lacks of chemical analysis technologies that meet the complexities of crude oils had made the description of asphaltenes properties, such as their molecular weight, variable for years. The past decade was fruitful in the gain of understanding on the molecular level of asphaltenes. Two main structures of asphaltene molecules were reported: the island type (single core of PAH with aliphatic side chains) and the archipelago type (several aryl connected cores of PAHs). Figure 1.3 shows schematics of both main structures. Mullins

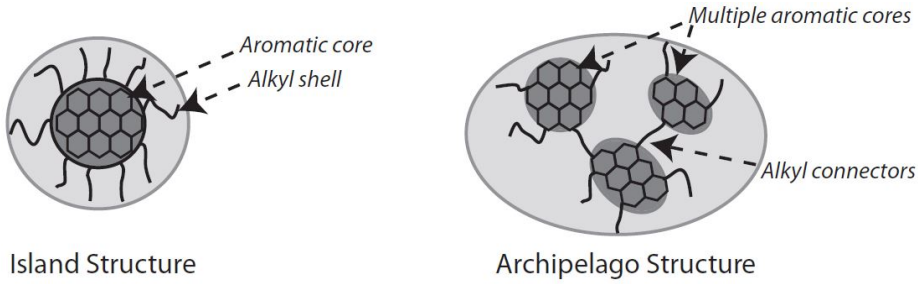

FIGURE 1.3: Schematic of the island and archipelago structures of asphaltene molecules (reproduced from Hoepfner[28])

et al.[55] have been leading extensive research and suggested that the island motifs of asphaltenes were predominant based on time resolved fluorescence depolarization experiments.
Recent studies significantly improved the molecular resolution of chemical structures and enabled analyzing samples of isolated asphaltene molecules by atomic force microscopy (AFM)[65;64] and by Fourrier transform ion cyclotron resonance coupled to mass spectrometry (FT-ICR MS)[13;14]. Findings eventually reach a consensus to define petroleum asphaltenes as a polydisperse continuum composed of polycyclic aromatic hydrocarbons (PAHs).
Elemental compositions of crude oil and asphaltene samples have been obtained by FT-ICR MS analysis that provides the abundance of chemical species as a function of their mass to charge ratios m/z. This technique enabled to verify the widespread

agreement on the significantly lower Hydrogen to Carbon ratio of asphaltenes (H/C $\sim$ 1) compared to maltenes[50]. Figure 1.4 is reproduced from McKenna et al.[50] and shows the example of larger hydrogen deficiency of asphaltenes compared to its parent oil.

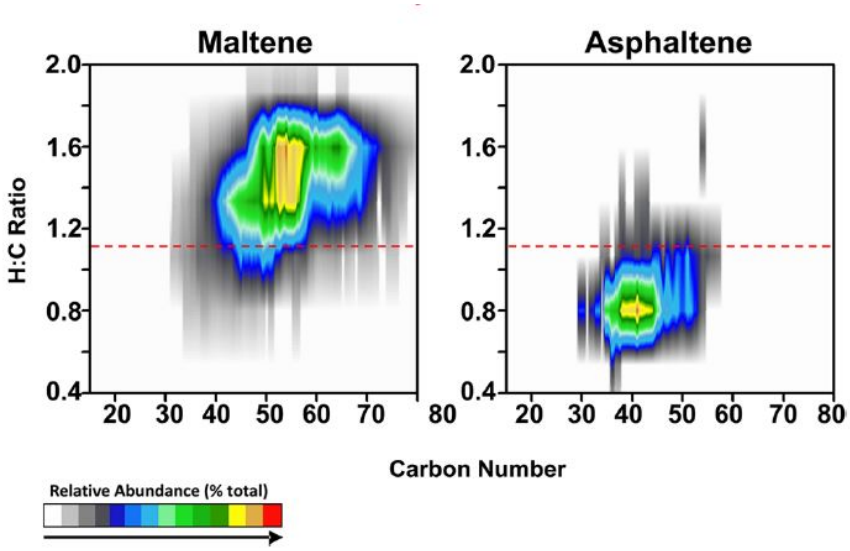

FIGURE 1.4: Isoabundance-contoured plots of H/C ratio of maltenes (left) and asphaltenes (right) of a heavy crude oil as a function of the carbon number (reprinted from McKenna et al.[50])

The concept of double bond equivalent (DBE) also uses FT-ICR MS measurements to further evaluate the level of unsaturation in organic molecules (double bonds + cyclic rings). This analysis enables another compact visualization of complex mixtures compositional space. An upper theoretical boundary line has been determined for planar PAHs on the plot of DBE against carbon number of structures, the limit is given by the following relation[31]:

$$\text{DBE} \approx 0.9 \text{ x (carbon number)} \tag{1.1}$$

More explorations on the extracted highly aromatic asphaltenes, showed in Figure 1.5, revealed clear experimental evidence of the planar PAH boundary.

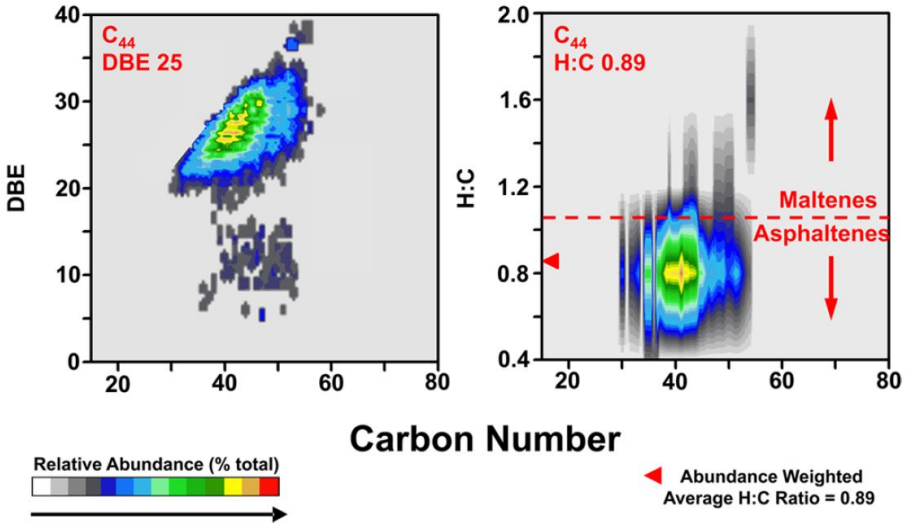

FIGURE 1.5: Isoabundance-contoured plots of DBE (left) and H/C ratio (right) of asphaltenes as a function of the carbon number (reprinted from McKenna et al.[50])

Several crude oils and asphaltenes from different origins were chemically analyzed by McKenna et al.[50]. Figure 1.6 shows the empirical compositional spaces defined by multiple samples. Indeed a boundary between asphaltenes and maltenes compositional spaces is represented by a line that complements the PAH planar limit. The delineation is equivalent to a H:C ratio of 1.10 and agrees with previous data reported on the form of H:C ratios versus carbon number.

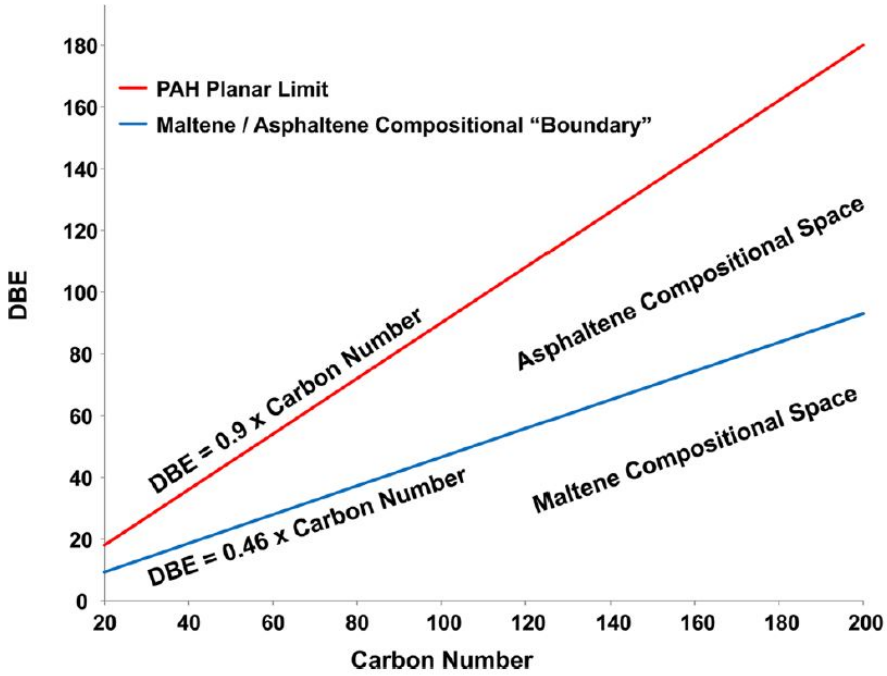

FIGURE 1.6: Experimentally determined boundary (blue) between asphaltene and maltene compositional space on the plot of DBE as a function of the carbon number (reprinted from McKenna et al.[50])

This powerful compositional method also facilitated the analysis of asphaltenes

fragments using different methods. This way Chacon-Patino et al.[13] clarified previous selective artifacts and revealed the coexistence of archipelago and island motifs of asphaltenes in crude oils as seen in Figure 1.7.

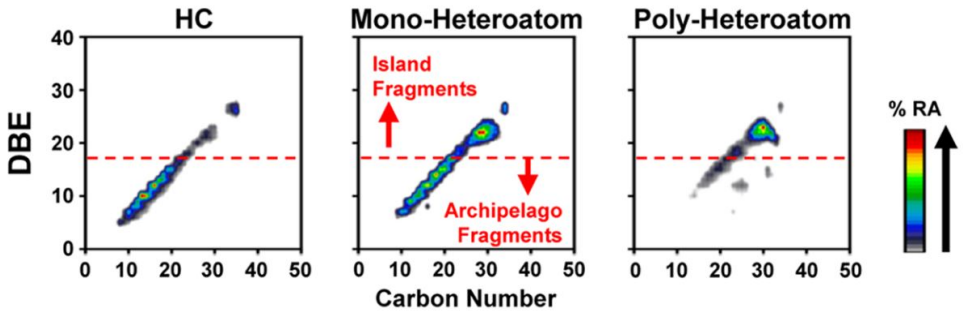

FIGURE 1.7: Isoabundance-contoured plots of DBE of several fractions of asphaltenes as a function of the carbon number (reprinted from Chacon-Patino et al.[13])

Although Chacon-Patino et al.[15] correlated the abundance of archipelago motifs to the molecular weight and polarity of the overall asphaltenes, the ratio *island/archipelago* is oil dependent.
Those results are completed by the impressive pictures of isolated asphaltenes molecules obtained by AFM[64]. Indeed images showed in Figure 1.8 were obtained on samples recovered from multiple industrial problematic operations and showed excellent agreements with mass spectrometry measurements.

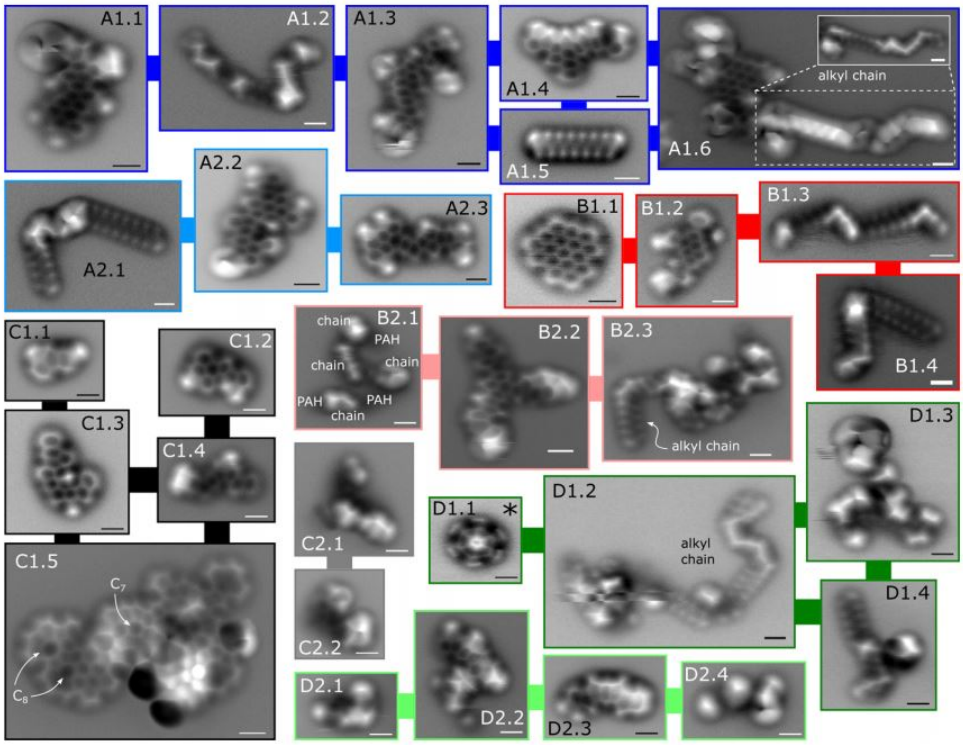

FIGURE 1.8: AFM raw images of individual heavy recovered components from industrial deposits (reprinted from Schuler et al.[64])
scale bars: 5 Å

The vast majority of the available catalogue of collected asphaltenes molecular weights have been found to belong to the range $\sim 250 - 1200$ g.mol^{-1} [55;13;52]. Exact measurement of asphaltenes molecular weights by FT-ICR MS might provide matters to argue with this widely accepted range. Indeed Chacon-Patino et al. [13] claimed selectivity artifacts of previously used processes of chemical analysis. They reported larger molecular weights using their "non-destructive" ionization technique.
Tens of thousands (or perhaps more) different molecular structures of asphaltenes can be found in a single crude oil. Attempting to account for all molecules with individual properties complicates the problem and is almost impossible. Instead, distributions are defined and are usually adjusted to exprimental measurements with equations of state[84]. The notion of apparent molecular weight considers an ensemble of molecules described by Gamma distribution functions. As illustrated in Figure 1.9 this practice requires to account for fractions that have much larger molar weights than orders reported above (M_w ~750 g/mol). Indeed asphaltenes self-association can generate structures with larger apparent molar weights. The apparent molar weight of associated asphaltenes increases with their concentration, this particular behavior is discussed in the following paragraph.

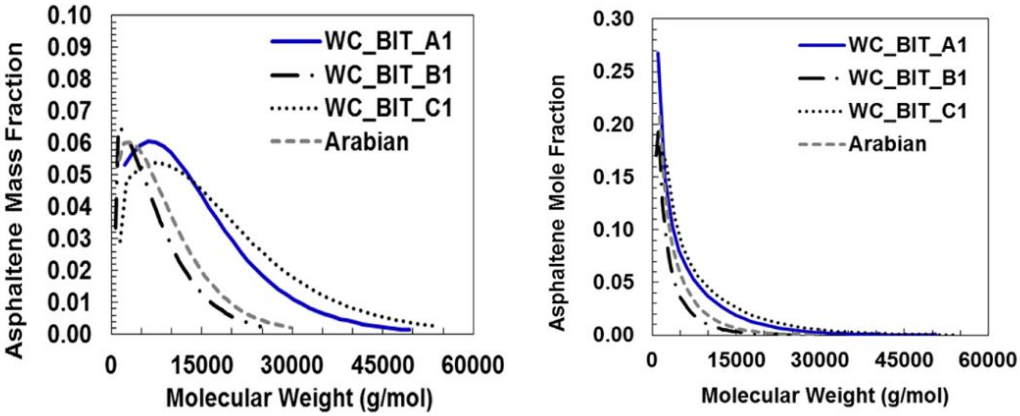

FIGURE 1.9: Comparison of molecular weight distributions of four different extracted asphaltenes at concentration of asphaltenes of 10 g/L (reprinted from Barrera et al.[9])

Yarranton and Masliyah[84] developed a power law correlation between the density and the molecular weight of asphaltenes found in bitumen samples (referred "Yarranton (1996)" in the following figure). However, as showed in Figure 1.10, Barrera et al.[9] suggested that asphaltenes from crude oils rather follow an exponential function given by the "correlation" curve shown in Figure 1.10:

$$\rho_{asph} = 1100 + 100\left[1 - \exp\left(-\frac{\mathrm{Mw}_{asph}}{3850}\right)\right] \tag{1.2}$$

where Mw_{asph} is the molecular weight of asphaltenes (in g.mol^{-1}) and ρ_{asph} is their density (in kg.m^{-3}).

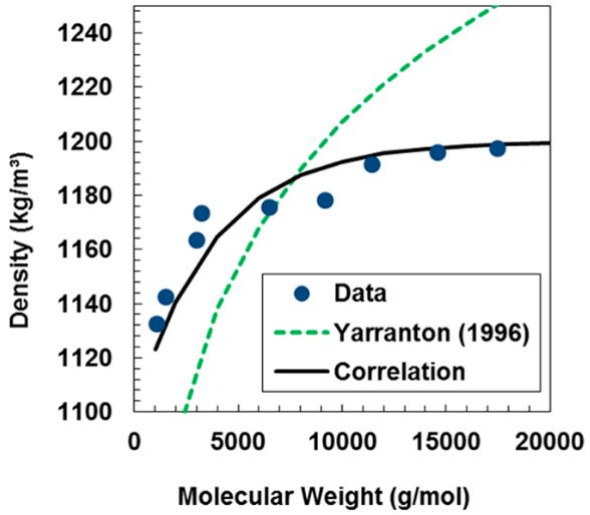

FIGURE 1.10: Density of extracted asphaltenes at 23°C as a function of the molecular weight at concentration of asphaltenes of 10 g/L (reprinted from Barrera et al.[9])

1.2.3 Asphaltenes in good solvents

Molecular properties of asphaltenes cannot directly be used to solve classical thermodynamics and transport equations as they are mainly present in forms of stabilized self-associated molecules in good (aromatic) solvents[56] and in (live) crude oils[33]. Indeed suspended elemental aggregates, more commonly referred to as nanoaggregates[29;17], have been extensively characterized with in-situ non-invasive techniques of small angle scattering X-ray and neutron scattering (SAXS/SANS)[66;16;29]. Direct-current conductivity measurements[66;21] and nuclear magnetic resonance (NMR)[19] were also used to investigate molecular and structural properties during the past decades. The aforementioned studies converged in a shape description of nanoaggregates corresponding to core-shell disc-like organizations composed of 5 to 8 molecules and made of $\pi - \pi$ stacked aromatic cores limited in size by steric repulsion from the peripheral chains[17;54]. Figure 1.11 exemplifies geometrical characteristics of nanoaggregates obtained by Hoepfner[28] who used wide angle X-ray scattering (WAXS) to study the molecular orders within nanoaggregates of asphaltenes.

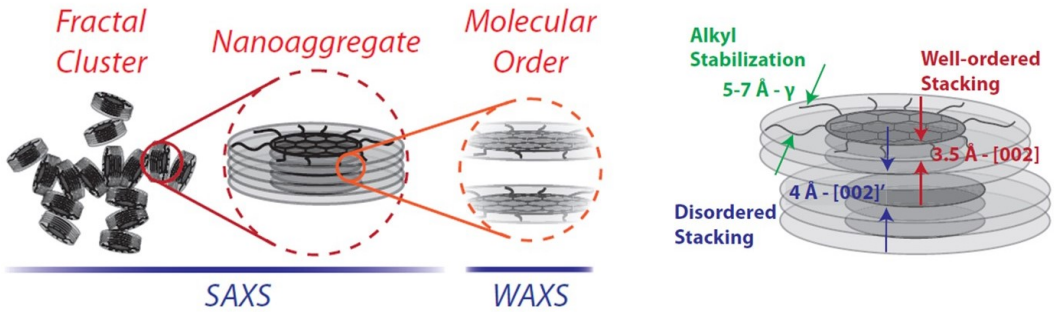

FIGURE 1.11: Schematic illustration of results on the molecular order of asphaltenes nanoaggregates obtained by WAXS (reprinted from Hoepfner[28])

The characteristic radius of nanoaggregates is reported as ∼1-2 nm, their molar mass is comprised in the range of $\sim 3000 - 10000$ g.mol^{-1} [29;17;85] depending on their level of association. Their fractal dimension is typically measured to be ∼1.7[56;29], which indicates high level of solvation of the structures. In analogy to the widely used critical micelle concentration (CMC) in colloidal science, the critical nanoaggregate concentration (CNAC) was defined as the concentration of asphaltenes above which the majority of asphaltene molecules in the system go to nanoaggregates. In good asphaltene solvents, the CNAC ranges from 10 mg/L to 150 mg/L according to experimental results from multiple techniques[21;7;17;19;29;57]. More recently, Svalova et al.[68] statistically studied interfacial active asphaltenes by interpreting ultrasound velocity measurements coupled to analyses of asphaltenes side-chains distribution by selective oxidation of aromatic rings. Svalova et al.[68] observed relation between the CNAC and the side chain distributions. Their results on the CNAC are in agreement with the range of values previously reported in the literature.
As seen in Figure 1.11, elemental aggregates of asphaltenes distinctly show a second stage of aggregation at one unit larger order of length scale by forming fractal clusters at concentrations above the reported critical cluster concentration ∼ 2-5 g/L[21;54]. Figure 1.12 shows a schematic representation of the asphaltenes structural hierarchy.

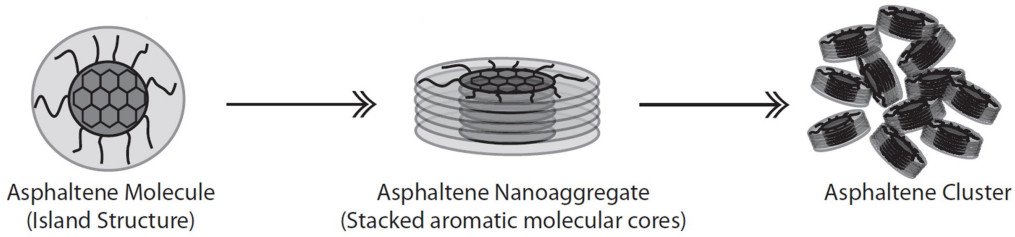

FIGURE 1.12: Schematic of the hierarchical self-association of asphaltenes in good solvents (reprinted from Hoepfner[28])

Clusters are generally accepted to be composed of less than 12 elemental nanoaggregates, they are described by a molar mass of $\sim 50000 - 10^4$ g.mol^{-1}, a characteristic radius of $\sim 5 - 7$ nm and a fractal dimension up to $D_f \sim 2$ still indicating loose particles with trapped solvent.
New simulation methods have been arising with the increase of computational power. Javanbakht et al.[36] were able to simulate the 2 stages of aggregation by long time molecular dynamics (MD). Their MD results provided realistic size, morphology and association energies of aggregated structures only when accounting for the polydisperse representation of the molecular weight, aromaticity and polarity of contributing species.

1.2.4 Asphaltenes in their natural state

Supported by experimental results exposed in the previous paragraph, the most used conceptual representation of the multiple stages of asphaltenes colloidal association is the Yen-Mullins description[53;55]. The characteristic dimensions in this hierarchical picture of the state of asphaltenes aggregation in good solvents is mainly used for the characterization of oil reservoirs. Indeed, Freed et al.[20] developed an equation of state (EOS) based on the regular solution theory[27;2;80;69;61]. This EOS

had originally been developed for macromolecules like polymers in solutions[32;42]. The so-called Flory-Huggins-Zuo (FHZ) EOS showed successful predictions of asphaltenes concentration gradients and presence of tar mats in geological reservoirs. Asphaltenes being much heavier than other components of crude oils, their observed segregation in continuously permeable reservoirs is in agreement with theoretical equilibrium reached during geological times. In practice it enables to identify reservoirs connectivity and to optimize the industrial strategy of oilfield developments.

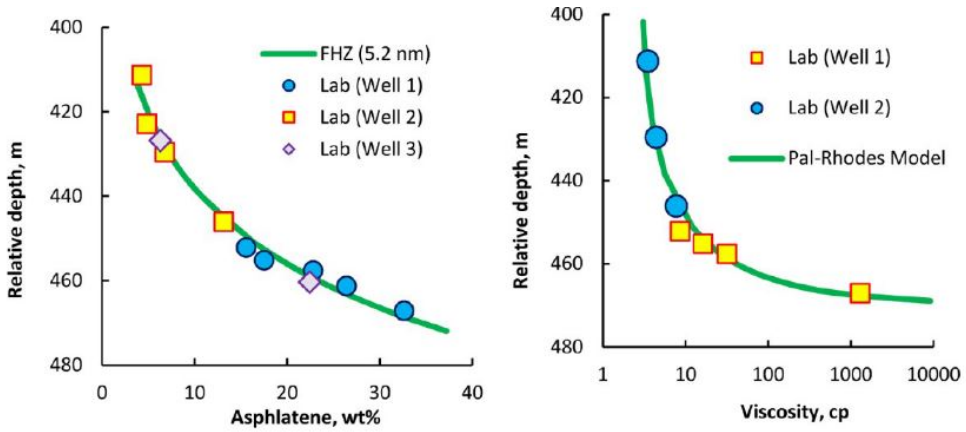

FIGURE 1.13: Predicted and measured gradients of asphaltene contents in three wells of a Saudi Arabian oilfield (reprinted from Mullins and Sheu[56])

Note that molar masses used by Mullins and Sheu[56] are in agreement with self-association concepts presented above and reinforces the reported average in molecular weight of asphaltene molecules (~ 750 g.mol^{-1}).
In parallel, Barré et al.[8] demonstrated consistent relations between structural parameters of clusters by considering asphaltenes as a suspension of fractal aggregates in good solvents. The results are in agreement with previous evidences of the fractal nature of asphaltenes[35] and are supported by small angle X-ray scattering (SAXS) and rheological measurements. As showed in Figure 1.14, Pal[59] was able to collapse viscosity measurements from 20 different sets of literature data with a single scaling law:

$$\frac{\eta_r - 1}{[\eta]_s} = \left(\frac{\phi_{eff}}{1 - \phi_{eff}} \right) \tag{1.3}$$

where $[\eta]_s$ is the intrinsic viscosity of asphaltene aggregates, η_r is the relative viscosity of dilute suspensions and ϕ_{eff} is the volume fraction of the solvated asphaltenes.

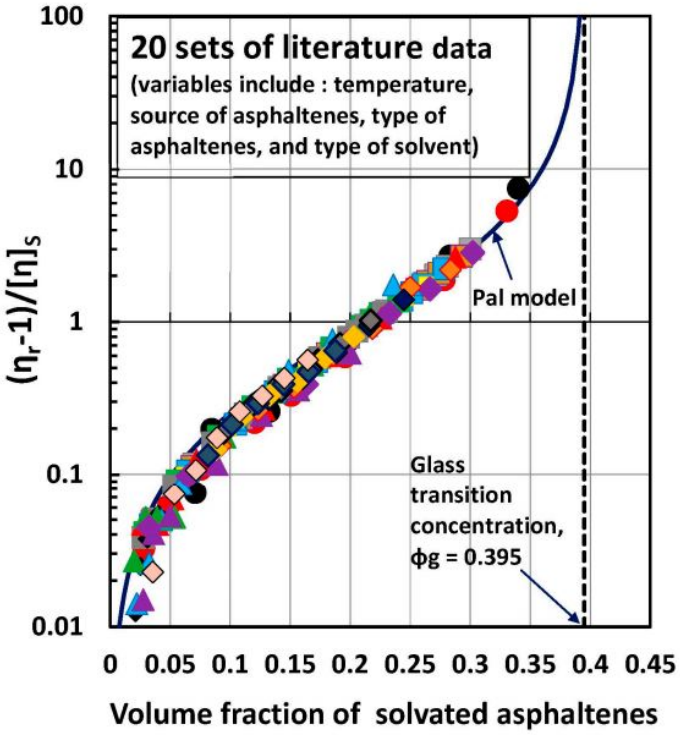

FIGURE 1.14: Semi-log viscosity scaling law applied to 20 sets of data available in the literature (reprinted from Pal[59])

In summary at this point, we have seen that the literature regarding asphaltenes in good solvents shows very rich and consistent results from multiple experimental and modeling techniques at length scales ranging from molecular to macroscopic scale. The understanding of the molecular structures of asphaltenes permits a good understanding of their gradual and balanced presence throughout geological reservoirs. Moreover, transport properties of oils containing stabilized nanoaggregates and clusters can be well calculated with relatively simple models accounting for their averaged size and morphology. However, the transit of crude oils enclosing large enough quantities of volatile components through the industrial network will occasion a destabilization process of asphaltenes related to their decrease of solubility in the carrier solvent. The decrease of solubility of the solution can be caused by a change in thermodynamic conditions (pressure or temperature) or by the change in oil composition.

1.2.5 Solubility of asphaltenes

Completely dissolved asphaltenes as individual molecular solutes rarely exist even in good solvents. However, the growth of self-associated asphaltenes is limited to the nano-scale in good solvents. This behavior has been attributed to the larger steric repulsion forces of side alkyl chains compared to attractive forces between clusters in certain conditions[77;76]. Therefore, it becomes natural to call those asphaltenes "stable" in reference to the stabilized colloidal suspensions formed by solvated asphaltenes in liquid solutions. In this dissertation, "unstable" or "destabilized" asphaltenes will only refer to components that contribute to the growth of aggregates to larger association levels. Indeed, Hoepfner et al.[30] showed that upon a change of

the surrounding solvent, a certain class of asphaltenes further grow through a flocculation process while others remain at a similar state to their original form (clusters of nanoaggregates). Figure 1.15 reprints a schematic that illustrates this statement.

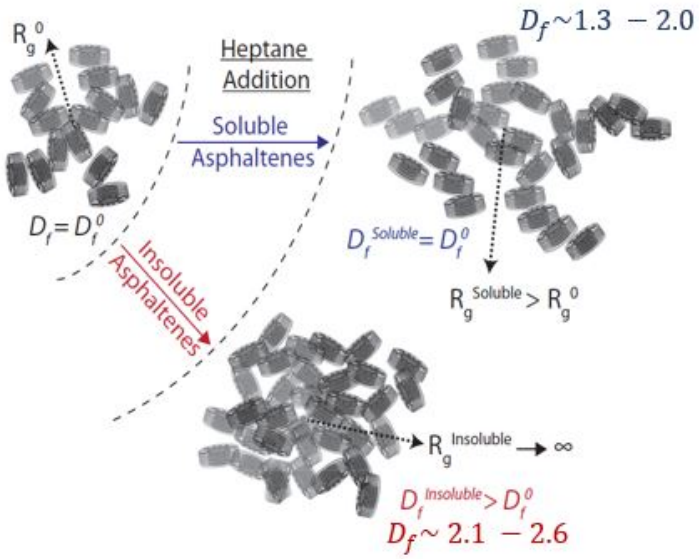

FIGURE 1.15: Schematic of the destabilization process of asphaltenes upon heptane addition (reprinted from Hoepfner et al. [30])

We note that the fractal dimension of "insoluble" asphaltenes is significantly increased in this process. This indicates that unstable aggregates expel the trapped solvent by shrinking inter-molecular distances and become more solid-like structures.

The widespread enthalpic driving force of colloidal stabilization, Gibbs energy of mixing[81], has been applied to asphaltenes flocculation since a long time[78;27]. This energy can be estimated by the difference in the solubility parameters of colloidal material and the solubility parameter of the solution ($\delta_{asph} - \delta_{solution}$)[46]. The solubility parameter δ_i of a liquid constituent i is equivalent to the degree of interaction between molecules[45]. Hildebrand[26] first suggested a numerical estimate of the solubility of non-electrolytes, given by Equation 1.4:

$$\delta = \sqrt{\frac{\Delta H_{vap} - RT}{v_m}} \tag{1.4}$$

The square root of the cohesive energy density is expressed by the energy of vaporization of the compound (ΔH_{vap}) divided by its molar volume (v_m) in the condensed phase. Materials with similar solubility parameters will be able to interact with each other, resulting in good miscibility. Hansen[24] developed a practical scale of solubility parameters and determined numerical values by addition of the three types of interactions in solvents: dispersion, polar and hydrogen ones.

Based on results of a large number of crude oils, authors[71] stated that asphaltenes stability was predominantly governed by Van der Waals (VdW) interactions[36]. A crude oil system contains very few permanent dipoles, for this reason generalizing VdW interactions to solely London dispersion interactions is a fair approximation.

Consequently, techniques to study asphaltene instability were designed using laboratory measurements of solvent parameters affecting dispersive forces such as densities[60;61;82;9], molar volumes[75;41;2], volume ratios[80] or refractive indices[11;73;74;12;73]. The solubility parameter of crude oils depend on their compositions and usually ranges between 16 $MPa^{1/2}$ (light oils) and 20 $MPa^{1/2}$ (heavy oils) at ambient conditions. In contrast the solubility parameter of problematic asphaltenes, which is often indirectly determined, is much larger (up to 26 $MPa^{1/2}$) than their parent oils (see Figure 1.16).

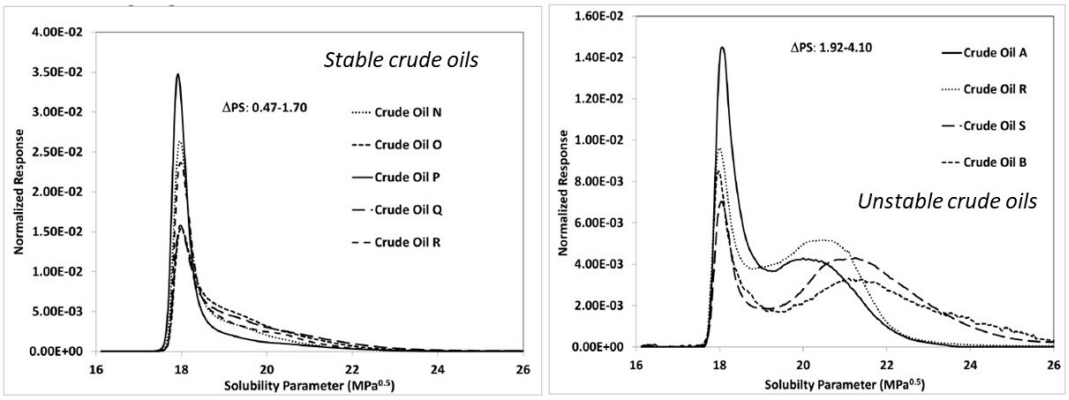

FIGURE 1.16: Indirectly measured solubility parameter profile of asphaltenes by re-solubilization (reprinted from Rogel et al.[62])

Let us consider a stabilized crude oil sample at ambient conditions, the addition of pure components, such as liquid alkanes, will decreases the average solubility parameter of the solution. Thus widening of the already existing gap between δ_{asph} and $\delta_{solution}$ can cause the destabilization of some asphaltenes. The predominant change of solubility parameter of a mixed organic solvents is described by the change in volume fraction ϕ_i of its constituents i and is given by:

$$\delta_{solution} = \sum_i \phi_i \delta_i \tag{1.5}$$

Consequently, the volume composition of oil-alkane mixtures is pre-supposed to be a relevant variable to study the asphaltenes destabilization.
Alternatively, a linear relation, given below, was proposed by Wang and Buckley[73] to relate the dispersion component of organic solutions solubility parameters and the Clausius-Mossotti or Lorentz-Lorenz refractive index function[18]. It is expressed as:

$$\delta_i = 52.042 \frac{(n_{D_i}^2 - 1)}{(n_{D_i}^2 + 2)} + 2.904 \tag{1.6}$$

where n_{D_i} is the refractive index of the pure constituent i at the conditions of interest. Figure 1.17 shows the graphic representation of pure liquid solubility parameters against the refractive index function. Buckley et al.[11] explained methane and ethane deviation from this curve due to measurements at conditions beyond their respective critical temperatures.

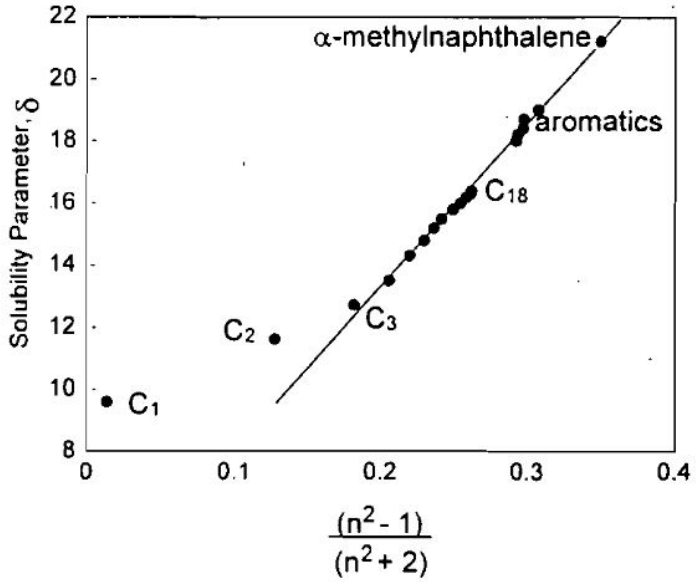

FIGURE 1.17: Comparison of the Lorentz-Lorenz function and the solubility parameters of organic components (reprinted from Buckley et al. [11])

In this work Equation 1.6 is applied and refractive indices (n_D) of crude oils are measured at the wavelength of yellow Sodium D line (589.3 nm) using a benchtop refractometer with a temperature control. The mentioned wavelength is usually chosen because it corresponds to the peak of absorption of organic matter and to a high enough frequency ($\sim 10^{15}$ Hz) to assume that the subsequent total polarizability of the molecules is well represented by the electronic polarizability[34].

We should note that Vargas and Chapman[70] related the density and refractive indices of more than 200 crude oil samples by the so-called "one-third rule" as shown in Figure 1.18.

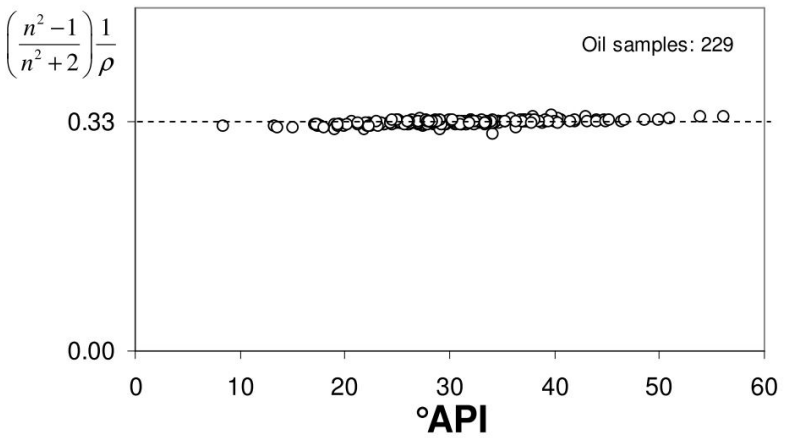

FIGURE 1.18: Consistency of the one-third rule applied to more than 200 stabilized crude oils at atmospheric pressure (reprinted from Vargas and Chapman[70])

Assuming that oils follow the same rule defined by Figure 1.18 with dissolved

light constituents, the calculation of live-oil refractive indices is simplified by only using routine thermodynamic reports of oils that usually provide the density of transported oils during their flow.
However, the extrapolation of simple laboratory measurements to industrial conditions is complex due to other influential variables, such as the nature of the constituents that cause the destabilization or "destabilizing agents".

1.3 Destabilization of asphaltenes induced by the expansion of light dissolved constituents

The most catastrophic upstream industrial problems related to asphaltenes are scenarios of unexpected well bore deposition or formation damage[86] that can irreversibly block wells. In those circumstances, the increased gap of solubility parameters is promoted by the volume expansion of light constituents (such as methane or carbon dioxide) in the carrier liquid. Indeed the pressure gradient, which promotes the fluid to move, also impacts volume composition to vary (signature from the change of density). Figure 1.19 illustrates the continuous process by which the asphaltenes are destabilized during the crude oil production in wells. The density of a reservoir fluid decreases as the pressure decreases until it reaches the saturation pressure (P_{sat}). At this point, a gas phase is created and the light dissolved constituents leave the liquid phase as the pressure further decreases.

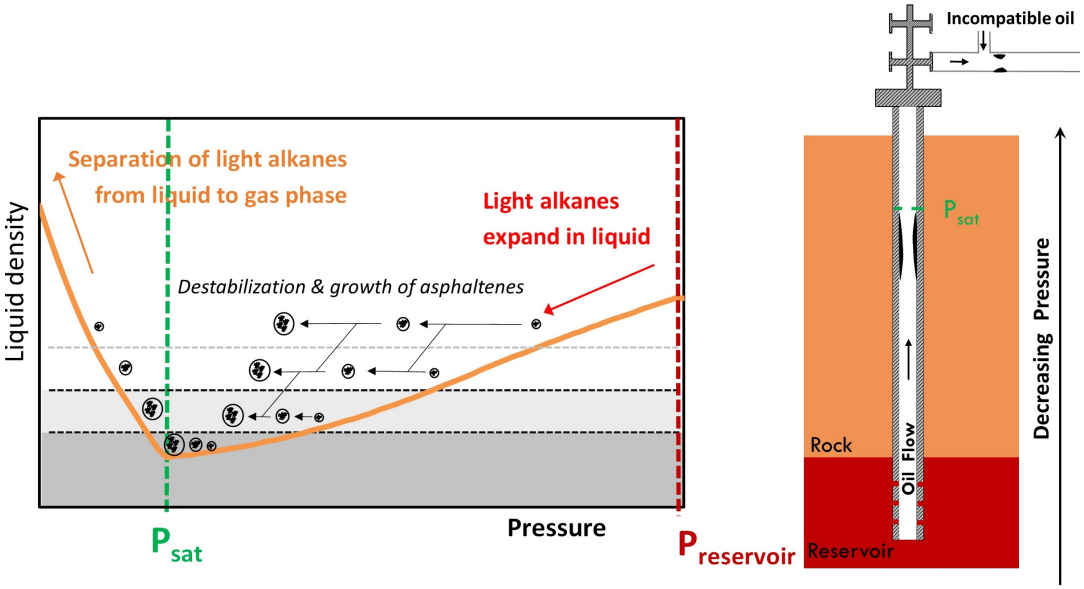

FIGURE 1.19: Typical live oil density profile as a function of the hydrostatic pressure along with the schematic of asphaltenes destabilization (illustrated by experimental microscope images) and their deposition in wells or pipelines

Consider one mole of fluid parcel that flows along the system, the steady decrease of the hydrostatic pressure causes an increase of its volume that is mainly driven by most volatile components as shown in Figure 1.20. The most sensitive constituents in the pressure range of interest (100 to 1000 bar) are ones with lighter molecular weights than propane.

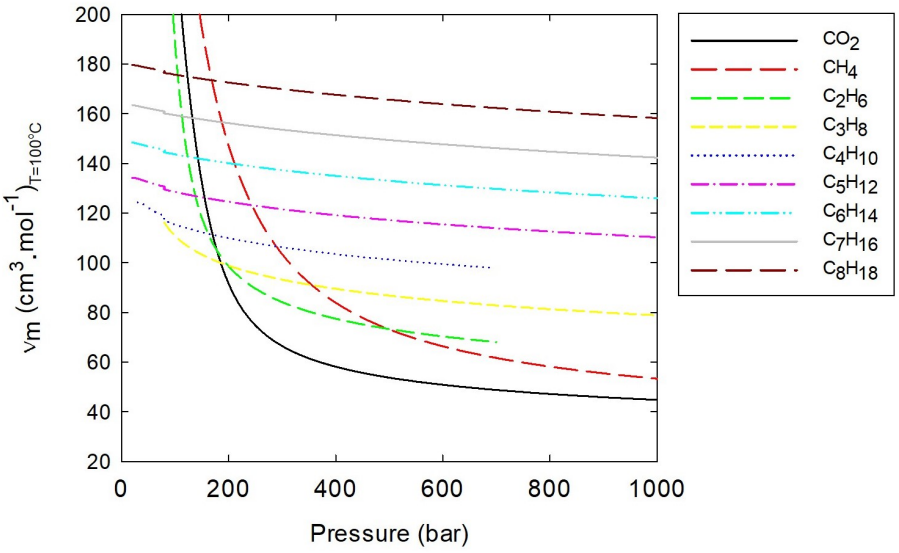

FIGURE 1.20: Pure molar volumes of the 9 lightest main components of live-oils as a function of the hydrostatic pressure in typical range of oil & gas industrial pressures at 100 °C(reprinted from NIST chemical web book)

Despite the strong economical implications of the presented process, general laboratory practices induce asphaltenes instability with addition of liquid *n*-alkanes (usually *n*-heptane or *n*-pentane) to crude oil samples at atmospheric pressure. Indeed liquid solvents are convenient for their easy use with good controls of their volumes and masses during experimentation.
Such inexpensive protocols are for example used to select the best chemicals for preventive actions. The low dosage continuous injection of dispersing agents is often chosen as a remediation strategy to the deposition of asphaltenes. Depending on the used method and conditions of tests, different mechanisms may be evaluated and can result in varying selected chemical. However relevant laboratory protocols to the field mechanisms are not yet understood, some injected chemicals are sometimes coincidentally discovered to be ineffective.

We should note that despite the lack of understanding, many qualitative risk evaluation methods related to asphaltenes stability are available and are rather based on statistical plots. The plot of average petroleum properties (such as density) as a function of characteristic properties of associated asphaltenes is the preferred format of such tools.
For example, Zhou et al.[87] and Rondon et al.[63] developed a database that correlates the density of crude oils at reservoir conditions (equilibrium) to a graduated scale of indices that classifies the most unstable asphaltenes of respective oils. The integer number in the range of 0 to 20 scale (asphaltene stability class index: ASCI) is related to the fraction of heptane in heptane-toluene mixtures where the first appearance of flocculated asphaltenes can be visually detected by adding a droplet of crude oil

$$\text{ASCI} = 100 \text{ x } \frac{\phi_{C_7,detection}}{5} \tag{1.7}$$

where $\phi_{C_7,detection}$ is the minimum volume concentration of heptane for visual detection of solid and black particles. The method is designed to provide a simple identification number of the most unstable fraction of asphaltenes. Safe and risky

zones are empirically identified with a statistical frontier. The evolution of the transported oil density along extraction conduits informs whether or not the fluid will cross risky conditions (see Figure 1.21). In the reprinted schematic of Figure 1.21 (b) P_{ini} is the initial pressure that represents reservoir conditions during oil production and P_b represents the conditions at saturation or "bubble" pressure. Conditions at saturation pressure correspond to the most risky potential where the lightest constituents are the most expanded in the liquid phase.

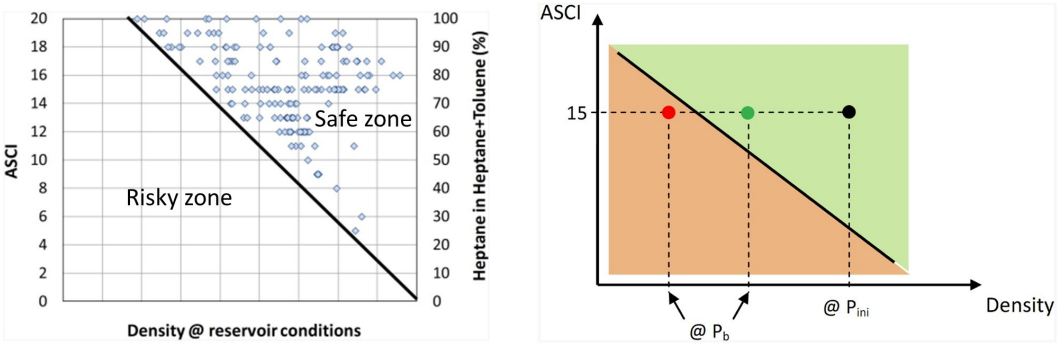

FIGURE 1.21: (a) Plot of the ASCI versus the density of crude oils at reservoir conditions database and (b) schematic of the ASCI method where the red marker predicts severe risks and the green one does not anticipate any destabilization (reprinted from Rondon et al. [63])

Such methods are usually powerful to identify potential risks with exploration samples, however they are not quantitative and show limitations when using them during field development stages.

1.4 Objectives of this work

Despite nearly a century of scientific investigation [47;39], upstream industrial practices have not changed much since disastrous cases of blocked wells have been reported [25]. The complexity of describing a general behavior under extraction conditions raise uncertainties in risk evaluations and remediation strategies related to the deposition of asphaltenes. Indeed a significant gap exists between the lastly acquired knowledge on the molecular level of asphaltenes and problems in oilfields production.
This research is taking part of an initiative to link both scales by identifying the major mechanisms by which asphaltenes destabilize, aggregate and deposit, under relevant conditions to the to upstream industrial applications. The fundamental objective is to understand effects of primary variables in liquid solutions on the asphaltenes behavior. This way inexpensive experimentation could be developed with procedures and conditions that can reasonably replicate the underlying physics taking place in oilfields.

This manuscript is organized in 5 Chapters in addition to this introductory Chapter.
Chapter 2 presents the main measurement techniques that were used in this work. It

clarifies key aspects of piezo-electrical resonators and lays solid experimental foundations based on relevant length scales to the asphaltenes destabilization, aggregation and deposition phenomena. Indeed this dissertation heavily relies on results obtained using immersed quartz crystal resonators to invetigate deposition mechanisms at the nanometer to micrometer length scales.
In Chapter 3, first principles of diffusion-limited deposition theory experimentally reveals the controlling kinetics of asphaltenes. Time-dependent destabilization is exposed to be the limiting process as opposed to the aggregation kinetics[23;48]. Indeed, bulk appearance of "unstable" asphaltenes is described as a slower process than their aggregation and a mathematical model is proposed for destabilization kinetics. The necessity to simplify the description of such complex mixtures is addressed by characterizing the unstable asphaltenes as a continuum of molecules with only two adjustable parameters. First insights of the asphaltene deposition are showed by comparing the deposition rates to the calculated destabilization rate along the deposition experiments. The addition rate of *n*-heptane is identified as a key parameter to the kinetics of destabilization
Chapter 4 revisits existing concepts of Brownian aggregation of unstable asphaltenes by incorporating findings on the kinetics of destabilization. Investigations reconcile the parameters adjustment in the coagulation modeling of asphaltenes with the extensive practice reported on colloidal solutions of polymers. A relation is proposed between the initial rate of generation of unstable asphaltenes and the appearance time of micron-sized unstable asphaltenes.
Chapter 5 is dedicated to a mechanistic investigation of asphaltenes deposition induced by a continuous change of oil-heptane solutions at various conditions. A deposition model is developed for interpreting the experimental results obtained by using a new apparatus. The model combines findings of the precedent Chapters with diffusive principles of asphaltenes deposition. A universal range of depositing aggregates size is found under the studied conditions and significantly simplifies the problem. Simplifications enable to study different effects: (i) the fluid superficial velocity over the studied surface, (ii) the presence of large unstable aggregates of asphaltenes and (iii) the rate of change of the liquid solution by varying the addition rate of *n*-heptane.
Chapter 6 investigates the mechanisms of asphaltenes destabilization, aggregation and deposition induced by the continuous and discontinuous addition of varying *n*-alkanes in crude oil. Developed concepts of precedent Chapters on oil-heptane mixtures are indirectly verified to apply to different *n*-alkanes. The validity of the so-called ASIST method of extrapolation of laboratory to field conditions is discussed.
Chapter 7 discusses the major conclusions of this dissertation and implications on the future research on this topic.
A list of references is provided at the end of each Chapter in Bibliography sections.

Bibliography

[1] Abraham, H.
1960. *Asphalts and Allied Substances: Their Occurrence, Modes of Production, Uses in the Arts, and Methods of Testing. v.* D. Van Nostrand Company, Incorporated.

[2] Alboudwarej, H., K. Akbarzadeh, J. Beck, W. Y. Svrcek, and H. W. Yarranton
2003. Regular solution model for asphaltene precipitation from bitumens and solvents. *AIChE Journal*, 49(11):2948–2956.

[3] Alboudwarej, H., J. Beck, W. Svrcek, H. Yarranton, and K. Akbarzadeh
2002. Sensitivity of asphaltene properties to separation techniques. *Energy & Fuels*, 16(2):462–469.

[4] Ancheyta, J., G. Centeno, F. Trejo, and G. Marroquin
2003. Changes in asphaltene properties during hydrotreating of heavy crudes. *Energy & fuels*, 17(5):1233–1238.

[5] Ancheyta, J., G. Centeno, F. Trejo, G. Marroquin, J. Garcia, E. Tenorio, and A. Torres
2002. Extraction and characterization of asphaltenes from different crude oils and solvents. *Energy & Fuels*, 16(5):1121–1127.

[6] Ancheyta, J., F. Trejo, and M. S. Rana
2010. *Asphaltenes: chemical transformation during hydroprocessing of heavy oils*. CRC press.

[7] Andreatta, G., N. Bostrom, and O. C. Mullins
2005. High-q ultrasonic determination of the critical nanoaggregate concentration of asphaltenes and the critical micelle concentration of standard surfactants. *Langmuir*, 21(7):2728–2736.

[8] Barré, L., S. Simon, and T. Palermo
2008. Solution properties of asphaltenes. *Langmuir*, 24(8):3709–3717.

[9] Barrera, D., D. Ortiz, and H. Yarranton
2013. Molecular weight and density distributions of asphaltenes from crude oils. *Energy & fuels*, 27(5):2474–2487.

[10] Boussingault, M.
1837. Memoire sur la composition des bitumes. In *Annales de Chimie et de Physique*, volume 64, P. 141.

[11] Buckley, J. S., G. Hirasaki, Y. Liu, S. Von Drasek, J. Wang, and B. Gill
1998. Asphaltene precipitation and solvent properties of crude oils. *Petroleum Science and Technology*, 16(3-4):251–285.

[12] Buckley, J. S., J. Wang, and J. L. Creek
2007. Solubility of the least-soluble asphaltenes. *Asphaltenes, Heavy Oils, and Petroleomics*, Pp. 401–437.

[13] Chacon-Patino, M. L., S. M. Rowland, and R. P. Rodgers
2017a. Advances in asphaltene petroleomics. part 1: asphaltenes are composed of abundant island and archipelago structural motifs. *Energy & fuels*, 31(12):13509–13518.

[14] Chacon-Patino, M. L., S. M. Rowland, and R. P. Rodgers
2017b. Advances in asphaltene petroleomics. part 2: selective separation method that reveals fractions enriched in island and archipelago structural motifs by mass spectrometry. *Energy & fuels*, 32(1):314–328.

[15] Chacon-Patino, M. L., S. M. Rowland, and R. P. Rodgers
2018. Advances in asphaltene petroleomics. part 3. dominance of island or archipelago structural motif is sample dependent. *Energy & fuels*, 32(9):9106–9120.

[16] Eyssautier, Joëlle; Frot, D. B. L.
2012. Structure and dynamic properties of colloidal asphaltene aggregates. *Langmuir*, 28.

[17] Eyssautier, J., P. Levitz, D. Espinat, J. Jestin, J. Gummel, I. Grillo, and L. Barré
2011. Insight into asphaltene nanoaggregate structure inferred by small angle neutron and x-ray scattering. *The Journal of Physical Chemistry B*, 115(21):6827–6837.

[18] Feynman, R. P., R. B. Leighton, and M. Sands
1989. The feynman lectures on physics, redwood city.

[19] Freed, D., N. Lisitza, P. Sen, and Y. Song
2009. A study of asphaltene nanoaggregation by nmr. *Energy Fuels*, 23(3):1189–1193.

[20] Freed, D. E., O. C. Mullins, and J. Y. Zuo
2010. Theoretical treatment of asphaltene gradients in the presence of gor gradients. *Energy & Fuels*, 24(7):3942–3949.

[21] Goual, L., M. Sedghi, H. Zeng, F. Mostowfi, R. McFarlane, and O. C. Mullins
2011. On the formation and properties of asphaltene nanoaggregates and clusters by dc-conductivity and centrifugation. *Fuel*, 90(7):2480–2490.

[22] Grutters, M., K. Ramanathan, D. Naafs, E. Clarke, Z. Huo, D. Abdallah, S. Zwolle, and A. Stankiewicz
2010. Integrated discipline approach to conquer asphaltene challenges in on-shore abu dhabi oil fields. In *Abu Dhabi International Petroleum Exhibition and Conference*. Society of Petroleum Engineers.

[23] Haji-Akbari, N., P. Masirisuk, M. P. Hoepfner, and H. S. Fogler
2013. A unified model for aggregation of asphaltenes. *Energy & Fuels*, 27(5):2497–2505.

[24] Hansen, C. M.
2004. 50 years with solubility parameters—past and future. *Progress in Organic Coatings*, 51(1):77–84.

[25] Haskett, C. E. and M. Tartera
1965. A practical solution to the problem of asphaltene deposits-hassi messaoud field, algeria. *Journal of petroleum technology*, 17(04):387–391.

[26] Hildebrand, J. H.
1936. Solubility of non-electrolytes.

[27] Hirschberg, A., L. DeJong, B. Schipper, and J. Meijer
1984. Influence of temperature and pressure on asphaltene flocculation. *Society of Petroleum Engineers Journal*, 24(03):283–293.

[28] Hoepfner, M. P.
2013. *Investigations into asphaltenes deposition, stability and structure*. PhD thesis, University of Michigan.

[29] Hoepfner, M. P. and H. S. Fogler
2013. Multiscale scattering investigations of asphaltene cluster breakup, nanoaggregate dissociation, and molecular ordering. *Langmuir*, 29(49):15423–15432.

[30] Hoepfner, M. P., C. Vilas Boas Favero, N. Haji-Akbari, and H. S. Fogler
2013. The fractal aggregation of asphaltenes. *Langmuir*, 29(28):8799–8808.

[31] Hsu, C. S., V. V. Lobodin, R. P. Rodgers, A. M. McKenna, and A. G. Marshall
2011. Compositional boundaries for fossil hydrocarbons. *Energy & Fuels*, 25(5):2174–2178.

[32] Huggins, M. L.
1964. A revised theory of high polymer solutions. *Journal of the American Chemical Society*, 86(17):3535–3540.

[33] Indo, K., J. Ratulowski, B. Dindoruk, J. Gao, J. Zuo, and O. C. Mullins
2009. Asphaltene nanoaggregates measured in a live crude oil by centrifugation. *Energy & Fuels*, 23(9):4460–4469.

[34] Israelachvili, J. N.
2015. *Intermolecular and surface forces*. Academic press.

[35] Janardhan, A. S. and G. A. Mansoori
1993. Fractal nature of asphaltene aggregation. *Journal of Petroleum Science and Engineering*, 9(1):17–27.

[36] Javanbakht, G., M. Sedghi, W. R. Welch, L. Goual, and M. P. Hoepfner
2018. Molecular polydispersity improves prediction of asphaltene aggregation. *Journal of Molecular Liquids*, 256:382–394.

[37] Kaminski, T. J., H. S. Fogler, N. Wolf, P. Wattana, and A. Mairal
2000. Classification of asphaltenes via fractionation and the effect of heteroatom content on dissolution kinetics. *Energy & Fuels*, 14(1):25–30.

[38] Katz, D. L. and K. E. Beu
1945. Nature of asphaltic substances. *Industrial & Engineering Chemistry*, 37(2):195–200.

[39] Katz, M.
1934. Alberta bitumen: I. the composition of blown alberta bitumen. *Canadian Journal of Research*, 10(4):435–451.

[40] Kilpatrick, P. K.
2012. Water-in-crude oil emulsion stabilization: Review and unanswered questions. *Energy & Fuels*, 26(7):4017–4026.

[41] Kraiwattanawong, K., H. S. Fogler, S. G. Gharfeh, P. Singh, W. H. Thomason, and S. Chavadej
2007. Thermodynamic solubility models to predict asphaltene instability in live crude oils. *Energy & fuels*, 21(3):1248–1255.

[42] Krigbaum, W. and D. Geymer
1959. Thermodynamics of polymer solutions. the polystyrene-cyclohexane system near the flory theta temperature. *Journal of the American Chemical Society*, 81(8):1859–1868.

[43] Leontaritis, K. and G. Mansoori
1987. Asphaltene flocculation during oil production and processing: A thermodynamic colloidal model. In *SPE International Symposium on Oilfield Chemistry*, Pp. 4–6. Society of Petroleum Engineers Richardson, TX, USA.

[44] Leontaritis, K. J. and G. A. Mansoori
1989. Fast crude-oil heavy-component characterization using combination of astm, hplc, and gpc methods. *Journal of petroleum science and Engineering*, 2(1):1–12.

[45] Lin, H.-M. and R. A. Nash
1993. An experimental method for determining the hildebrand solubility parameter of organic nonelectrolytes. *Journal of pharmaceutical sciences*, 82(10):1018–1026.

[46] Lindvig, T., M. L. Michelsen, and G. M. Kontogeorgis
2002. A flory–huggins model based on the hansen solubility parameters. *Fluid Phase Equilibria*, 203(1-2):247–260.

[47] Mack, C.
1936. J. physic. chem. 36, 2901 (1932). *Siehe auch J. Ph. Pfeiffer und PM van Doormaal, Kolloid*, (76):95.

[48] Maqbool, T., S. Raha, M. P. , and H. S. Fogler
2011. Modeling the aggregation of asphaltene nanoaggregates in crude oil- precipitant systems. *Energy & Fuels*, 25(4):1585–1596.

[49] Mason, T. and M. Lin
2003. Asphaltene nanoparticle aggregation in mixtures of incompatible crude oils. *Physical Review E*, 67(5):050401.

[50] McKenna, A. M., A. G. Marshall, and R. P. Rodgers
2013. Heavy petroleum composition. 4. asphaltene compositional space. *Energy & Fuels*, 27(3):1257–1267.

[51] Mitchell, D. L. and J. G. Speight
1973. The solubility of asphaltenes in hydrocarbon solvents. *Fuel*, 52(2):149–152.

[52] Muller, E., J. Law, T. Headen, M. Jimenez Serratos, E. Boek, and J. Murgich
2019. A catalogue of plausible molecular models for the molecular dynamics of asphaltenes and resins obtained from quantitative molecular representation.

[53] Mullins, O. C.
2010. The modified yen model. *Energy & Fuels*, 24(4):2179–2207.

[54] Mullins, O. C.
2011. The asphaltenes. *Annual review of analytical chemistry*, 4:393–418.

[55] Mullins, O. C., H. Sabbah, J. Eyssautier, A. E. Pomerantz, L. Barré, A. B. Andrews, Y. Ruiz-Morales, F. Mostowfi, R. McFarlane, and L. Goual
2012. Advances in asphaltene science and the yen–mullins model. *Energy & Fuels*, 26(7):3986–4003.

[56] Mullins, O. C. and E. Y. Sheu
2013. *Structures and dynamics of asphaltenes*. Springer Science & Business Media.

[57] Mullins, O. C., E. Y. Sheu, A. Hammami, and A. G. Marshall
2007. *Asphaltenes, heavy oils, and petroleomics*. Springer Science & Business Media.

[58] of Pharmacy, P. C. and Science
1838. *American Journal of Pharmacy*, number v. 9-10. Philadelphia College of Pharmacy.

[59] Pal, R.
2017. Modeling and scaling of the viscosity of suspensions of asphaltene nanoaggregates. *Energies*, 10(6):767.

[60] Passade-Boupat, N., H. Zhou, and M. Rondon-Gonzalez
2010. Asphaltene Precipitation From Crude Oils : How To Predict It And To Anticipate Treatment? *SPE Middle East Oil and Gas Show and Conference*.

[61] Powers, D., H. Sadeghi, H. Yarranton, and F. Van Den Berg
2016. Regular solution based approach to modeling asphaltene precipitation from native and reacted oils: Part 1, molecular weight, density, and solubility parameter distributions of asphaltenes. *Fuel*, 178:218–233.

[62] Rogel, E., C. Ovalles, M. Moir, J. Vien, and H. Morazan
2015. Solubility characterization of asphaltene deposits. In *SPE International Symposium on Oilfield Chemistry*. Society of Petroleum Engineers.

[63] Rondon, M., M. Kane, C. Quintero, N. Passade-Boupat, and H. Zhou
2014. Developing a field with asphaltenes risks: From diagnosis to cure. In *Abu Dhabi International Petroleum Exhibition and Conference*. Society of Petroleum Engineers.

[64] Schuler, B., S. Fatayer, G. Meyer, E. Rogel, M. Moir, Y. Zhang, M. R. Harper, A. E. Pomerantz, K. D. Bake, and M. Witt
2017. Heavy oil based mixtures of different origins and treatments studied by atomic force microscopy. *Energy & fuels*, 31(7):6856–6861.

[65] Schuler, B., G. Meyer, D. Peña, O. C. Mullins, and L. Gross
2015. Unraveling the molecular structures of asphaltenes by atomic force microscopy. *Journal of the American Chemical Society*, 137(31):9870–9876.

[66] Sheu, E. Y.
1998. Self-association of asphaltenes. In *Structures and dynamics of asphaltenes*, Pp. 115–144. Springer.

[67] Speight, J.
2015. *Asphalt Materials Science and Technology*. Elsevier Science.

[68] Svalova, A., N. G. Parker, M. J. Povey, and G. D. Abbott
2017. Determination of asphaltene critical nanoaggregate concentration region using ultrasound velocity measurements. *Scientific reports*, 7(1):16125.

[69] Tharanivasan, A. K., H. W. Yarranton, and S. D. Taylor
2010. Application of a regular solution-based model to asphaltene precipitation from live oils. *Energy & Fuels*, 25(2):528–538.

[70] Vargas, F. M. and W. G. Chapman
2010. Application of the one-third rule in hydrocarbon and crude oil systems. *Fluid Phase Equilibria*, 290(1-2):103–108.

[71] Vargas, F. M., D. L. Gonzalez, J. L. Creek, J. Wang, J. Buckley, G. J. Hirasaki, and W. G. Chapman
2009. Development of a general method for modeling asphaltene stability. *Energy & fuels*, 23(3):1147–1154.

[72] Vargas, F. M. and M. Tavakkoli
2018. *Asphaltene deposition: Fundamentals, prediction, prevention, and remediation*. CRC Press.

[73] Wang, J. and J. S. Buckley
2001. A two-component solubility model of the onset of asphaltene flocculation in crude oils. *Energy & Fuels*, 15(5):1004–1012.

[74] Wang, J. and J. S. Buckley
2003. Asphaltene stability in crude oil and aromatic solvents the influence of oil composition. *Energy & fuels*, 17(6):1445–1451.

[75] Wang, J., J. L. Creek, and J. S. Buckley
2006. Screening for potential asphaltene problems. In *SPE Annual Technical Conference and Exhibition*. Society of Petroleum Engineers.

[76] Wang, S., J. Liu, L. Zhang, J. Masliyah, and Z. Xu
2009. Interaction forces between asphaltene surfaces in organic solvents. *Langmuir*, 26(1):183–190.

[77] Wang, S., J. Liu, L. Zhang, Z. Xu, and J. Masliyah
2008. Colloidal interactions between asphaltene surfaces in toluene. *Energy & Fuels*, 23(2):862–869.

[78] Wiehe, I. A.
1996. Two-dimensional solubility parameter mapping of heavy oils. *Fuel Science and Technology International*, 14(1-2):289–312.

[79] Wiehe, I. A. and R. J. Kennedy
2000. Application of the oil compatibility model to refinery streams. *Energy & fuels*, 14(1):60–63.

[80] Wiehe, I. A., H. W. Yarranton, K. Akbarzadeh, P. M. Rahimi, and A. Teclemariam
2005. The paradox of asphaltene precipitation with normal paraffins. *Energy & Fuels*, 19(4):1261–1267.

[81] Wolf, B. A.
2010. Making floryr–huggins practical: Thermodynamics of polymer-containing mixtures. In *Polymer Thermodynamics*, Pp. 1–66. Springer.

[82] Yarranton, H., D. Powers, J. Okafor, and F. van den Berg
2018. Regular solution based approach to modeling asphaltene precipitation from native and reacted oils: Part 2, molecular weight, density, and solubility parameter of saturates, aromatics, and resins. *Fuel*, 215:766–777.

[83] Yarranton, H. W., H. Alboudwarej, and R. Jakher
2000. Investigation of asphaltene association with vapor pressure osmometry and interfacial tension measurements. *Industrial & engineering chemistry research*, 39(8):2916–2924.

[84] Yarranton, H. W. and J. H. Masliyah
1996. Molar mass distribution and solubility modeling of asphaltenes. *AIChE Journal*, 42(12):3533–3543.

[85] Yarranton, H. W., D. Ortiz, D. Barrera, E. Baydak, L. Barré, D. Frot, J. Eyssautier, H. Zeng, Z. Xu, and G. Dechaine
2013. On the size distribution of self-associated asphaltenes. *Energy & Fuels*, 27(9):5083–5106.

[86] Yuan, B. and D. A. Wood
2018. *Formation damage during improved oil recovery: Fundamentals and applications*. Gulf Professional Publishing.

[87] Zhou, H., N. Passade-Boupat, and M. Rondon Gonzalez
2012. Workflow for asphaltene precipitation assessment and mitigation strategies. In *Abu Dhabi International Petroleum Conference and Exhibition*. Society of Petroleum Engineers.

Chapter 2

Introduction to quartz crystal resonators (QCRs) and asphaltene deposition measurement

2.1 Introduction

After spending millions of years in geological porous media, destabilizing a fraction of asphaltenes will modify their molecular equilibrium such that dynamic exchange of molecules between nanoaggregates will be less frequent, distances between asphaltene molecules within fractal structures will shrink[17] and associated molecules will eventually reduce their contact with their surroundings[21] by further aggregating or by depositing. After forming a "solid-like" phase, a new equilibrium will be reached. Note that massive deposits found in wells are due to the continuous accumulation of asphaltenes fractions (mass divided by the cumulative volume of oil produced during a period of time) as opposed to sudden events with limited volumes of oil. The process that drives asphaltenes to destabilize and to deposit must be studied at the appropriate length scales within suitable scales of time. In laboratory studies, limited quantities of samples can be used and the subsequent scale of mass has to be adjusted to the problem. The use of macroscopic tools within short periods of experimental time at extreme supersaturations of asphaltenes might neither provide relevant information of the transition state nor information of the deposition process.

Piezoelectric techniques is one of the most appropriate techniques to study solid surface interactions of nano-scale species in a fluid environment[2] either at ambient conditions or under higher pressure than the atmospheric one. As the deposition of asphaltenes can be caused by liquid anti-solvent addition or by light-ends expansion upon depressurization, a portion of this Chapter will be devoted to describing the sensing techniques applied to pressurized conditions. The use of the exact same instrument was decided to liberate ourselves from potential experimental and interpretation discrepancies when comparing destabilization induced by addition of liquid alkanes at ambient pressure and volume increase of volatile dissolved components at elevated pressure conditions. The detection is suitable to the mass scale of interest and is monitored in live while the titrations or depressurizations are carried out. With this tool, the intention is to study mass transport to the surface with a much finer sensitivity than more commonly applied techniques (weight measurement of deposits[30] or back-calculation of thickness from measured pressure gradients[32;16]). Indeed, such sensitivity is advisable to study the asphaltene deposition with regards to the major sub-micrometer particles contributions that will be discussed in the following Chapters.

The rest of this dissertation will densely rely on a piezoelectric resonator technique to explore the destabilization and the deposition of asphaltenes. The purpose of this Chapter is to provide a brief and general overview of the measuring technique (immersed acoustic sensors) before carrying on. Researchers interested in a deeper introductory reading on the subject are directed to *The Quartz Crystal Microbalance in Soft Matter Research* by Johannsmann [22] and readers more familiar with the basics of piezoelectric materials are suggested to revert to *Piezoelectric Sensors and Actuators* by Rupitsch [27].

2.2 Methods and definitions

In this work, unless stated otherwise, experimental investigations refer to a single West African originated crude oil with characteristic properties summarized in Table 2.1. In order to avoid interactions between asphaltenes and wax crystals, the experimental work was performed on isotherms at 60 °C.

TABLE 2.1: Used stabilized (or "dead") crude oil properties at 60°C

Parameters	Units	Values
Density	$kg.m^{-3}$	872.3
Dynamic viscosity	$mPa.s$	14.5
n_D	-	1.4999
Average M_w	$g.mol^{-1}$	232
M_w of C20+ fraction	$g.mol^{-1}$	500
Saturates	wt %	35.7
Aromatics	wt %	42.8
Resins	wt %	11.1
n-C_5 Asphaltenes	wt %	10.3
ASCI classification	-	11
Wax appearance temperature	°C	41
Bottom hole static pressure	bar	492
Bottomhole static temperature	°C	79.2
Saturation pressure of live oil	bar	174

where ASCI stands for *Asphaltenes Stability Class Index*, M_w is the molar weight and n_D is the refractive index.

2.3 Quartz Crystal Microbalance background

Everyone knows crystal oscillators for their excellent properties to keep the track of time in our consumer devices such as wristwatches. The most common type of piezoelectric material is the quartz crystal. The principle of the laboratory measurement is based on distorting the crystal with electrical voltage applied on the crystal through electrodes. When the electric field is temporarily removed, the quartz oscillates in a precise frequency and generates an electric signal while equilibrating to its original shape. Laboratory measurements usually involve a quartz crystal in the form of a disc contacted to the fluid of interest, usually termed as quartz crystal microbalance with dissipation monitoring (QCM-D). The resolution of QCM-D can be as low as 1 Hz due to the high ratio of frequency over the bandwidth. The

narrow resonance peaks make the device accurate for sensing changes that are imperceptible by means of macroscopic mass scales. The theoretical sensitivity of a quartz crystal will depend on the fundamental resonant frequency of the crystal, usually perceptive of adsorbed monolayer of molecules to its surface[19]. A 3 MHz crystal, genuinely used in this work, will typically have responsive signals to tens of nanograms. When crystals are grown, cut and mounted properly, it can be made to mechanically distort in a thickness shear mode (see Figure 2.1).

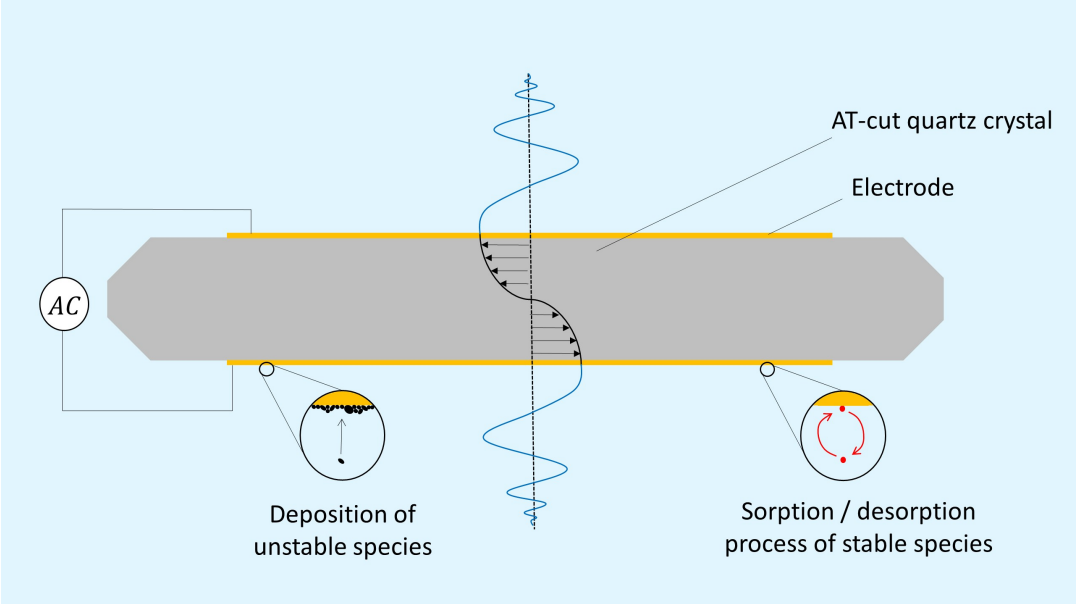

FIGURE 2.1: Schematic of a thickness shear mode resonator immersed in a liquid

In this mode, the reflective acoustic wave at the surface of the crystal depends on the impedance of the adjacent medium. The family of QCM sensors exploiting the surface acoustic wave are also termed "resonators". Then resonators have the particularity of not having the sole microgravimetric functionality. Indeed, viscoelastic properties of the surroundings are playing an essential role by damping the shear wave[2]. In fact, the finite decay of the transverse waves, as opposed to longitudinal ones, is an advantageous property that avoids reflection or transmission of wave from the surrounding interfaces. For the exposed reasons, in the remainder of this dissertation, we will refer to our measuring instrument as a quartz crystal resonator or QCR instead.

The electromechanical coupling is ensured by means of electrodes onto both sides of the sensing disc, in such way that the shear deformation is induced by an alternating current (AC) voltage. Gold electrodes are advocated to minimize the aging of the sensors thanks their optimal adhesion to the crystal and to the absence of formation of a metal oxides layer. An in-between layer of Titanium is used to improve the binding of the electrode to the crystal. Also part of the robustness of the method, surface polishing of sensors reduces their surface imperfections and makes them compatible with theoretical expressions for resonating behavior and shock-resistant. However minor fluctuations of the resonating frequencies f can still be caused by the thermal noise, crystal lattice imperfections, edge effects or adsorption/desorption of molecules on the surface of the crystal when exposed to a dynamic fluid environment.

Resonators can be excited at a number of odd harmonic overtones n that keep the

condition of inducing opposite sign of electric charges on both sides of the crystal. The number of harmonics that have a good agreement with the theory are limited due to side effects. The fundamental frequency (overtone n = 1) usually does not enable a good energy trapping effect (confinement of the acoustic wave in the center of sensor by an increased thickness compared to the peripheral thickness to avoid edge effects). Contrarily, the resonance of too large overtones usually results in an interference with anharmonic side band signals (see Figure 2.2 (b)).
An impedance analysis consists of monitoring the electric conductance G as a function of the driving frequency as illustrated by Figure 2.2. The profiles can be obtained by a network analyzer and the peaks of conductance correspond to the frequency of resonance while the bandwidth of the curve indicates an estimation of the dissipation Γ factor which quantifies the damping of the medium. As the viscous dissipation and the loaded mass both affect the responsive resonance frequency of the sensor, the analysis of the full peak signals becomes an essential factor to evaluate the predominant influence. Liquids have varying shear acoustic impedance, which more or less affects the propagation of the oscillation resulting in a shift in resonance frequency:

$$\Delta f = f - f_{vacuum} \tag{2.1}$$

and a change of the bandwidth:

$$\Delta\Gamma = \Gamma - \Gamma_{vacuum} \tag{2.2}$$

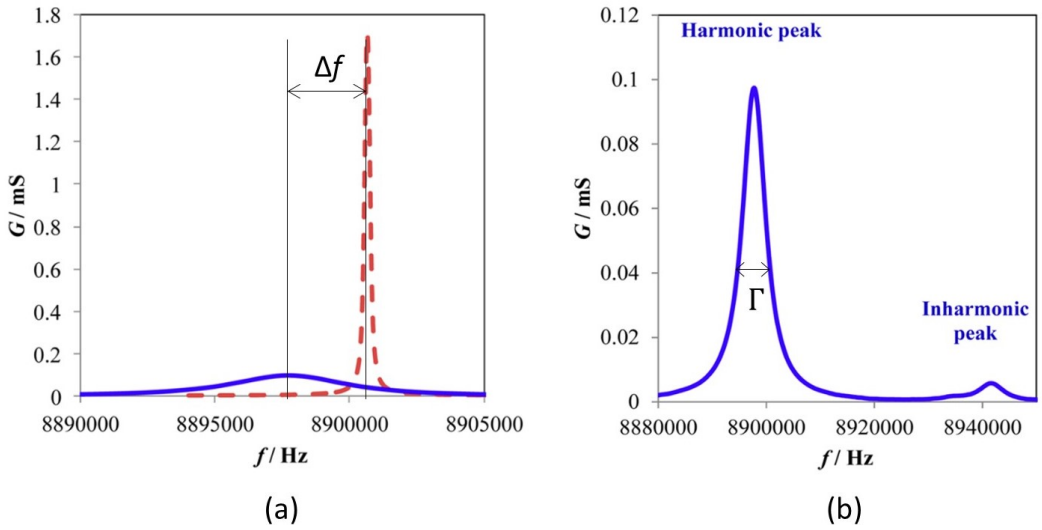

FIGURE 2.2: (a)Impedance analysis of the overtone n=3 for a 3 MHz QCR in vacuum (dashed line) and immersed in a crude oil (solid line) (b) Absence of interference showed for the overtone n=3 of a 3MHz QCR immersed in crude oil

King[24] used a QCM device for the first time, in 1964, to detect the sorption of components in the gas phase. Since the mid-1980s, oscillating sensors have then been thoroughly operated in liquid solutions to investigate interactions between flowing molecules in a dense phase, such as proteins, and a functionalized stationary surface (like specific bio-sites). Larger entities, like viruses or polymers present in a flowing solvent are also studied with usually contacting only one face of the crystal disc[10]. Goual et al.[12] used a QCM device to study the adsoprtion behavior of asphaltenes for the first time.

The interpretation of QCRs signal, when immersed in a dense phase, can be quite complicated when accounting for all the phenomena. However, frequency shifts induced by thin film of material rigidly coupled to the crystal ($\Delta f_{n,load}$) can be treated as an extension of thickness of the quartz and are described by the Sauerbrey Equation[28]:

$$\Delta f_{n,load} \sim -2nC_m\Delta m_{deposit} \tag{2.3}$$

where C_m is the Sauerbrey constant defined by Equation 5.3, $\Delta m_{deposit}$ is the cumulative mass of deposit per unit area of the sensor surface and n is the overtone investigated.

$$C_m = \frac{2f_0^2}{\sqrt{\rho_q\mu_q}} \tag{2.4}$$

where f_0 is the fundamental resonance frequency of the quartz crystal, ρ_q and μ_q are the density and the shear modulus of the quartz material.

2.4 Experimental methods used for this research

Holder mounted 3 MHz AT-cut quartz crystal resonators with diameters of 1.36 cm are used thorough the entire results of this dissertation. Each sensor was bought with polished finish surfaces and 7 mm diameter electrodes on both sides made of Gold-Titanium (respectively 100 and 1 nm thick). The effects of surfac roughness and liquid-trapping within asperities are accordingly neglected. The acoustic wave scans are generated at successive odd harmonics of the fundamental frequency of the crystal (1, 3, 5 and 7) by means of a network analyzer (Agilent E5071C) connected by coaxial cables to a monitor that has a LabVIEW internally automated program. Note that volumetric extensions of alkanes are conducted concurrently to the measurements, the full automated scanning is made within a relatively short time (< 60 s) by the network analyzer, which lets us average the composition of the solutions with errors lesser than $\pm$0.3 vol%. Resonance frequency and dissipation shifts (Δf & $\Delta\Gamma$) are both calculated by subtracting the monitored signal to a reference signal; the reference is calibrated prior to each experiment in the air for consistency and to account for the potential aging of the sensors. The record of quartz frequency and dissipation signals is started after the first immersion in the liquid, as shown in Figure 2.3 the signal drifts for a few minutes during the equilibration of the liquid at the temperature of work and then reaches a stable plateau comprised within a noise. As expected, the fluctuations are more or less important depending on the nature of the liquid. Variations of $\pm$ 0.5 Hz in pure solvents might be solely caused by viscoelastic and liquid trapping effects while the complex composition and the larger viscosity of crude oils imply larger fluctuations ($\pm$ 25 Hz) probably due to additional factors like the viscoelasticity, adsorption/desorption process of species, slippage of the contact liquid film and others.

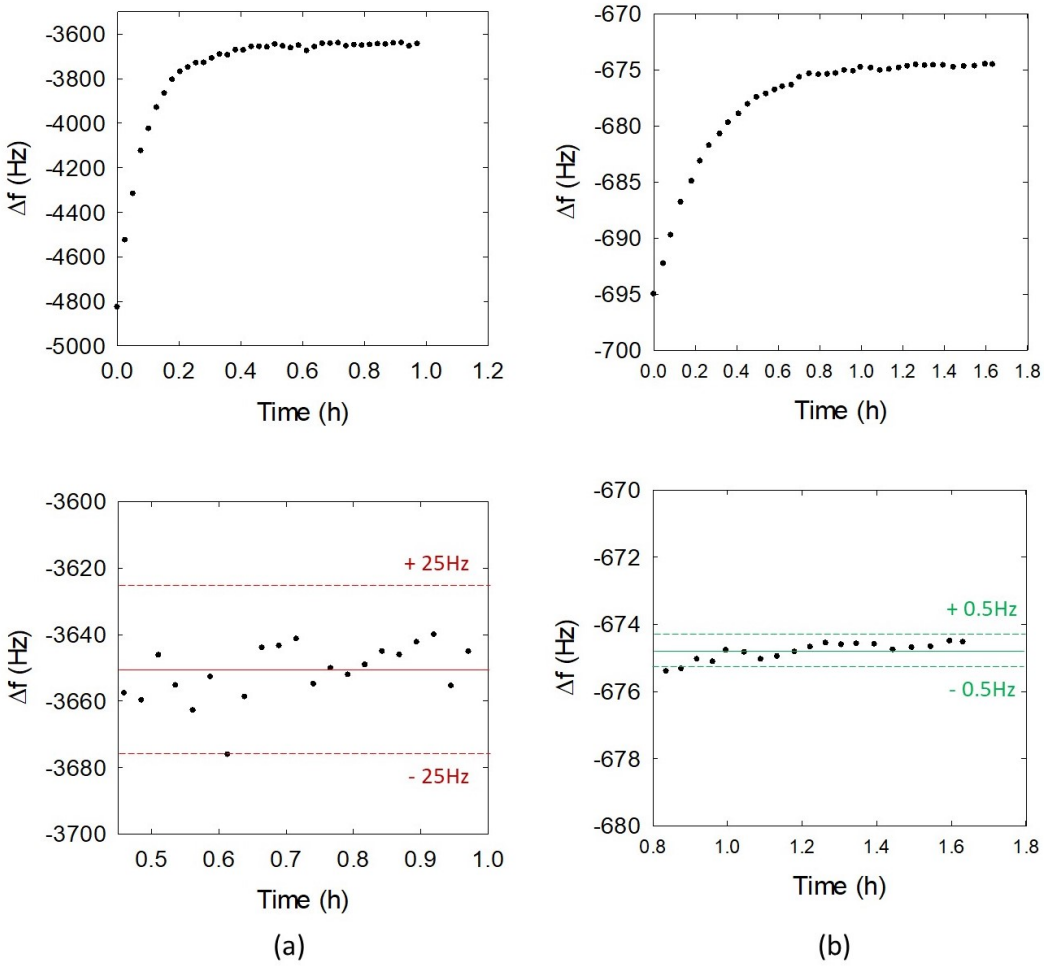

FIGURE 2.3: Frequency shift of the 3^{rd} overtone over time after immersion of the QCR in (a) crude oil (b) heptane.

Assuming a rigid deposit on the surface of the sensor, the dissipation can be considered to be exclusively affected by the density ρ_{liq} and the viscosity μ_{liq} of the contacted liquid. With such assumption, Cassiède et al. [5 6] and Daridon et al. [9] established that the frequency of resonance is sensitive to the pressure, to the loaded mass on its surface (deposit of unstable asphaltenes) and to the contact liquid transport properties within a certain penetration depth (typically hundreds of nanometers in liquids) at each overtone of the nominal frequency.
They demonstrated a good interpretation of their model for the response in resonance frequency and dissipation of a quartz crystal in contact with the same solvent medium on both faces. The frequency behavior is then explained[7] by a combination of Sauerbrey[28] and Kanazawa[23] equations resulting in Equations 2.5 and 2.6, respectively the shift of dissipation and the shift of resonant frequency signals:

$$\Delta\Gamma_{n,load} = \sqrt{n}\frac{C_m}{\pi f_0}\sqrt{\rho_{liq}\mu_{liq}}(1 + R_{interface}) \tag{2.5}$$

where $R_{interface}$ is an empirical term that corrects for the viscous friction of the liquid on rough surfaces of the sensor.

$$\Delta f_{n,load} = \underbrace{-2nC_m\Delta m_{deposit}}_{\text{surface mass load}} - \underbrace{\sqrt{n}\frac{C_m}{\sqrt{\pi f_0}}\sqrt{\rho_{liq}\mu_{liq}}}_{\text{bulk properties}} \tag{2.6}$$

During the volumetric increase of an alkane in crude oil, two competing effects on the frequency shift were identified[9]:

(1) the surface mass load

(2) the change of bulk properties of the surrounding media.

As both phenomena occur simultaneously during our experiments, both effects are complicated to decouple on a single harmonic overtone. In the case of a rigid layer of deposit, the damping effect of the surrounding fluid, quantified by dissipation shifts $\Delta\Gamma$ divided by $\sqrt{n}$, is theoretically independent of the overtone number. The shear wave promoted by the oscillator decays exponentially in the contacting media and the penetration length is given by:

$$\eta = \sqrt{\frac{\mu_{liq}}{n\pi f_0 \rho_{liq}}} \tag{2.7}$$

The order of values of this characteristic length is provided in Table 2.2 for a 3MHz resonator submerged in a typical petroleum liquid.

overtone (n)	penetration depth (η)
-	nm
1	364
3	210
5	163
7	137

TABLE 2.2: QCR sensitivity in a newtonian liquid with similar properties to mixtures of crude oil and alkanes μ_{liq}= 1 mPa.s^{-1} and ρ_{liq}= 800 kg.m^{-3}

In the presence of a rigid deposited layer on the surface of the oscillator, the wave is supposed to propagate without attenuation through the deposit (assumed integrally part of the crystal itself) and starts to fall off after entering in the fluid. The propagation of the wave becomes affected in presence of any bulk heterogeneity (e.g. interfaces, particles) with similar characteristic sizes to the length scale of the penetrated media, it will increase the damping of the response signal. However, in the case of a complex viscoelastic deposited material containing many in-situ interfaces, the decrease of the wave's amplitude will happen within the mechanically absorbing material. In such case, the damping of a shorter penetrating wave is expected to be more remarkable than the attenuation of longer invading waves. Indeed, this behavior might arise in our studies from the amorphous organization of unstable asphaltenes with trapping liquid in the interstices of the fractal solid structures[17]. As illustrated in Figure 2.4, the dependence of the dissipation signal on the overtone number in presence of unstable deposited asphaltenes typically follows the latter configuration.

Figure 2.4 shows how dissipation responses of the QCR differ when immersed in

a solution (a) of good asphaltene solvents compared to immersion in a mixture of crude oil and a flocculating agent. However the unfavorable conditions to asphaltenes stability exhibit a strong dependence of bandwidths of the resonance peaks per harmonic overtone number (Figure 2.4(b)).

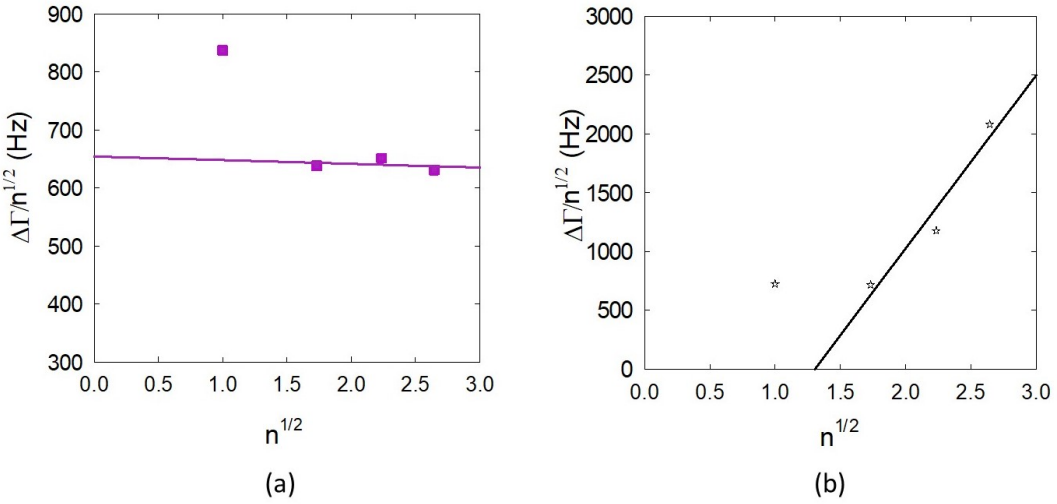

FIGURE 2.4: QCR resonance bandwidth shifts $\frac{\Delta\Gamma}{\sqrt{n}}$ as a function of the overtone $\sqrt{n}$ when immersed in mixtures of crude oil and (a) toluene or (b) heptane.

Consequently to the dependence of the response signal on the deposit properties, the validity of the simple model (Equation 2.6) to track the mass of asphaltenes deposit on the surface is questionable. Accounting for the damping effects, many authors[26;1;18;29] applied the QCM-D technique to observe the successive formation of layers (up to $\sim$ 400 nm thick) on solid surfaces in liquid media. Their results showed that despite the high hydration of sticking species, the rigid film approximation still holds as a good estimation of the deposited quantity. This literature review reveals that Sauerbrey's relation may underestimate the loaded mass with errors below 25% when compared to more complicated models[11] that combine viscoelastic and mass load repercussions. Although viscoelastic effects can be modeled for the interpretation of deposition, the frequency shifts primarily reflect the mass changes at the surface of the sensor.

For the sake of simplicity, in this research the estimation of the accumulated mass of deposited asphaltenes will be quantified with Equation 2.6. Effects related to compressional waves due to energy trapping, film slipping, viscoelasticity or to trapped material in asperities are all purposely neglected. However, we will keep in mind, for future perspectives, that accounting for the sensitivity to such effects may enable to study the morphology of the deposit.

With such assumptions, Equation 2.8 shows that the measurement of the conductance spectra along a stretched range of overtones (3 to 7 in this work) allows us to isolate the effect of mass load on surfaces of the sensor by dividing the measured shift in frequency by the square root of the relevant overtone.

$$\Delta f_{n,load}/\sqrt{n} \propto \Delta m_{deposit} \tag{2.8}$$

Moreover Cassiède et al.[6] reported that this method was adequate to eliminate effects of finite crystal (on the fundamental overtone) and interference with inharmonic modes. Treatment of the recorded raw data were performed manually through Microsoft Excel and coherency was guaranteed by analyzing data of each overtone recorded as shown by Figure 2.5.
In this work, sensors are immersed in an oil which contains asphaltenes in a "stable" state and the volume addition of a constituent is carried. During the first part of a titration experiment (Figure 2.5(a)) the shift in frequency response is first dominated by the modified viscosity and density of the fluid in the vicinity of the sensor. When the volumetric addition of precipitants is carried further (Figure 2.5(b)), a drastic (but continuously monitored) change in slope indicates accumulation of asphaltenes deposit on the surface of the sensor as opposed to a monolayer adsorption. This effect becomes predominant compared to the change of transport properties of the surrounding bulk (also termed dilution effects). Qualitatively, at fixed overtone an increase of the theoretical mass deposited per unit of area $\Delta m_{deposit}$ decreases the absolute value of the shift in frequency while the reduction of $\sqrt{\rho_{liq}\mu_{liq}}$ due to dilution by a lighter and less viscous n-alkane induces an increase of the absolute value $|\Delta f|$[23;28]. The Figure 2.5(a) provides an example of the very limited progression of the slopes dominated by a dilution effects while Figure 2.5(b) shows an enormous change in slope linked to the ongoing deposition when the addition of flocculating agents is carried further.

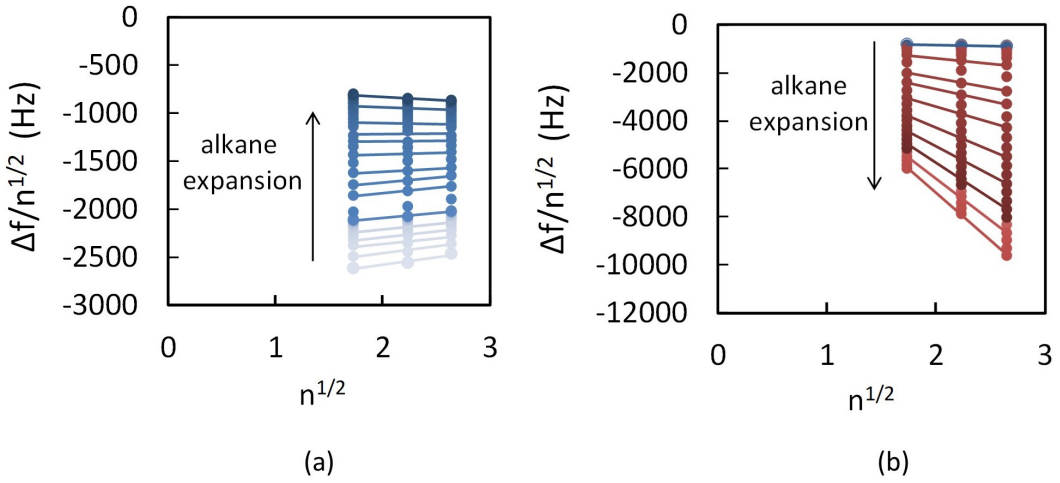

FIGURE 2.5: Evolution of the slope $\Delta f_{n,load}/\sqrt{n}$ vs $\sqrt{n}$ during titration of C_7 dominated by (a)dilution effects and (b) continuous deposition effects

The smooth response of the signals during the alkane addition advises of the continuous process of asphaltene destabilization and deposition. Indeed with this observation, it seems unreasonable arbitrary to decide of a single condition that separates stability from instability of asphaltenes. However, the possibility of conditions of instantaneous flocculation (according to the scale of time of interest: minutes) will be studied in the remainder of this dissertation.

2.4.1 Quartz crystal resonator immersed in a stirred tank reactor at atmospheric pressure

The used experimental set-up permits the continuous addition of solvents in a fixed volume of crude oil. In this experiment, the titration is carried out while recording the signal of an immersed sensor at atmospheric pressure. The apparatus consists of a custom-made vessel that is comparable to a continuous stirred tank reactor (CSTR) with the difference of not having an outlet, the total volume of the studied fluid becomes variable during the experiment. The following illustration provides a schematic view of the set-up.

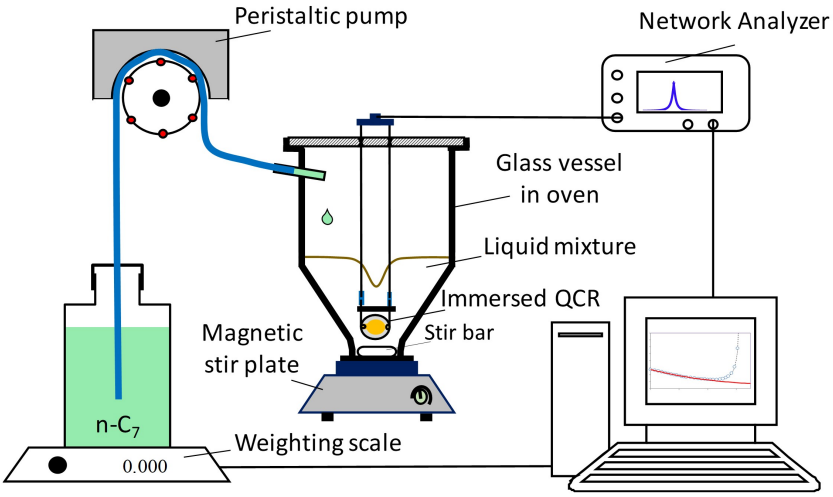

FIGURE 2.6: Schematic of the atmospheric pressure immersed QCR experimental apparatus

The rate of addition of the solvent is chosen such that it enabled a good mixing and a sufficient number of signal recording within acceptable change of composition. The agitation is provided by a rotating magnetic stir bar and the sealed glass vessel has a lower-conical and upper-cylindrical geometry. Such geometry was designed to reduce the consumption of oil samples and solvents. A constant volume of crude oil is initially introduced in the reactor and a pre-calibrated resonator is immersed in the oil in a centered position 1 cm above the top of the stir bar. The temperature is controlled by an oven ($\pm$ 0.5 °C) and continuously verified by an inserted thermo-couple probe. The experimental time was set to zero and the chronometer is started when the addition of solvent started. The promotion of solvents is achieved with a peristaltic pump into the vessel at a specified flow rate while the stirring is kept constant at minimum revolution speed enabling the visual presence of a vortex (subjective of relatively short mixing times). Working on a mass record basis augments the accuracy, the cumulative injected mass are automatically saved over time by measuring the weight of the solvent reservoir. However from a theoretical point of view, it is preferable to work with volume fractions instead of mass fractions. For that purpose, the volumetric concentrations are then calculated by converting masses into volumes using measured densities of the fluids. Figure 2.7 shows an example of raw signal data acquired for multiple overtones during additions of toluene or heptane.

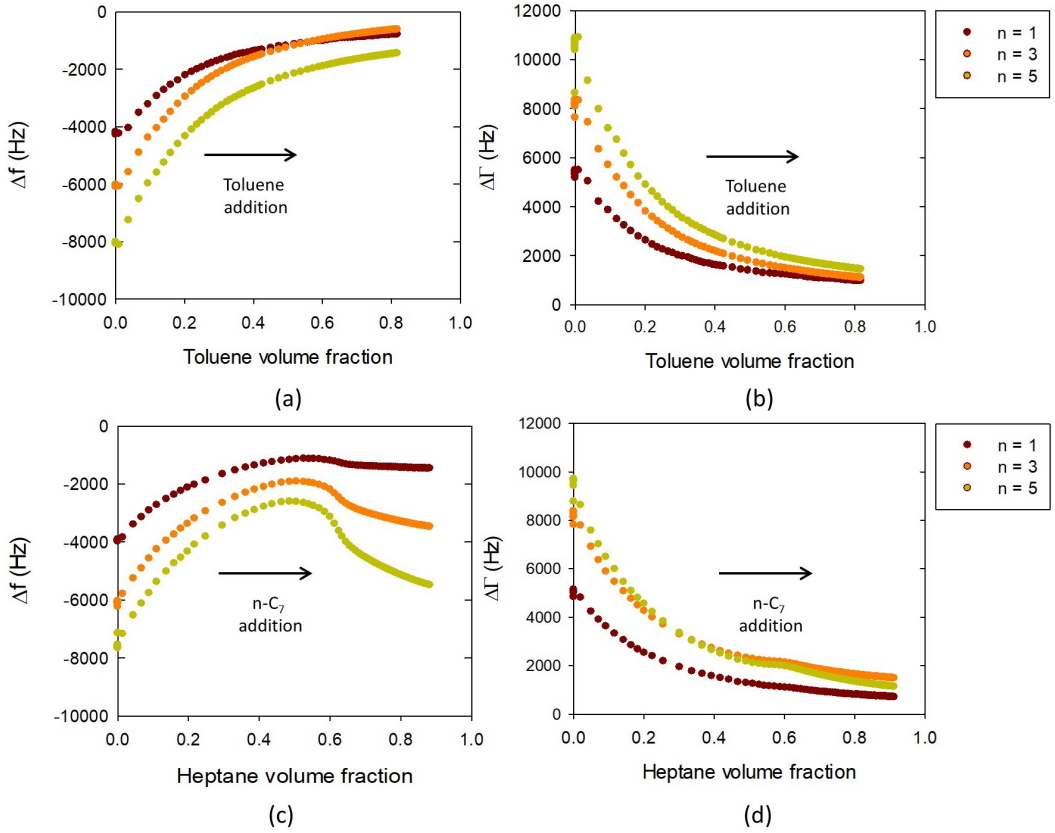

FIGURE 2.7: Example of shifts of frequency and dissipation recorded during experimental titrations of a crude oil as a function of the volume fraction of (a, b) toluene and (c, d) heptane

As the sole dilution effect related to changes in viscosity, the varying oscillating frequency caused by composition changes can be modeled using the Grunberg-Nissan[13] type of equation assuming a binary mixture composed of crude oil + solvent. When combined to Equation 2.6, the modeled square root of the density-viscosity product with a nullified surface mass load give rise to the following correlation for each overtone. This relation was used by Daridon et al.[9] to model the QCR responses in systems mainly composed of heptane and toluene. In our cases, crude oil will be assumed to be a single pseudo-component.

$$\Delta f_{mix} = e^{(xln\Delta f_{solvent}+(1-x)ln\Delta f_{oil}+x(1-x)G)} \tag{2.9}$$

where x is the mass fraction of the solvent in the mixture of oil + solvent, Δf_i is the shift of frequency of the overtone of interest when immersed in pure component i, G is an adjusted parameter of the Grunberg-Nissan type of correlation. Figure 2.8 shows the good agreement of the correlated values compared to experimental measurement for a system of crude oil titrated with a solvent that does not induce destabilization of asphaltenes (toluene) at 20°C. As it can be seen in Figure 2.8, maximum deviations observed between the correlation and the experiment reaches 4%. Such deviations are expected for huge changes of the frequency (5000 Hz), related to relatively complex and viscous medium. Indeed, impacts of the non-ideal side effects on quartz crystals resonance exposed in the previous section are neglected but still exist.

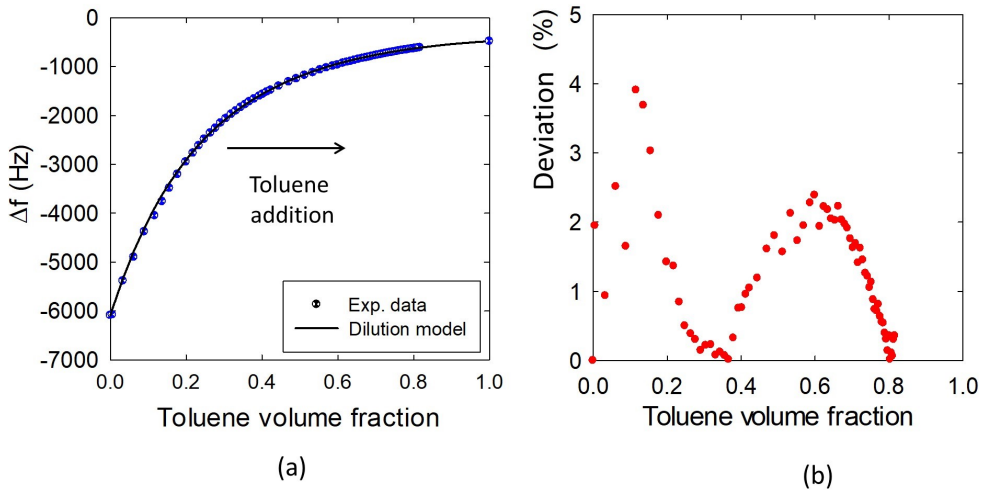

FIGURE 2.8: (a) Comparison between experimental and correlated (eq.2.9) frequency shifts versus toluene volume fraction for the 3^{rd} overtone
(b) Absolute deviation percentage of the correlated dilution curve compared to measured data

When addition of a bad solvent is carried out, the QCR detection of asphaltenes instability during the time of the titration can be highlighted by superposing a fitted dilution curve to the actual data. Figure 2.9 (a) presents the comparison between the calculated dilution curves with Equation 2.9 and the measured frequency shifts. Indeed, the curvature of the correlation can be adjusted with the parameter G to best match with experimental points at low heptane fraction or to numerically minimize the deviation within a larger range of composition. The two extreme possibilities are used to evaluate the error bars when comparing the deviation of the experimental data to dilution in Figure 2.9 (b). A geometrical construction by interpolated linearizable regions of the graphic allows us to estimate the instantaneous point (crossing point) of detection of unstable asphaltenes with the immersed probe. Unstable asphaltenes necessarily exist in the form of aggregates larger than the sensitivity beyond this particular content of alkane (Figure 2.9). However, as described in the introduction Chapter, asphaltenes belong to a continuum of molecules and defining strict solution conditions of destabilization is not consistent with the nature of such colloidal petroleum fractions.

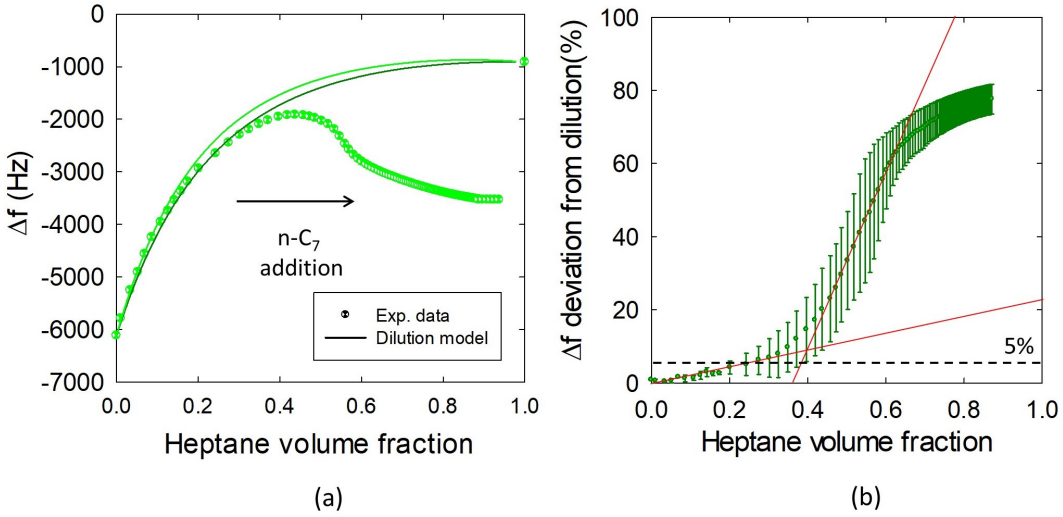

FIGURE 2.9: (a) Comparison between experimental and dilution correlated (eq.2.9) frequency shifts versus heptane volume fraction for the 3^{rd} overtone at 20^oC
(b) Percent deviation of the measured data from the calculated dilution curve.

The complicated interpretation and the large error bars are induced by the consequent difference of the viscosity-density products at low temperature between typical crude oils and solvents used throughout this research project. Therefore, although the goal was not to study the effect of temperature, higher temperatures were studied for practical reasons as illustrated by Figure 2.10. The limited curvature of the function brings more accuracy of the Grunberg-Nissan approximation (typical errors lesser than 1%). Additionally, this practice will approach typical temperatures found in oil-producing wells, usually larger than 50^oC. Note that such temperatures also present the advantadge of avoiding the formation of solid paraffins contained in crude oils (limit temperature usually termed as "wax appearance temperature" or WAT). The pseudo-exponential increase of the deviation, showed in Figure 2.10, is qualitatively in agreement with a continuous process of destabilization as opposed to well-defined conditions of destabilization. Delimiting an "onset" volume fraction of heptane for asphaltene destabilization with Figure 2.10 (b) is a matter of interpretation and would be ambiguous.

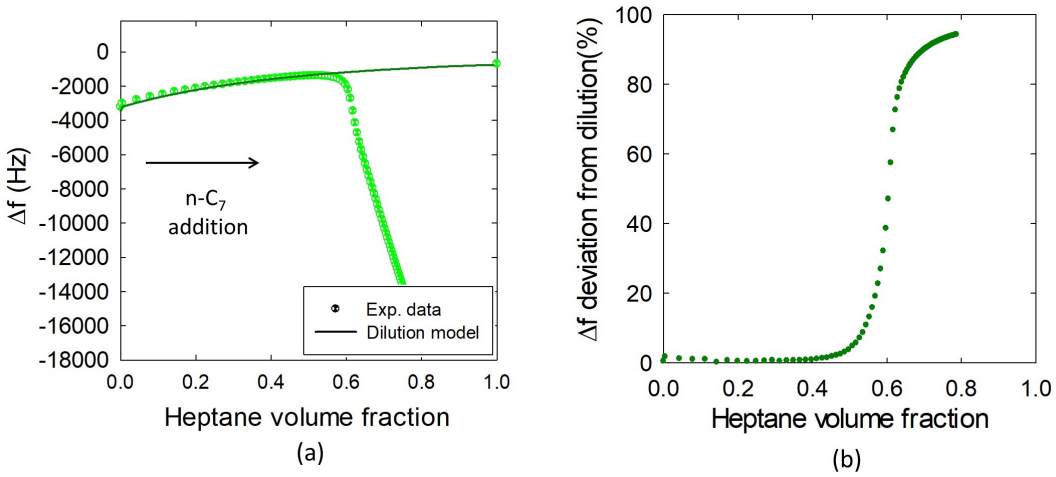

FIGURE 2.10: (a) Comparison between experimental and dilution correlated (eq.2.9) frequency shifts versus heptane volume fraction for the 3^{rd} overtone at 60^{o}C
(b) Percent deviation of the measured data from the calculated dilution curve.

After finding operational conditions for which experimental uncertainties related to changes of the bulk fluid properties are reduced, the surface mass load is then studied within the defined range using Equation 2.6. The deposited mass per unit of area is plotted (see Figure 2.11) and predominant physical parameters affecting the cumulative deposited asphaltenes are identified and further investigated in the following Chapters of this dissertation.

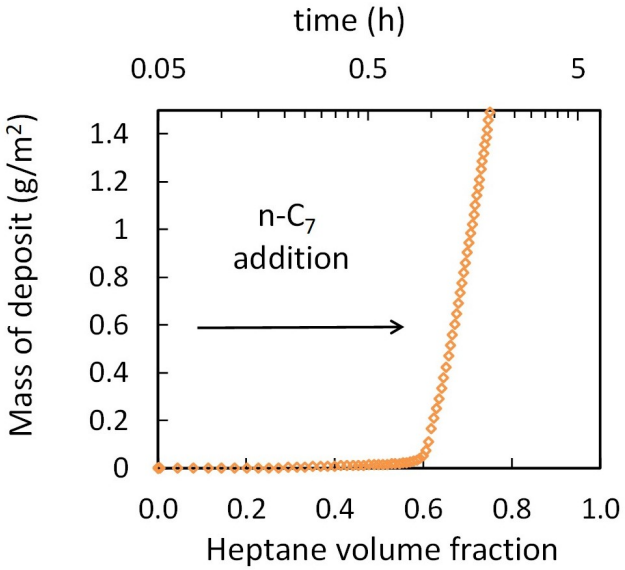

FIGURE 2.11: Cumulative mass of asphaltenes deposit on surfaces of the QCR interpreted with Equation 2.6 as a function of the heptane content in crude oil and as a function of the elapsed time from the begining of the titration.

Note that the utilization of the QCR apparatus not only enabled to extend nanoscale investigations to a larger range of alkanes concentrations, it also has the advantages of short experimental run-times (few hours) along with drastically shrinking

the necessary volume of oil by one order of magnitude compared to other experimental technique that seek similar goals.

Solubility parameter of liquid mixtures

During continuous addition of alkanes in crude oil, the quality of mixed solvents can be expressed in terms of solubility parameter (mainly dispersion component). All the following solubility parameters of liquid solutions were calculated by the linear proportionality to the Lorentz-Lorenz refractive index function proposed by Wang and Buckley [31]. In the following sections, Equation 2.10 is applied to the temperature of work: 60 °C ; we make the assumption that the predominant parameter affected by the temperature is the refractive index of the liquid solutions. According to van Laar-Lorenz definition of enthalpy, the other parameter affected by the temperature is the size of molecules. Using Equation 2.10 at different temperatures, compared to the temperature at which the expression was defined, makes the assumption that the distance between molecules (captured by the refractive index) is predominantly affecting the cohesive energy density and the internal variation in size of molecules is neglected.

$$\delta = 52.042\frac{(n_D^2 - 1)}{(n_D^2 + 2)} + 2.904 \tag{2.10}$$

The refractive indices (n_D) of crude oils and mixtures were measured at the wavelength of yellow Sodium-D line (589.3nm) using a bench-top refractometer apparatus with a temperature control (Mettler Toledo RM40). The mentioned wavelength is usually chosen because it corresponds to the peak of absorption of organic matter and to a high enough frequency ($\sim 10^{15}$ Hz) to assume that the subsequent total polarizability of the molecules is well represented by the electronic polarizability [20] (see Equation 2.18 in the following section). The solubility parameter of liquid mixtures containing i constituents is given by:

$$\delta_{mix}^T = \sum_i \delta_i^T \phi_i \tag{2.11}$$

where ϕ_i are the volume fractions of the constituents i in the mixture and δ_i is its solubility parameter at the temperature T of interest. Graphics involving changes of solution properties by addition of solvent components can now be plotted as a function of the solubility parameter of the solution (Figure 2.12) instead of the volume fraction of the injected solvent (Figure 2.11). This form of representation of the solution mixture conveniently displays data when one wants to study various mixtures made of different crude oils or different solvents, the graduated scale of the variable is constant.

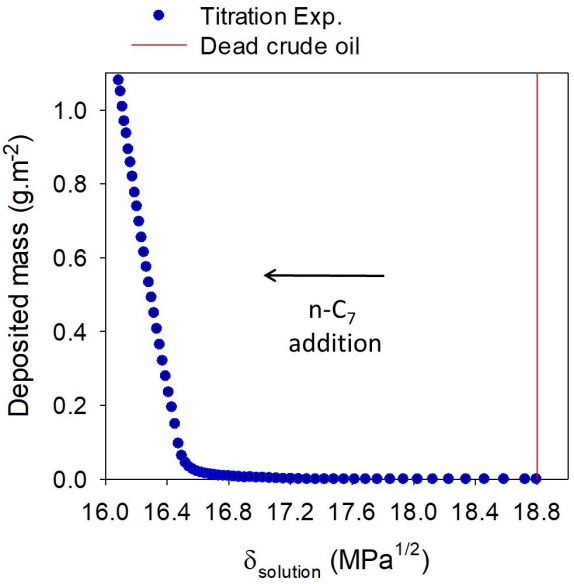

FIGURE 2.12: Cumulative mass of asphaltenes deposit on surfaces of the QCR interpreted with Equation 2.6 as a function of the solubility parameter of the solution made of heptane and crude oil

2.4.2 Quartz crystal resonator immersed in pressurized systems

Applicability to the range of pressures found in wellbores or oil reservoirs is another significant advantageous attribute of the QCR technique. Indeed, as explained in the introduction Chapter of this thesis, asphaltenes instability and deposition is a major concern when implied by the expansion of low molecular weight constituents, such as short hydrocarbons or carbon dioxide, upon pressure decrease during the oil extraction. The high pressure experimental set up is schemed on Figure 2.13. It consists of a stainless steel custom jacketed and continuously stirred cylindrical PVT cell (pressure, volume and temperature measurement cell) with an integrated QCR. The equipment can undergo pressures measured through a transducer up to 1000 bar and temperatures measured by an inserted thermocouple probe from 0 to 120°C. The total volume of the piston cylinder is about 50 cm^3. A high pressure microscope cell is optionally connected to visually observe the fluid through an infrared (IR) camera mounted on a 50x microscope lens placed above a sapphire window and a 10x eyepiece.

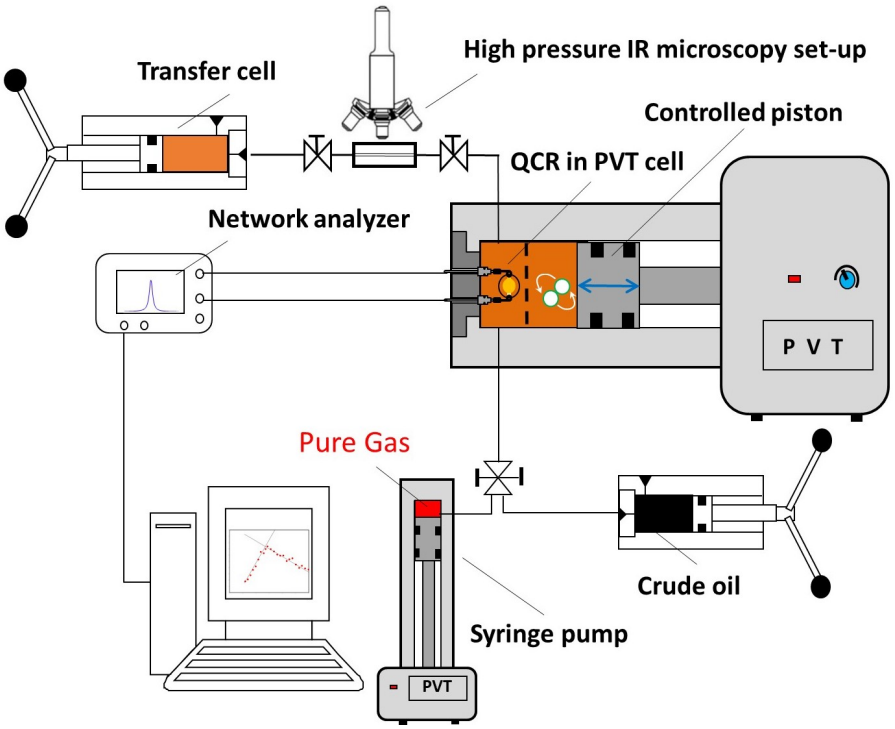

FIGURE 2.13: Schematic of the high pressure immersed QCR experimental apparatus

Sample preparation

As opposed to the volume addition of alkanes at constant pressure[25;15], experiments with mixtures of light constituents and oil were based on the volume expansion of a constant molar composition by isothermal depressurization of a liquid containing volatile components. For such experiments, it is crucial to reduce experimental uncertainties; one of them being the control of volumes and compositions. The parameters were precisely fixed by keeping simple gas compositions with well documented thermodynamic properties of the pure alkanes or the binary mixture of methane and carbon dioxide. Calibrations are achieved by means of mass basis inserted solvents (99%+ pure) prior to each experiment. The pressure and temperature measurement devices are calibrated using externally controlled probes. The calibration of the total volume of the cell is ensured by using the NIST chemical webbook database of pure solvents to calculate the according volume at each set of mass, pressure and temperature conditions. After calibration, a sensitivity analysis was made and resulted in measured pressures within $\pm$ 0.5% of error compared to the annually controlled calibrating sensor, the measured temperature has an error of less than $\pm$ 0.5^{o}C and the volumes are accurate to $\pm$ 0.1% compared to the NIST database.
Referring to previous work of Cassiède et al. [6] and Daridon et al. [8], this calibration is not only necessary to know the exact parameters of the piston cell body but also to account for the hydrostatic pressure effect on the immersed quartz sensor Δf_p:

$$\begin{aligned} \Delta f_{fluid} &= \Delta f - \Delta f_p \\ \Delta \Gamma_{fluid} &= \Delta \Gamma \end{aligned} \tag{2.12}$$

After calibration, the cylinder cell is heated and dried using a vacuum pump for several hours. A controlled mass of crude oil is first transferred to the experimental cell. Isothermal transfer of the desired volume of the gas used as a flocculating agent

is then performed by means of a syringe pump, initially calculated using the NIST data base for pure components and REFPROP software for binary blends. Gases were supplied by Linde France SA, one bottle of pure methane and one containing a blend of methane and carbon dioxide (80:20) molar composition.

Pressure scanning experiments

After preparing the blend, a constant mass compression is performed at a rate larger than 500 bar.min^{-1} and at non-mixing conditions in order to slowly dissolve the light components during the pressure increase. This practice enables a bypass of the instability zone, if any, during the pressurizing phase. The magnetic stirrer is then turned on after the stabilizing pressure is reached. The live graphical monitoring of pressure and volume enable to ensure the absence of any leakage or any remaining gas bubble while frequency and dissipation shifts are providing certainty that a stable zone is reached with no observable changes of resonance behavior overtime. After conditions are stabilized, the pressure is then isothermally decreased at specified rates ranging between 1 and 20 bar.min^{-1} (realistic depressurization rates compared to typical ones found in oil & gas production wells). Note that the temperature of the experiments is chosen larger than the WAT. In order to portray the typical measurement performed in this method, we are defining two example cases with no other variable than the methane content in the prepared mixtures. The Figures 2.14 (a) and (b) respectively show the hydrostatic pressure corrected frequency shift $\Delta f - \Delta f_P$ and the half-band half-width $\Delta\Gamma$ for a crude oil combined with methane at 30 mol%. Figures 2.14 (c) and (d) represent the evolution of the same response parameters for a blend of crude oil and methane at 57 mol%. For both compositions, one observes two regions separated by corner points upon depressurization. In the case of fewer CH_4 dissolved, one notices the linear behavior of the upper pressure region while higher content of methane trends the signal to slighlty bend.

Note that as expected, scattered data of the fundamental resonance frequency (overtone $n = 1$) are caused by the sensitivity of this overtone to side and imperfections effects related to the finite crystal. Only higher odd numbers of the overtone are therefore taken as references for interpretations.

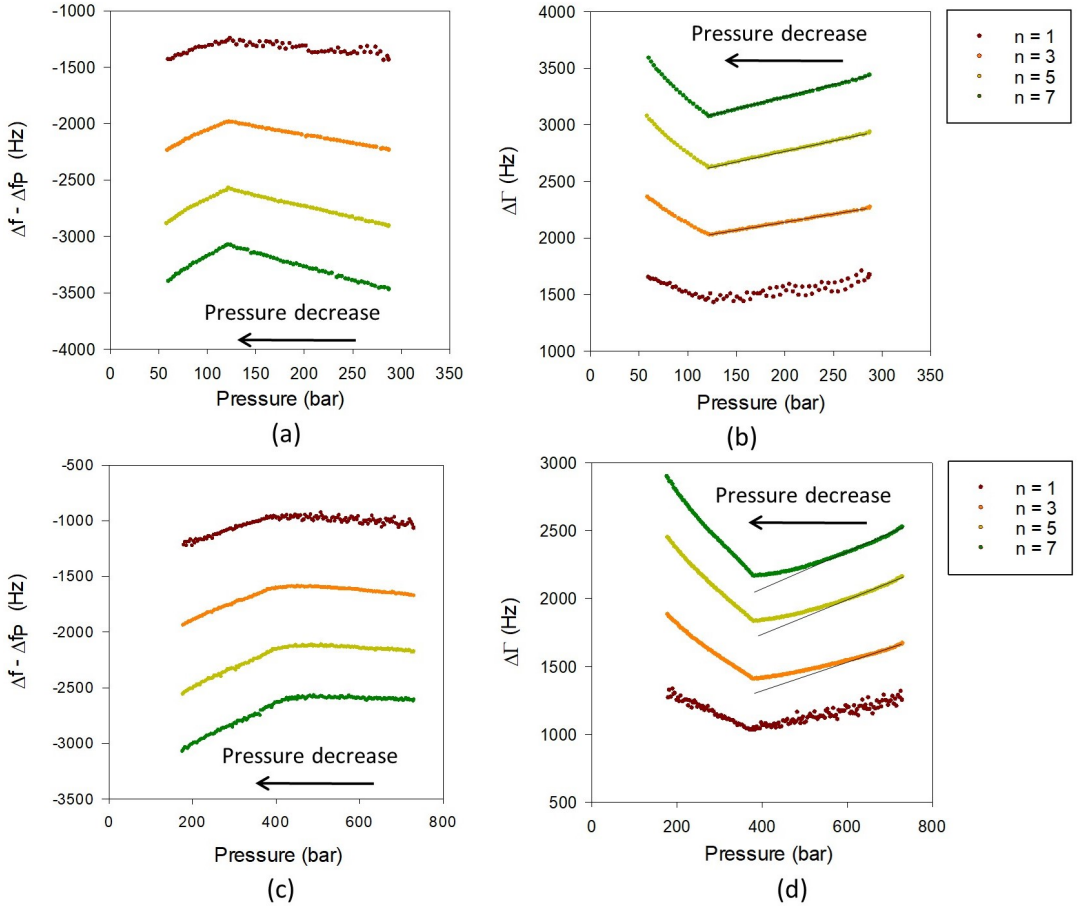

FIGURE 2.14: Frequency shift and dissipation signals evolution of harmonic overtones 1 to 7 upon depressurization for:
(a) and (b) a combination of crude oil and methane with 30 mol%$_{CH_4}$
(c) and (d) a combination of crude oil and methane with 57 mol%$_{CH_4}$

Daridon and Carrier [7]; Cardoso et al. [4] proposed a phase transition detection protocol. These authors showed that the abrupt slope inversion is the signature of the first gas bubble appearance or more commonly termed as the saturation pressure (P_{sat}) or the bubble point. At low molar content of methane, the comparison of normalized QCR signals to the volume of the total fluid as a function of pressure illustrates the presence of a gas phase. In order to plot both signals of the sensor on the same graph, they are respectively normalized onto 0 to 1 scale by dividing absolute value by reference values denoted with a zero subscript (maximum observed).

$$\frac{\left(\Delta f - \Delta f_p\right) / \left(\Delta f - \Delta f_p\right)_0}{\Delta\Gamma / \Delta\Gamma_0} \tag{2.13}$$

As shown in Figure 2.15), the significant increase of the isothermal compressibility of the fluid (relative volume response upon pressure change $\left[\frac{1}{V}\left(\frac{\partial V}{\partial P}\right)\right]$) is the signature of the gas phase appearance below the saturation pressure. A very good match is observed between the change of slopes of the QCR signal and the measured volume as a functin of pressure. The saturation pressure of a system depends on the composition of the mixture; larger molar contents of light constituents will cause saturation at larger pressures.

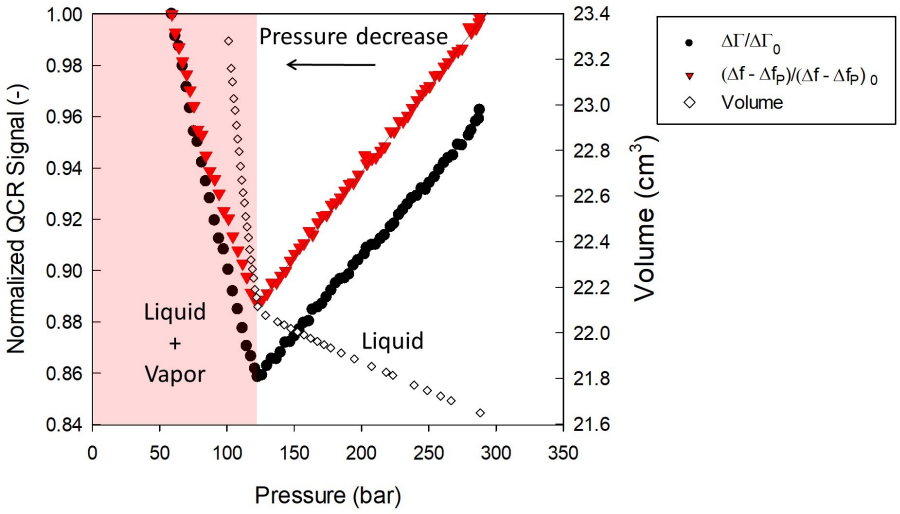

FIGURE 2.15: Records of volume and normalized change in QCR signals Δf and $\Delta\Gamma$ of the 3^{rd} overtone as a function of pressure during a constant mass expansion experiment of a blend crude oil-methane (30 mol%)

In single phase conditions (i.e. $P > P_{sat}$), Daridon and Carrier[7] evidenced the appearance of unstable asphaltenes and the growth of a deposit layer on the crystal's surface was well identified through an observed deviation from linearity of the resonance frequency shift, $(\Delta f - \Delta f_p)$, during pressure depletion experiments. Consequently, in a similar manner to the atmospheric pressure experiment, the frequency shift is the first interpreted criterion to detect conditions at which instability is observable at the acoustic waves length scale. Figure 2.16 exemplifies the case of non-linear behavior of the acoustic wave sensor signals at pressures larger than P_{sat}. Note that $\Delta\Gamma$ still interestingly exhibits a corner shape at the saturation pressure.

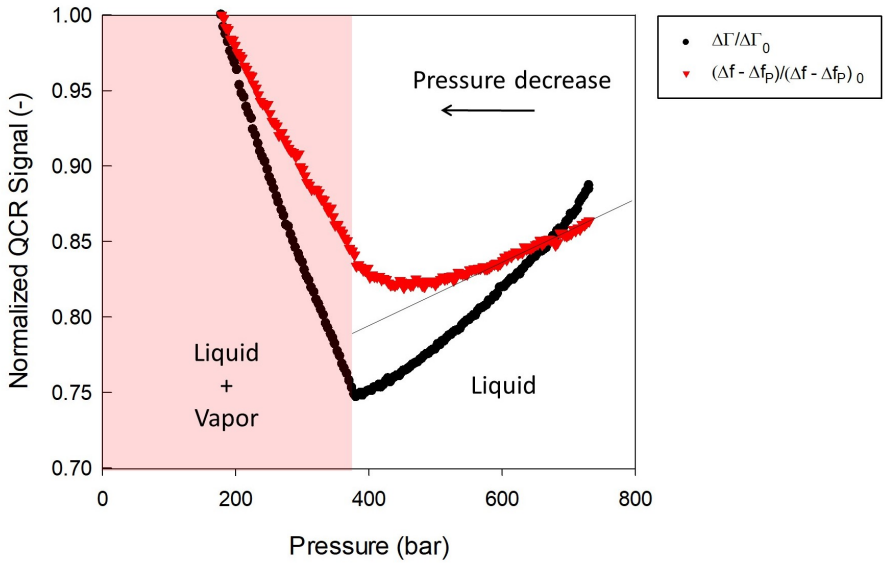

FIGURE 2.16: Records of volume and normalized change in QCR signals Δf and $\Delta\Gamma$ of the 3^{rd} overtone as a function of pressure during a constant mass expansion experiment of a blend crude oil-methane (57 mol%)

As advised in the precedent section, definite conditions are hardly delineated for asphaltenes stability as this class of compounds belong to a class of components as opposed to a single structure or molecule. Discussions on the extensive practice of defining an asphaltene "onset" pressure (AOP) will be extended in Chapter 6.
Figure 2.17 illustrates the more significant deviation of the frequency absolute signal than at lower concentrations of methane showed in Figure 2.16 (60 vs 57 mol%). The frequency deviation is in the order of thousands of Hertz and indicates that massive deposition occurs at the investigated conditions.

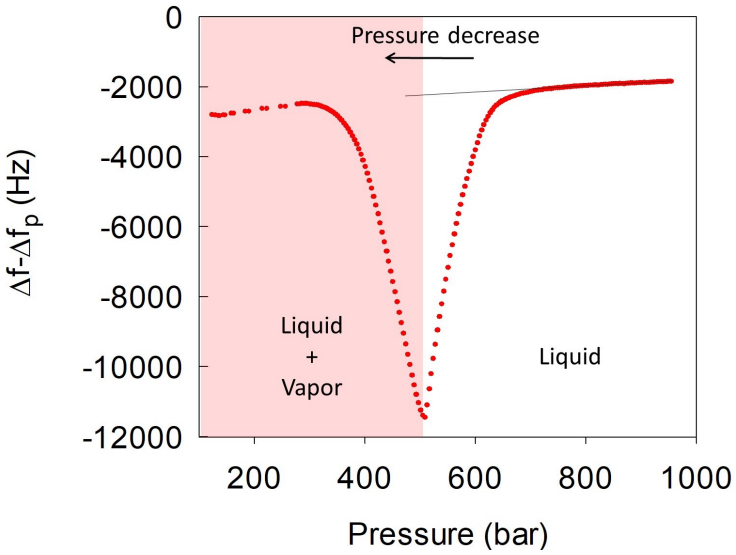

FIGURE 2.17: Measured shift of the frequency change as a function of the pressure during a constant mass expansion (CME) experiment of an oil-methane blend containing 60 mol% of methane

After identifying conditions at which large amounts of unstable asphaltenes are detected, further data treatments are then computed by combining Equation 2.6 and Equation 2.12 to calculate the deposited mass of asphaltenes per unit area (Figure 2.18).

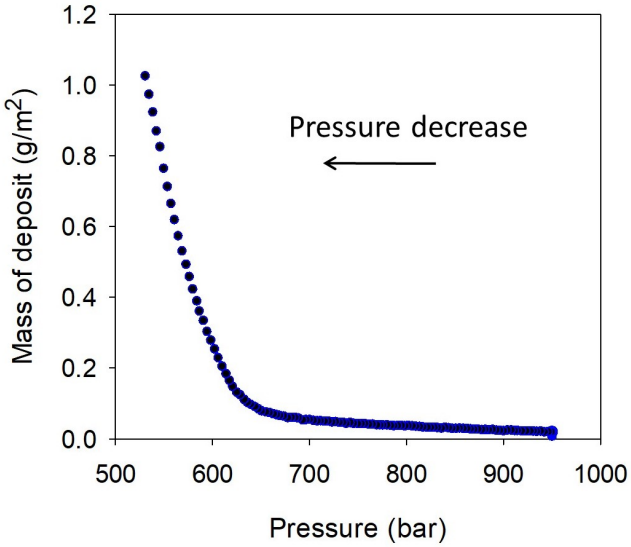

FIGURE 2.18: Calculated cumulative mass of deposit, using Equations 2.6 and 2.12, as a function of the pressure during a constant mass expansion (CME) experiment of an oil-methane blend containing 60 mol% of methane

As shown in the results involving addition of liquids at atmospheric pressure (precedent section), the appropriate track of solution properties can either directly be the volume fraction of destabilizing solvent or the solubility parameter of the solution. In Chapter 6, the goal of our research will be to understand the effect of light-ends dissolved in the extracted petroleum, such as methane, compared to more common liquid solvents used in laboratories to destabilize asphaltenes, such as *n*-heptane. It then becomes essential to know the volume fraction of the methane as a function of the pressure. Indeed, the pressure is a variable of secondary importance to the asphaltenes stability, it is actually a mean of varying the volumetric composition of the liquid solution when some of its components' properties strongly depend on the pressure, which in turn has direct implications on the asphaltenes stability. Additionally, industrial operations like blending of produced fluids, gas-lift injections in wells to reduce the hydrostatic column pressure or like gas injections to maintain reservoir pressures do not necessarily involve strong pressure gradients but can significantly alter the solubility of asphaltenes by locally modifying volumetric compositions. As illustrated in Figure 6.6 the molar volumes of pure carbon dioxide, methane, ethane and propane are expected to be the most predominant components that contribute to the variation in volume composition of a live oil during its transport.

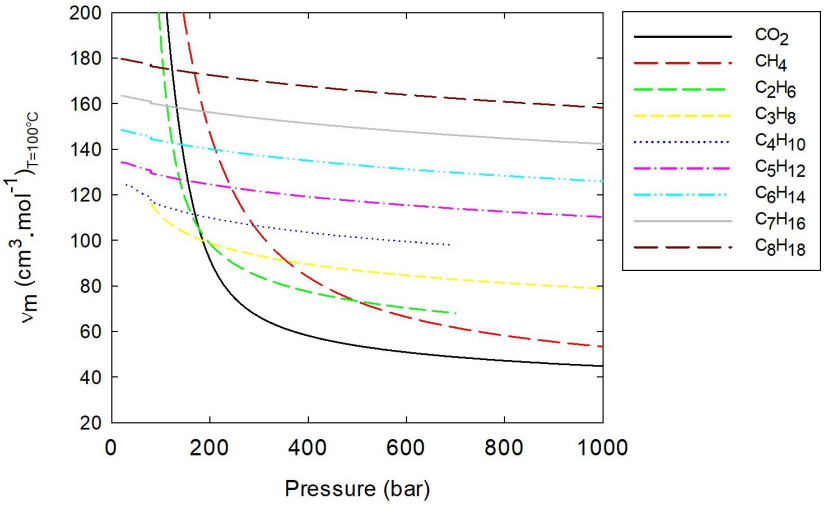

FIGURE 2.19: Comparison of molar volumes of pure fluids as a function of the pressure at constant temperature (100°C) (source: NIST chemical web book)

Calculation of the apparent molar volume of light dissolved components (e.g. methane)

Unlike heavy components present in the crude oil, $v_{gas}^{P,T}$ the apparent molar volume of light compressible constituents can be significantly different when dissolved in crude oil at elevated pressures compared to their pure molar volumes $v_{gas}^{*P,T}$ reported in the literature. The presence of other components can enhance or reduce their dissolution. Therefore experimental measurement can help us to calculate the actual volume percent of methane into the oil-methane mixtures that are first prepared on a molar basis. After recombining the crude oil with a well-known molar composition, the molar volume of the light-ends dissolved at specific pressure and temperature conditions is then given by:

$$v_{gas}^{P,T} = \frac{V_{gas}^{P,T}}{N_{gas}} = \frac{V_{solution}^{P,T} - \frac{m_{oil}}{\rho_{oil}^{*P,T}}}{N_{gas}} \tag{2.14}$$

where $\left(V_{solution}^{P,T}\right)$ is the measured volume of the recombined fluid, $\left(N_{gas}\right)$ is the number of moles of the injected light constituent and $\left(m_{oil}\right)$ is the injected mass of crude oil. Note that the measurement of several parameters instead of simulating them augments the accuracy of the experimental interpretation. Part of those parameters, the density of the crude oil at the test conditions $\left(\rho_{oil}^{*P,T}\right)$ is experimentally determined prior to adding other components like methane to compose the custom mixture. Alternatively, and as showed by Figure 2.20, the isothermal Tait Equation of state can be used to relate the liquid density to pressure with the following relationship[14]:

$$\rho_{oil}^{*P,T} = \frac{m_{oil}}{V_{oil}^{P,T}} = \frac{m_{oil}}{V_0(1-C)log\left(\frac{B+P}{B+P_0}\right)} \tag{2.15}$$

where V_0 is a reference volume (the volume at the pressure of reference P_0, usually conveniently chosen to be the atmospheric pressure), B and C are temperature dependent parameters specifically adjusted to the studied liquid with limited number of experimental measurements. Figure 2.20 shows the good agreement between the

calculation using Tait equation of state and the measured density of the pure crude oil.

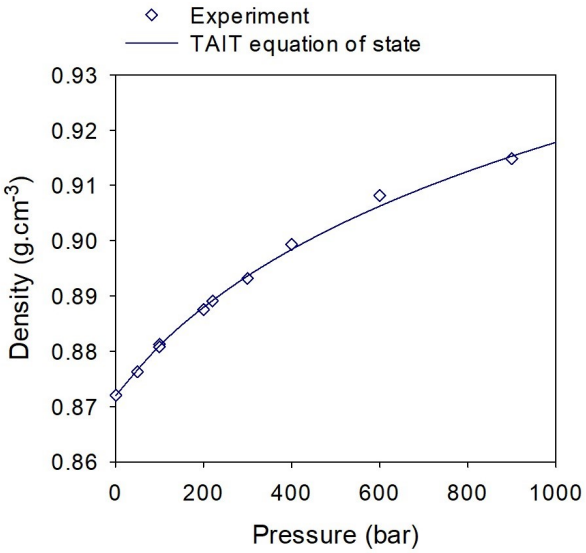

FIGURE 2.20: Relation between the crude oil density and the pressure at constant temperature (60°C)

The volumetric composition of the mixture is then calculated by converting the molar composition through the apparent molar volumes as a function of the pressure. The volume fraction of the dissolved gas is calculated using the following Equation:

$$\phi_{gas} = \frac{V_{gas}^{P,T}}{V_{solution}^{P,T}} = \frac{V_{solution}^{P,T} - \frac{m_{oil}}{\rho_{oil}^{*P,T}}}{V_{solution}^{P,T}} \tag{2.16}$$

Deposition measurements can be plotted as a function of the volume fraction of methane, as shown in Figure 2.21:

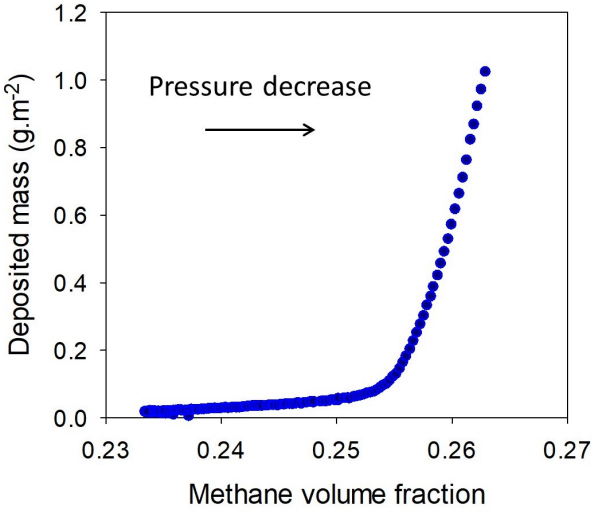

FIGURE 2.21: Calculated cumulative mass of deposit, using Equations 2.6 and 2.12, as a function of the methane volume fraction during a constant mass expansion (CME) experiment of an oil-methane blend containing 60 mol% of methane

Calculation of the refractive index of gas recombined oils at elevated pressures
The refractive indices (n_D) at elevated pressures with light component dissolved (single liquid phase) are calculated as proposed by Buckley et al. [3], assuming a volume fraction ϕ_i averaged Lorenz-Lorentz function of 2 pseudo-components in the mixture: the dead oil and its associated gas dissolved at the respective conditions of study.

$$\left(\frac{n_D^2-1}{n_D^2+2}\right)_{solution}^{P,T} = \phi_{oil}\left(\frac{n_D^2-1}{n_D^2+2}\right)_{oil}^{P,T} + \phi_{gas}\left(\frac{n_D^2-1}{n_D^2+2}\right)_{gas}^{P,T} \tag{2.17}$$

The use of Clausius-Mossotti and Lorenz-Lorentz Equations [20] lets us write Equation 2.18.

$$\left(\frac{n_D^2-1}{n_D^2+2}\right)_{i}^{P,T} = \frac{\alpha_i \rho_i^{*P,T} \mathcal{N}_\mathcal{A}}{3 M_{w_i} \epsilon_0} \tag{2.18}$$

Where $\rho_i^{*P,T}$ is density of pure components i at the pressure and temperature of interest, α_i and M_{w_i} are respectively the electronic polarizability and the molecular weight of the component i, ϵ_0 is the permittivity of free space and $\mathcal{N}_\mathcal{A}$ is the Avogadro Number. By using a convenient reference condition of pressure and temperature, e. g. ambient conditions thereafter denoted by the exponent 0, Lorenz-Lorentz Equation 2.17 combined to Equation 2.18 leads us to the following relation which allows to calculate the refractive index function of the mixture at each pressure and temperature.

$$\left(\frac{n_D^2-1}{n_D^2+2}\right)_{solution}^{P,T} = \frac{V_{oil}^0}{V_{solution}^{P,T}}\left(\frac{n_D^2-1}{n_D^2+2}\right)_{oil}^{0} + \frac{N_{gas}}{V_{solution}^{P,T}} Rm_{gas}^0 \tag{2.19}$$

Where V_{oil}^0 and $V_{solution}^{P,T}$ are volumes of oil at reference conditions and volume of the solution mixture at the pressure and temperature of test, N_{gas} and Rm_{gas}^0 are respectively the number of moles and the molar refractivity of the gas dissolved.
We should note that this relation assumes molecular polarizabilities of components to be independent of pressure and temperature in the oil industry operational range of conditions ($\sim$ 1 to 1000 bar and 0°C to 120°C). Indeed, the density of the mixture is the only pressure and temperature dependent parameter in Equation 2.18.
Note that the density is a measured value for single liquid phase conditions, i. e. at pressures greater than the saturation pressure. Volume measurements no longer enables us to calculate the density of the liquid phase at under saturated pressures due to the presence of both phases in the total volume. This reinforces the choice of CME experiments instead of compression at pressures lower than the saturation pressure or constant pressure experiments. This way, the destabilization and deposition of asphaltenes by means of presence of light constituent is studied at conditions in which properties of the carrier liquid are measured and can help understanding the effect of different destabilizing agents.
Combining Equations 2.19 and 2.10, the solubility parameter of the solution at high pressure is calculated and the measured properties related to asphaltenes destabilization and deposition can be plotted as a function of the solubility parameter of the solution along the CME experiment as illustrated in Figure 2.22.

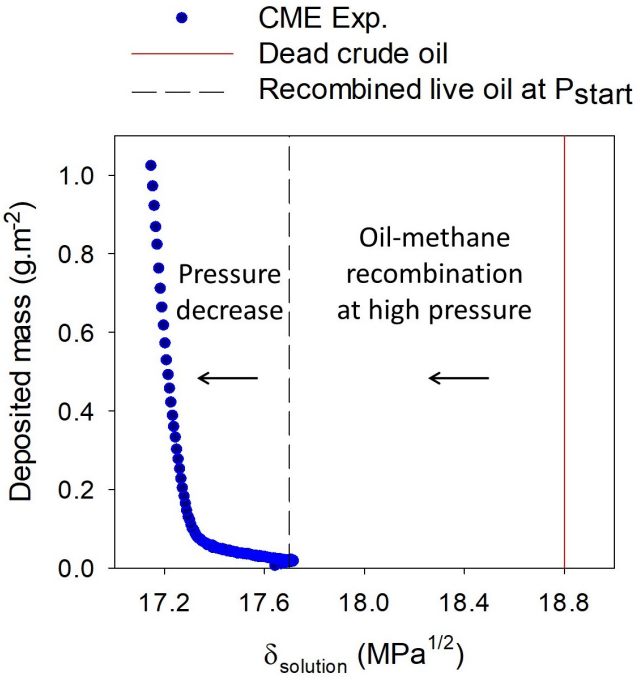

FIGURE 2.22: Calculated cumulative mass of deposit, using equations 2.6 and 2.12, as a function of the solubility parameter of the liquid solution during a constant mass expansion (CME) experiment of an oil-methane blend containing 60 mol% of methane

This practice presents the advantage of reconciling data from different mixtures of oil and anti-solvent on the same graphic representation. It will therefore be used when studying the effect of the nature of the flocculating agent (alkane chain length or molar volume of the agent) in Chapter 6.

Bibliography

[1] Aulin, C., I. Varga, P. M. Claesson, L. Wågberg, and T. Lindström
2008. Buildup of polyelectrolyte multilayers of polyethyleneimine and microfibrillated cellulose studied by in situ dual-polarization interferometry and quartz crystal microbalance with dissipation. *Langmuir*, 24(6):2509–2518.

[2] Bruckenstein, S. and M. Shay
1985. Experimental aspects of use of the quartz crystal microbalance in solution. *Electrochimica Acta*, 30(10):1295–1300.

[3] Buckley, J. S., G. Hirasaki, Y. Liu, S. Von Drasek, J. Wang, and B. Gill
1998. Asphaltene precipitation and solvent properties of crude oils. *Petroleum Science and Technology*, 16(3-4):251–285.

[4] Cardoso, F., H. Carrier, J.-L. Daridon, J. Pauly, and P. Rosa
2014. Co2 and temperature effects on the asphaltene phase envelope as determined by a quartz crystal resonator. *Energy & Fuels*, 28(11):6780–6787.

[5] Cassiède, M., J.-L. Daridon, J. Paillol, and J. Pauly
2010. Impedance analysis for characterizing the influence of hydrostatic pressure on piezoelectric quartz crystal sensors. *Journal of Applied Physics*, 108(3):034505.

[6] Cassiède, M., J.-L. Daridon, J. Paillol, and J. Pauly
2011. Characterization of the behaviour of a quartz crystal resonator fully immersed in a newtonian liquid by impedance analysis. *Sensors and Actuators A: Physical*, 167(2):317–326.

[7] Daridon, J.-L. and H. Carrier
2017. Measurement of phase changes in live crude oil using an acoustic wave sensor: Asphaltene instability envelope. *Energy & Fuels*, 31(9):9255–9267.

[8] Daridon, J.-L., M. Cassiède, J. Paillol, and J. Pauly
2011. Viscosity measurements of liquids under pressure by using the quartz crystal resonators. *Review of Scientific Instruments*, 82(9):095114.

[9] Daridon, J. L., M. Cassiede, D. Nasri, J. Pauly, and H. Carrier
2013. Probing asphaltene flocculation by a quartz crystal resonator. *Energy & Fuels*, 27(8):4639–4647.

[10] Dickert, F. L., O. Hayden, R. Bindeus, K.-J. Mann, D. Blaas, and E. Waigmann
2004. Bioimprinted qcm sensors for virus detection—screening of plant sap. *Analytical and Bioanalytical Chemistry*, 378(8):1929–1934.

[11] Domack, A., O. Prucker, J. Rühe, and D. Johannsmann
1997. Swelling of a polymer brush probed with a quartz crystal resonator. *Physical Review E*, 56(1):680.

[12] Goual, L., G. Horváth-Szabó, J. H. Masliyah, and Z. Xu
2005. Adsorption of bituminous components at oil/water interfaces investigated by quartz crystal microbalance: Implications to the stability of water-in-oil emulsions. *Langmuir*, 21(18):8278–8289.

[13] Grunberg, L. and A. H. Nissan
1949. Mixture law for viscosity. *Nature*, 164(4175):799.

[14] Hayward, A. T. J.
1967. Compressibility equations for liquids: a comparative study. *British Journal of Applied Physics*, 18(7):965.

[15] Hirschberg, A., L. DeJong, B. Schipper, and J. Meijer
1984. Influence of temperature and pressure on asphaltene flocculation. *Society of Petroleum Engineers Journal*, 24(03):283–293.

[16] Hoepfner, M. P., V. Limsakoune, V. Chuenmeechao, T. Maqbool, and H. S. Fogler
2013a. A fundamental study of asphaltene deposition. *Energy & fuels*, 27(2):725–735.

[17] Hoepfner, M. P., C. Vilas Boas Favero, N. Haji-Akbari, and H. S. Fogler
2013b. The fractal aggregation of asphaltenes. *Langmuir*, 29(28):8799–8808.

[18] Hovgaard, M. B., M. Dong, D. E. Otzen, and F. Besenbacher
2007. Quartz crystal microbalance studies of multilayer glucagon fibrillation at the solid-liquid interface. *Biophysical journal*, 93(6):2162–2169.

[19] Huang, X., Q. Bai, J. Hu, and D. Hou
2017. A practical model of quartz crystal microbalance in actual applications. *Sensors*, 17(8):1785.

[20] Israelachvili, J. N.
2015. *Intermolecular and surface forces*. Academic press.

[21] Javanbakht, G., M. Sedghi, W. R. Welch, L. Goual, and M. P. Hoepfner
2018. Molecular polydispersity improves prediction of asphaltene aggregation. *Journal of Molecular Liquids*, 256:382–394.

[22] Johannsmann, D.
2015. The quartz crystal microbalance in soft matter research. *Fundamentals and modeling. Switzerland: Springer International Publishing*.

[23] Kanazawa, K. K. and J. G. Gordon II
1985. The oscillation frequency of a quartz resonator in contact with liquid. *Analytica Chimica Acta*, 175:99–105.

[24] King, W. H.
1964. Piezoelectric sorption detector. *Analytical Chemistry*, 36(9):1735–1739.

[25] Kraiwattanawong, K., H. S. Fogler, S. G. Gharfeh, P. Singh, W. H. Thomason, and S. Chavadej
2007. Thermodynamic solubility models to predict asphaltene instability in live crude oils. *Energy & fuels*, 21(3):1248–1255.

[26] Rickert, J., A. Brecht, and W. Göpel
1997. Qcm operation in liquids: constant sensitivity during formation of extended protein multilayers by affinity. *Analytical chemistry*, 69(7):1441–1448.

[27] Rupitsch, S. J.
2018. *Piezoelectric Sensors and Actuators*. Springer.

[28] Sauerbrey, G.
1959. The use of quarts oscillators for weighing thin layers and for microweighing. *Z. Phys.*, 155:206–222.

[29] Steinmetz, N. F., E. Bock, R. P. Richter, J. P. Spatz, G. P. Lomonossoff, and D. J. Evans
2008. Assembly of multilayer arrays of viral nanoparticles via biospecific recognition: a quartz crystal microbalance with dissipation monitoring study. *Biomacromolecules*, 9(2):456–462.

[30] Vilas Bôas Fávero, C., A. Hanpan, P. Phichphimok, K. Binabdullah, and H. S. Fogler
2016. Mechanistic investigation of asphaltene deposition. *Energy & Fuels*, 30(11):8915–8921.

[31] Wang, J. and J. S. Buckley
2001. A two-component solubility model of the onset of asphaltene flocculation in crude oils. *Energy & Fuels*, 15(5):1004–1012.

[32] Wang, J., J. S. Buckley, and J. L. Creek
2004. Asphaltene deposition on metallic surfaces. *Journal of dispersion science and technology*, 25(3):287–298.

Chapter 3

On the controlling kinetics of unstable asphaltenes

3.1 Introduction

Asphaltenes are defined as a class of relatively heavy, highly aromatic and polar molecules present in native crude oils at concentrations naturally ranging from units of g/L to hundreds of g/L depending on the oil origin[2;24] and on the used procedure for extraction[1;25;30]. Volumetric addition of bad solvents like n-alkanes, generally called precipitants or flocculating agent of asphaltene constituents, causes them to move out of stable nanoaggregate or cluster states into a destabilized state of insoluble agglomerated clusters. Previous authors have been describing this process by several terminologies, such as precipitation[6;41;38;32], destabilization[39], aggregation[19;28;33] or flocculation[3;8;14;22]. In all cases "precipitation" might not be the most suitable term for this process, since stable asphatenes are colloidal suspensions of species in liquids and not actually dissolved in solutions. Previous research on asphaltenes destabilization was for a long time focused on the determination of the "onset" conditions during addition of a bad solvent[3;5;12;20;9], defined as a well-delineated concentration of bad solvent under which asphaltenes would all be in a stable state and above which they would become unstable by fractions. This past definition gave way to a better understanding of time-dependent onset point first revealed by Angle et al.[4].
Maqbool et al.[27] further showed how small fractions of unstable asphaltenes were neglected by previous researchers who did not wait long enough for their growth until unstable flocs would reach detectable size below the onset volume. Since then, studies involving the aging time of prepared mixtures at fixed composition were multiplied[16;29;35;38]. Precipitation, aggregation, destabilization and flocculation were sometimes interchangeably used to describe the slow kinetics of a single reaction-limited process[7;42] associated with detecting asphaltenes instability. In this research, we will theorize two distinct mechanisms: (i) destabilization of stable units and (ii) aggregation of unstable asphaltenes. The main objective is to reveal, if any, the dominating kinetic effect between both processes.

3.1.1 Review of the destabilization and aggregation modeling approaches

For an unchanged mixture prepared at time = 0, destabilization of asphaltenes can mathematically be modeled as a first-order reaction described by an elementary step[11] where nanoaggregates or clusters of asphaltenes convert from a "stable" state (A_{stable}) to an "unstable" state ($A_{unstable}$). After becoming incompatible with their

surrounding fluid, the converted clusters of nanoaggregates are termed primary aggregates (or particles) of unstable asphaltenes and have a characteristic size of 2 to 10 nm. Further aggregation of unstable asphaltenes occurs throughout another reaction with other particles to form larger aggregates (A_k) composed of k number of primary units. Primary units can be considered to be the converted nanoaggregates or clusters as mentioned above.

$$[\mathrm{A}_{stable}] \xrightarrow[\mathrm{k_N}]{(\mathrm{t_{aging}})} [\mathrm{A}_{unstable}] \xrightarrow[\mathrm{k_{agg}}]{(\mathrm{t_{agg}})} [A_k]$$

The mass basis reaction rate r_1 of destabilization is then described by:

$$r_1 = k_N C_{A_{t\to\infty}} \tag{3.1}$$

where $C_{A_{t\to\infty}}$ or later referred as C_{A_∞} is the equilibrated total mass concentration of unstable asphaltenes,k_N is the nucleation rate constant and k_{agg} is the aggregation rate constant usually represented by a Kernel[28].
Determining the dominant effect, if any, between aggregation and destabilization kinetics is a fundamental concern that will have significant implications on the following Chapters of this dissertation. In one scenario, all the unstable asphaltene particles will have relatively long lifetimes at small sizes (slow aggregation) and their number will be immediately fixed. In the opposite one, the lifetime of small particles will be short but their number will be dictated by their generation rate (slow destabilization).

Literature review on aggregation kinetics
As summarized by Fávero et al.[14], the phenomenon that is believed to take the longest time is the aggregation process of destabilized nanoaggregates or clusters ($k_{agg} << k_N$). Consequently, previous authors[28;37;29;18] focused their efforts to understand the aggregation kinetics and built population balance mathematical models based on the population balance equation developed by Smoluchowski[15]. In their modeling, Maqbool et al.[28] considered a fraction of asphaltenes that immediately becomes unstable and form an initial number of unstable primary particles $C_1(t = 0)$ after an alkane is added. The main assumption made by the authors is that the initial mass concentration of primary particles is constant over time ($C_1(0) = C_A(t \to \infty)$). In other words, the total number of primary nanoparticles across all agglomerates at any instant was assumed equal to the total primary units immediately formed after addition of the flocculating agent. The initial concentration of larger than primary aggregates was assumed:

$$C_k(0) = 0 \text{ for } k > 1 \tag{3.2}$$

According to their model, these nanoparticles undergo a Brownian aggregation process and the rate of change of the number concentration of particles formed with k primary units is given by the Smoluchowski coagulation Equation:

$$\frac{dC_k}{dt} = \frac{1}{2}\sum_{i+j=k} K_{ij}C_iC_j - C_k\sum_{i\geqslant 1} K_{ik}C_i \tag{3.3}$$

where C_k is the number concentration of $k-th$ species, K_{ij} is the collision kernel between i and j species, t is the aging time.
The collision kernel is a constant that describes the rate at which particles of size

i aggregate with the particles of size j. K_{ij} is therefore related to the interaction between colliding particles and is expressed as the product of the flocculation rate constant between i-j species K^*_{ij} and their collision efficiency β_{ij} :

$$K_{ij} = K^*_{ij}\beta_{ij} \tag{3.4}$$

For the agglomeration of Brownian particles, the rate constant can be calculated as follows according to the work of Smoluchowski[36]:

$$K^*_{ij} = 2\pi(d_i + d_j)(D_i + D_j) = \frac{2k_BT}{3\mu_{liq}}\frac{(d_i + d_j)^2}{d_i d_j} \tag{3.5}$$

where d_i and d_j represent the hydrodynamic diameters of colliding particles i-j, D_i and D_j are their respective diffusion coefficients in the medium, k_B is the Boltzmann constant, μ_{liq} the viscosity of the liquid medium, T is the absolute temperature.
The geometric population balance model proposed by Maqbool et al.[28] was numerically solved through ordinary differential equations (ODEs). They fixed the initial conditions with the total concentration of primary particles ($C_1(0)$) and the collision efficiency β was adjusted to fit the experimental data. As shown in Figure 4.3(a), the reorganization of nanoparticles reaches an equilibrium in particle size distribution of agglomerates indicated by a plateau value of the separated mass after waiting an appropriate time. Maqbool et al.[28] estimated $C_1(0)$ using the measured separated concentration of asphaltenes per unit volume of the mixture C_{A_∞} by the centrifugation technique of oil-heptane mixtures. Authors used the following Equation to calculate the number of primary units (nanoaggregates) at time = 0 :

$$C_1(0) = C_{A_\infty}\frac{\mathcal{N}_\mathcal{A}}{M_{w_{\text{asph}}}N_{\text{agg}}} \tag{3.6}$$

where $\mathcal{N}_\mathcal{A}$ is the Avogadro number, $M_{w_{\text{asph}}}$ is the molecular weight of the asphaltene molecules averaged at 750 g.mol^{-1} and N_{agg} is the number of asphaltenes per nanoaggregate ($N_{agg} \approx 8$ based on previous structural measurement[31]).
They reported adjusted values of the collision efficiency between 10^{-4} and 10^{-6} for the investigated range of heptane content smaller than the instantaneous onset (see Figure 4.3(b)).

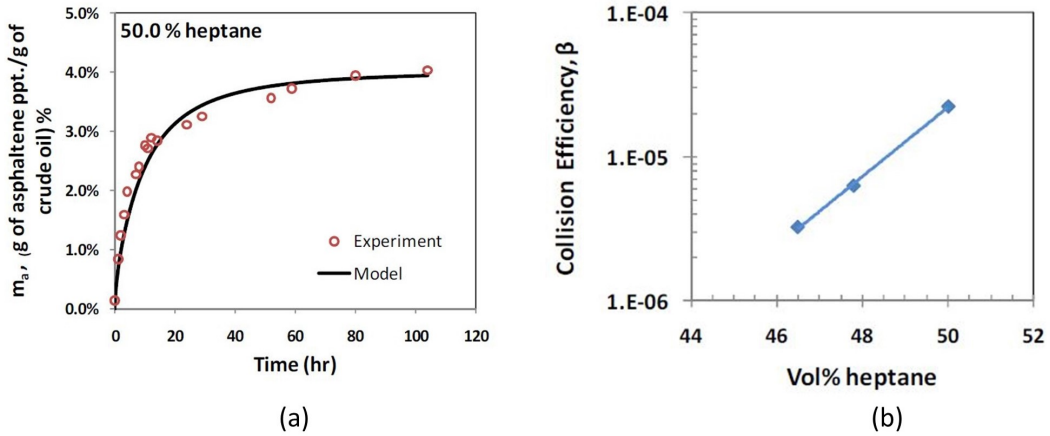

FIGURE 3.1: Reported by Maqbool et al. [28]
(a) Experimental and simulated increasing evolution of the mass of separated unstable asphaltenes (Equation 4.1
(b) Tuned collision efficiency as a function of heptane concentration in blends of crude oil and heptane.

Multiple authors followed a similar modeling approach based on the adjustment of a collision Kernel K_{ij} to study the effect of external parameters such as shear[37] or temperature[29]. Moreover, other investigators[18] derived a relation between the collision efficiency β_{ij} and the widely accepted driving force of colloidal flocculation[26;21]: $(\delta_{asph} - \delta_{solution})$. The postulated proportionality (Equation 5.3) published by Haji-Akbari et al.[18] collapsed many experimental data collected with several crude oils and various anti-solvent n-alkanes in a single master curve by tuning the unknown solubility parameter profile of asphaltenes.

$$\ln(t_{detection}\sqrt{C_1(0)}/\mu_{liq}) \propto \frac{1}{(\delta_{asph} - \delta_{solution})^2} \tag{3.7}$$

Literature review on destabilization kinetics

Despite the few publications found on destabilization kinetics, recent authors have investigated the effect of incorporation of destabilization kinetics into a population balance model[10]. Motivated by experimental observations of non-zero slopes in the plateau region, precedent attribution of time independent $C_1(0)$ values[28] was challenged by allowing a progressive appearance of destabilized asphaltenes. Indeed Duran et al.[10] modified the population balance model described in the previous paragraph by incorporating a mathematical term r_1 for the generation of primary particles over time. In their approach, the rate of change of the number concentration of primary particles is expressed as follows.

$$\frac{dC_1}{dt} = -C_1 \sum_{j=i}^{N-1} K_{1j}C_j + r_1 \tag{3.8}$$

Additionally, Duran et al.[10] made other modifications to represent the behavior of agglomerates larger than the micrometer size for contents of heptane higher than the instantaneous "onset" point. Authors[10] estimated Van Der Waals (VdW) forces with

Hamaker constants to modify the collision frequency of non-Brownian particles with an attractive term and their collision efficiency was made time-dependent ($\beta_{ij}(t)$. The authors have also improved the predictability of the particle size distribution at excessive heptane concentrations by introducing two input parameters:

- a micrometer scaled size of primary particles after 0.1s of solution aging
- a maximum fractal dimension.

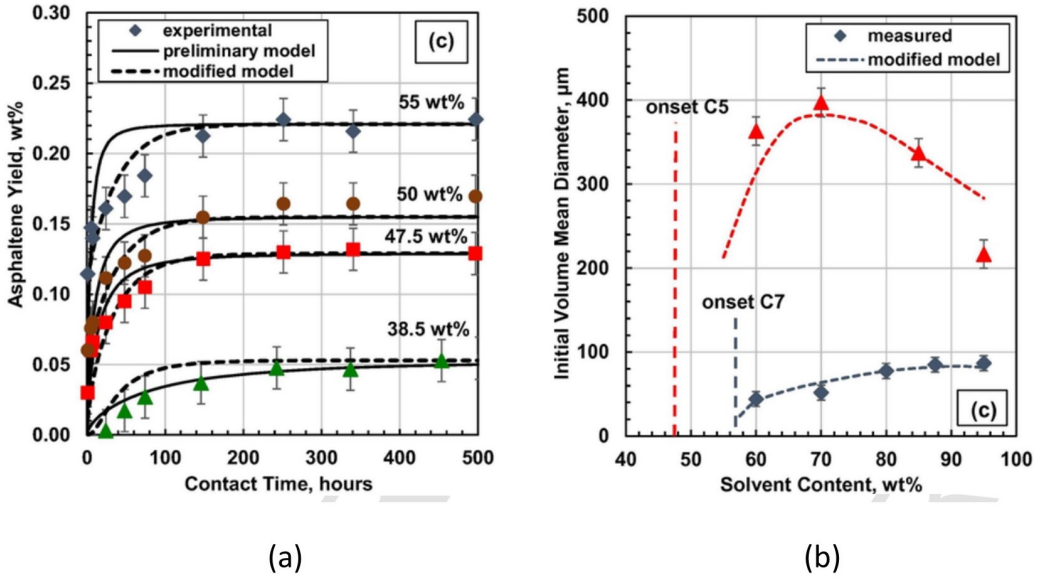

FIGURE 3.2: Reported by Duran et al. [10]
(a) Experimental and simulated evolution of the mass of separated unstable asphaltenes.
(b) Experimental and simulated average size of unstable asphaltenes as a function of flocculating agent concentration in blends of crude oil and solvent.

Although their results (see Figure 3.2) are in good agreement with experimental values, the use of multiple fitting parameters can raise doubts in the validity of some adjusted factors. In spite of the better agreement found between experiments and their population balance model by considering generation of particles, the factual existence of destabilization kinetics has not been demonstrated yet.

3.1.2 Aim of this work

As a result of the present literature review, we distinguish two phenomena upon volumetric addition of a bad solvent:

(i) destabilization is a generation of primary units with a characteristic radius of a few nanometers

(ii) aggregation is the process of agglomeration of primary and larger units evolving into larger aggregates.

Although the slow process attributed to aggregation may be revisited, the fundamental kinetic modeling of this part is well understood thanks to extensive research in the past decade [28;29;19] while only first insights of destabilization kinetics (time dependent generation of primary units) are drawn [10]. Nevertheless, the concentration of unstable constituents experiences a sharp increase upon addition of a flocculating agent at a particular concentration usually called the "onset point" of flocculation.

Bulk kinetics effects (including both destabilization and aggregation) cause a shift of this particular point of interest to predict deposition risks. The differentiation of destabilization and aggregation kinetics is accordingly an important point to clarify as it directly has impacts on applications to evaluate severity of industrial problems and could be implemented in remediation methods. As suggested by Duran et al. [10] in their aggregation modeling procedure, slow kinetics of destabilization would generate new unstable asphaltenes over time at fixed composition of oil and n-alkane mixture. Their generation rate constant k_N was set to $\sim 10^{-6} - 10^{-5} s^{-1}$ as opposed to previous studies where k_N was assumed infinitely large [14] compared to k_{agg}, the aggregation rate constant. In this work, we aimed to verify the above postulate of competing time-dependent phenomena: aggregation and destabilization. Direct experimental differentiation between the simultaneous destabilization and aggregation kinetics at the nanometer length scale is quite difficult, not to say impossible. Nonetheless, it is now established that destabilization is a precursor to deposition and that mass transport of unstable asphaltenes from a contact liquid toward a surface can be modeled considering diffusion-limited equation [40;13;23;17]. Consequently in this work, deposition was chosen to indirectly observe evidences of destabilization kinetics. Two available experimental devices were used to respectively probe asphaltene deposition at the macroscopic scale and at the sub-microscopic scale: 1) a packed-bed apparatus [40], 2) an immersed quartz crystal resonator (QCR) [8;34]. The comparison of the concentration of unstable asphaltenes (obtained by centrifugations) with both deposition experiments, along with an analysis of the deposition rates at several conditions provide answers to complete expectations with experimental evidences supported by a mechanistic study.

3.2 Methods

3.2.1 Sample preparation

Liquid solvents (e.g. n-alkanes) were 98+% purity supplied. The 3 dead crude oil samples later referred as crude oil A, B and C provided by operators from 3 different fields. All received samples were inspected by microscopy and by centrifugation to make sure that they were free from contamination of water, solid particles, production additives or drilling fluid. The preparation of crude oils and alkane mixtures at specified concentrations was as follows for all experiments (unless stated otherwise). Crude oil, n-alkane and vials were all incubated at the temperature of the study until reaching a stable temperature. A known volume of oil was placed into the vial. The solvent was added at 3 mL/min until the desired concentration was obtained. During the addition a good agitation was ensured with a magnetic stirrer to minimize localized high concentrations. The solution was then aged in a sealed vial and kept agitating at the temperature of interest during the entire study. All the liquid mixtures were prepared on a mass basis in order to increase the accuracy, final volume fractions were calculated using the respectively measured densities with a density meter (make Anton Paar model DMA 5000 M) at the temperature of work.

3.2.2 Measurement of microscopy detection-time

The microscopy detection-time corresponds to the tracking time of appearance of particles larger than 500 nm in a prepared blend of crude oil with a flocculating agent, measured by time-resolved optical microscopy [27]. For specific concentrations of heptane, Maqbool et al. [27] and Haji-Akbari et al. [19] found that the time for unstable

asphaltenes to reach a microscopical size varies linearly with the volume concentration of alkanes on a semi-logarithmic graphic. Aliquots of the prepared mixture are taken over time to observe them by shooting images with a CCD camera mounted on a consistently configured optical microscope with a 50x objective lens and a 10x eyepiece. The time it takes for solid opaque particles to be detected after heptane addition with this method is called the microscopy detection-time. The procedure is repeated at multiple concentrations of flocculating agent (heptane in this study) in order to obtain a detection-time curve typically ranging from a few minutes to 1000h. The lowest concentrations of n-alkanes for which the detection-time is less than 5 minutes is considered to be the instantaneous microscopy detection condition.

3.2.3 Measurement of the concentration of unstable asphaltenes

The content of unstable asphaltenes per unit volume of crude oil $C_A(t)$ is measured by the time-resolved centrifugation method reported by Maqbool et al.[27]. For the sake of simplicity, the total mass of separable unstable asphaltenes (larger than the cut-off size determined by the method described in Appendix) will be recalled as C_{A_t} when referring to a specific aging time. Aliquots of 1.5mL are taken over time from the prepared blend of crude oil and heptane. They are centrifuged for calculated periods of time at 24000x the relative centrifugal force (or g-force). The centrifugation time is calculated in order to keep the separation efficiency constant, depending on the density and the viscosity of the solution, and comply with a constant cut-off size of 100 nm (more details of the calculation is described in Appendix). The shortest aging that can be measured for the separation of unstables asphaltenes equals the sum of the time of preparation and the calculated centrifugation run-time that enables to collect Stokes particles larger than the mentioned cut-off size (here $\sim$ 100 nm). The minimum aging time with our centrifuge equipment (Eppendorf brand model 5418) is therefore between 20 minutes and 3h. Consequently, $C_{A_{3h}}$ will be assumed as an approaching value to $C_{A_{t\to 0}}$ for practical reasons in this study.
During centrifuge experiments, asphaltenes aggregates larger than the cut-off size are projected to the bottom of the centrifuge tube and can be collected as a "wet" cake (containing unstable asphaltenes and trapped liquid solution) by removing the supernatant at the end of the experiment. Traces of solution mixtures sticking to the inside walls of the centrifuge tubes are wiped with a cleaning tissue. The cake is then washed with heptane several times, re-dispersed and re-centrifuged until the supernatant remains transparent. The cakes are dried and their mass are recorded to calculate the concentration of "dry" unstable asphaltenes larger than the cut-off size per unit volume of crude oil. Indeed. one must note that the mass of collected asphaltenes with this method reflects a portion of the mass of the total number of created particles due to the washing out of the trapped solvent. This concentration of pure or "dried" unstable asphaltenes C_A increases with the aging time for a fixed mixture and eventually tends to a plateau region. By definition, the distribution size of unstable asphaltenes reaches an equilibrium and the variation of the separable matter over time is null when the plateau region is attained. The plateau value named C_{A_∞} is then estimated when the slope of C_A as a function of time can be lumped within experimental errors (usually few hours to hundreds of hours).
The goal of our study is to determine whether the evolution of C_A before reaching the plateau region is predominantly caused by ongoing aggregation or by slow destabilization. In the first eventuality, aggregation of a fixed number of initial particles makes existing small unstable particles grow larger than the cut-off size upon

aging, resulting in an increase of the separable mass. In the second possibility, unstable asphaltenes are generated over time, once formed their fast aggregation immediately brings them to stick to larger particles and will cause an increase of C_A . In this research, all the solutions have been aged for 750h as estimations resulted in a plateau region after 700h. For several oil-heptane compositions, only 3 aging points are measured: the first is the shortest time ($\sim$ 1-3 hours), the second after waiting 700h and the last point after 750h confirmed that the plateau region was reached at 700h. The two extreme times will provide 2 yield curves of "dry" separable material as a function of the heptane content. Any solution aged for a time comprised between those two extremes is expected to yield to an amount of unstable asphaltenes in between the extreme aging times.

3.2.4 Asphaltene deposition

Packed-bed experiment

The experimental set-up consists of a 40 cm long jacketed glass column (10 mm inner diameter). A total of 108 units of 3 mm-diameter and 440 units of 4mm-diameter SS316 stainless steel beads were disposed in the column in square close-packing motifs with centered small beads. The mixture is connected to a peristaltic pump in order to generate an upward flow in the packed-bed at a definitive flow rate. Identical mixtures are prepared to replace the previous one at frequencies ensuring the absence of particles larger than 500 nm (conditions cautiously chosen according to indications of the detection-time curve). Aliquots of the ongoing mixture are taken over time for microscopy verification for the entire duration of the experiment. The liquid is drained at a flow rate of 0.05g/min after the specified run-time has been reached. Chloroform is then streamed through the bed to collect the retained material composed of deposit (if any) and trapped liquid. The mass of deposit is obtained by measuring it after complete evaporation of the chloroform and by subtracting the collected mass of trapped liquid for a 1 min run-time experiment at the same conditions. Note that in order to collect a measurable weight, it usually takes liters of oil and days of experiment to access to results for one set of conditions. Figure 3.3 gives a schematic view of the apparatus.

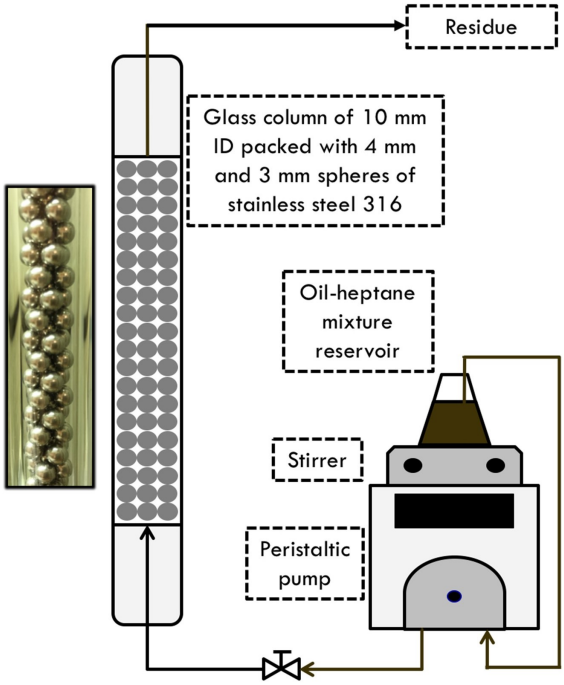

FIGURE 3.3: Packed bed asphaltene deposition apparatus[40]

Quartz crystal resonator immersed in a stirred tank reactor
The immersed QCR set-up that was used in this Chapter corresponds to the one described in Chapter 2. Heptane was used to favour the destabilization and deposition of asphaltenes. The continuous injection rate was set to 0.3 $cm^3.min^{-1}$ in an initial volume of 20 cm^3 of crude oil. 3 different overtones were monitored during experiments in order to determine the mass of deposit in the post-treatment data processing.

Deposition modeling
Principles of the surface deposition of asphaltenes comprehensively lean on a process limited by the rate of diffusion of unstable asphaltenes in the mass-transfer boundary layer that envelops the surface of deposition[40;13;23;17]. The local deposition rate is indeed physically materialized by a flux of unstable asphaltenes J_A toward the solid interface:

$$Rate_{dep} \propto J_A = D_A \frac{C_{A,d} - C_{A,s}}{\zeta_{\text{mass transfer}}} \tag{3.9}$$

where D_A is the diffusion coefficient of the asphaltenes depositing particles, $C_{A,d}$ is the concentration of unstable asphltenes available to deposit, $C_{A,s}$ is the concentration of unstable asphltenes at the surface of deposition and $\zeta_{\text{mass transfer}}$ is the thickness of the mass-transfer boundary layer. A mathematical simplification arises in Equation 3.9 from considering $C_{A,s}$ as a null value by rationally postulating that all the transported unstable particles that reach the wall necessarily deposit by a reaction process at a much larger rate than the mass transfer one in a diffusion-limited mechanism. The simplification on Equation 3.9 lets us write:

$$Rate_{dep} \propto C_{A,d} \tag{3.10}$$

It is important to note that $C_{A,d}$ is somewhat related to $C_A(t)$ and the relation must indirectly derive from a better understanding of kinetics. The presence of unstable asphaltenes available to deposit ($C_{A,d} > 0$) necessarily implies a positive quantity of unstable particles in the bulk ($\sum_{k=1}^{\infty} C_k > 0$).

3.3 Results and discussions

Microscopy detection-time

Following the procedure introduced by Maqbool et al.[27], the detection-time curve of particles that are $\sim 0.5\mu$m in diameter, provided in Figure 3.4, is an indication of the minimum range of composition at which the content of unstable asphaltenes and their size come into a macroscopic scale. In this study, the detection-time information was mainly used as an indication for the mixture reservoir replacement frequency during the packed-bed deposition runs.

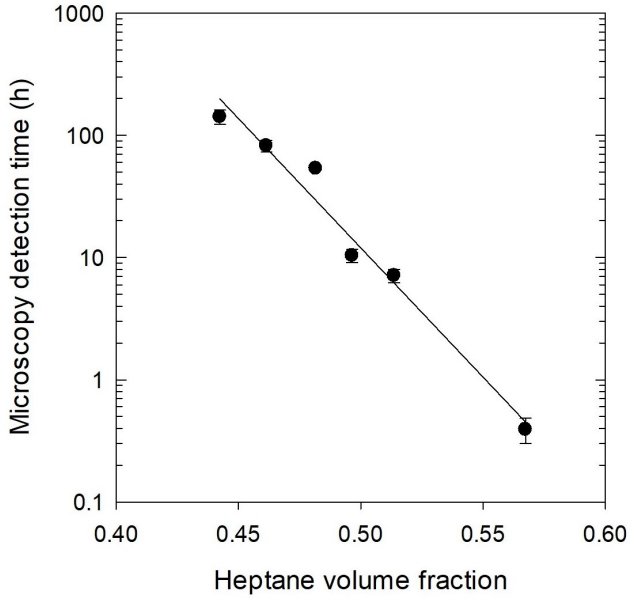

FIGURE 3.4: Necessary aging time to detect particles by microscopy visual observations as a function of the volume fraction of C_7 in heptane-oil blends

Separation of unstable asphaltenes

Content of unstable asphaltenes collected by centrifugation was studied as a function of the aging time for fixed compositions of crude oil and C_7 mixtures. Figure 3.5(*a*) reports the evolution of C_A for a mixture containing 51 vol% of C_7 in crude oil A, the plateau region is reached after aging the solution for more than 700h and C_{A_∞} is effectively estimated by extrapolating a fitted exponential trend curve.

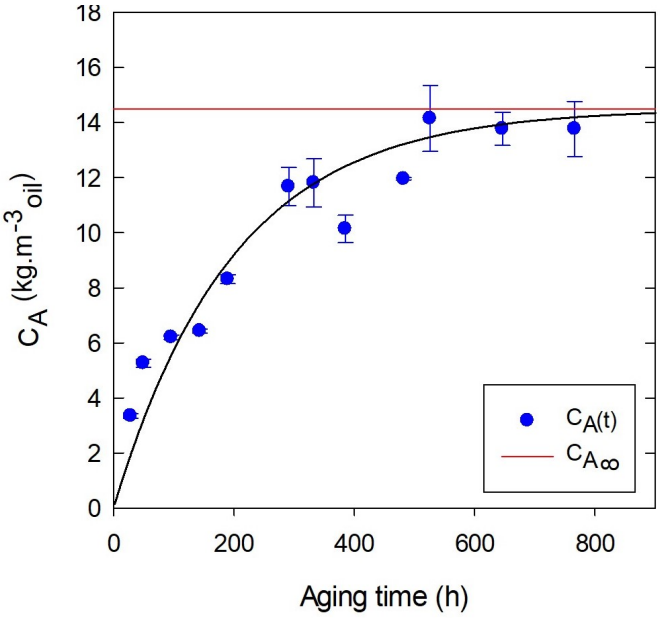

FIGURE 3.5: Concentration of unstable asphaltenes larger than 100 nm separated by centrifugation as a function of the aging time of a prepared blend of crude oil A and heptane (51 vol% C_7). Solid line is an exponential regression and markers are experimental data points.

Figure 3.6 reports the aging evolution of the concentration of separable particles of various heptane contents ranging from 48 vol% to 91 vol%. The same data are represented in two different ways (Figures (a) and (b)) respectively as a function of each variable; the aging time and the heptane content in the mixtures. As expected, for a given concentration of heptane in Figure 3.6(*b*), the total content of unstable asphaltenes is significantly smaller if considering destabilization kinetics compared to the values of C_{A_∞} at equilibrium of destabilization when waiting for long time enough after addition of the flocculating agent. In this particular example, the characteristic minimum aging time that was practically achieved is of 3h for solutions of oil and heptane.

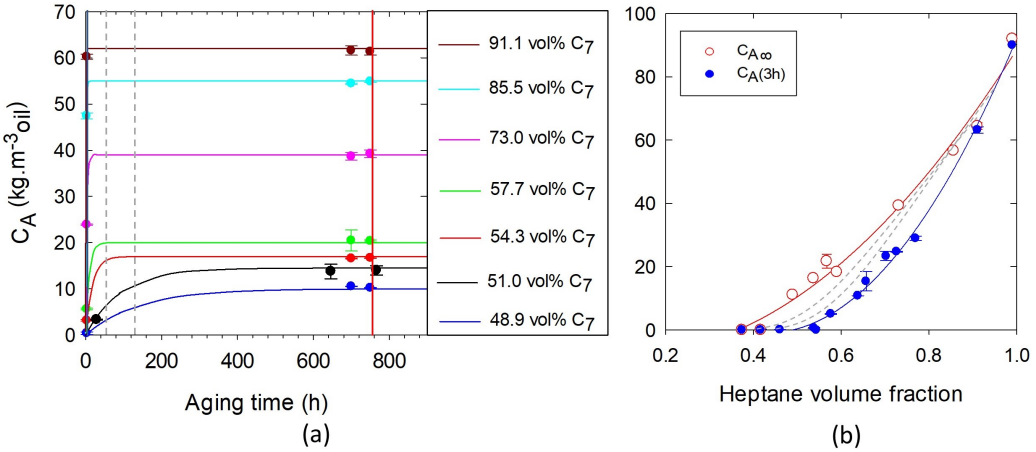

FIGURE 3.6: Concentration of unstable asphaltenes larger than 100 nm separated by centrifugation as a function of:
(a) the aging time of several blends of crude A and heptane at various contents of heptane
(b) the volume fraction of heptane in the blends for extremes of aging times: $\sim$ 3h ($C_{A_{3h}}$) and $\sim$700-750h (C_{A_∞})
Solid line is an exponential regression and markers are experimental data points.

Any yield curve corresponding to an aging between 3h and infinite time is hypothesized by the thin dashed curves in both Figures 3.6.

Packed-bed deposition results

Vilas Bôas Fávero et al.[40] extended the generic principles of the previous paragraph with established correlations of the mass transfer coefficient to derive Equation 3.11 for asphaltenes deposition rate in the packed-bed geometry:

$$Rate_{dep} = 6A_c^{1/2} d_b^{-3/2} \frac{(1-\theta)^{3/2}}{\theta} \rho_{liq}^{-1/3} \mu_{liq}^{-1/6} D_A^{2/3} q^{1/2} L C_{A,d} \tag{3.11}$$

where A_c is the cross-sectional area of the bed, L is its length, d_b is the mean diameter of the beads, θ is the porosity of the bed, q is the mass flow rate of the liquid mixture. The experimentally verified relation expressed by Equation 3.11 is coherent with a theoretically linear increase of the deposition rate with $C_{A,d}$. The dependence on the superficial velocity was also experimentally retrieved, which fundamentally confirmed a diffusion-limited regime. In their study, destabilization kinetics was neglected by adhering to suggestions of previous studies[28;18], thus they assumed the presently questioned equality between $C_{A,d}$ and C_{A_∞}, and found fair agreements between experimental results and the conceptual behavior.

In this model, the diffusion coefficient of depositing asphaltenes was the only adjusted parameter of the model. Equivalent size of diffusing asphaltenes aggregates was then back-calculated from the tuned diffusivities using the Stokes-Einstein Equation:

$$D_A = \frac{k_B T}{6\pi \mu_{liq} R_A} \tag{3.12}$$

where k_B is the Boltzmann constant, T is the temperature and R_A is the hydrodynamic radius of diffusing aggregates of unstable asphaltenes. Authors[40] obtained

radius ranging from 10 to 100 nm for 6 crude oils and for all the investigated conditions. This result is in excellent agreement with the absence of particles under microscopy observation during the experiment. Nevertheless, values obtained from Equation 3.11 and plotted in Figure 3.7 ($C_{A,d} = C_{A_\infty}$) are in conflict with the proportionality behavior expected by Equation 3.10. Actually, it is expected from Equation 3.10 that an extrapolated line should cross the origin of the graphic but it was not observed by considering fast destabilization kinetics.

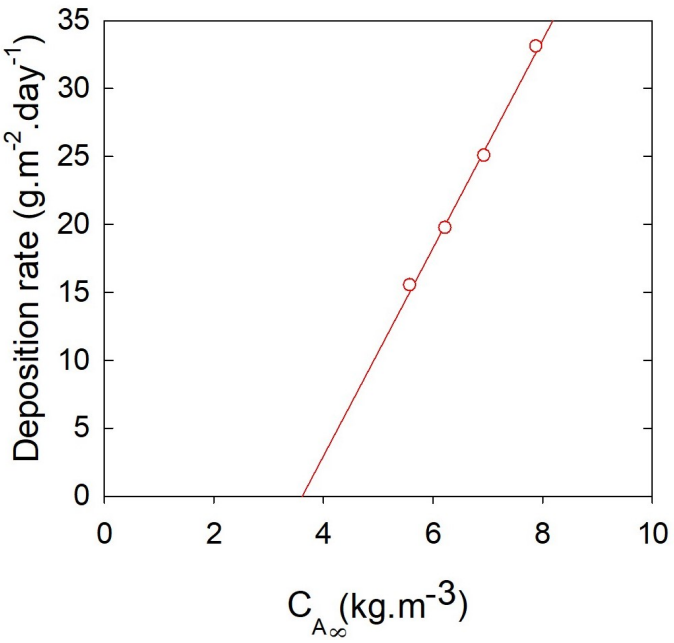

FIGURE 3.7: Experimental asphaltene deposition rate as a function of the plateau concentration (C_{A_∞}) of unstable asphaltenes in crude oil C and C_7 mixtures obtained from experimental set-up in Figure 3.3[40]; markers are experimental data and the solid line is a linear interpolation

As a repercussion of the centrifugation trends summarized by Figure 3.5, one can forecast that taking asphaltene destabilization kinetics into account would diminish the $C_{A,d}$ value by equalizing it to $C_A(t)$, thus shifting the line of Figure 3.7 toward values in better harmony with the theory. The aging time of the flowing mixtures through the packed-bed ranges between 0 and the time between each reservoir replacement. For practical reasons, in order to evaluate effects of the destabilization kinetics, the aging time of centrifuged mixtures was chosen equal to the time between each reservoir replacement during the packed-bed deposition experiments. Results displayed in Figure 3.8 are in excellent agreement with expectations and indicate that $C_{A,d} = C_A(t)$ should be posited in order to comply with the theoretical behavior. After the mixture was aged for a given time, results indicate that centrifuged-out masses provide a good approximation of the total content of unstable asphaltenes at the respective moment.

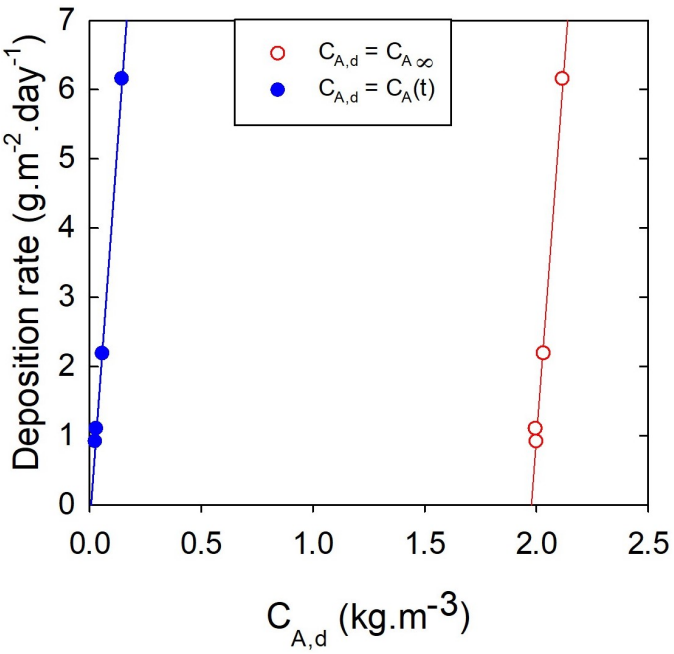

FIGURE 3.8: Asphaltene deposition rate as a function of the concentration of unstable asphaltenes in crude oil B and C_7 mixtures

We know from Figure 3.6 that C_{A_∞} value is necessarily larger than $C_A(t)$ for any mixture of oil and a flocculating agent. Consequently, accounting for destabilization kinetics must engender larger tuned diffusion coefficient of depositing particle according to Equation 3.9. Therefore, revising the results of Vilas Bôas Fávero et al. [40] with incorporating the destabilization kinetics would lead to even smaller-in-size depositing particles for each studied case. Particle sizes would therefore still be in agreement to the microscopy observations (absence of micron-sized particles). In order to verify this trend, reciprocal results were obtained by strictly applying their method [40]. Two mixtures of different oil-heptane compositions were specifically chosen in the range of composition exhibiting large differences between $C_A(3h)$ and C_{A_∞} (51 and 55 vol% of heptane as showed in Figure 3.6(b)). The diffusion-limited model presented in Equation 3.11 was able to match experimental data with the set of parameters summarized in table 3.1. In this experiment, the replacement of the reservoir mixture was made every hour and every 3h, respectively for the 51 and 55 vol% of heptane contents. Results of both conditions are presented in the following Figure:

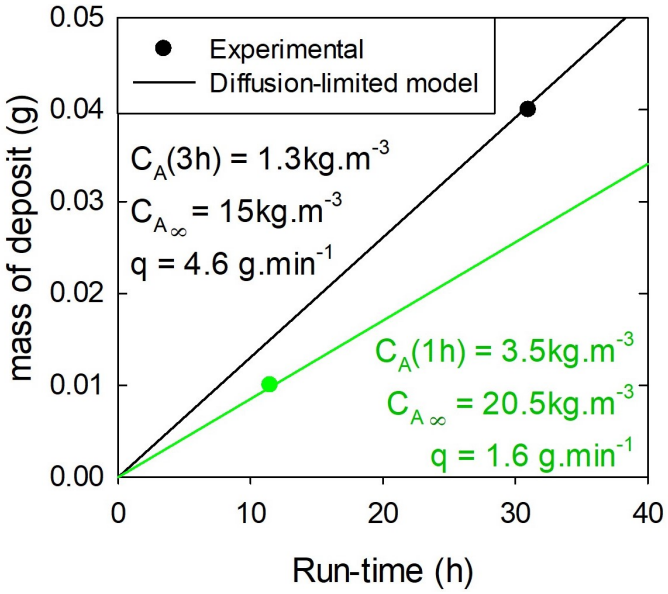

FIGURE 3.9: Deposited mass of asphaltenes as a function of the run-time in the packed-bed experiment for volumetric concentrations of heptane equal to 51 vol% (black) and 55 vol% (green)

TABLE 3.1: Particle diameters calculated by the Stokes-Einstein equation from the set of parameters used in Equation 3.11 to match the deposition experimental data

Destabilization kinetics	C_7 **concentration**	$C_{A,d}$	**Diffusion coefficient**	**Asphaltene particle diameter**
-	$vol\%$	$kg.m^{-3}$	$(m^2.s^{-1})\mathbf{x}10^{-12}$	nm
$k_N \rightarrow \infty$	51	15	0.36	850
$C_{A,d} = C_{A_\infty}$	55	20.5	0.25	1400
$k_N << 1$	51	1.3	14.10	22
$C_{A,d} = C_{A_{3h}}$	55	3.5	3.50	100

It is important to note the incoherence of the resulting particle sizes for the cases of extremely fast destabilization ($C_{A,d} = C_{A_\infty}$), the calculated diameters are in conflict with the experimental observations by optical microscopy which certified the absence of particles exceeding 500 nm in diameter. However, the calculated hydrodynamic diameters of depositing unstable asphaltenes by considering slow destabilization kinetics reconcile to the microscopy observations. In addition, the comparison of sizes between both conditions logically indicates larger aggregate diameters at greater heptane concentration (100 nm compared to 22 nm).

Independently, one observes that the collected mass are very constrained ($\sim$ 10 - 100 mg) for an experimental duration situated within the order of days. Consequently, it is more suitable to use a technique that is sensitive to the length and mass scale of interest; i. e. the QCR experiment. The need for a sensitive technology is augmented by the fact that the concentration of asphaltenes in a crude oil can be as low as 0.1 wt%.

QCR results

Figure 3.10 reports the deposited mass (Equation 2.6) on the sensing electrodes upon addition of heptane in crude oil A up to 79 vol% within a duration of approximately 2h. The final cumulative recorded mass on both surfaces of the sensor is $\sim 2 g.m^{-2}$. In this experiment, one can see that the important departure of the curve (so-called "onset" point signaled by a red arrow) occurs after a titration time of approximately 1h. As the composition is continuously changed upon time, the titration time differs from the aging time concept presented in previous centrifugation results. As for the packed-bed reference time of aging equal to the reservoir replacement time, we can affirm that in the case of a continuous titration ; the corresponding average aging time of the solution mixture is necessarily less than the total run-time of the experiment. Actually the time of "onset" conditions of deposition corresponds to $\sim$ 59 vol% of heptane, the solution mixture was less than one hour old at this given composition.

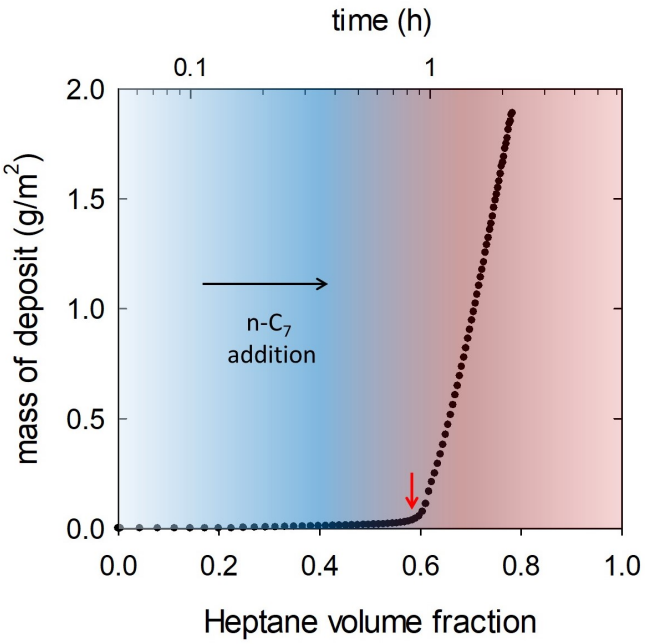

FIGURE 3.10: Asphaltene deposited mass as a function of the volume fraction of C_7 and run-time of the QCR experiment

In other words, if the mass concentration of unstable asphaltenes is immediately at equilibrium after addition of heptane, most of the unstable asphaltenes particle would have to be smaller than 100 nm (cut-off size of centrifugation) as they could not be observed in the centrifuged masses. As predicted by Equations 3.10 and 5.2, if a large enough number of particles are smaller than 100 nm, they should likely contribute to the diffusive deposition and engage a sharp increase of the detected deposit by the nano-sensitive sensor. In accordance to the hypothesized increase of deposited mass caused by the amplified concentration of unstable asphaltenes suspending in the surrounding solution, it becomes interesting to compare the point of departure of the centrifugation curves (at extreme aging times, i. e. short = 3h and long = 700h) to the mass of deposit recorded. The firm growths of the time-dependent separated unstable asphaltenes and of the deposit during the titration appear at a nearly coincident volume fraction of heptane, as opposed to the separated mass of particles from solutions aged for longer than 700h.

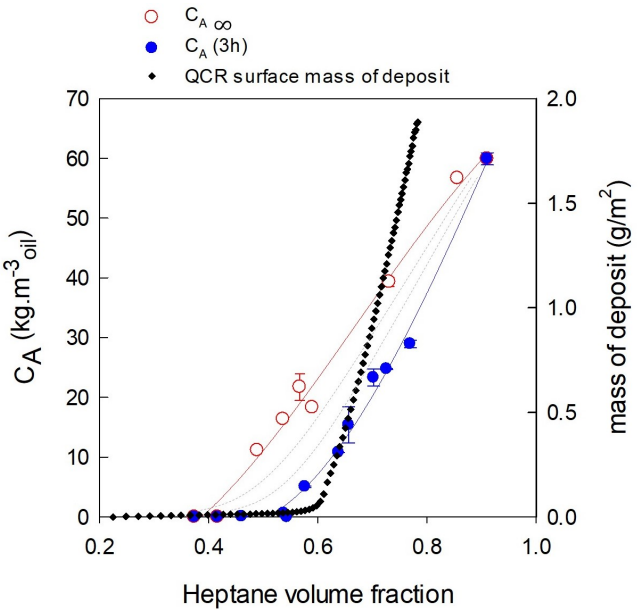

FIGURE 3.11: Comparison of asphaltene deposited mass profile to the centrifuged concentrations of unstable asphaltenes as a function of the volume fraction of C_7

The measured deposition on the QCR during the titration of heptane further complements observations in the packed-bed apparatus. Indeed, the consistency of results reinforces the notion of process controlled by the destabilization kinetics over the kinetics of aggregation. In addition, the aging time of the mixture in which the sensor was immersed being less than 1h at the particular composition (∼59 vol%), the departure of the curve is lightly shifted to larger C_7 fraction compared to the centrifuged $C_{A_{3h}}$.

3.4 Mathematical modeling of destabilization with kinetics

In previous paragraphs, we have examined bulk separation and surface deposition data to experimentally examine the limiting process of the quantitative growth of unstable asphaltenes upon time in fixed mixtures. The results suggest that the generation rate constant k_N is less than the aggregation rate constant k_{agg} of unstable asphaltenes. The increasing mass of separated material is then belonging to newly generated particles rapidly becoming larger than the cut-off size of 100 nm. Other terms, such as the dissociation by shear forces or the adhesion and inter-particles attraction forces will likely affect the larger orders of particle sizes and can be neglected to analyze our centrifugation data. In the present section, letting k_{agg} be significantly larger than k_N implies the generation term to be the main mathematical kinetic parameter.

Destabilization kinetics in mixtures of fixed composition over time

According to experimental observations, the rate of destabilization r_1 appears as proportional to the rate of concentration increase observed in curves of C_A versus time (Equation 5.16). The heptane content 51 vol% in heptane-crude oil (reported in Figure 3.5 is taken as an example case with a large number of data. The rate of primary units generation can be estimated by the local increments of separated

concentration ΔC_A over an increment of time Δt. As illustrated by Figure 3.12 for this example; k_N ranges from 10^{-6} s^{-1}, a few minutes after last addition of C_7, to 10^{-7} s^{-1} at aging times larger than 700h.

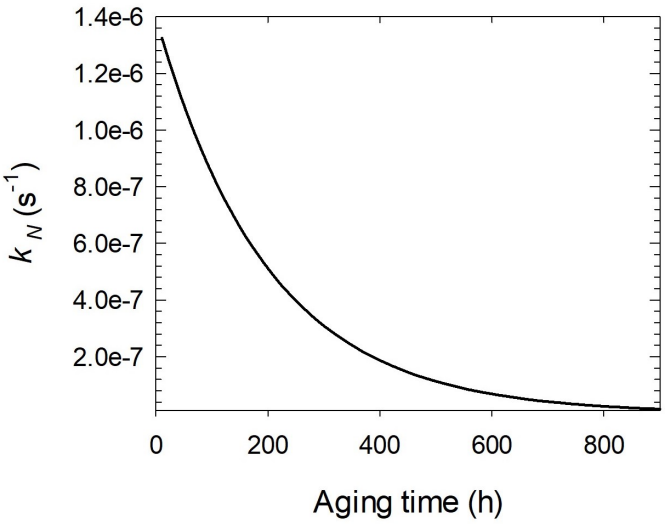

FIGURE 3.12: Evolution of the constant of unstable asphaltenes generation k_N for an aged mixture of C_7 and crude oil A with 51 vol% of heptane

The range of generation constant found at conditions approaching the "onset" agrees with reported values of $\sim 10^{-6}$ s^{-1} by Duran et al.[10]. Besides, our results indicate a strong time-dependence with a notable abrupt decay of k_N shortly after the addition of heptane was completed. In addition, the profile of k_N must also be a function of the solvent quality (volume fraction of the added alkane). With extensively reported trends of centrifugation data similar to Figure 3.5, we observed that k_N has the following mathematical form:

$$k_N = \frac{1}{\tau}\left(1 - \frac{C_{A_i}}{C_{A_\infty}}\right) e^{-\frac{t}{\tau}} \tag{3.13}$$

where C_{A_i} is the initial concentration of previously destabilized asphaltenes and τ is a coefficient representing the characteristic time of equilibration of a system with a given composition. In other words, the value of τ will determine the time at which k_N will fall to insignificant values such that generation will become negligible and the plateau region will be reached. The set of parameters τ and C_{A_∞} will dictate the initial slope of k_N when aging a given solution. Both parameters depend on the initial thermodynamic driving force: the anti-solvent concentration.
In this way, by replacing k_N in Equation 5.16, the mass balance of unstable asphaltenes in a prepared solution of crude oil and alkane is:

$$\frac{dC_A}{dt} - C_{A_\infty}\frac{1}{\tau}\left(1 - \frac{C_{A_i}}{C_{A_\infty}}\right) e^{-\frac{t}{\tau}} = 0 \tag{3.14}$$

Integrating Equation 3.14 with the initial conditions $C_A(0) = C_{A_i}$ for an aged solution with a fixed composition at the initial time t_i until the final time, we get:

$$C_A(t) = (C_{A_\infty} - C_{A_i})\left(e^{-\frac{t_i}{\tau}} - e^{-\frac{t}{\tau}}\right) \tag{3.15}$$

Equation 3.15 is then applied to separated asphaltenes by centrifugation with the following initial conditions:

$$t_i = 0$$
$$C_{A_i} = 0$$
$$C_{A_\infty} = C_A(700\text{h})$$

With those bound conditions, Equation 3.13 reduces to:

$$k_N = \frac{1}{\tau} e^{-\frac{t}{\tau}} \tag{3.16}$$

and Equation 3.15 becomes:

$$C_A(t) = C_{A_\infty} \left(1 - e^{-\frac{t}{\tau}}\right) \tag{3.17}$$

The only unknown parameter, the constant τ, is adjusted for each composition of oil-heptane such that the modeled concentration of unstable asphaltenes at early times (aging less than 700h) fits the separated amount by centrifugation. As shown in Figure 3.13, good agreements are found between the measured concentration of unstable asphaltenes and the calculated curves.

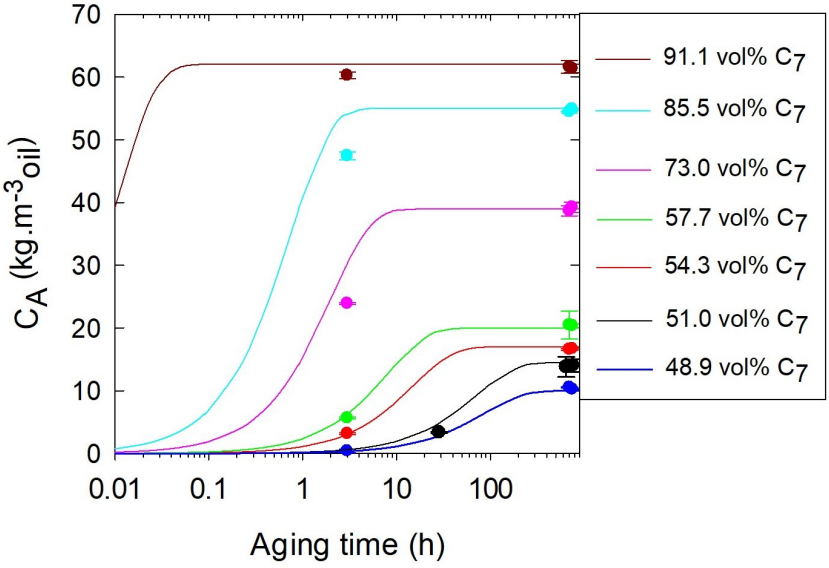

FIGURE 3.13: Concentration of unstable asphaltenes as a function of the aging time for several concentrations of heptane in the blend of crude oil-heptane; symbols are measured data by centrifugation and solid lines are modeled with Equation 3.15.

Consequently, the yield of unstable asphaltenes is function of both variables; the aging time and the composition of the solution. As explained, the dependence on the aging time of the solution is incorporated through the parameter τ whereas C_{A_∞} fixes the plateau value. In order to reach a continuity through the entire range of concentrations of heptane, we must define continuous dependencies of both parameters on solution compositions. Despite the limited range covered by the experimental data (due to practical reasons) within the possible compositions, regression analyses showed in Figure 3.14 produce the following power relationships as a function of

the anti-solvent volume fraction ϕ_{C_7}:

$$\tau = \tau_{max} {\phi_{C_7}}^{c} \tag{3.18}$$

$$C_{A_\infty} = C_{A_{max}} {\phi_{C_7}}^{b} \tag{3.19}$$

where τ_{max} and $C_{A_{max}}$ are respectively the equilibration time and the total content of separable material at infinite dilution of crude oil in the alkane, b and c are oil-dependent constants that must be determined by Equations 3.18 and 3.19 to match the experimental data.

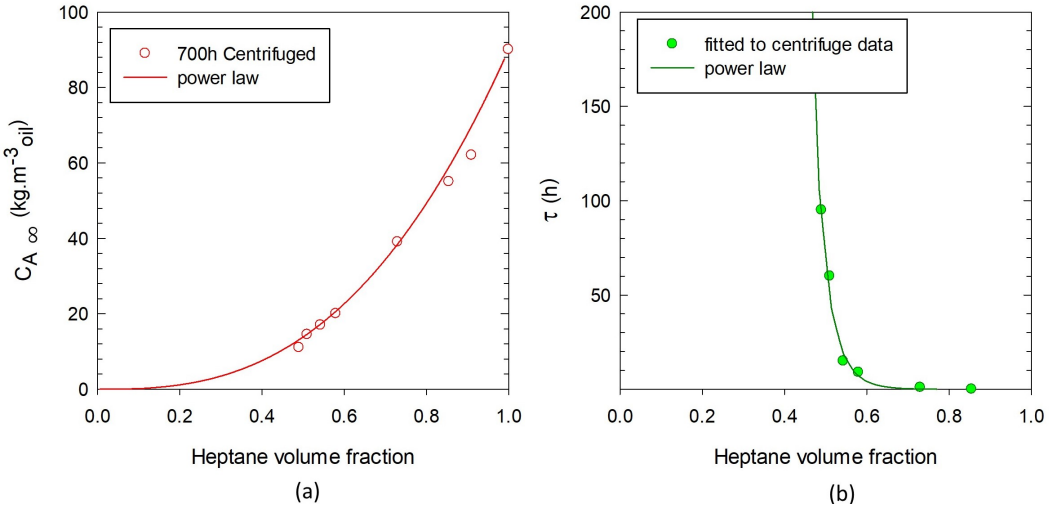

FIGURE 3.14: (a) Plateau concentration of unstable asphaltenes C_{A_∞} and (b) constant of destabilization kinetics τ as functions of the volume fraction of heptane in the blend of crude oil-heptane; symbols are measured data by centrifugation and solid lines are calculated with Equations 3.18 and 3.19.

We note that the adjusted parameter τ is significantly lower than 700h for the experimentally investigated conditions. This comparison confirms that experimental consideration of a reached equilibrium for the acquired data after waiting for 700h or longer is a fair approximation.
With the proposed scaling laws, the immense polydispersity of asphaltenes is described as a compositional continuum. After adjusting functions of τ and C_{A_∞} with experimental data, the mass rate at which components will leave the solution can be calculated by substituting parameters from Equations 3.18 and 3.19 into Equation 3.15. Calculations are plotted in Figure 3.15 which reports results of independent mixtures (assuming each composition prepared individually at t_i=0) for several aging times.

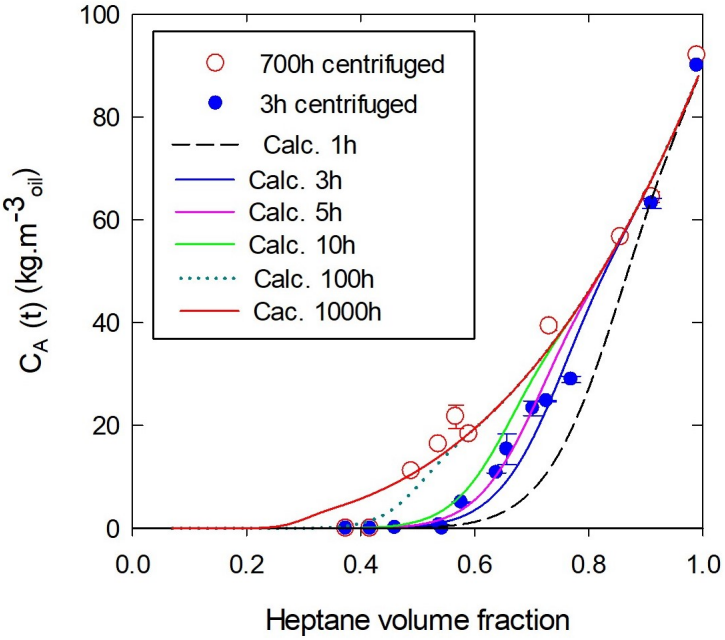

FIGURE 3.15: Concentration of unstable asphaltenes C_A versus the heptane content for solutions aged for different times

A good agreement is observed between the 3h aged experimental data points and the modeled curve. The pairs of composition and aging time conditions all logically show calculated concentrations of unstable asphaltenes inferior or equal to the assumed plateau values (t_{aging} >700h).
A sensitivity analysis (see Figure 3.16) of the generation constant k_N is made by independently varying the aging time and the heptane fraction of the solution.

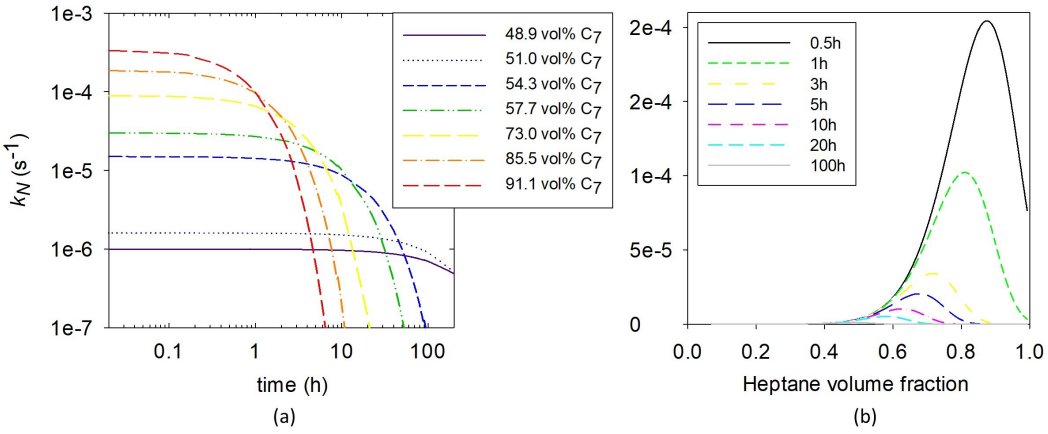

FIGURE 3.16: Sensitivity analysis of the unstable asphaltenes generation coefficient k_N as a function of:
(a) the aging time for solutions containing various contents of heptane
(b) the heptane content for solutions aged for different times

The plotted results indicate 4 important tendencies:

- the maximum generation rate of primary particles monotonously decreases with the aging time of a fixed solution and takes its maximum value immediately after the addition of heptane

- the generation rate remains relatively constant during a certain period of time for fixed solution mixtures
- the equilibrium is reached after waiting shorter periods as the heptane content gets larger
- the initial generation rate is increased for larger heptane volumetric contents.

Destabilization kinetics during continuous variation of the volumetric mixture composition

In the following analysis, we will be interested in destabilization when caused along a continuous addition of heptane, in reference to the industrial case where destabilization is caused by expansion of light constituents. The change of stability must then be encouraged by the steady change in solubility parameter of the solution ($\Delta\delta_{\text{solution}}$) during the flow. As previously said for the titration experiment, it is complicated to isolate the aging time in such a cases. In this situation, the whole unstable fraction of asphaltenes becomes partially composed of older and fresher units. According to the sensitivity analysis of k_N in the previous paragraph, the unceasing volume expansion of bad solvent must promote the particles generation at a faster rate than the aging effects by recreating a non-aged fraction of unstable asphaltenes. Destabilization kinetics and aging functions should then be interdependent with the rate of change of solvent properties. In order to decouple the various scales of time, the process can be discretized in series of durations upon which only aging occurs without any change of composition. At each change of time step, new initial and final conditions (t_i, t_f, C_{A_i}, τ and C_{A_∞}) must be defined to solve Equation 3.15 during the actual aging.

As illustrated by the example on Figure 3.17, punctual additions of heptane can be modeled by finding the appropriate initial and final times. Finding the corresponding aging time of the new composition that equalizes the actual C_A as if it was prepared at initial time zero will let us solve the integration through corrected limits t_i and t_f at each step. Rearranging Equation 3.15, we then find:

$$\begin{aligned} t_i(t+\Delta t) &= -\tau ln\left(1-\frac{C_A(t)}{C_{A_\infty}}\right) \\ t_f(t+\Delta t) &= t_i(t+\Delta t)+\Delta t = -\tau ln\left(1-\frac{C_A(t)}{C_{A_\infty}}\right)+\Delta t \end{aligned} \tag{3.20}$$

Substituting the found limits of Equation 3.20 into Equation 3.15, it then becomes:

$$C_A(t+\Delta t) = (C_{A_\infty}-C_A(t))\left[\left(1-\frac{C_A(t)}{C_{A_\infty}}\right)\left(1-e^{-\frac{\Delta_t}{\tau}}\right)\right] \tag{3.21}$$

In this way, the adjusted parameters are kept with the same dependence on both the aging time and the heptane fraction for the appropriate time interval corresponding to fixed solutions in composition. τ and C_{A_∞} are re-calculated at each step of time with the set of Equations 3.18 and 3.19 for successive compositions of oil-heptane in order to solve the problem numerically.

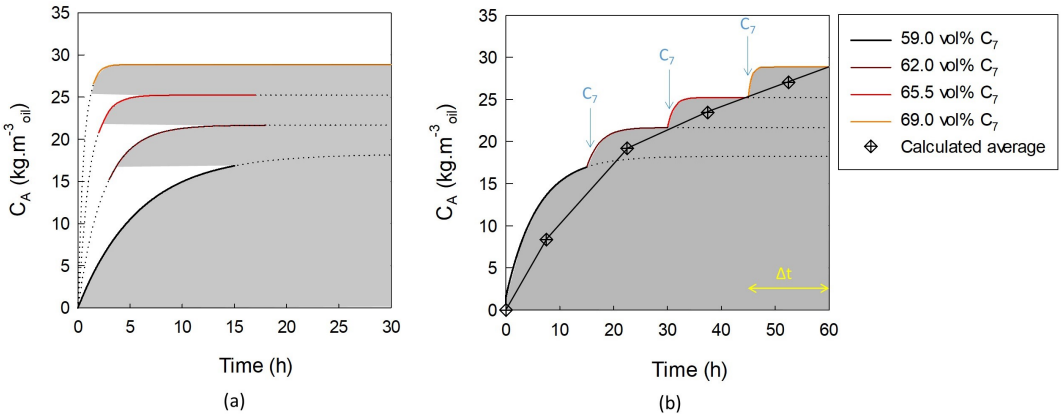

FIGURE 3.17: Comparison of the modeled evolution of the total concentration of unstable asphaltenes C_A as a function of time for:
(a) independent solutions prepared at time = 0
(b) a tracked solution with series of step additions of heptane

Assuming that the composition does not change during the incremental time, an average C_A is attributed to the ongoing composition. One observes that for non-linearizable C_A profiles at successive conditions, the choice of too large Δt in Equation 3.21 can significantly underestimate the amount of unstable asphaltenes. However, when choosing an adapted temporal discretization (short enough) to the rate of change of solution, the errors become lesser as Δt is decreased and the profile is fairly represented through series of linearizable regions as showed by Figure 3.18.

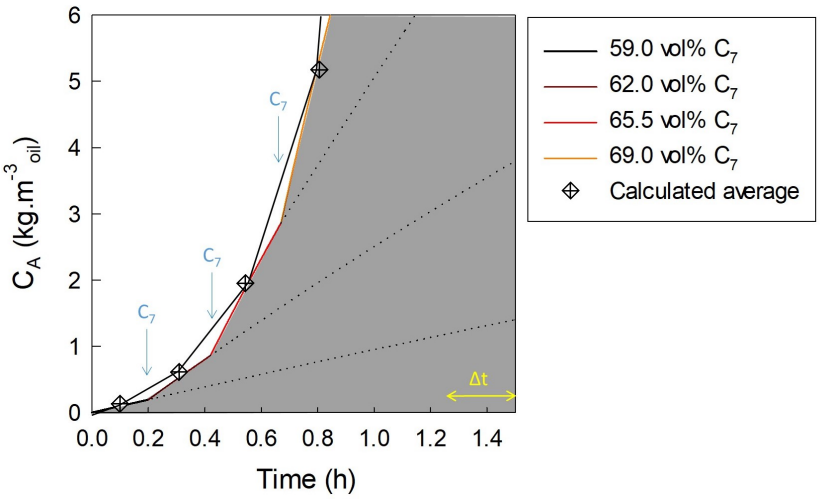

FIGURE 3.18: Modeled evolution of the total concentration of unstable asphaltenes C_A as a function of time during the continuous addition of heptane at a flow rate q_{C_7} = 0.3 cm^3.min^{-1}

The applicability of this estimation is appraised by simulating an incremental time equal to the typical order of elapsed-time between the records of the immersed QCR data ($\sim$ 0.02h to 0.2h). The obtained average values are then plotted in Figure 3.19 to compare to simulations with much shorter time steps. We find that this practice enables to estimate the evolution of the unstable asphaltenes concentration without error propagation.

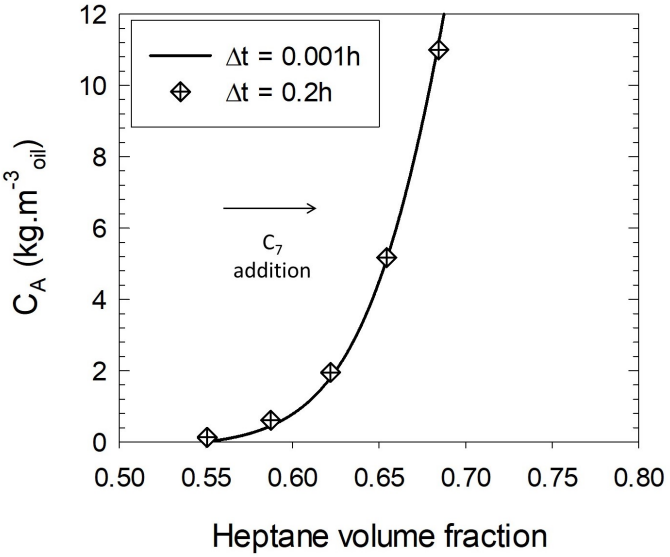

FIGURE 3.19: Modeled evolution of the total concentration of unstable asphaltenes C_A as a function of the heptane fraction during the continuous addition of heptane at a flow rate q_{C_7} = 0.3 cm^3.min^{-1}

The calculated profile shows a good match when compared to experimental data obtained by centrifugation after addition of heptane was steadily ensured at a rate of 0.2 g.cm^{-3}. Starting with a given mass of crude oil (18 g), the experiment was repeated to reach different compositions. We should note that due to the additional handling and centrifuging times, the aging of samples are 20 minutes longer than if we were to instantaneously separate asphaltenes while the titration is running. An excellent agreement between the model calculation and the centrifugation data is depicted in Figure 3.20.

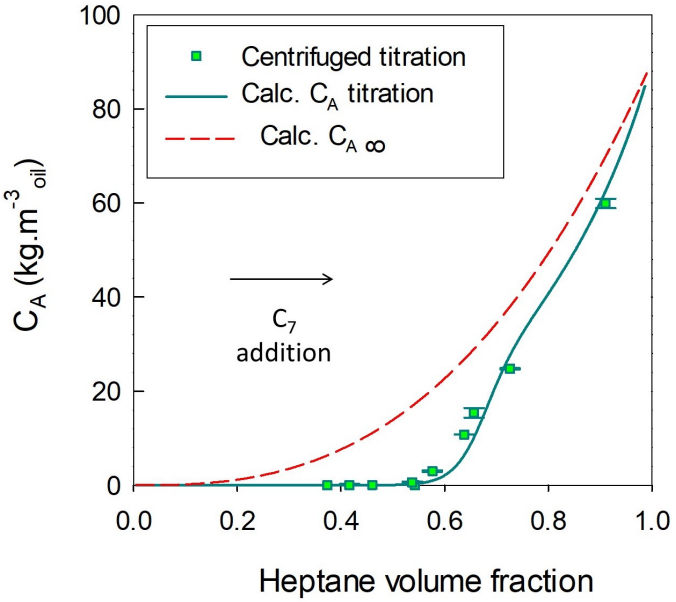

FIGURE 3.20: Comparison between experimental and modeled evolution of the total concentration of unstable asphaltenes C_A as a function of the heptane fraction during the continuous change of composition at a flow rate q_{C_7} = 0.2 cm^3.min^{-1}

The aging time of the liquid solution is naturally linked to the rate of composition variation and to the residence time of the fluid in the system for an open loop flowing mixture. In a closed system with volume expansion, three competing effects should be captured in modeling the expansion of an alkane: (i) elevated addition rates will promote larger generation rates of unstable asphaltenes, (ii) larger addition rates will shorten the aging time of the solution through the experiment and should result in lower cumulative C_A during the experiments, (iii) the dilution effect during the alkane extension reduces the generation rate by cutting down the number of asphaltenes per unit volume of solution. The generation constant k_N is incrementally assessed by using Equation 3.13 with setting $C_{A_i(t)} = C_A(t - \Delta t)$.
The expected behavior is verified in Figure 3.21. Indeed, cumulative effects due to increased aging put the concentration curve with the slowest addition rate above the two others, however the greater generation rates are found when the bad solvent is added at the fastest pace. We also note that due to the mentioned competing effects, the generation rate goes through a maximum value at different heptane volume contents depending on the speed of heptane inclusion.

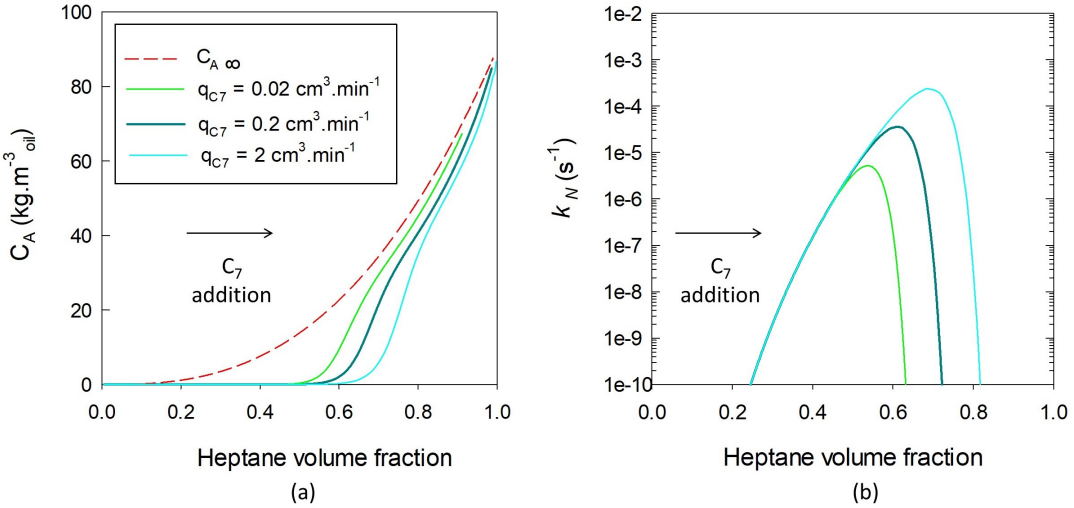

FIGURE 3.21: (a) Calculated profiles of C_A with Equation 3.21 for several rates of addition of heptane
(b) Calculated constant of unstable asphaltenes generation k_N upon continuous volumetric addition of heptane at several rates

During the titration, the rate of particle generation increases until reaching its maximum value. This first part, combined to the augmenting equilibrium concentration C_{A_∞}, provokes the amount of unstable asphaltenes to sharply engage into a large slope versus the heptane fraction. Logically, when k_N decreases, less primary particles are generated per unit of time and the slope of C_A becomes less important. Subsequent values reported in Figure 3.21(b) support that the simultaneous promotion of heptane results in larger generation of primary units of unstable asphaltenes over time than the sole aging effect.
Finally and as expected, the results indicate that the rate of asphaltenes destabilization is controlled by the rate of volume expansion of flocculating agents.

Relation between destabilization kinetics and deposition
As the aggregation rate is suggested extremely fast compared to the generation rate of unstable asphaltenes; the diffusive deposition rate of asphaltenes should evolve

into a dependence on the rate of generation of unstable asphaltenes. The generated entities might constitute the fraction of few remaining small particles which have large diffusion coefficients. The recorded mass of deposited material on the quartz sensor during the continuous addition of heptane gives us access to local deposition rates along the titration:

$$rate_{deposition} = \frac{\Delta m_{deposit}}{\Delta t} \tag{3.22}$$

As time elapses during the experiment the cumulative deposit grows, however the deposition rate interestingly passes through a maximum value. As graphically analyzed in Figure 3.22 (a), the composition at which the maximum deposition rate is measured nearly coincides with the maximum calculated generation constant k_N using Equation 3.13 from centrifugation data. We note that those conditions also correspond to the significant increase of concentration of unstable asphaltenes (Figure 3.22(b))

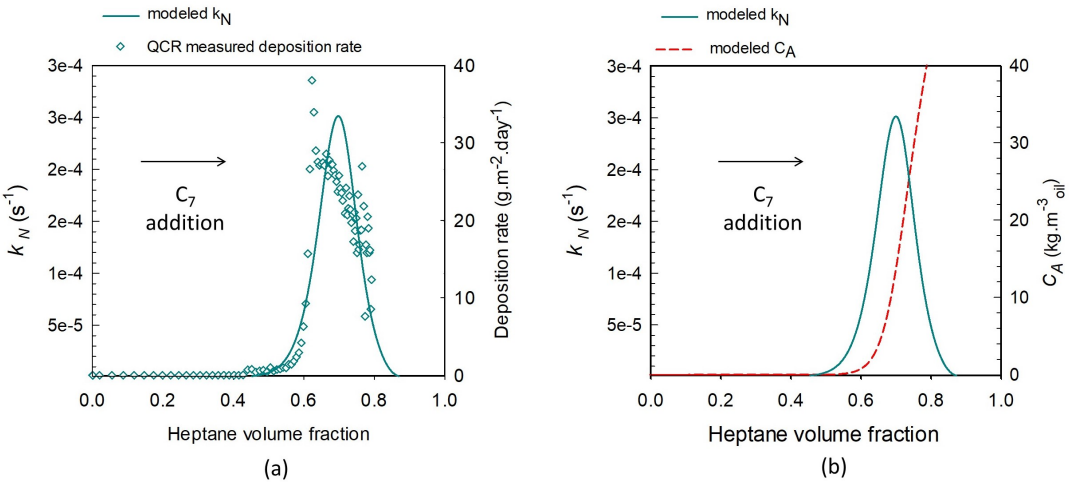

FIGURE 3.22: (a) Comparison of the calculated generation constant of unstable asphaltenes generation k_N upon continuous volumetric addition of heptane to the deposition rate of unstable asphaltenes (b) Calculated profiles of C_A with Equation 3.21 using the generation constant rate of unstable asphaltenes k_N during addition of heptane

The generation of unstable asphaltenes promises to play an important role in the deposition process and necessitate further investigations in order to jointly elucidate the mechanisms of destabilization, aggregation and deposition.

3.5 Conclusions

Deposition measurements by two different techniques combined to time-resolved centrifugation results recommend that the evolution of separable mass of unstable asphaltenes over time is mainly driven by the destabilization kinetics (and secondarily by the aggregation kinetics). According to this study, the Brownian collision of unstable particles thereupon is suggested to have a larger efficiency than values reported in the literature[28], perhaps approaching 100% at conditions of instantaneous flocculation.

Consequently the total mass concentration of unstable asphaltenes is not constant over time for a fixed mixture and should not be termed as the initial concentration

of primary units $C_1(0)$. The existing models that are developed based on the assumption that destabilization attains immediate equilibration while aggregation is a slow process can provide misleading and overestimating predictions about the amount of unstable asphaltenes. In support to those conclusions, excellent proportional relation between the deposition rate in the packed-bed apparatus and the time dependent concentration of "dry" unstable asphaltenes is observed with an experimentally estimated $C_A(t)$, for sets of conditions at given times, with single centrifugation runs per condition (calculated cut-off size of $\sim$ 100 nm).
With this observation, a mathematical model was proposed to calculate the constant of generation k_N with two adjusted parameters on regression power laws; (i) the equilibrium concentration C_{A_∞} and (ii) the characteristic time of equilibration τ. Both parameters are dependent on the oil-heptane mixture composition. The applicability of the analytical calculations was first appraised by comparison with experimental data of fixed mixtures of crude oil and heptane prepared at time = 0 and evolving over aging times up to 700h.
Additionally, an iterative method was proposed to calculate the mass concentration of "dry" unstable asphaltenes during the continuous change of composition together with the effect of destabilization kinetics. Based on an interative integration with corrected initial and final conditions at each time interval, the calculations showed fair agreements with centrifuge laboratory data. The sensitivity analysis of the particle generation rate provided expected trends with larger constants as the heptane fraction is increased and as the aging time is shortened. With this logic, for systems varying in composition, the generation of primary unstable asphaltenes is shown to have a strong dependence on the rate of heptane volumetric additin, making the consequent generation constant orders of magnitude larger than during the aging of a fixed mixture. This result has direct applications on the understanding of industrial problems, the volumetric rate of heptane content should be compared to the expansion rate of light constituents in the field (which has a direct relation to the pressure profile along the production network).
The indications of such results are beyond the concepts of destabilization and aggregation modeling, it has implications on the simulation approach of the deposition of asphaltenes in tubulars. It advises that comparing the sole concentration profiles of unstable asphaltenes at equilibrium as a function of the composition is not sufficient to evaluate the severity of diffusive deposition. The generation rate of primary unstable asphaltenes showed to have a strong similarity to the deposition rate against the heptane content. Such similarity was expected in a diffusion-limited deposition process as k_N parameter controls the number of small unstable asphaltenes available to deposit.
In the following Chapters, those concepts will be further evaluated with incorporating them into a coagulation model and a conventional deposition model will be designed. Indeed, the two following simplifications are valuable by cutting down the number of adjustable parameters in the modeling approaches. In the case of steady volume addition of a bad solvent, asphaltenes destabilization is promoted at an elevated pace all along the expansion as fresh promoting conditions are constantly being produced. A single yield centrifugation curve of the unstable asphaltenes can be used with accounting for the aging time of the fluid during its flow over a surface of interest. Both simplifications provide room to understand the major unclear points related to the deposition of asphaltenes:

- how to reduce the number of adjusted coefficients to quantitatively predict the deposition rate ?

- how to fundamentally relate destabilization caused by the addition of liquid alkanes to the expansion of light constituents dissolved caused by the pressure decrease ?

Finally, the immersed quartz crystal vessel showed promising results to study asphaltene deposition, it was able to quantify the deposit. Its sensitivity, in the order of micrograms, enables to study a continuous process of solvent addition that is analogous to the mechanism driven by depressurization in the industrial conditions. In such dispositions, the rate of change of solution properties ($\Delta\delta_{\text{solution}}$)is theoretically identified as a key parameter to the deposition of asphaltenes and will be further investigated in Chapter 5 and 6.

Bibliography

[1] Alboudwarej, H., J. Beck, W. Svrcek, H. Yarranton, and K. Akbarzadeh
2002. Sensitivity of asphaltene properties to separation techniques. *Energy & Fuels*, 16(2):462–469.

[2] Ancheyta, J., G. Centeno, F. Trejo, G. Marroquin, J. Garcia, E. Tenorio, and A. Torres
2002. Extraction and characterization of asphaltenes from different crude oils and solvents. *Energy & Fuels*, 16(5):1121–1127.

[3] Andersen, S. I.
1999. Flocculation onset titration of petroleum asphaltenes. *Energy & Fuels*, 13(2):315–322.

[4] Angle, C. W., Y. Long, H. Hamza, and L. Lue
2006. Precipitation of asphaltenes from solvent-diluted heavy oil and thermodynamic properties of solvent-diluted heavy oil solutions. *Fuel*, 85(4):492–506.

[5] Buckley, J. S.
1999. Predicting the onset of asphaltene precipitation from refractive index measurements. *Energy & Fuels*, 13(2):328–332.

[6] Buckley, J. S., G. Hirasaki, Y. Liu, S. Von Drasek, J. Wang, and B. Gill
1998. Asphaltene precipitation and solvent properties of crude oils. *Petroleum Science and Technology*, 16(3-4):251–285.

[7] Burya, Y. G., I. K. Yudin, V. A. Dechabo, V. I. Kosov, and M. A. Anisimov
2001. Light-scattering study of petroleum asphaltene aggregation. *Applied optics*, 40(24):4028–4035.

[8] Daridon, J. L., M. Cassiede, D. Nasri, J. Pauly, and H. Carrier
2013. Probing asphaltene flocculation by a quartz crystal resonator. *Energy & Fuels*, 27(8):4639–4647.

[9] David Ting, P., G. J. Hirasaki, and W. G. Chapman
2003. Modeling of asphaltene phase behavior with the saft equation of state. *Petroleum Science and Technology*, 21(3-4):647–661.

[10] Duran, J., F. Schoeggl, and H. Yarranton
2019. Kinetics of asphaltene precipitation/aggregation from diluted crude oil. *Fuel*, 255:115859.

[11] Érdi, P. and J. Tóth
1989. *Mathematical models of chemical reactions: theory and applications of deterministic and stochastic models*. Manchester University Press.

[12] Escobedo, J. and G. A. Mansoori
1995. Viscometric determination of the onset of asphaltene flocculation: a novel method. *SPE production & facilities*, 10(02):115–118.

[13] Eskin, D., J. Ratulowski, K. Akbarzadeh, and S. Pan
2011. Modelling asphaltene deposition in turbulent pipeline flows. *The Canadian Journal of Chemical Engineering*, 89(3):421–441.

[14] Fávero, C. V. B., T. Maqbool, M. Hoepfner, N. Haji-Akbari, and H. S. Fogler
2017. Revisiting the flocculation kinetics of destabilized asphaltenes. *Advances in colloid and interface science*, 244:267–280.

[15] Filbet, F. and P. Laurençot
2004. Numerical simulation of the smoluchowski coagulation equation. *SIAM Journal on Scientific Computing*, 25(6):2004–2028.

[16] Goual, L., M. Sedghi, X. Wang, and Z. Zhu
2014. Asphaltene aggregation and impact of alkylphenols. *Langmuir*, 30(19):5394–5403.

[17] Guan, Q., Y. Yap, A. Goharzadeh, J. Chai, F. Vargas, W. Chapman, and M. Zhang
2017. Integrated one-dimensional modeling of asphaltene deposition in wellbores/pipelines. In *Modeling, Simulation, and Applied Optimization (ICMSAO), 2017 7th International Conference on*, Pp. 1–6. IEEE.

[18] Haji-Akbari, N., P. Masirisuk, M. P. Hoepfner, and H. S. Fogler
2013. A unified model for aggregation of asphaltenes. *Energy & Fuels*, 27(5):2497–2505.

[19] Haji-Akbari, N., P. Teeraphapkul, A. T. Balgoa, and H. S. Fogler
2015. Effect of n-alkane precipitants on aggregation kinetics of asphaltenes. *Energy & Fuels*, 29(4):2190–2196.

[20] Hammami, A., C. H. Phelps, T. Monger-McClure, and T. Little
2000. Asphaltene precipitation from live oils: An experimental investigation of onset conditions and reversibility. *Energy & Fuels*, 14(1):14–18.

[21] Hansen, C. M.
2004. 50 years with solubility parameters—past and future. *Progress in Organic Coatings*, 51(1):77–84.

[22] Hirschberg, A., L. DeJong, B. Schipper, and J. Meijer
1984. Influence of temperature and pressure on asphaltene flocculation. *Society of Petroleum Engineers Journal*, 24(03):283–293.

[23] Kurup, A. S., F. M. Vargas, J. Wang, J. S. Buckley, J. L. Creek, J. Subramani, Hariprasad, and W. G. Chapman
2011. Development and application of an asphaltene deposition tool (adept) for well bores. *Energy & Fuels*, 25(10):4506–4516.

[24] Leontaritis, K. and G. Mansoori
1987. Asphaltene flocculation during oil production and processing: A thermodynamic colloidal model. In *SPE International Symposium on Oilfield Chemistry*, Pp. 4–6. Society of Petroleum Engineers Richardson, TX, USA.

[25] Leontaritis, K. J. and G. A. Mansoori
1989. Fast crude-oil heavy-component characterization using combination of astm, hplc, and gpc methods. *Journal of petroleum science and Engineering*, 2(1):1–12.

[26] Lindvig, T., M. L. Michelsen, and G. M. Kontogeorgis
2002. A flory–huggins model based on the hansen solubility parameters. *Fluid Phase Equilibria*, 203(1-2):247–260.

[27] Maqbool, T., A. T. Balgoa, and H. S. Fogler
2009. Revisiting asphaltene precipitation from crude oils: A case of neglected kinetic effects. *Energy & Fuels*, 23(7):3681–3686.

[28] Maqbool, T., S. Raha, M. P. , and H. S. Fogler
2011a. Modeling the aggregation of asphaltene nanoaggregates in crude oil- precipitant systems. *Energy & Fuels*, 25(4):1585–1596.

[29] Maqbool, T., P. Srikiratiwong, and H. S. Fogler
2011b. Effect of temperature on the precipitation kinetics of asphaltenes. *Energy & Fuels*, 25(2):694–700.

[30] Mitchell, D. L. and J. G. Speight
1973. The solubility of asphaltenes in hydrocarbon solvents. *Fuel*, 52(2):149–152.

[31] Mullins, O. C., E. Y. Sheu, A. Hammami, and A. G. Marshall
2007. *Asphaltenes, heavy oils, and petroleomics*. Springer Science & Business Media.

[32] Powers, D., H. Sadeghi, H. Yarranton, and F. Van Den Berg
2016. Regular solution based approach to modeling asphaltene precipitation from native and reacted oils: Part 1, molecular weight, density, and solubility parameter distributions of asphaltenes. *Fuel*, 178:218–233.

[33] Rogel, E.
2002. Asphaltene aggregation: A molecular thermodynamic approach. *Langmuir*, 18.

[34] Saidoun, M., T. Palermo, N. Passade-Boupat, J.-P. Gingras, H. Carrier, and J.-L. Daridon
2019. Revisiting asphaltenes instability predictions by probing destabiliztion using a fully immersed quartz crystal resonator. *Fuel*, 251:523–533.

[35] Seifried, C. M., J. Crawshaw, and E. S. Boek
2013. Kinetics of asphaltene aggregation in crude oil studied by confocal laser-scanning microscopy. *Energy & Fuels*, 27(4):1865–1872.

[36] Smoluchowski, M. v.
1918. Versuch einer mathematischen theorie der koagulationskinetik kolloider lösungen. *Zeitschrift für physikalische Chemie*, 92(1):129–168.

[37] Solaimany-Nazar, A. R. and H. Rahimi
2009. Investigation on agglomeration- fragmentation processes in colloidal asphaltene suspensions. *Energy & Fuels*, 23(2):967–974.

[38] Tavakkoli, M., M. R. Grimes, X. Liu, C. K. Garcia, S. C. Correa, Q. J. Cox, and F. M. Vargas
2015. Indirect method: a novel technique for experimental determination of asphaltene precipitation. *Energy & Fuels*, 29(5):2890–2900.

[39] Vargas, F. M., D. L. Gonzalez, J. L. Creek, J. Wang, J. Buckley, G. J. Hirasaki, and W. G. Chapman
2009. Development of a general method for modeling asphaltene stability. *Energy & fuels*, 23(3):1147–1154.

[40] Vilas Bôas Fávero, C., A. Hanpan, P. Phichphimok, K. Binabdullah, and H. S. Fogler
2016. Mechanistic investigation of asphaltene deposition. *Energy & Fuels*, 30(11):8915–8921.

[41] Wiehe, I. A., H. W. Yarranton, K. Akbarzadeh, P. M. Rahimi, and A. Teclemariam
2005. The paradox of asphaltene precipitation with normal paraffins. *Energy & Fuels*, 19(4):1261–1267.

[42] Yudin, I., G. Nikolaenko, E. Gorodetskii, E. Markhashov, V. Agayan, M. Anisimov, and J. Sengers
1998. Crossover kinetics of asphaltene aggregation in hydrocarbon solutions. *Physica A: Statistical Mechanics and its Applications*, 251(1-2):235–244.

Chapter 4

Revisiting the aggregation modeling of unstable asphaltenes with incorporation of destabilization kinetics

4.1 Introduction

The destabilization of asphaltenes exhibits a complex behavior, however the occurring process leading to the growth of particles physically remains a flocculation or aggregation. The aggregation can take significant time depending on the oil sample (mainly viscosity) and on the conditions. Indeed, previous authors have identified key parameters to the flocculation process which are summarized by Fávero et al.[7]. Some of these parameters, such as the number concentration of initially available particles, are cross-linked with destabilization kinetics discussed in the previous Chapter. Some of other parameters can be assumed independent from the destabilization, such as the initial population size or the aggregation rate constant that will be further discussed in this investigation. However, most of the previous researchers did not account for the kinetics of destabilization in their estimated rates of aggregation. The number of available particles was fixed to an equilibrium at initial time when the mixtures of oil-alkane are first prepared. Over-estimations of the number of available particles might arise from such assumptions.
Duran et al.[4] incorporated the time generation of unstable asphaltenes along with multiple other phenomena (e. g. dissociation by shear effect or interaction forces between large particles) into their numerical population balance model. Despite the good agreements found between their model and their experimental data, the use of various adjustable parameters does not let us conclude on the mechanism with the possibility that effects can cancel each other. The adjustment of too many parameters at the same time can lead to unreasonable choices and goes against our willingness to simplify the modeling of asphaltenes behavior. For example, the mentioned authors[4] tuned the size of primary units to values exceeding 1μm in some of their simulations. This order of initial particle size is in contradiction with the immense number of measurements on the primary size of unstable asphaltenes during the past decade[12;2;20;9;7].

Literature review on the coagulation modeling of Brownian particles
Referring back to the general form of the Smoluchowski coagulation Equation[23] with neglecting the generation of primary particles over time, the concentration of

particles formed with k primary units of unstable asphaltenes is given by:

$$\frac{dC_k}{dt} = \frac{1}{2}\sum_{i+j=k} K_{ij}C_iC_j - C_k\sum_{i\geqslant 1} K_{ik}C_i \tag{4.1}$$

where C_k is the number concentration of k^{th} species, t is the aging time and K_{ij} is the aggregation rate constant between i-j Brownian spherical species, sometimes termed the aggregation kernel. This aggregation kernel is usually reported to be dependent on the size of aggregating particles and is given by:

$$K_{ij} \sim K^*_{ij} = \frac{2k_BT}{3\mu_{liq}}\frac{(d_i + d_j)^2}{d_id_j} \tag{4.2}$$

where K^*_{ij} is the theoretical aggregation rate constant in a diffusion-limited clusters aggregation process (DLCA), d_i and d_j are the hydrodynamic diameters of colliding aggregates i and j, k_B is the Boltzmann constant, μ_{liq} the viscosity of the liquid medium and T is the absolute temperature. For Browninan particles of nearly equal size, the aggregation kernel reduces to a size independent form:

$$K^*_{ij} = \frac{8k_BT}{3\mu_{liq}} \tag{4.3}$$

This behavior is explained by Elimelech[5] to be the result of compensating effects of smaller diffusion coefficients with larger collision radius for grown particles that have the same size. More importantly, Equations 5.5 and 4.3 highlight a major aspect in the case the collisions of polydisperse asphaltenes aggregates. Indeed, the aggregation rate constant K^*_{ij} for Brownian particles of different sizes is necessarily larger than for particles having equivalent sizes regardless of their absolute size. K^*_{ij} gets larger as the size difference between colliding i-j particles increases. This feature is specially important in the circumstances of nanoparticles aggregating with much larger existing particles in suspension.
A coefficient of collision efficiency β_{ij} has been introduced by Maqbool et al.[16] when applying Equation 5.5 to the flocculation of unstable asphaltenes. The factor β_{ij} of the Brownian coagulation kernel was defined by the following ratio:

$$\beta = \frac{\text{Number of successful collisions}}{\text{Total number of collisions}} \tag{4.4}$$

With such collision efficiency, the aggregation rate constant presented in Equation 5.5 becomes:

$$\begin{aligned} K_{ij} &= K^*_{ij}\beta_{ij} \\ K_{ij} &= \frac{2R_gT}{3\mu_{liq}}\frac{(d_i + d_j)^2}{d_id_j}\beta_{ij} \end{aligned} \tag{4.5}$$

In practice the coefficient β_{ij} is tuned to reduce the difference between measured physical quantities and modeled ones. Therefore β_{ij} might be the result of additional effects to the sole collision efficicency for asphaltenes during their flocculation process.
The stability of colloidal suspensions has been extensively studied in electrolyte solutions, usually analyzed by the Derjaguin–Landau–Verwey–Overbeek (DLVO) theory of colloid stability[3;26] that describes the energy from summation of interaction

potentials. Modeling have arisen from many studies in the past century, mainly based on the general differential equation first proposed by Smoluchowski[3;8;18;22;23]. Assuming that the coagulation involves spherical particles, the "collision efficiency" β_{ij} corresponds to the inverse of the more commonly used Fuchs stability ratio W. The stability ratio of two colliding particles of equal size a, can fundamentally be related to their total interaction potential U as a function of their separation distance r by:

$$\frac{1}{\beta} = W = 2a \int_{2a}^{\infty} exp\left(\frac{U}{k_B T}\right) \frac{dr}{r^2} \tag{4.6}$$

An approximation of W is given by Elimelech[5]:

$$W = \frac{1}{2\kappa a} exp\left(\frac{U_{max}}{k_B T}\right) \tag{4.7}$$

where $1/\kappa$ is the thickness of the diffusive layer and U_{max} is the maximum positive value of the particle-particle interaction energy. Typical curves of interaction energies are plotted in Figure 4.1 for illustration.

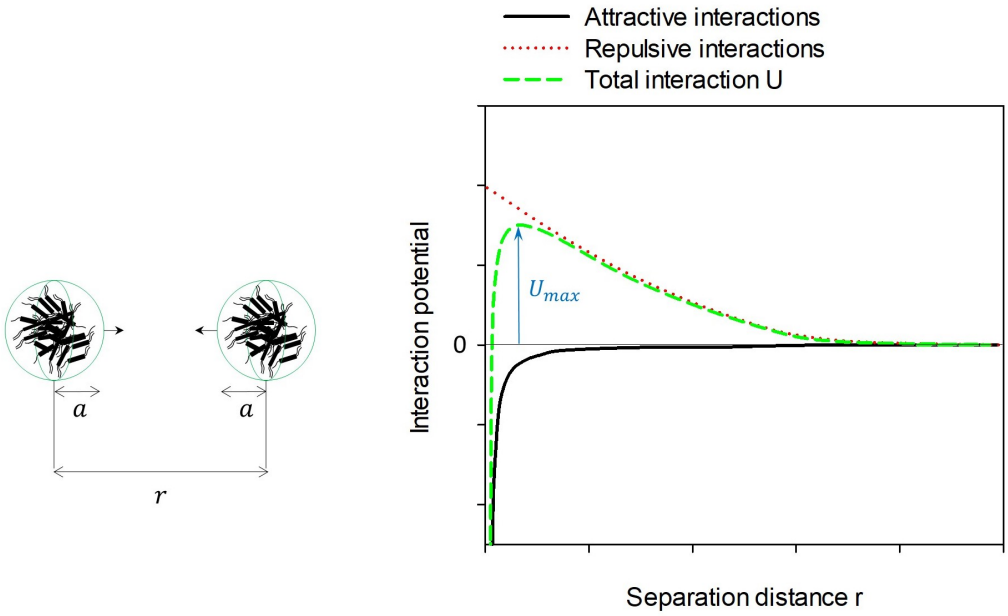

FIGURE 4.1: Example of potential curves for repulsive, attractive and the total interaction energies of two particles approaching each other

Fuchs[8] described the unfavorable or "slow" aggregation when repulsive interactions dominate and U_{max} is large. The presence of a repulsive energy barrier between particles (e. g. due to steric repulsions) makes the aggregation process to be controlled by the interparticle potential[3]. In such conditions, W>1 and this is often referred to as a reaction-limited clusters aggregation (RLCA). We note that W>1 can also be interpreted by a reduced concentration gradient where despite the Brownian motion, the number of particles is so small that concentration gradients cannot produce a sufficient Brownian flux to compensate for the large distances between particles.

Wang et al.[27] have experimentally measured the interaction energy between asphaltenes in various solvents using an atomic force microscope (AFM). The repulsion force between asphaltenes was found to be dependent on the solvent in which

the measurement was performed, as shown in Figure 4.2.

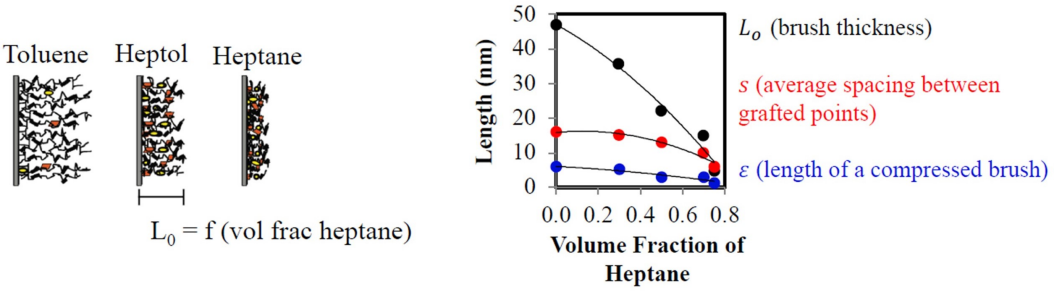

FIGURE 4.2: Measured repulsive interactions between asphaltenes particles using an AFM and interpreted length of steric brushes [28;27]

The steric repulsion between asphaltenes was found to have a decreasing trend with the heptane concentration and eventually becomes null at some composition of the mixture.
In this particular situation, the aggregation becomes entirely controlled by the Brownian motion, the "fast" or favorable process is qualified as a diffusion-limited clusters aggregation (DLCA) and $W = 1$. In the colloidal science literature, this "onset" condition is often reached by varying the concentration of electrolytes that play the role of a double-layer in aqueous environments. At this point, the electrolyte concentration defines the critical coagulation concentration (CCC). The tempting analogy with the so-called onset concentration of alkanes for the flocculation of asphaltenes in oil-alkane mixtures will later animate the results discussions of this Chapter.
Fuchs [8] had considered two possible mechanisms of aggregation where (i) in RLCA only fractions of the Brownian motion driven collisions would result in aggregation and (ii) in DLCA all the Brownian motion driven collisions are successful. Most of the studies on the aggregation of asphaltenes are based on a method developed around the maximum value of the interaction potential U_{max} that symbolizes the energy barrier. The validity of such applications holds at conditions when U_{max} is greater than the thermal energy $k_B T$. McGown and Parfitt [17] extended Fuchs's research and considered the total interaction energies given by the sum of repulsive and attractive forces between particles. The effect of Van der Waals (VdW) forces, neglected in Fuch's formula, could now explain the rapid coagulation in certain situations. Although further improvement were later proposed to account for viscous interactions between particles [24], the inclusion of an attractive VdW term is a major change for a process mainly controlled by London dispersion forces like asphaltenes in crude oil [1;29].
Indeed at augmented favorable conditions of coagulation, the effective stability ratio W can then take values artificially lower than the unity due to the predominant contribution of attractive forces (U<0) as particles get close to each other [22;25]. This behavior is also indirectly related to the stronger increase of attractive than repulsive forces for enlarged particles. The direct observation of such behavior is well described when computing the VdW interaction forces of approaching particles with Hamaker constants with varying their size [14;10].
We have seen that W is defined as the ratio of the "fast" flocculation rate constant to the "slow" one within the timescales of interest (minutes to hours). In the case of primary colliding particles under RLCA and substituting the "collision efficiceny"

parameter by a stability ratio; we retrieve the expression of the kernel used by Maqbool et al. [16] (Equation 4.5) given by:

$$K_{ij} = \frac{K^*_{ij}}{W} \tag{4.8}$$

with K^*_{ij} representing the aggregation rate constant for DLCA and above defined by Equation 5.5. The expression of K_{ij} becomes more complicated if we adjoin factors to account for the role of clusters morphology and their associated mass-to-size relation. Therefore for simplicity in our work, we will consider that morphological effects can be lumped into the adjusted values of the stability ratio W and are minor compared to the particles interaction.

Previous work on the asphaltenes aggregation modeling
As seen in the below reprinted Figure from Maqbool et al. [16] (Figure 4.3), their data suggested that the aggregation process of unstable asphaltene particles is reaction-limited within the investigated range of heptane concentrations ($\beta << 1 \equiv W >> 1$).

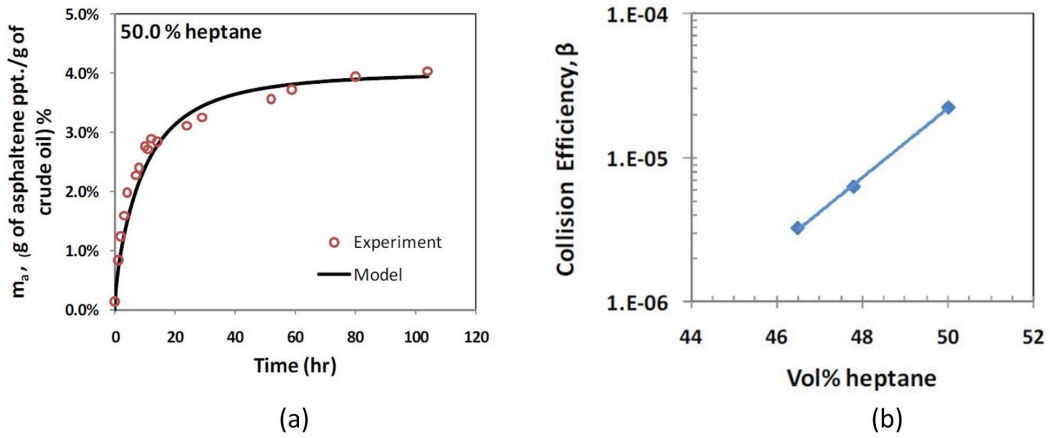

FIGURE 4.3: Reported by Maqbool et al. [16]
(a) Experimental and simulated increasing evolution of the mass of separated unstable asphaltenes.
(b) Tuned collision efficiency as a function of heptane concentration in blends of crude oil and heptane.

A theoretical calculation of W with Equation 4.6would require too many compositional details that are not available on asphaltene fractions. Therefore W needs to be experimentally determined due to the unknown chemical composition of asphaltenes molecules in the studied crude oil. In practice, the stability ratio is usually adjusted to experimental observations rather than directly measured in most cases of application to colloidal systems.
For a given oil-heptane mixture, the necessary time of appearance of micro-sized aggregates in the bulk is indicative of the aggregation kinetics and can be measured by time-resolved microscopy. Maqbool et al. [16] were able to calculate the change in particle size distribution (PSD) across the aging time and found excellent agreements between simulation and experimental results with tuning β (see reprinted Figure 4.4).

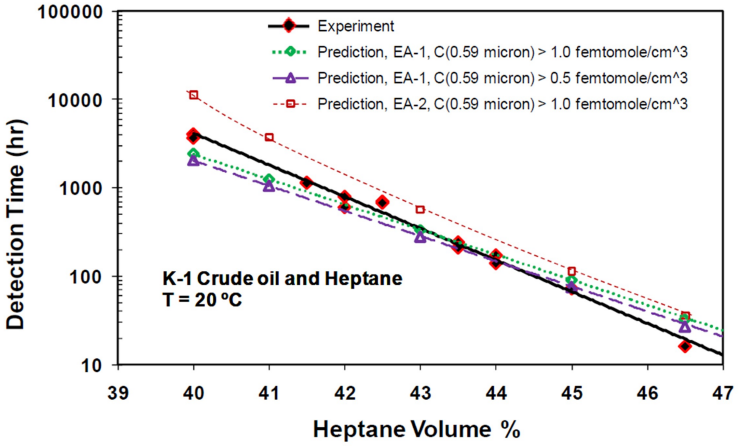

FIGURE 4.4: Results of experimental and simulated microscopy detection-times of unstable asphaltenes reported by Maqbool et al. [16] using adjusted values of β showed in Figure 4.3 in the population balance model of Equation 4.1

According to Haji-Akbari et al. [10], the value of the maximum repulsive interaction between aggregates of asphaltenes U_{max} is proportionally related to the difference in solubility parameters between the solution and the least stable asphaltenes ($\delta_{solution} - \delta_{asph}$). The solubility parameter of the solution is linked to the volume fraction of its components ϕ_i and is given by:

$$\delta_{solution} = \sum \phi_i \delta_i \tag{4.9}$$

Combining Equations 4.7 and 4.9 for a fixed δ_{asph}, we get:

$$W \propto exp(\delta_{solution} - \delta_{asph}) \propto exp(\phi_{n-C_7}) \tag{4.10}$$

where ϕ_{n-C_7} is the volume fraction of n-heptane in oil-heptane mixtures. We note that the adjusted coefficient accordingly exhibited an exponential trend in the work of Maqbool et al. [16] (see Figure 4.3(b)). The extrapolation of the reported collision efficiencies with an exponential regression can give us an indication of conditions at which "fast" flocculation should occur (W = 1) according to the colloidal science practice. As shown by the red circle in Figure 4.5 (a), favorable aggregation is predicted at heptane concentration $\sim$ 70%vol. However, the experimental measurement obtained by microscopy indicated an instantaneous detection (less than a few minutes) of particles larger than 1 μm at concentrations of heptane between 50 and 55%vol (Figure 4.5 (b)).

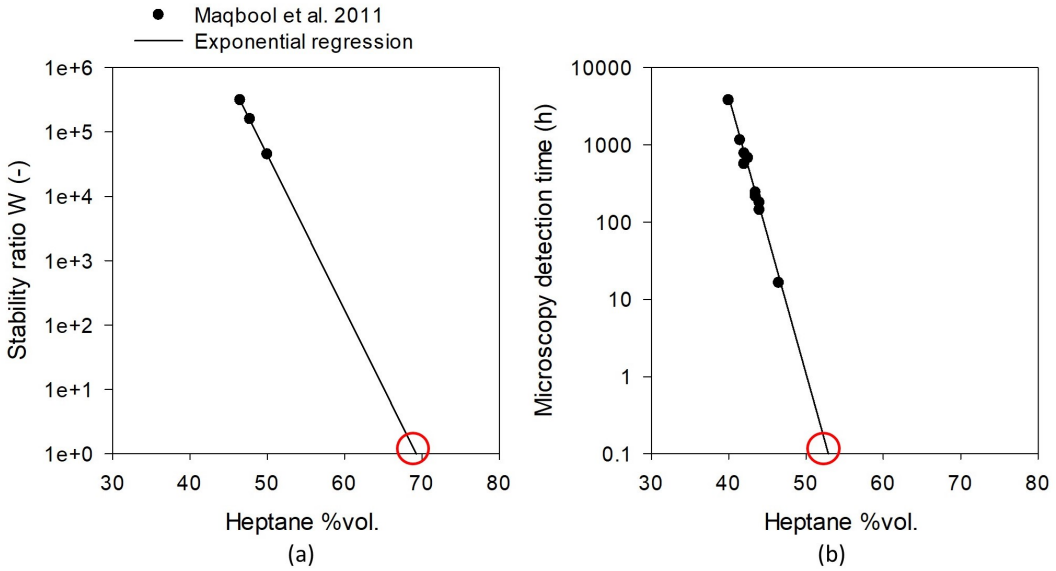

FIGURE 4.5: Regression analysis of data from Maqbool et al.[16] as a function of the heptane fraction in oil-heptane mixtures for the:
(a) adjusted stability ratio W
(b) experimentally measured detection-time of unstable asphaltenes having sizes larger than 500 nm

When exploring the limits of the tuned coefficient β or W, the regression analysis reveals a discrepancy between the immediate appearance of flocs under microscope observations and the adjusted W as a function of the heptane content. This examination suggests that W was overestimated compared to the experimental values. A lower stability ratio could be obtained if the aggregation is relatively faster than the proposed solutions by Maqbool et al.[16]. This parameter is intrinsic to the aggregation for a fixed number of particles. However if the number of particles is reduced, the aggregation rate will have to be faster in order to find a constant result. On the other hand, the authors[16] neglected generation kinetics of primary particle into their computations and assumed immediate availability of all particles found at equilibrium (plateau value of a centrifugation experiment against time). One can therefore suspect that overestimates of the number of particles in the system certainly emerged into their work and lead to underestimations of the aggregation rate constant K_{ij}.
Incorporating the time dependent generation of primary particles, r_1 becomes the time dependent source term into the differential Equation 4.1, we get:

$$\frac{dC_k}{dt} = \left[\frac{1}{2}\sum_{i+j=k} K_{ij}C_iC_j - C_k\sum_{i\geqslant 1} K_{ik}C_i\right] + r_1 \tag{4.11}$$

and according to our pevious work (Chapter 3), in absence of initial particles, the generation rate r_1 is described by:

$$r_1 = \frac{dC_1}{dt} = \frac{1}{\tau}e^{-\frac{t}{\tau}}\sum kC_{k_\infty} \tag{4.12}$$

where τ is the characteristic thermodynamic equilibration time of the system, $\sum kC_{k_\infty}$ is the total number concentration of primary units across all the aggregated entities at equilibrium.

The integration of Equation 4.12, with an initial time equal to zero, gives the following analytical solution:

$$\sum kC_k(t) = \left(1 - e^{-\frac{t}{\tau}}\right) \sum kC_{k_\infty} \tag{4.13}$$

The latter parameter is estimated with the measured "dry" mass concentration of unstable asphaltenes at equilibrium C_{A_∞} by centrifuge and converted to a number concentration as follows:

$$\sum kC_{k_\infty} = C_{A_\infty} \frac{\mathcal{N}_\mathcal{A}}{M_{w_{\text{asph}}} N_{\text{agg}}} \tag{4.14}$$

where the Avogadro number $\mathcal{N}_\mathcal{A}$, the molecular weight of asphaltenes $M_{w_{\text{asph}}}$ and the number of asphaltene molecules per primary particle N_{agg} lets us evaluate the mass of "dry" primary particles with the following generally accepted[20;19;6] average values:

$M_{w_{\text{asph}}}$ = 750 g/mol

N_{agg} = 80 = [(8 molecules/nanoaggregates) x 10 (nanoaggregates/cluster)]

As primary clusters of unstable asphaltenes are generated along the aging time for a fixed solvent as opposed to instantaneously at initial time in the work of Maqbool et al.[16], one should expect the aggregation rate constant to be adjusted with larger values in order to match the experimental data. With the described mechanism, the adjusted stability ratio W is expected to shift down in Figure 4.5 (a).
In the following sections, a simple numerical method will be applied to a similar system with a different crude oil compared to Maqbool et al.[16]. The expected behavior of combined asphaltenes kinetics of destabilization (primary particles generation) and aggregation will be verified by comparison to microscope observations. Results will be presented for mixtures of one crude oil with various concentrations of heptane, all other parameters being left constant during the study.

4.2 Materials and methods

4.2.1 Sample preparation

Liquid solvents (e.g. n-alkanes) were 98+% purity supplied. One dead crude oil sample was used throughout this study, it was inspected by microscopy and by centrifugation to make sure that the samples were free from contamination of water, solid particles, production additives or drilling fluid. The preparation of crude oil and alkane mixtures at specified concentrations was as follows for all experiments (unless stated otherwise). The crude oil, the alkane and vials were all incubated at the temperature of the study until reaching a stable temperature. A known volume of oil was placed into the vial. The solvent was added by means of a peristaltic pump at an addition rate of 3 cm^3/min until the desired concentration was obtained. During the addition, a good agitation was ensured with a magnetic stirrer to minimize localized high concentrations. The solution was then aged in a sealed vial and kept agitating at the temperature of interest during the entire study. All the liquid mixtures were prepared on a mass basis in order to increase the accuracy, final volume fractions were calculated using the respectively measured densities with a density meter (make Anton Paar model DMA 5000 M) at the temperature of work.

4.2.2 Microscopy detection-time measurement of unstable asphaltenes

The microscopy detection-time was chosen to track the appearance of particles larger than 500 nm in a prepared blend of crude oil with a flocculating agent, measured by time-resolved optical microscopy[15]. For specific concentrations of heptane, Maqbool et al.[15] and Haji-Akbari et al.[11] found that the time for unstable asphaltenes to reach a microscopical size varies linearly with the volume concentration of alkanes on a semi-logarithmic graphic. Aliquots of the prepared mixture are taken over time to observe them by shooting images with a CCD camera mounted on a consistently configured optical microscope with a 50x objective lens and a 10x eyepiece. The time it takes for solid opaque particles to be detected after heptane addition with this method is called the microscopy detection-time. The procedure is repeated at multiple concentrations of flocculating agent (heptane in this study) in order to obtain a detection-time curve typically ranging from a few minutes to 1000h. The lowest concentrations of n-alkanes for which the detection-time is less than 5 minutes is considered to be the instantaneous microscopy detection condition.

4.2.3 Quartz crystal resonator immersed in a stirred tank reactor

The immersed QCR set-up that was used in this Chapter is described in Chapter 2. Heptane was used to favour the destabilization and deposition of asphaltenes. The continuous injection rate was set to 0.3 cm^3/min.

4.2.4 Simultaneous modeling of primary particles generation and aggregation

Numerical methods need to be employed to resolve coagulation differential equations (Equation 4.11 when choosing physically realistic coagulation kernels (particle size and morphology dependent). Otto and Fissan[21] summarized the modeling approaches to describe the time change of the number concentrations of submicron suspending entities in aerosols. In this work, the mathematical form of the equations is supposed to remain the same for colloidal systems of nanoparticles in a liquid media. The built models enable to evaluate the size distribution of aggregated liquid or solid particles as a function of time to a certain level of details on the particle size distribution.
If the size distribution is fixed in shape, analytical solutions can be obtained with relatively simple equations. Among the analytical solutions; self-preserving and log-normal PSDs can provide the most realistic results[21]. In our case, the purpose of calculations is to compare the computed kinetic of destabilization and aggregation of unstable asphaltenes to the experimental microscopy detection-time that might itself include some associated uncertainties. For that purpose a mono-disperse size distribution was considered to correspond to the mean size of particles resulting from the aggregation process. This is the simplest assumption that shrinks the distribution to a single value of particle size that contains k number of primary units. For the specific case of an initialized instantaneous generation, the time dependent concentration of primary particles is expressed as:

$$C_1(t) = \frac{C_1(0)}{1 + \frac{1}{2}K_{ij}C_1(0)t} \tag{4.15}$$

where the dependence of the aggregation rate constant K_{ij} on the size of coagulating particles can be relaxed with assuming equal size of colliding particles along the experiment.
Equation 4.15 lets us analytically compute the decay in number concentration of the initial clusters of unstable asphaltenes (primary particles). With this Equation, Otto and Fissan [21] reported the time evolution of the average diameter of particles from a mass conservation perspective and was given by:

$$d_{A_k}(t) = d_{A_k}(0)\left(1 + \frac{1}{2}K_{ij}C_1(0)t\right)^{1/3} \tag{4.16}$$

where $d_{A_k}(t)$ is the mean diameter of particles in the system as a function of time.
According to Chapter 3, the generation of new unstable asphaltenes primary particles takes a significant time depending on the conditions of work. The equilibrium is sometimes slowly reached after waiting hours to hundreds of hours for low enough concentrations of *n*-heptane. As discussed in the introduction, the Brownian nature of newly born nanoparticles will likely make them contribute to enlarge already existing aggregates rather than start to form new aggregates of intermediate sizes. Therefore the generation of primary particles must have an important impact on coagulation. Unfortunately, the simultaneous calculations of nanoparticles generation and growth of aggregates restrict the possibility of finding analytical solutions. This forces us to discretize the problem in time in order to numerically account for the concurrently happening processes. We will therefore use a simple numerical method derived from the respective analytical solutions to solve both processes. Only the aggregation will be impacted by the number of generated particles, we assume that the generation of particles is not cross-linked to the aggregation and is controlled by other forces. The model has to account for lastly generated particles into the aggregation calculation at each iteration step. To do so, the time counter is cleared down between each interval of time used to solve the coagulation process. At the end of each step, Equation 4.15 is modified by re-injecting results into the initial conditions of the following time step. The Equation is resolved with appropriate time intervals Δt to satisfy a good convergence:

$$\begin{aligned} &C_1(t+\Delta t) = \frac{C_1'(t)}{1 + \frac{1}{2}K_{1A}C_1'(t)\Delta t} \\ &\text{with: } C_1'(t) = C_1(t) + \sum kC_k(t+\Delta t) - \sum kC_k(t) \end{aligned} \tag{4.17}$$

The preferential aggregation between primary particles and larger existing entities justifies the use of K_{1A} in this Equation, the aggregation rate constant between generated nanoparticles and particles having the average size (larger than primary ones) obtained at the previous time step. Equation 4.8 then develops into:

$$K_{1A}(t+\Delta t) = \frac{2R_gT}{3\mu_{liq}}\frac{(d_1 + d_A(t))^2}{d_1 d_A(t)}\frac{1}{W} \tag{4.18}$$

Discrete time intervals are implemented in Equation 4.16 along with results of the previous time step to account for both processes; the destabilization and the aggregation kinetics of unstable asphaltenes. We therefore obtained the numerical expression for the average size of aggregated particles:

$$d_A(t + \Delta t) = d_A(t) \left(1 + \frac{1}{2} K_{1A} C_1'(t) \Delta t\right)^{1/3} \tag{4.19}$$

In this way, the results from the precedent step of remaining number of primary particles $C_1(t)$ and the average size of particles $d_A(t)$ are passed on to the following time steps. The following initial conditions are considered when the last drop of heptane is added to crude oil:

$$\begin{aligned} t_0 &= 0 \\ \sum k C_k(0) &= 0 \\ d_A(0) &= d_1 = 10 \text{ nm} \end{aligned}$$

For a given oil-heptane solution mixture, the computed mean diameter of agglomerated particles d_A is then plotted as a function of time and the time at which d_A exceeds 500 nm is recorded. This process is repeated for several compositions of oil-heptane in the range of heptane contents that compare to observable detection-times under microscopy. The plot of simulated times at which the particles have an average size of 500 nm as a function of the heptane volume fraction in oil-heptane preparations is compared to the experimental observations. The profile of the stability ratio W is then adjusted in order to fit computed results to the experimental microscope observations.
Note that for consistency, the total number of primary units across all species is verified to be significantly larger than the minimum necessary concentration to form observable particles in the experiments. This number concentration C_{k_0} is evaluated in the next paragraph.

Minimum concentration of primary particles C_{k_0}
The sensitivity analysis provided by Haji-Akbari et al. [10] evaluated a minimum concentration equal to $\sim$ 30 particles with sizes larger than 500 nm within the field view of the microscope images. Authors [10] had used rough calculations to evaluate the minimum number concentration of primary particles. The number k_0 of primary units p into a fractal aggregate A is given by:

$$k_0 = \left(\frac{R_A}{R_p}\right)^{D_f} \tag{4.20}$$

where D_f is the fractal dimension of the aggregates. According to non-invasive measurements on the structural morphologies of unstable asphaltenes [4;12], flocculated unstable asphaltenes have fractal dimensions ranging within $D_f \sim$ 2.1 - 2.6. R_p is assumed equivalent to the average size of clusters in good solvent, reported $\sim$ 5 nm [20;6]. With this expression, the minimum number of primary particles in observable flocs of radius R_A = 500 nm is $k_0 \sim$ 15000 to 150000 depending on the assumed fractal dimension.
The monitored volume $V_{\text{monitored}}$ of fluid between microscope slides can be estimated by multiplying the spanned area through the microscope lenses ($\sim 3.10^4$ μm^2) to the thickness of the layer of liquid solution. Assuming that the droplets of 0.05

cm^3 evenly spread between the microscope slides with negligible losses, the thickness is estimated to ~ 0.1 mm and results in:

$$V_{\text{monitored}} \sim 3.10^{-12} \text{m}^3$$

With the above mentioned sensitivity analysis made by Haji-Akbari et al.[10], the minimum concentration of primary particles for the microscope observation of asphaltenes instability is:

$$C_{k_0} \sim 2.10^{17} - 2.10^{18} \text{ m}^{-3}$$

or in mass concentration:

$$C_{k_0} \sim 0.02 - 0.2 \text{ g.m}^{-3}$$

If the births of generated particles hypothetically occur inside or over existing structures, the aggregation process could be instantaneous (not limited). In this fictional scenario, the microscopy detection-time would then equal the time at which the cumulative number of generated primary particles exceeds C_{k_0}. This mechanism is not realistic because considering that primary particles can only contribute to a fixed number of growing particles (equal to the one that we are supposing) without any degree of freedom to form new flocs. However it is interesting to plot such results in order to quantify the additional time that aggregation takes compared to the destabilization. Note that verification of extremely fast aggregation (past "onset" conditions) will be conducted to confirm the realistic assumptions made to develop our model on the destabilization kinetics.
In the following section, results considering the sole destabilization kinetics or destabilization along with aggregation kinetics are compared.

4.3 Results and discussions

4.3.1 Microscopy detection-time of unstable asphaltenes

In this study, the detection-time information provides a quantitative indication of the aggregation rate and will let us adjust the only tuning parameter W.
The time-resolved microscope experimental observations are same as Chapter 3. As expected, the experimental points show a linear trend in the semi-logarithmic graphic. The intersection of the linear trend with the x-axis at 0.1h (6 min) corresponds to the instantaneous microscopy detection of unstable asphaltenes (marked by a red circle).

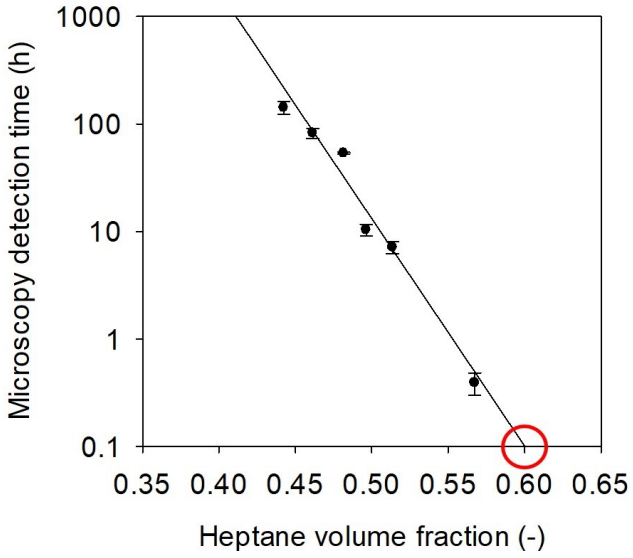

FIGURE 4.6: Necessary aging time to detect particles by visual microscopy observations as a function of the volume fraction of C_7 in heptane-oil blends

4.3.2 Destabilization and aggregation models application

Destabilization only

The generation rate of unstable asphaltenes is computed using Equation 4.13. Figure 4.7 illustrates how the micro-level detection-time of unstable entities is read when considering instantaneous aggregation by direct inclusion of generated particles inside a fixed number of suspending flocs. As presented above the considered fractal dimension has an effect on C_{k_0}, the minimum concentration of particles for observations logically grows as D_f increases. Indeed, if one wants to create objects of equal hydrodynamic size but different fractal characteristics, the object will have to be filled with more primary units as the fractal dimension gets large. The maximum D_f is 3 and corresponds to hard spheres.

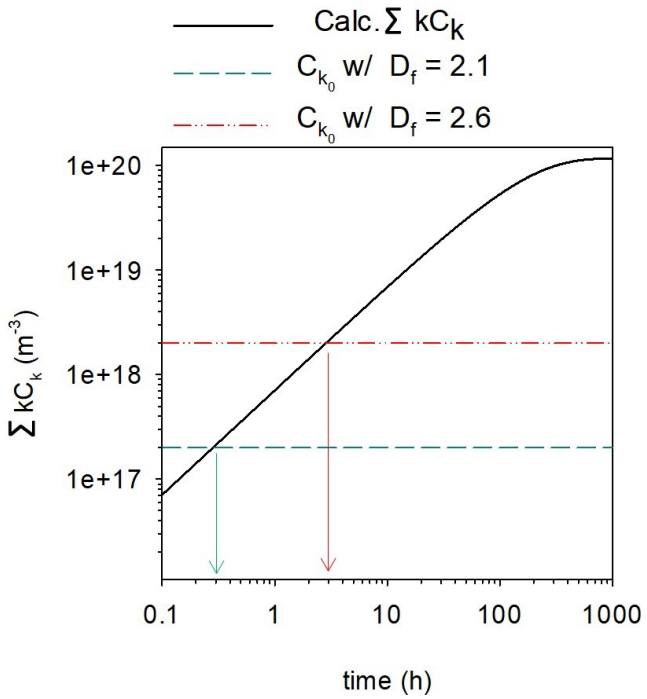

FIGURE 4.7: Comparison between the total number of primary particles across all entities and the minimum concentration of particles C_{k_0} to enable microscope observations for the case of heptane content = 47 vol%

The aging time at which the calculated particle concentrations exceed the estimated minimum concentrations is read as illustrated by Figure 4.7 by assuming instantaneous aggregation. The reading process is repeated for several contents of heptane. Figure 4.8 shows the results when considering this "unrealistic" mechanism that assumes generated particles to only contribute to the flocs that we see under microscope experiments.

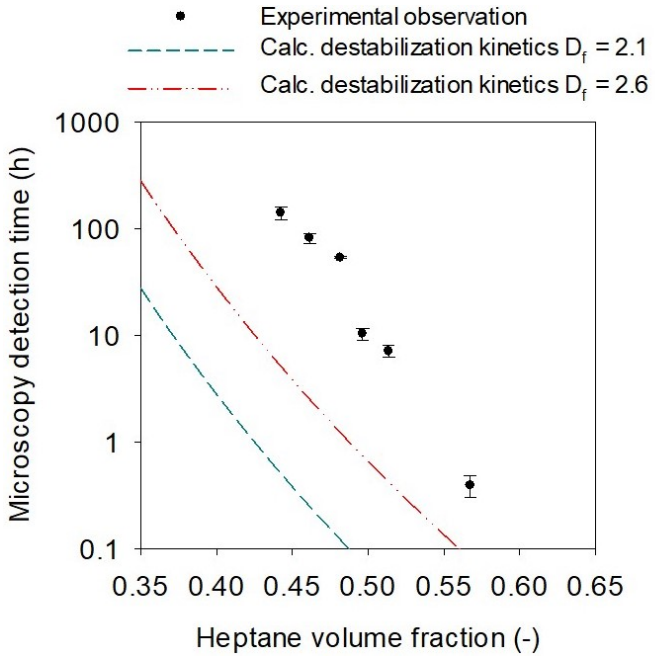

FIGURE 4.8: Comparison between experimental observations by microscopy and the calculated curves for a mechanism considering only kinetics of destabilization and instantaneous aggregation as a function of the heptane volume fraction in mixtures

As it can be seen, an offset of one to two orders of magnitude separates the modeled curves from the experimental observations. The calculated curves envisage an extremely fast aggregation and provide underestimations of the time we have to wait after preparing the mixture to observe micro-particles. The modeled detection-time was naturally expected to under-estimate the observations and confirms that the aggregation plays a role within the investigated range of conditions. However, it is also important to note that this plot confirms our precedent results that suggested kinetics to be dominated by the destabilization. Indeed, the results remain fairly comparable to the experiments (same order of magnitude) for fractal dimensions approaching hard spheres and for relatively large n-heptane contents.

Simultaneous destabilization and aggregation kinetics

In the case of simultaneous resolution of Equations 4.12 and 4.17, the detection-time of micro-particles is directly read on the plot of the computed average diameter of aggregates d_A as a function of the aging time for a given solution remaining fix in composition with time. Figure 4.9 shows the reading process for a chosen example, the detection-time is defined when d_A exceeds the resolution limit of the used microscope, i. e. 0.5μm.

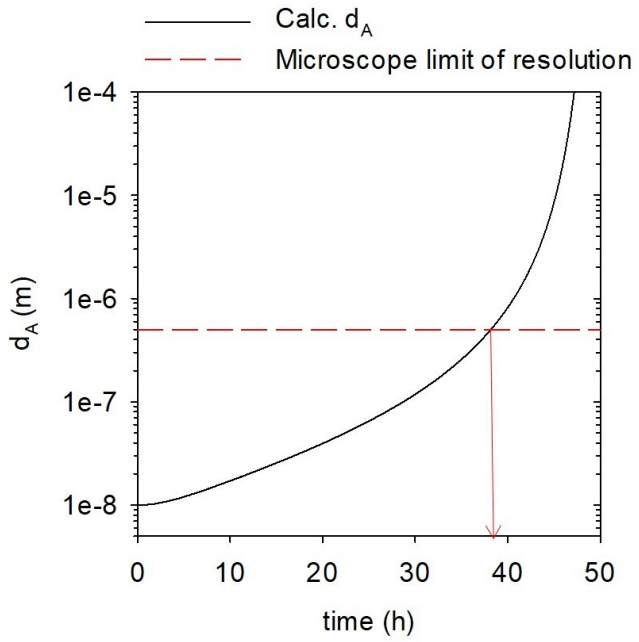

FIGURE 4.9: Computed mean diameter of aggregated structures as a function of time for a given solution (47'vol% of C_7) compared to the minimum detected size of distinct objects by microscopy

As expected, the obtained profile illustrates well the self-amplification process of nanoparticles generation into an environment containing increased number of large entities, which itself favors hetero-aggregation. As advertised by Equation 5.5, this leads to the preferential growth of the largest solid bodies. It is also important to remark that the initial size of unstable asphaltenes is an input value that was set to 10 nm at time zero ($\sim$ size of stable clusters of asphaltenes), when the mixture had just been prepared.
Along with the adjustment of appropriate stability ratios W, the reiteration of this process for several composition of oil-heptane mixtures lets us complete Figure 4.8 with the modeled detection-time curve that physically accounts for the aggregation of primary generated particles over time.

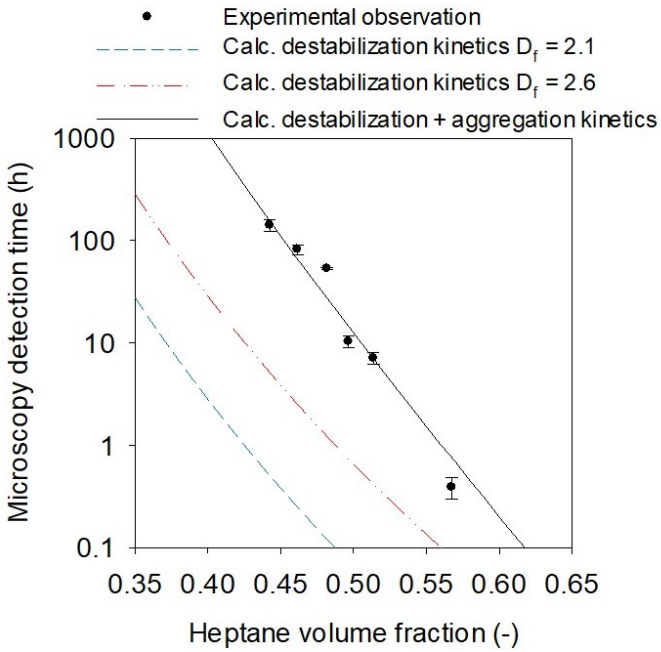

FIGURE 4.10: Comparison between experimental observations by microscopy and the calculated curves as a function of the heptane volume fraction in oil-heptane mixtures

An excellent agreement is obtained in Figure 4.10 between the simulated destabilization + aggregation and the experiments with the appropriate profile of W plotted as a function of the n-heptane fraction in Figure 4.11. The results confirm that the additional time that the system takes to acquire large enough particles for microscope observation can be captured by coagulation equations.

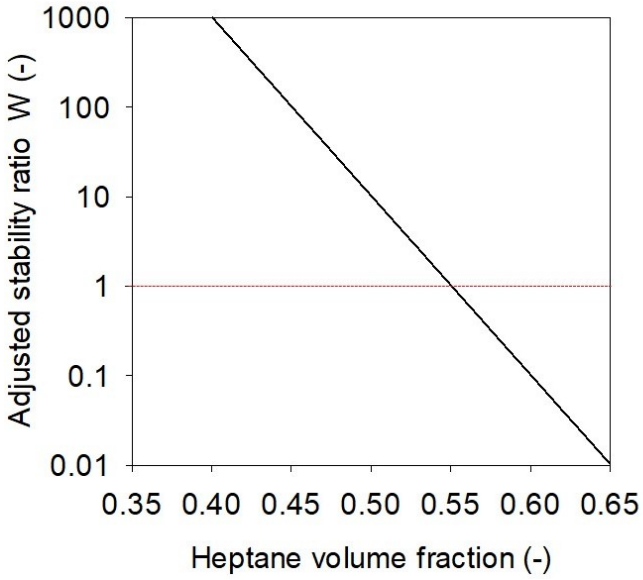

FIGURE 4.11: Tuned profile of the stability ratio W as a function of the heptane content in oil-heptane mixtures that satisfies the observed detection-time curve showed in Figure 4.10

4.3.3 Interpretation of the destabilization and flocculation modeling

The outcomes indicate that, for our oil-heptane system the aggregation process belongs to a RLCA regime at low enough heptane content in the mixtures and moves to more favorable coagulation conditions as the heptane fraction gets large. The behavior observed for *n*-heptane contents lower than 55 vol% can be interpreted as an increasing collision efficiency with the *n*-heptane concentration[16;7].
According to the colloidal definition of the stability ratio, the physical meaning of artificially transitioning values to $W < 1$ suggests an extremely fast aggregation process encouraged by a strong attractive potential when the *n*-heptane content becomes significant enough. In the aforementioned conditions, the conventional interpretations of the stability ratio as equal to the inverse of a collision efficiency does not hold anymore.
Besides the fact that more collisions than the sole Brownian driven ones are caused by the attractive forces between existing particles, other mechanisms might be at the origin of *W* divergence from the Brownian coagulation theory. This can be explained by the occurrence of multiple coinciding incidents at those conditions, that are first triggered by the escalation of the generation rate of primary particles. This is illustrated, in Figure 4.12, by the trends of the computed generation rate constant k_N and the characteristic time of thermodynamic equilibration τ. Indeed, Figure 4.12 (a) shows that the characteristic thermodynamic equilibrium time sharply decreases and reaches time scales of a few hours(or less) at heptane concentrations between 50 and 60 vol%.

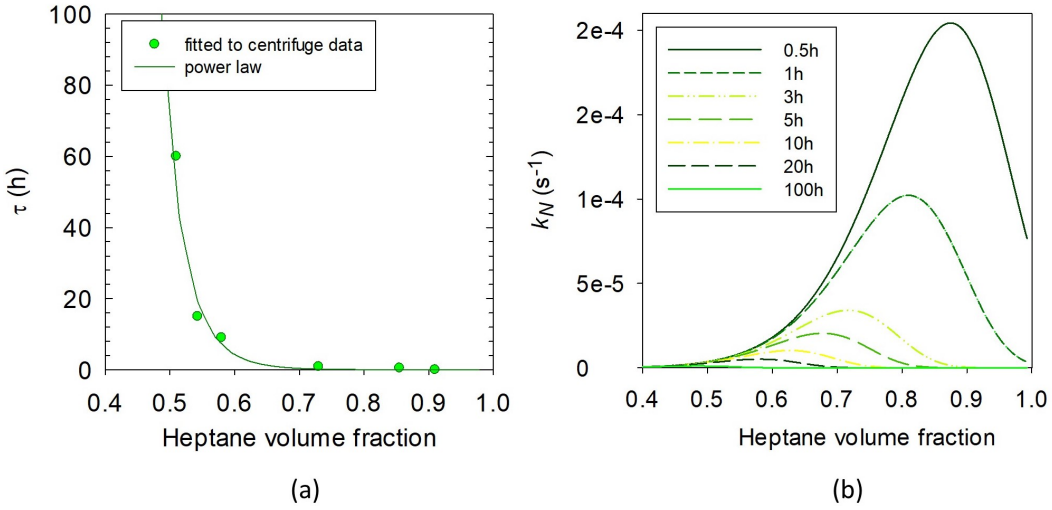

FIGURE 4.12: Plots of (a) the characteristic time of thermodynamic equilibrium τ and (b) the generation rate constant k_N at several times for various compositions of oil-heptane mixtures

Following intense particle generation events, the number of existing aggregates gets quickly big and the probability that a generated particle of unstable asphaltenes emerge nearby or inside an existing flocculated entity is extended.
For produced primary particles which are already contacting or approaching larger entities, the time for their aggregation is reduced to zero. The multiplication of such happening events can engender the tuned stability ratio to take abnormal values ($W << 1$). Actually, conforming to our introductory hypothesis, the immediate coagulation should be observed when the system transitions from dominating repulsive particle interaction to attractive interactions (i. e. $W = 1$). The experimentally

observed instantaneous flocculation is compared, in Figure 4.13, to the obtained stability ratio in our simultaneous primary particle generation and aggregation computation process.

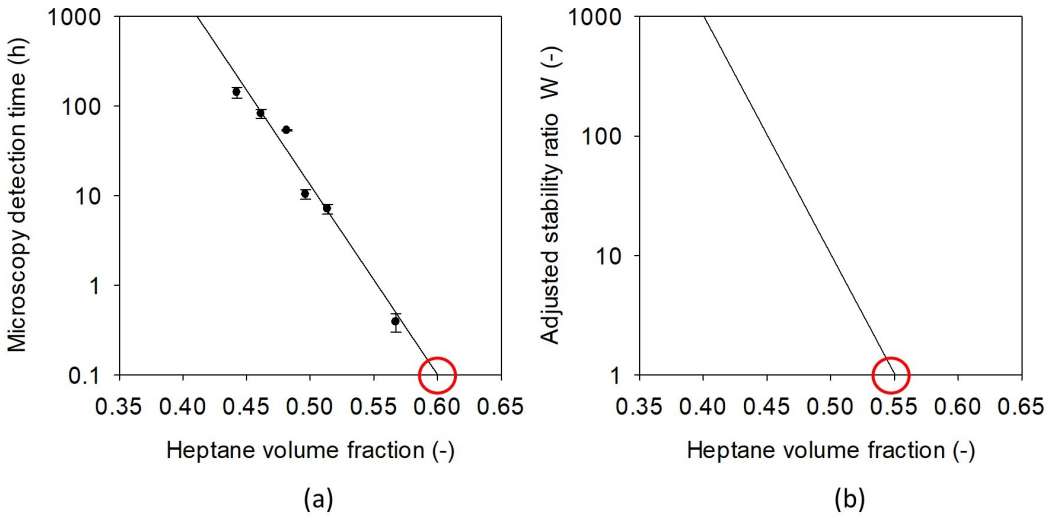

FIGURE 4.13: Plots of (a) the detection-time of experimentally observed micro-particles of unstable asphaltenes and (b) fitted stability ratio W for various compositions of oil-heptane mixtures

A relatively good agreement is observed. Experimental errors, chosen initial conditions and number of approximations made in our simple model (mono-disperse size of hard spheres without morphological influence of aggregates) may explain the slight difference between the experimental instantaneous observation (heptane content ~ 60 vol%) and the theoretical transition predicted by the stability ratio (heptane content ~ 55 vol%).
For the sake of consistency, we might want to verify the total number of primary particles across all entities when the micro-detection of unstable asphaltenes is simulated. Not surprisingly, Figure 4.14 confirms that the cumulative number of generated primary clusters of asphaltenes is larger than the minimum estimated concentrations C_{k_0} for microscope observation. This is naturally due to the larger number of aggregating seeds compared to the fictive case where all primary particles were assumed to grow the exact needed number of aggregates for our microscope observations.

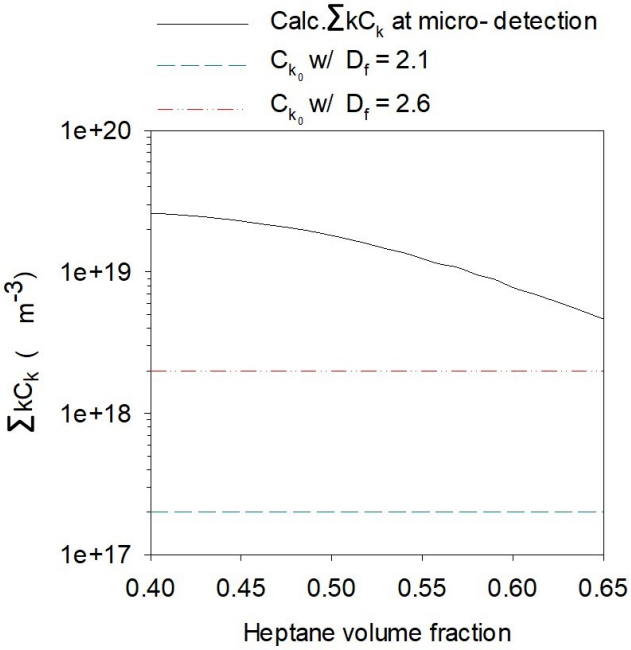

FIGURE 4.14: Calculated cumulative number of primary clusters across all the aggregates at the time of microscope detection

The total number concentration of primary units at micro-detection adopts a decreasing trend against an increasing heptane content, this behavior is related to the enlarged aggregation rate constant when larger volumetric percents of the alkane are mixed with oil. The observed effect reflects the different evolution of the aggregation and destabilization kinetics as a function of the *n*-heptane content. Indeed, simulation results indicate that the increase of the aggregation rate of unstable asphaltenes with the content of *n*-heptane is more significant than the evolution of the rate of destabilization. The preferential aggregation between aggregates of different sizes is an indirect associated effect that tends to promote the growth of the largest particles and reduce the number of aggregates with intermediate sizes.

4.3.4 Relation between the generation of primary units and the growth of asphaltenes aggregates

As already showed, the generation of new clusters of unstable asphaltenes ($r_1 = \frac{dC_1}{dt}$) is without doubt connected to the detection-time of micro-particles since the aggregation process needs to be supplied with Brownian entities. It is important to note that for each mixture composition, the generation rate of primary particles ($\frac{dC_1}{dt}$) remains relatively constant during longer periods of time than the microscopy detection-times (see example in Figure 4.15).

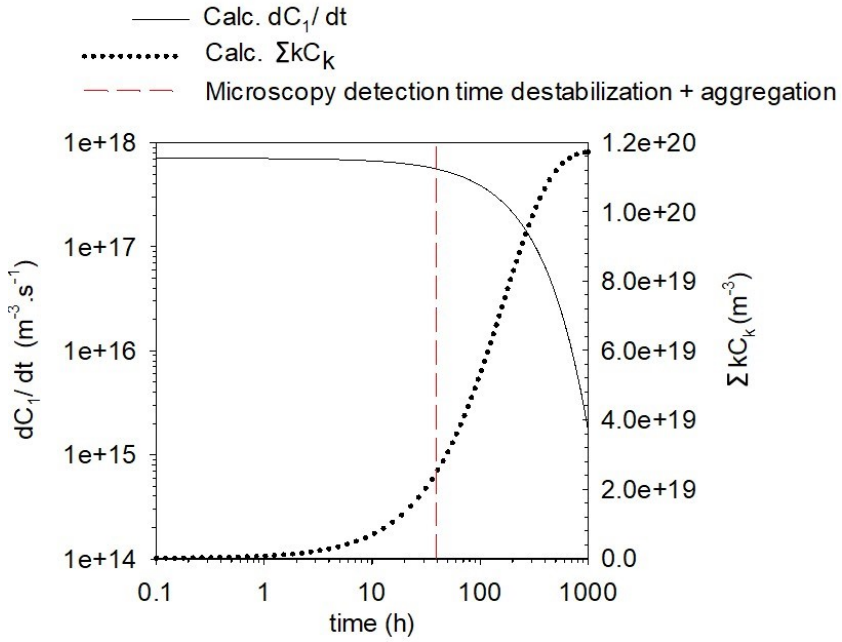

FIGURE 4.15: Comparison between the time evolution of the generation rate of primary clusters, the cumulative number concentration of generated primary units and the detection-time of micro-sized particles for the heptane concentration = 47 vol%

In fact, for aging times shorter than the micro-detection one, the rate of generation of primary units can be considered roughly equal to the initial one when the solution is prepared. As shown by the logarithmic plot of simulations in Figure 4.16, the mandatory time for the colloidal suspensions to reach micro-sizes is undeniably related to the initial generation rate of unstable asphaltenes $\frac{dC_{1_i}}{dt}$.

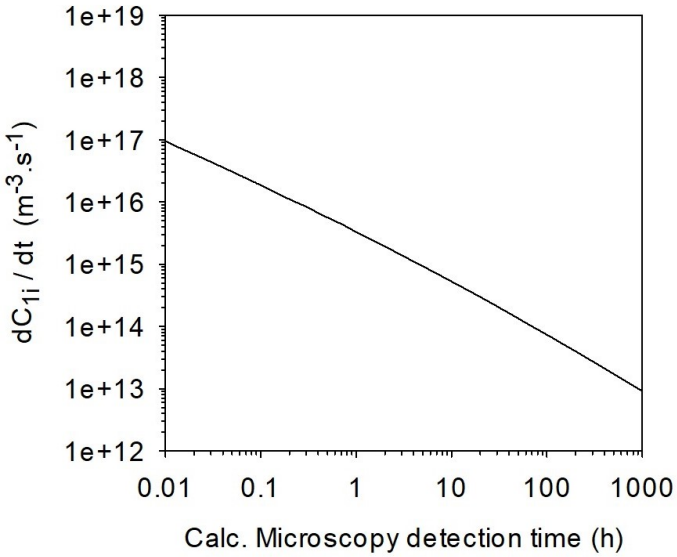

FIGURE 4.16: Computed initial generation rate against microscopy detection-time of unstable asphaltenes

Logically, the microscope detection-time increases with slower generation of particles. More importantly, a relationship can be derived between both output parameters when combining the issues of the two precedent plots resulting from the simultaneously computed destabilization and aggregation processes. The scaling relation between the detection-time of particles under microscope visualization and the generation rate of primary units is given, within a domain of time shorter than the detection-time, by:

$$\log\left(\frac{dC_{1_i}}{dt}\right) \propto \log\left(t_{detection}\right) \tag{4.21}$$

4.3.5 Insights of simultaneous destabilization, aggregation and deposition

Previous results suggest that the generation rate of unstable particles has directly an impact on the deposition process, however the aggregation may also have an indirect consequences. Indeed, we have seen that smaller particles will travel faster toward a surface a deposition in the presupposed regime controlled by diffusion. Therefore at fixed primary particles generation; if the aggregation is much faster than the diffusive deposition: the available particles for deposition can be assumed equal to generated ones at the considered instant, other being to large to be considered in the deposition process. Reversely if the aggregation is much slower than the deposition: the system may accumulate large number of unstable units available to deposit. The stability ratio, indicative of the flocculation kinetics, is compared in Figure 4.17 to the deposition rate measured with an immersed resonating sensor during the addition of heptane in crude oil.

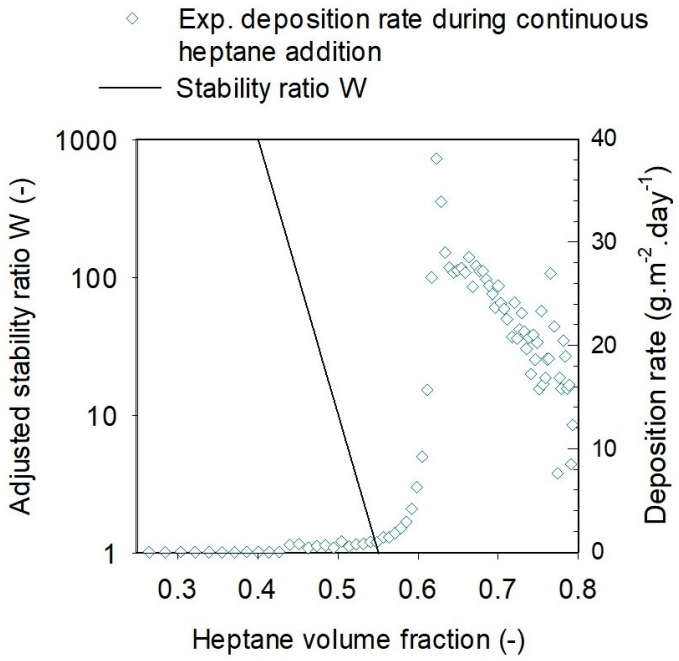

FIGURE 4.17: Stability ratio compared to the QCR measured deposition rate as a function of the heptane content

The results gives the indication that considerable deposition occurs only at conditions of oil-heptane mixtures when the aggregation is extremely fast (W <1). The

mesured deposition rate is null at extremely low heptane concentrations and becomes slightly positive in the range of heptane concentrations corresponding to the detection-time curve (40 to 55 vol%). The deposition rate then reaches tens of $g.m^2.day^{-1}$ at larger heptane contents.
Consequently to this observation, the aggregation rate can be assumed immediate and reduces our number of adjusting coefficients in asphaltenes deposition modeling.

4.4 Conclusions

In this work, the Smoluchowski's coagulation model has been combined to a mathematical expression for the time-dependent generation of unstable asphaltenes. An existing analytical solution for the aggregation part is computed with considering a mono-disperse size of aggregates. However the simultaneous generation of unstable clusters, also analytically resolved using described functions in our previous work, brings the problem into a numerical dimension along the aging time. A numerical approach has been proposed by simply adding the generated number of primary particles to the existing ones after solving the aggregation during a given time interval. The aggregation rate constant K_{ij} is calculated for the preferential aggregation of particles with extreme sizes (primary ones and largest ones) and is adjusted with a colloidal stability ratio W. An excellent agreement is found between the experimental observations and the simulation of the time of aggregates growth to a micro-size as a function of the heptane content. Despite a minor offset, the model fairly correlates the immediate appearance of large flocs to the change of regime predicted by the tuned stability ratio. The found "onset" conditions at which fast flocculation occurs compare to the concepts of the extensively reported critical coagulation concentration of dissolved salt in aqueous colloidal systems. Those conditions basically correspond to the transition from stabilized suspensions by predominant repulsive interactions (likely steric for asphaltenes[27] or more commonly electrostatic for aqueous systems) to favorable conditions for the coagulation when attractive interactions dominate (most likely VdW dispersion forces for asphaltenes). A critical concentration of alkanes can indirectly be defined as the corresponding unity of the stability ration for the aggregation of asphaltenes.
It is important to note that in this work, "onset" conditions refer to the alkane volume concentrations at which the aggregation of asphaltenes transitions from a regime where repulsive interactions dominate to a process controlled by attractive interactions. This interpretation is the result of a comprehensive data processing that incorporate both time-dependent phenomenon; the destabilization and the aggregation of asphaltenes after addition of *n*-heptane to crude oil. The attention of the reader is brought to this particular point as many studies use a different definition of the "onset", usually referred to as the point at which instantaneous detection of unstable asphaltenes is observed. Depending on the sensitivity of the used protocol in laboratory measurements, some results can logically diverge. With the proposed definition, the "onset" conditions become independent of the experimental apparatus but are rather obtained through the determination of the colloidal stability ratio profile, W versus the alkanes content in oil.
The aggregation is experimentally showed to contribute to the slow process within a low enough range of heptane contents, however results indicate that the aggregation takes infinitely short times at concentrations of heptane larger than the so-called "onset" conditions. This study suggests that the driving force of unstable asphaltenes

aggregation is their interaction potential. Consequently, the number of aggregation mechanisms can be reduced to two depending on the surrounding solvent. As particles of unstable asphaltenes approach each other due to the Brownian motion;
- (i) if the concentration of alkanes is sufficiently low in the liquid solvent, repulsive interactions will dominate and the aggregation will follow a typical RLCA slow behavior behavior with stability ratios larger than 1
- (ii) if the concentration of alkanes is sufficiently large in the solvent (larger than the "onset"), attractive interactions will dictate the extremely fast aggregation, characterized by a stability ratio smaller than 1.
Therefore, the importance of accounting for both destabilization and aggregation kinetics of asphaltenes upon addition of a flocculating agent (heptane in this work) is restricted to only certain compositions of oil-alkane mixtures.
As showed in this work, this practice seems compatible with the description of asphaltene constituents as a continuum of molecules with a coupled model for destabilization kinetics. Therefore the combination of the present work with the extensive reported research on the regular solution theory (or more commonly referred as the Flory-Huggins[13] theory) might enhance the quantitative accuracy of predictive tools on the flocculation of asphaltenes.
After consistent verification of the modeling techniques, a scaling relationship is found between the initial generation rate of primary units r_1 and the particle detection-time of micro-aggregates. Finally, the deposition of unstable asphaltenes is found to happen in the region where the aggregation is extremely fast and suggests that the aggregation can be assumed instantaneous in asphaltene deposition models.

Bibliography

[1] Buckley, J. S., G. Hirasaki, Y. Liu, S. Von Drasek, J. Wang, and B. Gill
1998. Asphaltene precipitation and solvent properties of crude oils. *Petroleum Science and Technology*, 16(3-4):251–285.

[2] Campen, S., B. Smith, and J. S. Wong
2018. Deposition of asphaltene from destabilized dispersions in heptane-toluene. *Energy & Fuels*.

[3] Derjaguin, B.
1940. On the repulsive forces between charged colloid particles and on the theory of slow coagulation and stability of lyophobe sols. *Transactions of the Faraday Society*, 35:203–215.

[4] Duran, J., F. Schoeggl, and H. Yarranton
2019. Kinetics of asphaltene precipitation/aggregation from diluted crude oil. *Fuel*, 255:115859.

[5] Elimelech, M.
1995. *Particle deposition and aggregation: measurement, modelling, and simulation*, Colloid and surface engineering series. Butterworth-Heinemann.

[6] Eyssautier, Joëlle; Frot, D. B. L.
2012. Structure and dynamic properties of colloidal asphaltene aggregates. *Langmuir*, 28.

[7] Fávero, C. V. B., T. Maqbool, M. Hoepfner, N. Haji-Akbari, and H. S. Fogler
2017. Revisiting the flocculation kinetics of destabilized asphaltenes. *Advances in colloid and interface science*, 244:267–280.

[8] Fuchs, v. N.
1934. Über die stabilität und aufladung der aerosole. *Zeitschrift für Physik*, 89(11-12):736–743.

[9] Goual, L., M. Sedghi, X. Wang, and Z. Zhu
2014. Asphaltene aggregation and impact of alkylphenols. *Langmuir*, 30(19):5394–5403.

[10] Haji-Akbari, N., P. Masirisuk, M. P. Hoepfner, and H. S. Fogler
2013. A unified model for aggregation of asphaltenes. *Energy & Fuels*, 27(5):2497–2505.

[11] Haji-Akbari, N., P. Teeraphapkul, A. T. Balgoa, and H. S. Fogler
2015. Effect of n-alkane precipitants on aggregation kinetics of asphaltenes. *Energy & Fuels*, 29(4):2190–2196.

[12] Hoepfner, M. P., C. Vilas Boas Favero, N. Haji-Akbari, and H. S. Fogler
2013. The fractal aggregation of asphaltenes. *Langmuir*, 29(28):8799–8808.

[13] Huggins, M. L.
1964. A revised theory of high polymer solutions. *Journal of the American Chemical Society*, 86(17):3535–3540.

[14] Israelachvili, J. N.
2015. *Intermolecular and surface forces*. Academic press.

[15] Maqbool, T., A. T. Balgoa, and H. S. Fogler
2009. Revisiting asphaltene precipitation from crude oils: A case of neglected kinetic effects. *Energy & Fuels*, 23(7):3681–3686.

[16] Maqbool, T., S. Raha, M. P. , and H. S. Fogler
2011. Modeling the aggregation of asphaltene nanoaggregates in crude oil- precipitant systems. *Energy & Fuels*, 25(4):1585–1596.

[17] McGown, D. N. and G. D. Parfitt
1967. Improved theoretical calculation of the stability ratio for colloidal systems. *The Journal of Physical Chemistry*, 71(2):449–450.

[18] Morrison, I. D. and S. Ross
2002. *Colloidal dispersions: suspensions, emulsions, and foams*. Wiley-Interscience New York.

[19] Mullins, O. C.
2011. The asphaltenes. *Annual review of analytical chemistry*, 4:393–418.

[20] Mullins, O. C. and E. Y. Sheu
2013. *Structures and dynamics of asphaltenes*. Springer Science & Business Media.

[21] Otto, E. and H. Fissan
1999. Brownian coagulation of submicron particles. *Advanced Powder Technology*, 10(1):1–20.

[22] Petosa, A. R., D. P. Jaisi, I. R. Quevedo, M. Elimelech, and N. Tufenkji
2010. Aggregation and deposition of engineered nanomaterials in aquatic environments: role of physicochemical interactions. *Environmental science & technology*, 44(17):6532–6549.

[23] Smoluchowski, M. v.
1918. Versuch einer mathematischen theorie der koagulationskinetik kolloider lösungen. *Zeitschrift für physikalische Chemie*, 92(1):129–168.

[24] Spielman, L. A.
1970. Viscous interactions in brownian coagulation. *Journal of Colloid and Interface Science*, 33(4):562–571.

[25] Tadros, T.
2013. *Stability Ratio*, Pp. 1047–1048. Berlin, Heidelberg: Springer Berlin Heidelberg.

[26] Verwey, E. J. W.
1947. Theory of the stability of lyophobic colloids. *The Journal of Physical Chemistry*, 51(3):631–636.

[27] Wang, S., J. Liu, L. Zhang, J. Masliyah, and Z. Xu
2009. Interaction forces between asphaltene surfaces in organic solvents. *Langmuir*, 26(1):183–190.

[28] Wang, S., J. Liu, L. Zhang, Z. Xu, and J. Masliyah
2008. Colloidal interactions between asphaltene surfaces in toluene. *Energy & Fuels*, 23(2):862–869.

[29] Wiehe, I. A.
2012. Asphaltene solubility and fluid compatibility. *Energy & Fuels*, 26(7):4004–4016.

Chapter 5

A simplified model for the deposition of asphaltenes

5.1 Introduction

Asphaltenes destabilization corroborates to various reported industrial problems [32;15;41;3;9]. The deposition of asphaltenes in conduits can constrain the transport of crude oils from geologic reservoirs to surface facilities by locally reducing inner tubular cross-sections [22;25;27;14]. Experimental deposition has been observed by flowing mixtures of oil and n-alkanes through various geometries [4;37;28;23;11].
The lack of mechanistic understanding lead researchers to investigate the transport mechanisms of destabilized asphaltenes from the bulk to the surface. Kurup et al. [26] first attempted to solve mass conservation equations coupled to a thermodynamic module of asphaltenes destabilization with equilibrium assumptions. Similarly, Guan et al. [17] developed an integrated tool solving conservation equations including mass transport, aggregation and dissociation of particles while still assuming thermodynamic equilibrium with cubic equations of state (EoS). As opposed to a phenomenon limited by suface reaction, successive authors [37;21] revealed the diffusive behavior of the asphaltene deposition process happening at the liquid/solid interface. Indeed, the deposition process can be modeled as a chemical reaction controlled by a deposition coefficient k_{dep} in which destabilized asphaltenes are idealized by spherical particles. As per the schematic on Figure 5.1, the deposition reaction is separated into two actions: the convective mass transfer that has a coefficient k_c and the sticking reaction of unstable particles to the solid interface characterized by a coefficient k_r.

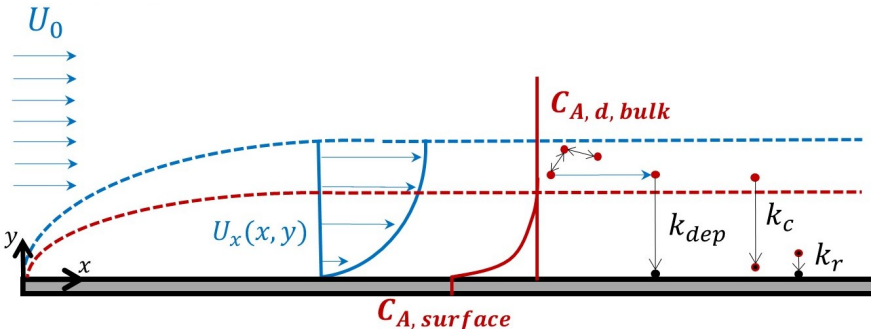

FIGURE 5.1: Schematic of unstable asphaltene particles travelling at a velocity $U_x(x, y)$ in the momentum boundary layer (blue dashed line) over a parallel solid surface and depositing through a mass transfer boundary layer (red dashed line) at a rate controlled by the constant k_{dep}

Assuming a diffusion controlled surface reaction, a gradient of concentration of asphaltenes available to deposit ($\Delta C_{A,d} = C_{A,d,bulk} - C_{A,surface}$) will reside through a mass transfer boundary layer as shown in the schematic of figure 5.1. $C_{A,d}$ is the mass concentration of unstable asphaltenes available to deposit and needs to be defined.
The presupposed mass transfer limited process adverts that $k_r >> k_c$. Hence the deposition rate of asphaltenes might be directly function of the square rooted pace at which fluid material is delivered in the vicinity of the solid surface[13] (see Figure 5.2).

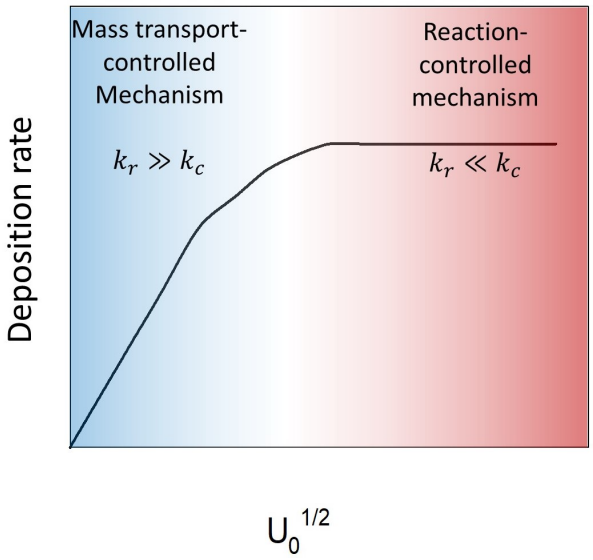

FIGURE 5.2: Surface deposition rate as a function of the square root of fluid superficial velocity U_0

Qualitatively, the ability of a diffusing asphaltenes particle to adhere to another existing solid entity can be compared to its Brownian collision efficiency (β) when aggregating to another particle. By analogy, the results of the precedent Chapters suggested slow destabilization kinetics and fast aggregation in range of conditions showing large deposition rates, a relatively large surface reaction coefficient k_r seems therefore rational with large collision efficiencies. As the deposition rate evolves into a dependence on the superficial velocity U_0 over the solid wall, the Sherwood dimensionless number will let us analyze the ratio of the rate of convective mass transfer, represented by the coefficient k_c, over the diffusion rate of particles toward the solid wall. The diffusion rate of unstable asphaltenes is calculated through the coefficient D_A (where A stands for depositing unstable asphaltenes) for a geometry that have a characteristic length L. As showed in precedent Chapters, unstable asphaltenes can have various sizes and this work will further investigate the main contributing aggregates to the deposition process.

$$\text{Sh} = \frac{\text{convective mass transfer}}{\text{diffusive mass transfer}} = \frac{k_c L}{D_A} \tag{5.1}$$

5.1.1 Properties of depositing unstable asphaltenes

With the abundantly reported diffusion-limited mechanism of asphaltene deposition, the size of depositing particles will play an important role[33]. According to

Stokes-Einstein, the diffusion coefficient of a low Reynolds particles scales inversely proportionally to the hydrodynamic radius R_A of depositing particles when immersed in a liquid medium with a dynamic viscosity μ_{liq}:

$$D_A = \frac{k_B T}{6\pi\mu_{liq} R_A} \tag{5.2}$$

where k_B is the Boltzmann constant and T is the temperature.
Eskin et al.[11] measured masses of asphaltene deposits formed by a turbulent flow of a live-oil in a couette-like device at constant pressure. They reached fair agreements between the measurements and their model that combined aggregation, deposition and shear removal. Those results first introduced the concept of a critical asphaltene particle size (tens of nanometers) by hypothesizing that larger particles motion is controlled by fluid mechanics. Indeed, re-suspension of particles in the flow stream is a well known phenomenon that mainly affect particles larger than few micrometers. The mass transfer boundary layer is typically tens of micrometers thick for parallel viscous flow regimes[40]. It then becomes evident that particles of the same order of sizes than the boundary layer will unlikely contribute to the diffusive process and will rather be subject to hydrodynamic forces, such as the inertial-lift ones[1]. On the other hand, intermittently striking large particles with an oblique trajectory may stick or bounce-off to more or less long distances from the solid surface. The particles can eventually be re-entrained[38] depending on the viscous sub-layer thickness. For example Chamberlain and Little[6] reported low deposition efficiencies of dry particles hydrodynamically travelling at velocities exceeding 0.5 m/s toward the solid surface.
Accordingly to the above exposed concepts, non-invasive measurements of the size and morphology of destabilized structures have been applied to solutions containing growing asphaltenes. Hoepfner et al.[24] have reported extremely slow growth of unstable asphaltenes before reaching the micro-scale at sufficiently low *n*-alkane contents. The extremely long lifetimes of particles at the nano-scale measured by scattering techniques[24] tended to suggest that unstable asphaltenes are subject to fast diffusive deposition fluxes during their entire residence in transport systems like pipelines. However when placed into their context, we note that the testing conditions were cautiously chosen in a range of low enough heptane concentrations permitting their visualization by microscopy after waiting hundreds of hours[30]. We must acknowledge from an equilibrium perspective[19;18;12] that for a given liquid viscosity, Equation 5.3 developed by Haji-Akbari et al.[18] indicates that conditions implying long microscopy detection-times of particles necessarily contain a relatively poor quantity of unstable asphaltenes and vice versa.

$$\ln(t_{detection}\sqrt{C_{A_\infty}}/\mu_{liq}) \propto \frac{1}{(\delta_{asph} - \delta_{solution})^2} \tag{5.3}$$

where δ_i is the solubility parameter of the component i, $t_{detection}$ is the necessary aging time of a given solution before observing particles by microscopy and C_{A_∞} is the concentration of unstable asphaltenes at equilibrium. When taking the destabilization kinetics into account, the concentration of unstable asphaltenes is further reduced compared to the amount at equilibrium. For example, the comparison of separated asphaltenes by centrifugation to their detection-time by microscopy in Figure 5.3, shows that larger equilibrium concentration (C_{A_∞} of unstable asphaltenes correspond to lower microscopy observation times.

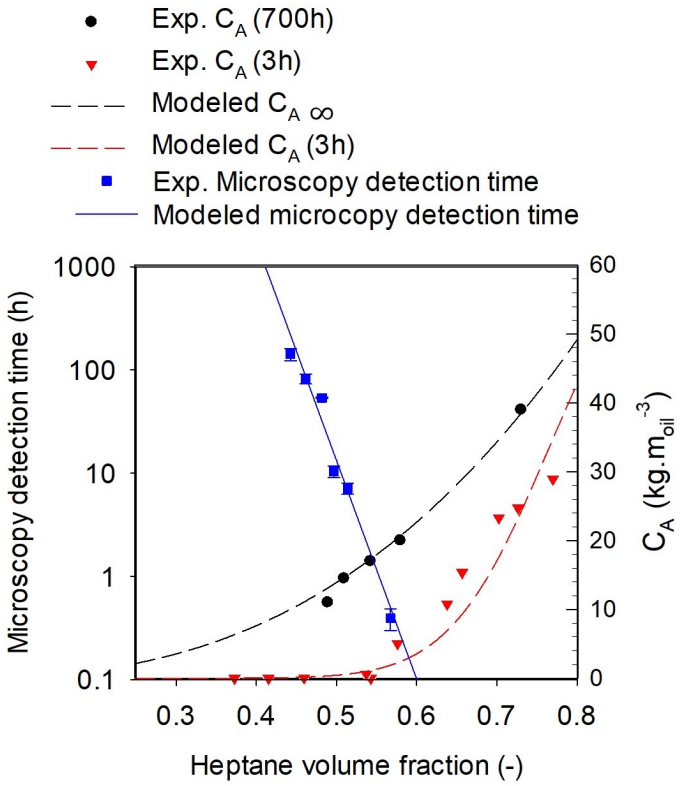

FIGURE 5.3: Comparison between the detection-time of unstable asphaltenes by microscopy and the separated unstable asphaltenes by centrifugation

Consider constant sizes of unstable asphaltenes, according to Equation 5.4, larger content of asphaltenes available to deposit will make the deposition rate to increase. Consequently, severe diffusive deposition might not arise from conditions chosen to study extremely slow appearance of micro particles of unstable asphaltenes [18;24;30].

$$Rate_{dep} \propto C_{A,d} \tag{5.4}$$

In the range of heptane contents beyond the microscopy detection-time region, reported results of dynamic light scattering (DLS) and centrifugations coupled to UV-visible spectroscopy have demonstrated that the particle size distributions reach micrometer sizes within seconds [29;5]. Other authors reported even larger particle sizes at more aggressive conditions or for solutions aged for longer duration [8]. At those conditions, the fast aggregation kinetics necessarily involves a short residence time of small unstable particles. Therefore the majority of asphaltenes available to deposit might be limited to destabilized structures aged for lesser time than the characteristic time that lets the aggregation to happen. As explained in Chapter **??**, this phenomena is described by the collision kernel K_{ij} between colliding particles i and j. For agglomeration of Brownian particles immersed in a fluid of much smaller particles (atoms or small molecules), the collision frequency is given by:

$$K_{ij} = \frac{2R_g T}{3\mu_{liq}} \frac{(d_i + d_j)^2}{d_i d_j} \frac{1}{W} \tag{5.5}$$

where d_i and d_j represent the hydrodynamic diameters of colliding aggregates i and j, R_g is universal gas constant, μ_{liq} the dynamic viscosity of the liquid medium, T is

the absolute temperature and W is the colloidal stability ratio of the solution. The diameter of Brownian particles in a liquid usually varies between 1 nm and 1 μm. Considering that typical dynamic viscosities of petroleum mixtures is 10^{-3} to 1 Pa.s, the aggregation rate constant K_{1j} of newly generated unstable clusters to nearby particles will be larger than 10^4 s^{-1}. New unstable asphaltenes are asphaltenes that pass from the state of dispersed clusters of nanoaggregates that have a constant size of $\sim$ 10 nm to growing particles. According to the previous results of this dissertation, the colloidal stability ratio of unstable asphaltenes in solutions approaches the unity. Those estimations let us reasonably assume that the prevailing generated unstable asphaltenes are existing only during the ongoing simulated time step ($\Delta t >>$ 1 s). Indeed, with the preferential coagulation of particles that have different sizes (large values of kernels K_{1j}), newly generated unstable asphaltenes at the time t can be considered as aggregated to larger entities at next simulated time ($t + \Delta t$).
As reported in the introductory Chapter, stable or dispersed colloidally stable asphaltenes behave like loose, meta-stable and highly porous solid suspending structures characterized by fractal dimensions D_f between 1.3 and 2. When escaping from the meta-stability state upon volumetric addition of alkanes, clusters will shrink and asphaltene nanoaaggregates will force the solvent molecules out of the suspending structures. This behavior has been experimentally evidenced by measurements of larger fractal dimensions ($D_f \sim$ 2.1 to 2.8) using nano[24] and micro-scale[7;8] experimental methods. Their contact with the surrounding solvent molecules will then be further reduced by aggregating to other particles and grow in size while trapping solvent. It then seems rational to approximate primary destabilized asphaltenes as hard and porous spheres of sizes in the same order of clusters described by the Yen-Mullins[34] hierarchical representation ($R_A \sim$ 5 to 10 nm).
On the other hand, diffusing clusters can contain significant amounts of trapped solvent depending on their internal packing. It involves that the effective density ρ_{eff} of the depositing fractal structures will be less than the one of "dry" asphaltenes ρ_{asph} (broadly accepted as $\rho_{asph} \sim$ 1200 kg.m^{-3}), ρ_{eff} needs to be calculated. An expression of the effective density of clusters arises from the work of Barré et al.[2]. The effective density of the aggregates is designated by ρ_{eff} is expressed as a function of the density of the mixture components and is given by:

$$\rho_{eff} = \left(\frac{\phi_{asph}}{\rho_{asph}} + \frac{(1 - \phi_{asph})}{\rho_{liq}} \right)^{-1} \tag{5.6}$$

where ρ_{liq} is the density of the trapped liquid solvent. Equation 5.7 relates the volume of "swollen" structures (termed as the effective volume v_{eff}) to the "dry" volume of asphaltenes v_{asph} with the fractal dimension of asphaltene clusters in good solvents. For a dilute system of solvated aggregates, the actual volume fraction of asphaltene components within a cluster is the ratio of these quantities defined by Barré et al.[2] as:

$$\phi_{asph} = \frac{v_{asph}}{v_{eff}} = \left(\frac{R_A}{R_p} \right)^{D_f - 3} \tag{5.7}$$

where R_p is the hydrodynamic radius of units composing the considered particle of a radius R_A; nanoaggregates of asphaltenes with an average hydrodynamic radius of 1.3 nm have frequently been reported to be the primary units of asphaltenes aggregates[2;36;31;18], this value of R_p is therefore fixed in our calculations. The mass

fraction of asphaltene molecules within the fractal structure x_{asph} is then given by:

$$x_{asph} = \frac{\rho_{asph}}{\rho_{eff}} \phi_{asph} \tag{5.8}$$

Combining the three precedent equations, we obtain the mass fraction of "dry" unstable asphaltenes in diffusing particles toward the solid surface:

$$x_{asph} = \frac{1}{\rho_{liq} + \rho_{asph} \left(\left(\frac{R_A}{R_p} \right)^{D_f - 3} - 1 \right)} \tag{5.9}$$

5.1.2 Previous deposition modeling investigations

Gradual understanding of asphaltene destabilization and deposition over years motivated researchers to complicate deposition modeling with multiple coefficients and account for all the simultaneously occurring phenomena during the oil flow: destabilization, aggregation, dissociation, mass transport, adhesion and shear removal[3;11]. Authors were able to numerically compute predictions and compare results to experimental data and to few reported field observations. With one exception[39], deposition modeling approaches found in the literature hence adopted the tuning of adjustable parameters and respective coefficients to each considered phenomena that are enumerated above (at least 3). Excellent agreements were accordingly observed, but such multi parameter tuning make a fully predictive application of models unreasonable. Indeed the possibility of compensating errors from incorrectly (though realistic) estimated parameters arises from the implementation of numerous adjusted restrictions.
As discussed in the previous Chapter, Vilas Bôas Fávero et al.[39] further reinforced previous discoveries by modeling asphaltene deposition in a packed-bed geometry at various conditions (crude oils, n-alkane contents, flow rates, packed-bed lengths). For the first time, asphaltene deposition modeling was limited to only one tuning parameter: the diffusion coefficient of depositing asphaltenes, all other parameters being measured. They have found very good agreements to their experimental results, in line with the mentioned critical size of $\sim$ 100 nm[11]. Results of Vilas Bôas Fávero et al.[39] can be revisited with accounting for results of precedent Chapters relating the destabilization kinetic and faster aggregation process. In this case, the concentration of asphaltenes available to deposit $C_{A,d}$ will take time-dependent values that are necessarily smaller than the equilibrium values C_{A_∞}. With this and according to Equation 5.10, the adjustment of depositing particles diffusion coefficient will take larger values.

$$Rate_{dep} \propto C_{A,d} D_A^{2/3} \tag{5.10}$$

According to the combined equations 5.2 and 5.10 used to model the deposition in a packed-bed geometry, such amendment will lead to even smaller back-calculated particle sizes than the ones found by the authors. This important result suggests that the average size of diffusing particles approaches the size of primary unstable particles or the size of stable clusters.
On the other hand, findings on the destabilization kinetic (Chapter3) suggest that the generation of primary particles decays exponentially over time for a given solution of oil-alkane. Combining the observations on destabilization kinetics to the small size indication of depositing entities[5;29;39;11], one would expect lighter deposition rates with flowing a beforehand prepared and aged mixture than the flow of fresh

solutions. The most severe conditions of deposition might therefore exist immediately after the solution was changed by adding anti-solvents, when the generation of primary particles equals its maximum composition. As expected from this rough analysis, Campen et al.[5] experimentally observed significantly increasing deposition rates on a one-face contacted quartz crystal when the aging time of the solution was decreased (by shortening the tube length between their mixing-tee and their measurement device).

5.1.3 Objectives and assumptions of this work

The principal purpose of the present investigation is to improve the understanding of deposition with restrained number of adjustable parameters. The incorporation of the destabilization kinetics to the deposition models found in the literature suggests that the generation of primary particles might play a predominant role linked to the parameter $C_{A,d}$.
In this Chapter, an analytical deposition model was developed for a immersed disc in a stirred tank reactor at atmospheric pressure with parallel viscous flow of a solution that contains unstable asphaltenes. The diffusion-limited regime is verified and simplifications on the particle size distribution are drawn. Indeed, the intention of the study is to verify the applicability of simplifications arising from conclusions of Chapters 3 and 4. The following adaptations are proposed:
(i) the rate of destabilization of asphaltenes is exclusively controlled by the continuous volumetric expansion rate of the flocculating agent due to the large decay of the generation constant k_N by multiple orders of magnitude upon the aging of solutions
(ii) the aggregation of generated particles to larger entities is immediate at conditions of alkane contents larger than the "onset" due to the observed behavior of the colloidal stability ratio W
(iii) the size distribution of unstable asphaltenes can be considered bi-modal with at alkane contents larger than the "onset" (see schematic in figure 5.4).

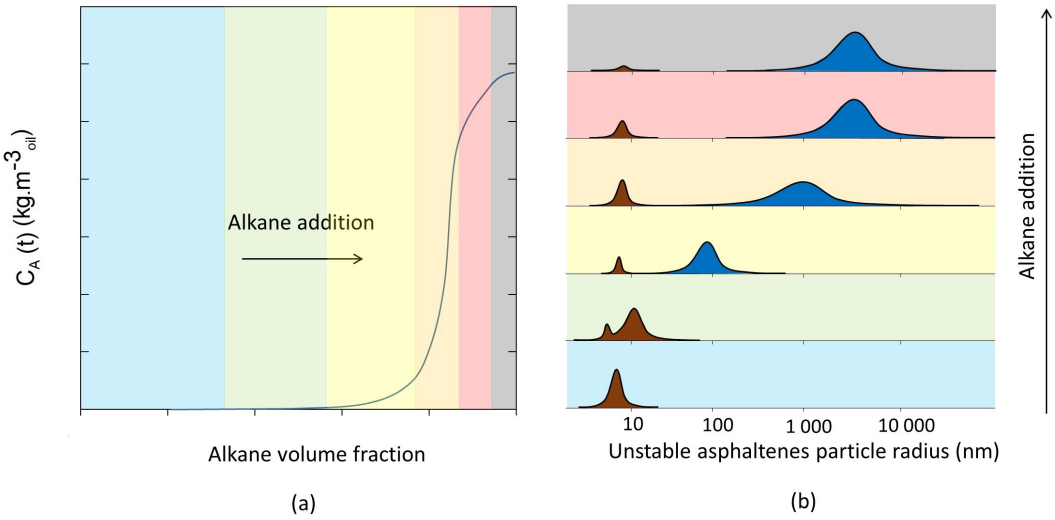

FIGURE 5.4: (a) Usual total concentration profile of unstable asphaltenes C_A during a volumetric alkane addition
(b) Schematic depiction of the hypothetical evolution of the particle size distribution upon expansion of an alkane with respective zones to C_A profile.

As explained, under those circumstances the large collision efficiencies of generated unstable asphaltenes force them to immediately associate with their nearest neighbor particles. New primary particles will likely belong to the already existing particles distribution at the next time step when discretizing the problem. At large concentrations of unstable asphaltenes the size distribution of most particles typically ranges within hundreds to thousands of nanometers[29;5]. Although their respective residence time is short at large alkane contents, significant quantities of primary particles are continuously generated as long as the alkane expansion continues over time. In this way, very few particles of intermediate size might reside while two distinct distributions will coexist: the first one around the size order of clusters of nanoaggregates and the second one in the order of the oldest aggregates. When the concentration of unstable asphaltenes becomes significant, the average size of particles exceeds 1μm. For this reason, the member objects of the largest size distribution (colored in blue in figure 5.4 (b)) are neglected in the solved transport equations of this work.
The signal of the immersed QCR gives us access to a large number of deposition measurements in order to verify this assumption. The mass transfer of unstable asphaltenes toward a solid surface is studied for the specific case of continuous addition of heptane to crude oil. Relevant parameters to the deposition process in our apparatus are accordingly identified and varied; the superficial fluid velocity, the addition rate of C_7 and the initial presence of particles larger than 200 nm. Their respective implications on the deposition implied by continuous change of composition of the solvent are observed.

5.2 Materials and methods

The experimental apparatus and the data processing to calculate the deposited mass on the quartz surfaces are described in Chapter 2 of the dissertation. In order to

avoid any redundancy, the present section is dedicated to the description of complementing details and assumes that the reader has earlier referred to the section *Experimental methods used for this research* in Chapter 2. The temperature of work was set to 60°C within the present investigations. A single crude oil was used throughout the study and some properties of the crude oil at the temperature of interest are provided in the following table. Considered as a relevant variable to verify the contribution of primary unstable particles to the deposit, the promotion rate of heptane ranges between 0.1 and 5 $cm^3.min^{-1}$.

TABLE 5.1: Crude oil properties at 60°C and atmospheric pressure

Density	Viscosity	Refractive Index	Average molecular weight	C_7 Asphaltenes content
$kg.m^{-3}$	$mPa.s$	-	$g.mol^{-1}$	$wt\%$
876	12.0	1.4938	232	10.3

5.2.1 Superficial velocity surrounding the sensor

The effect of the superficial velocity U_0 is deterministic of diffusion-limited regimes. Halász et al.[20] studied the vertical, radial and tangential velocity components of a vortex flow induced by a magnetic stirrer in a beaker using particle image velocimetry (PIV). Dye tracing and particle tracking both indicated a dominant downwelling behavior in the central region below the visual liquid-air interface funnel. By analogy, hypothesized vertical component streamlines are drawn for our geometry in Figure 5.5.

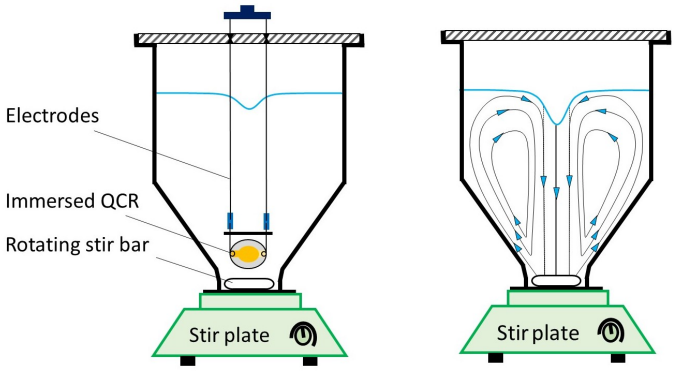

FIGURE 5.5: Qualitative schematic of the streamlines in the vessel used in this research

The sensor being centered above the stir bar at a very near distance (∼1 cm), the vertical flow is the only considered component. A dye tracing visual method was employed to measure the velocity of the liquid nearby the piezoelectric resonator as a function of the revolution speed of the magnetic stirrer. Note that water was chosen for practical reasons (transparent and suitable refractive index to enable image treatment), different density and viscosity of the liquid might have minor impacts on the velocity, those effects are neglected. The reactor was filled with water and equipped with a vertically placed 100 μL syringe that contained a 3 wt% aqueous solution of fluorescein. The concentration of the solution was adjusted to ensure a good track

of the encouraged flow by the stirring of the mixture. The difference in density between the initial water and the injected solution was verified to be sufficiently low such that it had a minor impact on measurements within the investigated scale of time, the sedimentation of the injected solution could not not observed. A 180° bent injection needle promoted the tracer in the upward vertical direction to guarantee a null downward initial velocity. A fixed 240 frame per second camera was activated in front of the glass reactor to record each pulse of tracer at various stirring speed. Video editing enabled to increase the contrast of the emission color (yellow/orange in the case of our tracer). The vertical movement of the darkened area could then be carefully tracked for individual frames taken every ∼4 ms. The injection point was first positioned in a central position (with and without sensor: Figures 5.6 and 5.7) below the visible funnel during the first part of the measurements to verify the predominance of vertical flow.

FIGURE 5.6: Snapshot pictures of the dye average velocity measurements below in the central region in absence of the sensor

FIGURE 5.7: Snapshot pictures of the dye average velocity measurements below in the central region in presence of the sensor

The width of the funnel and the measured average velocity significantly differed in presence of the sensor and the electrodes, a dependence of the velocity on the vertical position was also observed. Therefore, the injection point was placed next to the sensor and the video was focused on the specific area of interest to improve the local accuracy of this estimation. Figure 5.8 shows the physical location of the needle for dye injection next to the sensor.
A tracker video tool (from Open Source Physics Java framework) facilitated the

data analysis by pointing a 2D-located marker on the extreme lowest threshold (black/yellow interface) of the focused area over time.

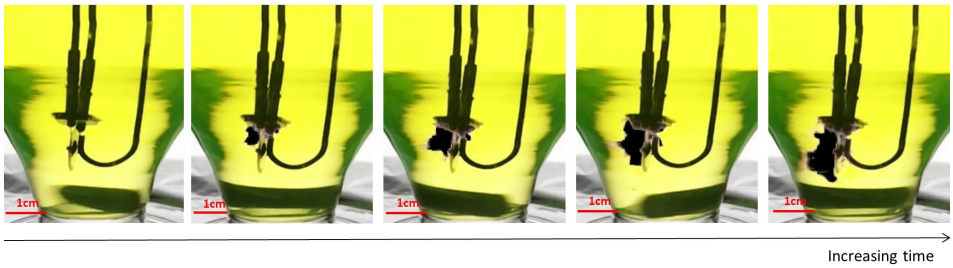

FIGURE 5.8: Zoomed snapshot pictures of the dye velocity measurement next to the sensor

The analysis of the tracked data points then provided estimations of the downward velocity with results exposed in a later section.

5.2.2 Concentration of unstable asphaltenes available to deposit $C_{A,d}$

The concentration profile of unstable asphaltenes along titrations is an input parameter of our deposition model, it can be measured or modeled as shown in Chapter 3. In this study, an experimentally determined C_A profile is preferable in order to reduce uncertainties on the entered deposition modeling parameters. For that, the mixtures of oil-heptane are first prepared with adding heptane at a rate of 0.2 cm^3 in a constant mass of crude oil (18 g) until the desired composition is reached. The mass of unstable asphaltenes is then measured with centrifuging 1.5mL aliquots during 10 to 15 minutes at an acceleration of 24000x the g-force. The centrifugation time is adjusted to establish a constant cut-off size of separated particles to 150 nm (see Appendix). Table 5.2 is reported from centrifugation data to input the time-resolved concentration of unstable asphaltenes to the model as a function of the volume fraction of heptane in the mixture ϕ_{c_7}:

$$\phi_{c_7} = \frac{V_{c_7}}{V_{oil} + V_{c_7}} \tag{5.11}$$

where V_i is the volume of the component i calculated from its measured mass and density.

TABLE 5.2: Concentration of unstable asphaltenes separated by time-resolved centrifugation along the titration

ϕ_{C_7} -	$C_{A>150\text{nm}}$ $kg.m^{-3}$
0	0
0.416	0
0.46	0.0774
0.538	0.0387
0.543	0
0.576	2.989
0.638	10.778
0.656	15.381
0.726	24.748
0.91	59.904

A linear regression interpolates the C_A measured data points by centrifugation with a slope later termed a_1. The trend is thereafter used to calculate C_A for larger volume fractions than the x-axis intercepting point $\phi_{c_7 min}$ = 0.5696. At volume fractions inferior to $\phi_{c_7 min}$, the concentration of unstable asphaltenes is assumed null. For comparison, computed results with expressions of the C_A profile from the proposed model of destabilization kinetics (defined in the precedent Chapter) along the titration are also showed throughout this study. The obtained curves fairly compare to each other as observed in the following Figure:

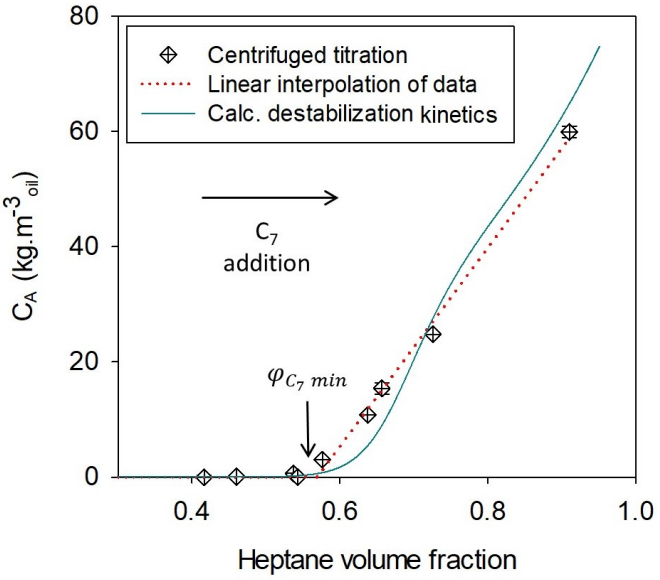

FIGURE 5.9: Concentration of unstable asphaltenes as a function of the volume fraction of heptane during continuous addition

During the continuous addition of the anti-solvent, estimates of the mass quantity of generated unstable particles per unit volume of solution is an information contained in the slope of the concentration profile C_A multiplied by the volume fraction of oil in the mixture to account for the dilution effect. Discretization of the time will be used to resolve the quantity of available primary particles at a particular times t_k during the titration. With respect to extremely short characteristic times of

aggregation suggested by previous results, generated particles are assumed to no longer exist in the form of primary units at the following time step t_{k+1} and are rather already considered larger entities. Note that with such an approach, the depletion of asphaltenes due to the deposition (on all solid surfaces) does not require to be accounted for in the model. Indeed the concentration profile of primary particles is independent from the total concentration of unstable asphaltenes itself but is rather dependent on the evolution of C_A with time. The estimated profile of primary particles concentration in the solution along the experiment is given by:

$$C_1(t) \approx \Delta C_{A_k} = \epsilon_{10} \left(\frac{\partial C_A}{\partial \phi_{c_7}} \frac{\partial \phi_{c_7}}{\partial t} \right)_{t_k} (1 - \phi_{c_7})_{t_k} \Delta t = \epsilon_{10} a_1 \frac{\partial \phi_{c_7}}{\partial t} (1 - \phi_{c_7})_{t_k} \Delta t \tag{5.12}$$

where ϵ_{10} takes the value of 1 when $\phi_{c_7} > \phi_{c_7 min}$ and equals 0 when $\phi_{c_7} < \phi_{c_7 min}$. In order to minimize discretization errors, the grid size of time was refined until converging to relative errors of less than 1% when back-calculating C_A in the following manner:

$$C_A(t_k) = \sum_{k=0}^{k} \Delta C_{A_k} \tag{5.13}$$

Expressing the volume fraction of heptane in the mixture as a function of time t and its volumetric addition rate q_{c_7}, we get:

$$\phi_{c_7} = \frac{q_{c_7} t}{V_{oil} + q_{c_7} t} \tag{5.14}$$

Replacing the time derivative of Equation 5.14 into Equation 5.12, the concentration of primary unstable particles during the period of time Δt becomes:

$$C_1(t_k) \approx \Delta C_A = \epsilon_{10} a_1 \frac{V_{oil} q_{c_7}}{(V_{oil} + q_{c_7} t_k)^2} \left(\frac{V_{oil}}{V_{oil} + q_{c_7} t_k} \right) \Delta t \tag{5.15}$$

We note that the time t elapses normally starting from zero when the addition of heptane is first engaged. As observable in Figure 5.10, results from computations of the destabilization kinetics with Equation 5.16 provide comparable orders of values of the evaluation of the generation rate employed from linear regression of C_A.

$$r_1 = \frac{dCA}{dt} = k_N C_{A_\infty} \tag{5.16}$$

where C_{A_∞} is the mass concentration of unstable asphaltenes at equilibrium. This equation represents the kinetics of destabilization and gives access to the incremental concentration of unstable asphaltenes in the solution mixture ΔC_A upon an increment of time Δt while the addition of heptane is carried. With choosing an appropriate Δt, ΔC_A approaches the concentration of generated unstable asphaltenes C_1 at an instant t.
The sharp increase in $\frac{dC_A}{dt}$ showed in the linear interpolated regression in Figure 5.10 is related to a_1 in Equation 5.15.

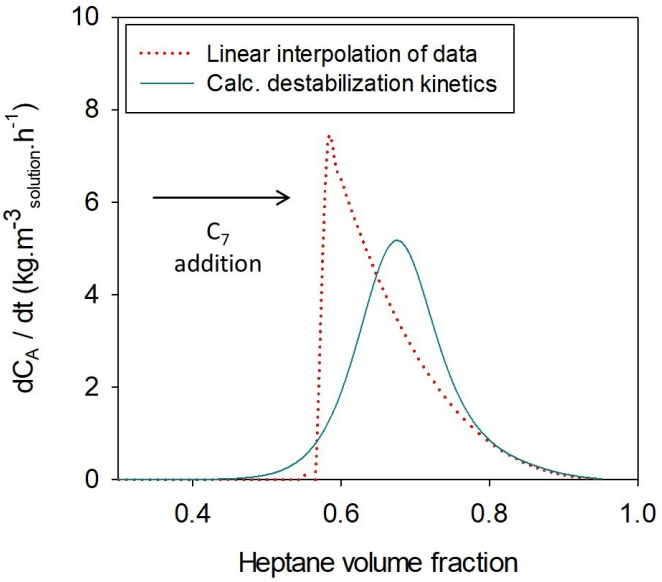

FIGURE 5.10: Generation rate of unstable asphaltenes $\frac{dC_A}{dt}$ as a function of the heptane-oil composition during the addition of heptane in oil

The sensitivity analysis of the Equations 5.15 and 5.16 show the response of the calculated generation rate $\frac{dC_A}{dt}$ at several heptane addition rates within the range of investigation in Figure 5.11.

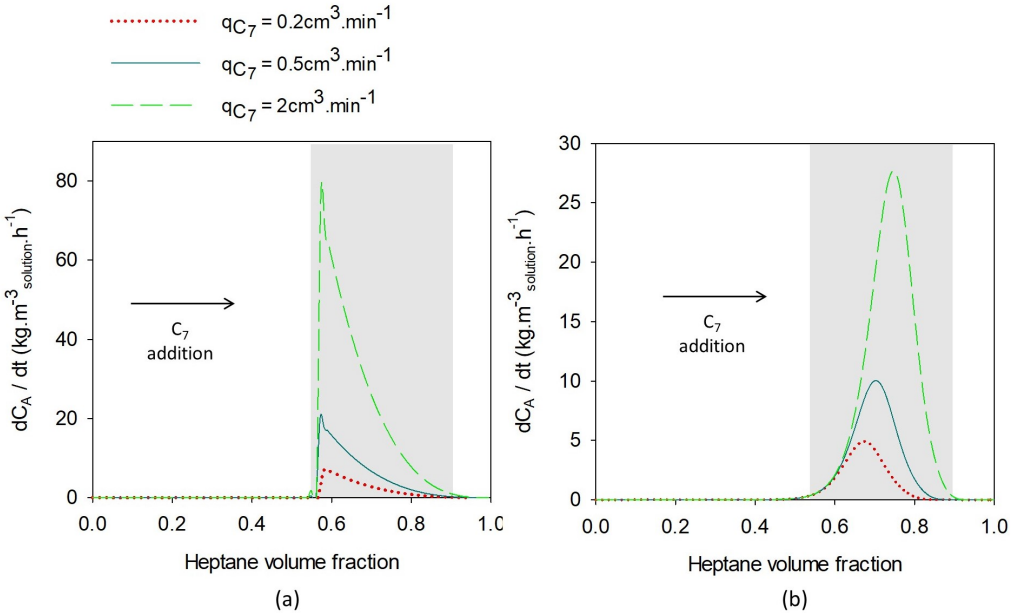

FIGURE 5.11: Calculated generation rates $\frac{dC_A}{dt}$ of unstable asphaltenes from (a) a linear C_A profile and (b) with destabilization kinetics as a function of the heptane-oil composition for several addition rates of heptane in oil

Besides indicating larger quantities of small unstable asphaltenes available to deposit per unit of time as the addition rate of heptane gets large, we should note that the cumulative mass of deposit at a given run-time will depend on the residence time at favorable deposition conditions (qualitatively expected by the greyed area).

Indeed, it is important to highlight the expected effect of residence time; faster promotion of heptane will induce larger generation rates of unstable asphaltenes and larger associated deposition rates. However the mixture will also last for less time than for cases of relatively slower heptane addition as showed in Figure 5.12.

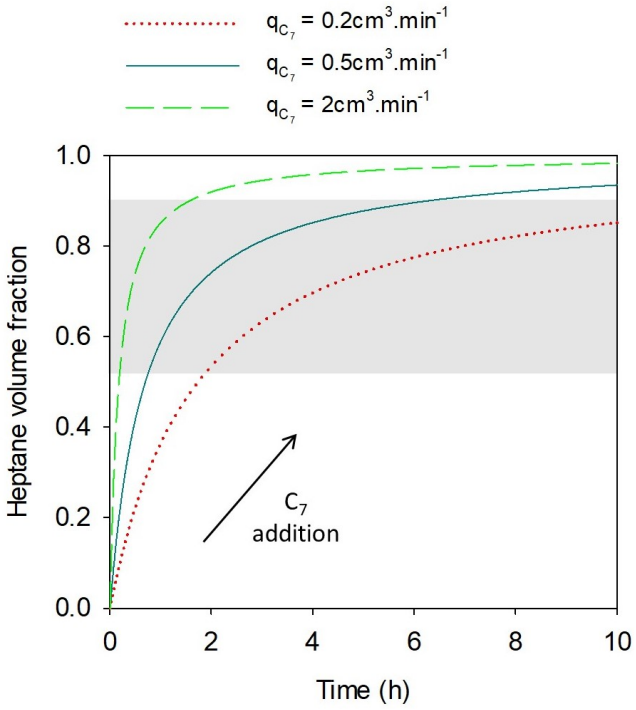

FIGURE 5.12: Heptane volume fraction as a function of time at various addition rates of heptane

5.3 Modeling deposition on the immersed disc-like sensor with parallel viscous flow

Assuming an infinite volume surrounding the sensor and an exclusive downward flow parallel to the disc sensor, the geometry is similar to the broadly used flat plate to study mass transport over a solid surface[40]. The surface phenomena can be mathematically modeled as a first-order reaction with the mass transfer coefficient k_c. Therefore, the diffusive deposition mass rate of unstable asphaltenes ($Rate_{dep}$) flowing over both sides of the sensor follow the relation:

$$Rate_{dep} = a_s k_c \left(C_{A,d} - C_{A,surface}\right) \tag{5.17}$$

where a_s is the total surface area of the sensor accounting for both sides of the disc. In this way, the process is driven by the concentration gradient of "dry" unstable asphaltenes denoted ΔC_A as previously defined. Considering that particles reaching the liquid/solid interface necessarily deposit; Equation 5.17 is subject to the following simplification: $C_{A,surface} = 0$. Mass-transfer experimental studies between flowing fluids and solid surfaces have lead to empirical correlations of the mass transfer coefficient k_c moving over certain shapes like flat plates, spheres or cylinders[40]. In the case of a laminar (Re<2.10^5) parallel stream with a superficial velocity U_0, Welty et al. [40] reports the following mass transfer coefficient correlation as a function of the

average Sherwood number, the Reynolds and Schmidt dimensionless numbers:

$$k_c = \frac{D_A}{L}\overline{Sh} = 0.664\frac{D_A}{L}Re^{1/2}Sc^{1/3} \tag{5.18}$$

Expressing the dimensionless numbers with measurable parameters, we get:

$$k_c = 0.664\frac{D_A}{L}\left(\frac{U_0 L\rho_{liq}}{\mu_{liq}}\right)^{1/2}\left(\frac{\mu_{liq}}{\rho_{liq}D_A}\right)^{1/3} \tag{5.19}$$

Substituting the obtained mass transfer coefficient from the last equation into Equation 5.17, the deposition rate of available "dry" asphaltenes takes the form:

$$Rate_{dep} = 0.664 a_s D_A^{2/3}\left(\frac{U_0}{L}\right)^{1/2}\left(\frac{\rho_{liq}}{\mu_{liq}}\right)^{1/6} C_{A,d} \tag{5.20}$$

The mathematical description of the deposition process requires to account for the captured mass of solvent that travels inside the contributing aggregates. Since the obtained C_A profile by centrifugation is based on the dried mass of asphaltenes, we then introduce the dimensionless factor ψ to correct for the swollen diffusing mass with respect to the solvent components of clusters:

$$\psi = x_{asph} + (1 - x_{asph})\frac{\rho_{liq}}{\rho_{asph}} \tag{5.21}$$

where x_{asph} is given by Equation 5.9. If we postulate an equality between the concentration of asphaltenes available to deposit $C_{A,d}$ and the transient concentration of generated unstable particles C_1. In addition to the incorporation of the factor ψ, combination of Equations 5.15 and 5.20 lets us develop the deposition rate into the following expression:

$$Rate_{dep}(t) = 0.664 a_s D_A^{2/3}\left(\frac{U_0}{L}\right)^{1/2}\left(\frac{\rho_{liq}}{\mu_{liq}}\right)^{1/6}\psi C_1 \tag{5.22}$$

where C_1 is a mass concentration of "dry" generated unstable asphaltenes provided by Equation 5.15 or alternatively by the modeled mass balance of destabilization with kinetics (refer to Equation 3.14). The only unknown parameter of Equation 5.22 becomes the average diffusion coefficient D_A of depositing aggregates. The cumulative deposited mass m_{dep} after running the titration experiment for a given time is:

$$m_{dep}(t) = \int_0^t Rate_{dep} t dt \tag{5.23}$$

As multiple parameters of Equation 5.22 will vary with the composition of the solution (and implicitly with time), the integral of the rate of deposition is approximated within the interval of experimental run-time by a finite sum using a Riemann summation method with N_t partitions of time (Δt) equal to the one used in computing Equation 5.15. The mass of deposit is then given by:

$$m_{dep}(t) = \sum_{k=0}^{N_t} Rate_{dep}(t_k^*)\Delta t \tag{5.24}$$

where k is described by $N_t = \frac{t}{\Delta t}$ and t_k^* is the midpoint of the current interval $t_k^* = (t_k + t_{k-1})/2$.

5.4 Results & discussions

5.4.1 Measurement of the superficial velocity

The vertical tracking of the moving colored fluid lets us plot the vertical coordinate as a function of time for different revolution speeds of the stir bar as showed in Figure 5.13 (a). In any case, the behavior appears linear and the slope of regressions contain the average superficial velocity information of the fluid. As expected, according to the vertical movement of the dye tracer, U_0 depends on the revolution per minute (rpm) of the stir bar placed 1 cm under the disc-sensor. Plotted velocities as a function of the stir bar revolution speed show a linear behavior within the investigated range (Figure 5.13(b)).

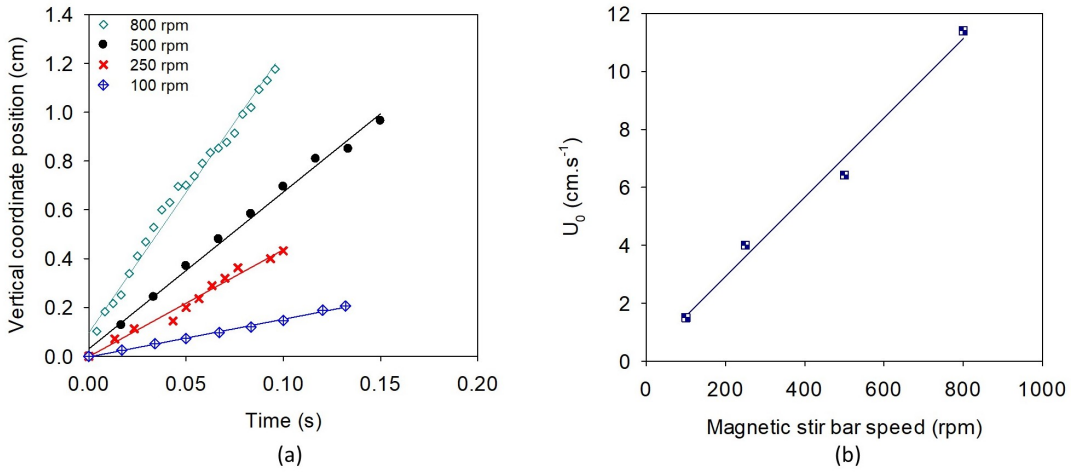

FIGURE 5.13: (a) Position of the tracer as a function of time for various stirring speed and (b) average superficial velocities U_0 as a function the stirring speed

The following sections will involve the analysis of multiple parameters of Equation 5.22. When studying the effect of other parameters, U_0 is therefore fixed with the values determined from Figure 5.13 (b).

5.4.2 Asphaltene deposition

Before proceeding to the analysis of the effect of the suspected important variables, it is interesting to note that the deposition of unstable asphaltenes on the sensor's surface during the continuous heptane addition significantly accumulates at conditions of heptane contents larger than the "onset" of immediate microscopy detection for individually prepared mixtures. Figure 6.15 shows that the conditions of the immediate detection of flocs by visual inspection and the departure of the deposition rate roughly coincide.

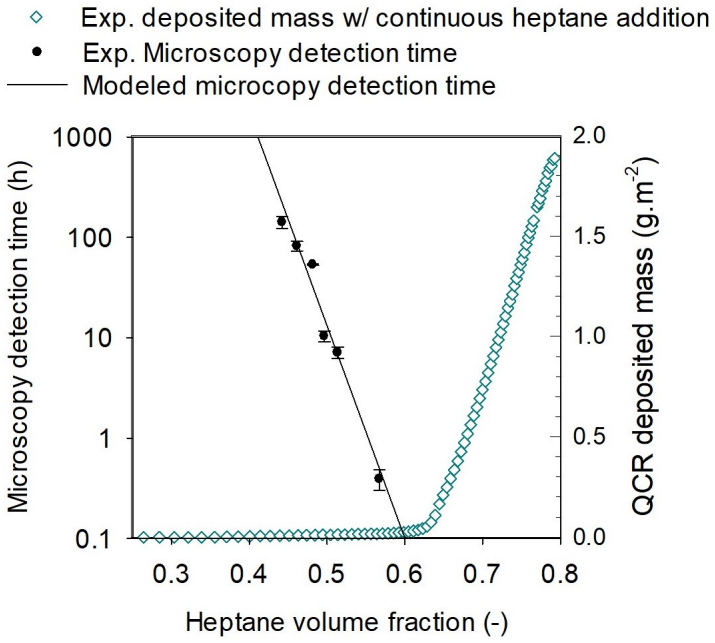

FIGURE 5.14: Comparison of the microscopy detection-time results of individual solutions to the cumulative mass of deposit during the heptane addition as a function of the mixture composition

This first result reinforces the assumptions of this study listed in the introduction section of this Chapter. This similarity in mixture composition observed for both events is interpreted by the consequence of larger amounts of destabilized asphaltenes at those conditions. Indeed, it is predicted from the aggregation theory that larger amounts of unstable particles will increase the collision frequency and will decrease the stability ratio of the colloidal mixture. It is also expected, using first principles of diffusive deposition processes, that larger numbers of generated particles will aggravate the deposition rate.
In the next paragraphs, although some example cases of titration experiments are chosen in order to illustrate the results, this section involves 3 experimental variables: the rate of heptane addition, the superficial velocity of the fluid and the initial presence or absence of large particles. Each of the respective effects were individually studied. It is important to recall that the concentration profile of primary unstable asphaltenes C_1 is entered as an input in Equation 5.22 and can be described with two possible options; (i) a linear regression from centrifugation data or (ii) modeled destabilization kinetics using Equation 3.21.

Size identification of depositing asphaltenes

This investigation has the purpose of identifying the contributing particles of unstable asphaltenes to the deposition process by analyzing their average size. The following example showed in Figure 5.15 was obtained with a fixed addition rate of 0.5 $cm^3.min^{-1}$ and a measured superficial velocity of 1.62 $cm.s^{-1}$. In a first step, the diffusivity of depositing aggregates D_A is adjusted using Equation 5.22. The fitted diffusion coefficients are entered in Equation 5.2 calculate the average radius of depositing particles along the experiment. For this example, the best fit is found to correspond to particles with an average radius R_A = 7 nm. This value is more compatible with the size of clusters than with nanoaggregates, meaning that primary particles able to deposit in the investigated conditions correspond to clusters.

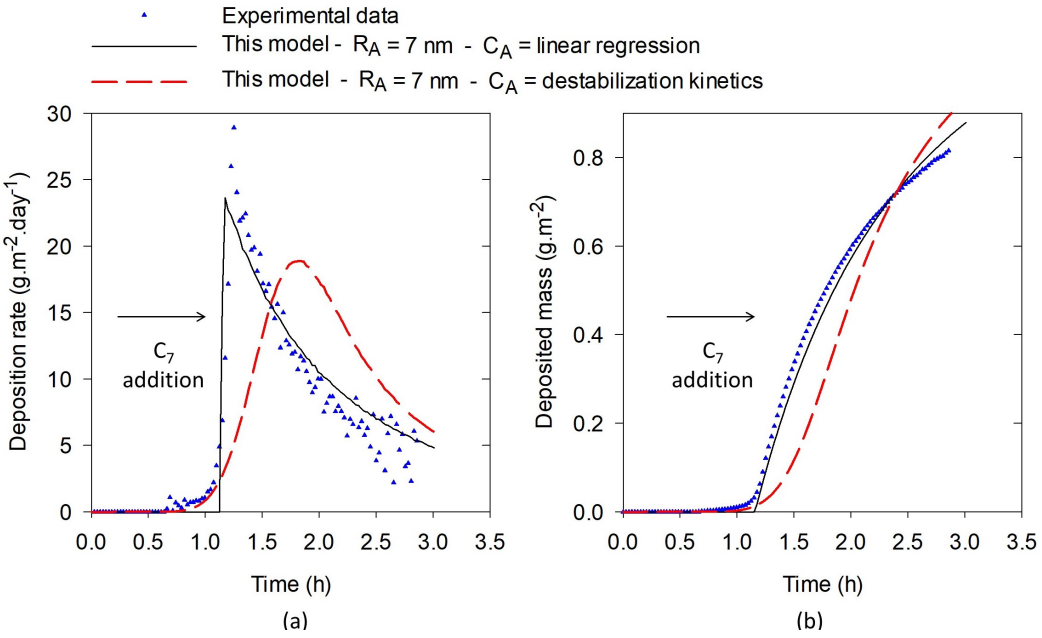

FIGURE 5.15: Comparison of experimental measurement to the computed values of (a) the deposition rate using Equation 5.22 and (b) the cumulative mass of deposit using Equation 5.24 as a function of time during the heptane addition

As it can be seen in Figure 5.15, the deposition model given by Equation 5.22 provides good estimates of the measured data when adjusting the diffusion coefficient with appropriate values. According to the Stokes-Einstein relation for the diffusivity of spherical particles (Equation 5.2), those values are in excellent agreement with reported sizes of clusters of nanoaggregates[36;24] in good solvents ($R_A \sim 5$ to 10 nm). More importantly, the back-calculated size of 7 nm supports the first assumption of our model that considers only freshly generated aggregates to contribute to the deposit in the concentration term of Equation 5.20 ($C_{A,d} = C_1$).
Although very good estimations are obtained from the fully predictive modeled curves, the analysis of the data is important in order to explain inconsistencies. We note that the smooth increase of the deposition rate between 0.5h and 1h in Figure 5.15 (a) is better captured by the model when considering a profile of C_A with destabilization kinetics. The discrepancy of the model when considering a linear profile is in line with the unrealistic "onset" considerations.
We can also notice a larger disparity between the curve considering the destabilization kinetics and the experimental data. This observation may indicate that the equilibration time parameter k_N of Equation 3.21 could be represented with a sharper profile near the departure of the curve. However, adjusting the profile of the generation constant k_N might induce inconsistencies with the measured unstable asphaltenes content separated by centrifugation. Consequently, this parameter is purposely left as previously found using centrifugation data and adjustement are focused on the size of depositing aggregates. In the next paragraph, the assumption of a single particle size along the experiment is reconsidered and the possibility of a progressing average particle size is introduced using a statistical observation.

Size investigation of depositing particles
With the C_A profile accounting for slow destabilization, the deviation of our computed results can individually be reduced by fitting a diffusion coefficient to each

data point of measured deposition rates. As expected, the trial and error process leads to an excellent match between the experimental data and the fluctuating modeled curve in Figure 5.16.

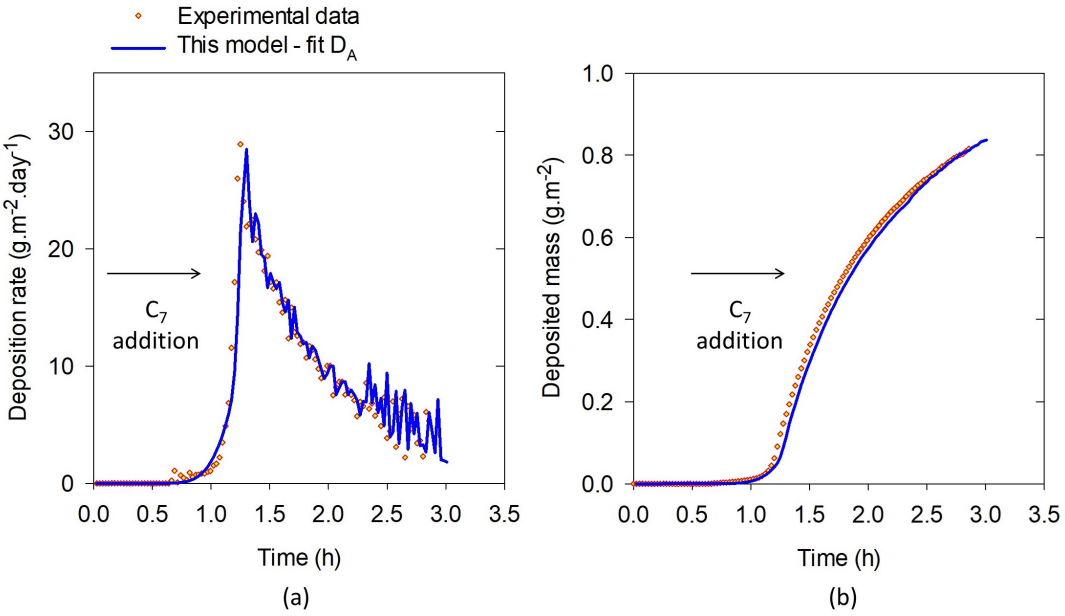

FIGURE 5.16: Comparison of experimental measurement to the computed values of (a) the deposition rate using Equations 5.22 and (b) the cumulative mass of deposit using Equations 5.24 as a function of time during the heptane addition

This process was repeated with all the experimental records and a statistical analysis was performed with more than 800 data points of deposition rates corresponding to 30 titration experiments performed on a single oil at various injection speeds. The covered area of parameters in this analysis is summarized in the following table:

TABLE 5.3: Investigated ranges of experimental parameters

	U_0 $cm.s^{-1}$	C_7 addition rate $cm^3.min^{-1}$	C_A kg.m$^{-3}_{solution}$
minimum	1	0.1	0
maximum	12	5	9

The calculated sizes of depositing asphaltenes with Equation 5.2 are then mapped as a function of the deposition rate and versus the concentration of initial particles in suspension at the respective conditions C_{A_i} obtained from centrifuge experiments of sample aliquots. The results are showed in Figure 5.17. The experimental data interestingly spread within an upper and a lower bound. The results indicate that the average hydrodynamic radius of depositing particles is 7.2 nm, most of the data are comprised between 2 nm and 10 nm, more particularly when no initial particles are present in the bulk. Again, the results of this analysis further support the postulated mechanism in this Chapter.

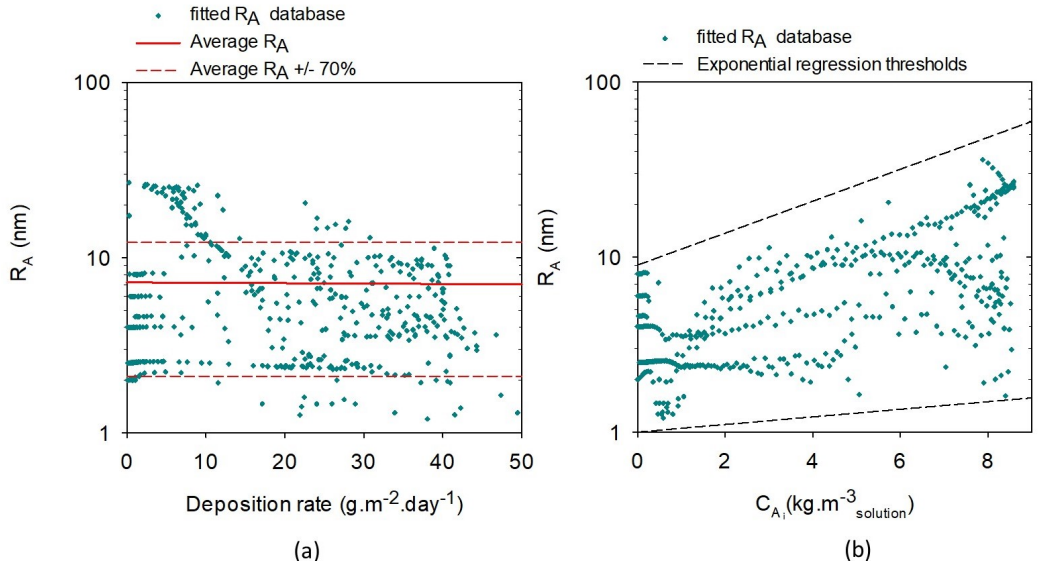

FIGURE 5.17: Depositing asphaltene particle radius R_A calculated from Stokes-Einstein Equation as a function of (a) the measured deposition rates and (b) the initial concentration of unstable particles C_{A_i} in the solution mixture

Although other unstable asphaltenes form observable suspending macro-solids in the bulk, the order of particle sizes contributing to the deposition process obtained in this study remains between 1 nm and 30 nm. The obtained statistics seem to indicate an increasing trend of the average size of contributing entities to the deposition as the initial concentration of bulk particles increases. We therefore can suspect from the trends that the presence of other solids might affect the diffusion properties of freshly generated aggregates toward the surface of interest. The presence of other particles will likely increase the coarsening probability before reaching the solid surface. Logically, larger depositing particles will provoke a slower diffusive process. Therefore, in those specific conditions, the results suggest that reduced deposition rates are caused by a larger average size of depositing particles at extended bulk concentrations of other particles as shown in Figure 5.17.
In consequence of the results presented in this paragraph, the effect of the presence of larger flocs in the bulk is specifically studied and results are reported in the following paragraph.

Effect of the presence of flocs of asphaltenes in the bulk
Those investigations involve the combination of successive heptane titrations and centrifugations as presented by the schematic of the procedure in Figure 5.18. The centrifugation time was adjusted between 10 and 30 minutes in order to satisfy a constant cut-off size of separated particles equal to 200 nm as well as a short enough centrifuge run-time that lets us neglect the aging effects.

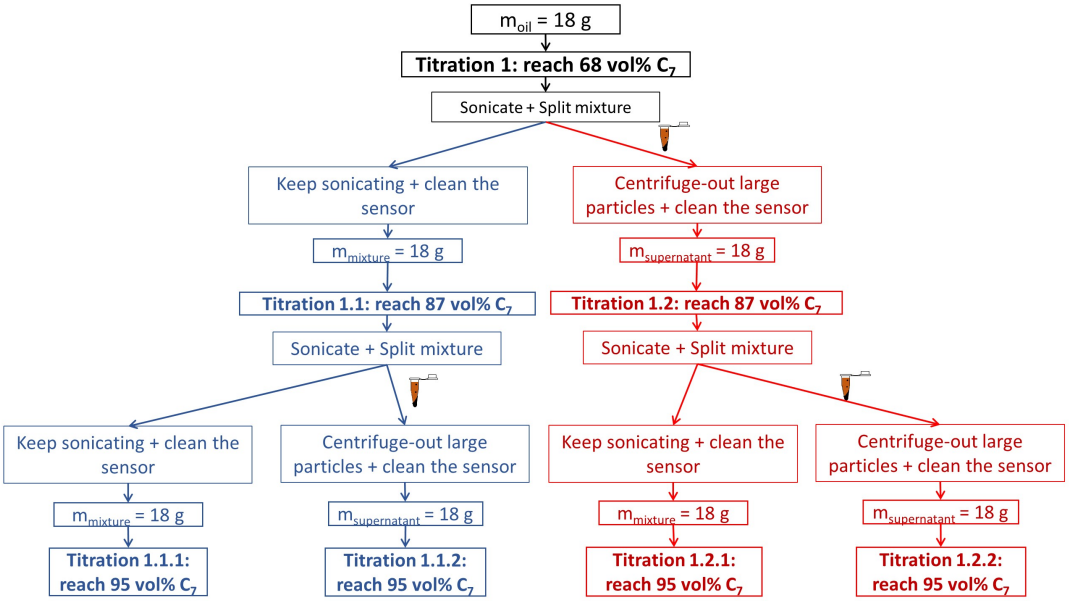

FIGURE 5.18: Schematic of the successively combined heptane titration and centrifugation processes

The procedure was specifically designed to observe the influence of the presence of large unstable asphaltenes flocs. Therefore the heptane adition rate (q_{c_7}=0.5 $cm^3.min^{-1}$) and the stirring velocity (500 rpm) are kept constant during all the experiments of this paragraph. Note that the starting mass of each titration is also kept identical and implies discontinuities in the rate of variation of the heptane fraction when starting from a new mixture (see Figure 5.19).

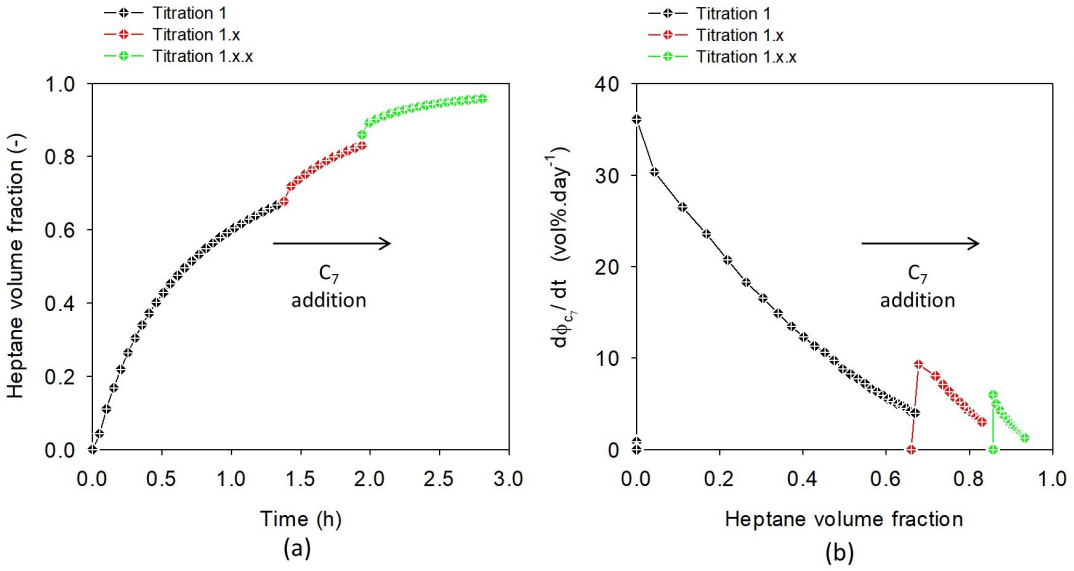

FIGURE 5.19: (a) Variation of the heptane volume fraction in the mixture as a function of cumulative time during the experiment
(b) Rate of variation of the heptane volume fraction as a function of the heptane volume fraction

After splitting the solutions, the following start of heptane addition behaves as if we had pushed up the flow rate at these particular times during a continuous experiment. Consequently, one expects the rate of generation of unstable asphaltenes

to follow the same trend. This should stimulate jump-starts of the deposition rate when initiating a new titration. The obtained results from the exposed process are communicated in the form of measured deposition rates in Figure 5.20.

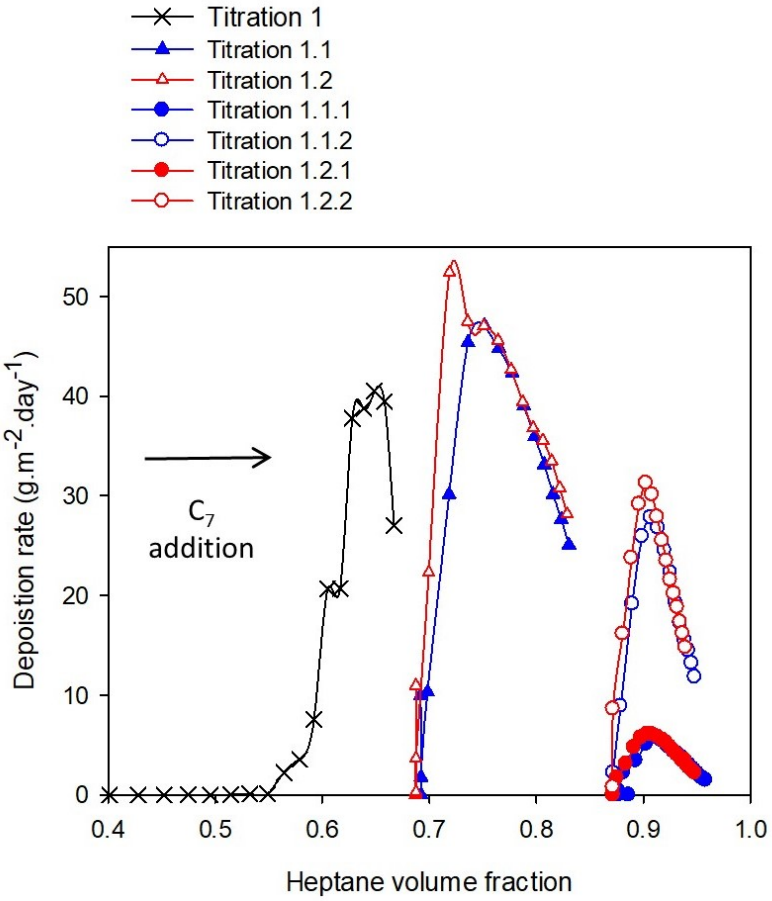

FIGURE 5.20: Results in deposition rates from successively combined heptane titrations and centrifugations; filled symbols contain initial particles and empty ones were centrifuged prior to starting the deposition experiments

As anticipated, the boosted rate of generation of unstable asphaltenes at the restart of experiments heightens the deposition rate at the exception of the experiments 1.1.1 and 1.2.1 that will be individually discussed later.
The graphic indicates that the presence of more unstable asphaltenes in the form of large aged particles does not increase the deposition rate. In fact, their presence appears to slow down the deposition in certain cases. Between 68 vol% to 70 vol% of heptane in oil, the presence of micrometer-sized particles (titration 1.1) temporary reduces the deposition rate compared its analogous case (titration 1.2). However when carrying on the heptane addition of the same experiments, both curves follow the same behavior. This can first be explained by the initial absence of solids in suspension, which gives a free path for generated particles toward the deposition surface. In parallel, the number of flocs grows after a few additional percents of heptane and their presence will disturb the transport of newly formed particles, making their diffusivity to decrease.
In the final studied region of composition during this process (87 to 95 vol% of C_7), a stronger effect prevents the generated particles from depositing when huge flocs are

kept in suspension before starting the heptane additions (1.1.1 and 1.2.1). Indeed, those cases repeatably show that the deposition rate is ∼4 times superior in cases when suspending flocs are limited in number by pre-centrifuging the sample.
Those results qualitatively show that the existence of other solids in the bulk seem to play a preventive role and lessens the mass transfer of generated unstable asphaltenes toward the surface of interest. The declining effect seems to be more pronounced as the quantity of suspending flocs is larger. As presented in the previous paragraph, the average radius of depositing particles R_A can be estimated from the experimental data with appropriately adjusting diffusivities D_A. Table 5.4 reports the back-calculated hydrodynamic radius of particles with the presented method and Figure 5.21 plots the data of this part comparing it to the regression limits previously found in Figure 5.17. The resulting particle sizes as a function of the average mass concentration of unstable asphaltenes in suspension are in good agreement with the precedent statistics.

TABLE 5.4: Concentration of unstable asphaltenes separated by centrifugation along the titration

Titration #	$C_{A>200nm}$ at start	$C_{A>200nm}$ avg	R_A
-	$kg.m^{-3}_{solution}$	$kg.m^{-3}_{solution}$	nm
1	0	4	4.5
1.1	2.56	6.64	10
1.1.1	8.06	8.32	60
1.1.2	0	0.26	9
1.2	0	4.08	3
1.2.1	7.02	7.28	25
1.2.2	0	0.26	3

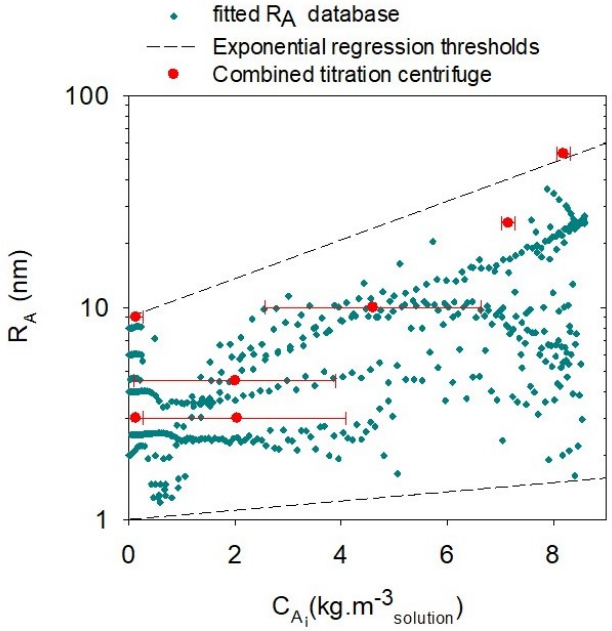

FIGURE 5.21: Fitted radius R_A of depositing asphaltenes to the measured deposition rates (figure 5.20) as a function of the mass concentration of initially suspending solids

Since minor deposition occurs if the addition of heptane is stopped, the process is still controlled by the influx of young generated particles. However the results show that their average size can be larger with greater initial concentrations of unstable asphaltenes. The observed trend can be explained by the increased collision probabilities of generated particles to some suspending solid entities before reaching the deposition surface, which diminishes their diffusing speed. On average, the calculated radius of generated particles increases by less than an order of magnitude in the extent of investigated conditions. Actually, the sizes remain relatively small compared to the majority of other agglomerates (larger than 1 μm observed by microscopy). For this reason, the range of depositing asphaltenes radius is still in excellent agreement with already reported dimensions[39;10].
The showed computation in Figure 5.15 is then revisited by defining a profile of depositing particle radius as a function of C_{A_i}. As empirically suggested by the statistical study, R_A profiles correlate to C_{A_i} using a regression function of the form:

$$R_A = R_{nanoaggr} exp\left(\zeta C_{A_i}\right) \tag{5.25}$$

where $R_{nanoaggr}$ is the minimum radius of depositing unstable asphaltenes particles corresponding to the radius of nanoaggregates and ζ is a fitting parameter.
The quality of the model is verified by comparing to the results to experimental data. The matching curvatures indicate that the model captures the underlying physics of the surface deposition. After optimizing the radius of particles R_A, the slight remaining disparities can be attributed to the errors related to the representations of C_A profiles.

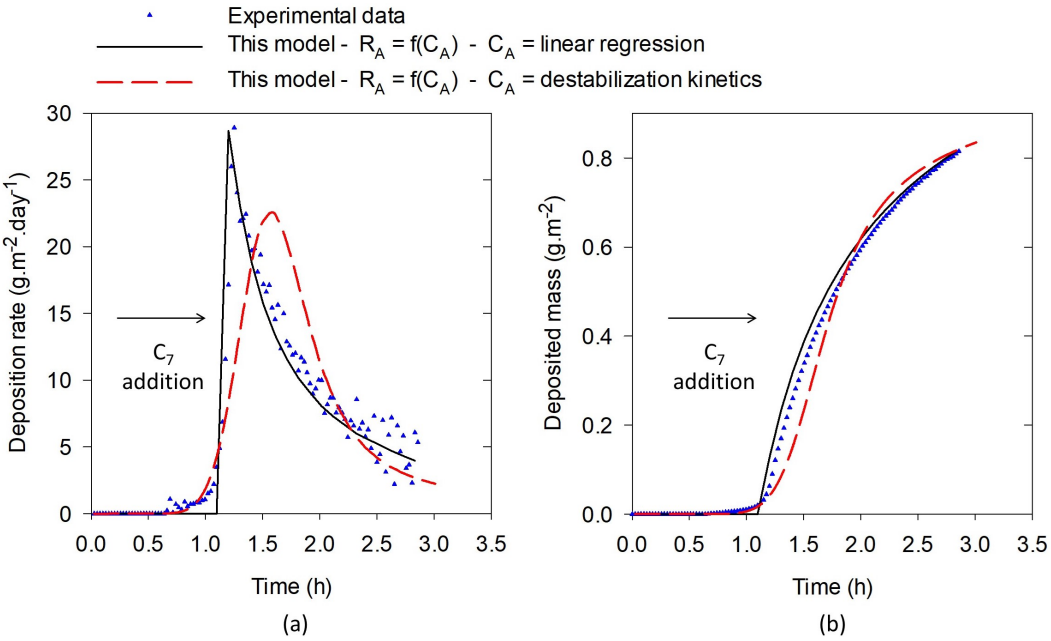

FIGURE 5.22: Comparison of experimental measurement to the computed values of (a) the deposition rate using Equation 5.22 and (b) the cumulative mass of deposit using Equation 5.24 as a function of time during the heptane addition with a size profile of depositing asphaltenes

The matching radius profiles appear in Figure 5.23 to lay between the previously empirically observed thresholds, which is consistent with antecedent results.

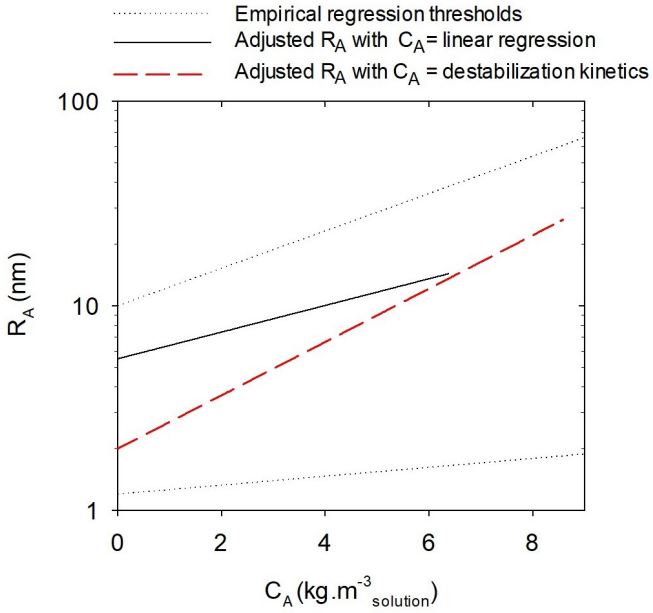

FIGURE 5.23: Comparison of the adjusted radius R_A profile with Equation 5.25 for a continuous titration to the extreme thresholds previously defined

The results confirm that the average size of depositing asphaltenes (radius between 2 and 20 nm) corresponds to the order of size of "stable" clusters of nanoaggregates[24;35;16].
In the following paragraphs; diffusivities are computed using Equation 5.2 with radius profiles laying between the empirical bounds presented in the Figures of this study, the other parameters of the equation are measured. According to results showed in this part, the deposition model provides reasonable estimates using a single average radius of depositing aggregates of 7 nm. Typical error bars related to the evaluation of the diffusion coefficients can be represented by fluctuating the hydrodynamic radius of primary aggregates by +/- 50% (3.5 nm to 10.5 nm).

Effect of the heptane addition rate

In this part, the anti-solvent injection rate is varied with the objective to again check for the self-consistency of the proposed idea of diffusing generated units of unstable asphaltenes. This part involves several destabilization rates by varying the addition rate of heptane at fixed superficial velocity (~ 7 cm.s^{-1} according to Figure 5.13 (b)).

The investigated conditions correspond to values of the generation constant k_N ranging from infinitely slow kinetics to $10^{-3}s^{-1}$. We recall that the destabilization constant is directly controlling the rate of unstable particles generation according to Equation 5.16. On the other hand, rearrangement of Equation 5.22 in order to express $C_{A,d}$ gives us5.26:

$$\frac{Rate_{dep}}{0.664 a_s D_A^{2/3} \left(\frac{U_0}{L}\right)^{1/2} \left(\frac{\rho_{liq}}{\mu_{liq}}\right)^{1/6}} = C_{A,d} \tag{5.26}$$

where D_A is calculated following the description of a particle size profile using Equation 5.25 entered in Stokes-Einstein equation, parameters of the left part of this Equation are measured. Our deposition model suggests that the plot of the experimentally obtained $C_{A,d}$ vs $\Delta C_A, centrif$ from Equation 5.15 should fall onto an equality line. Figure 5.24 compares all the experimentally obtained $C_{A,d}$ as a function of ΔC_A that estimates C_1 from the linear regression of centrifuged masses exposed in Table 5.2.

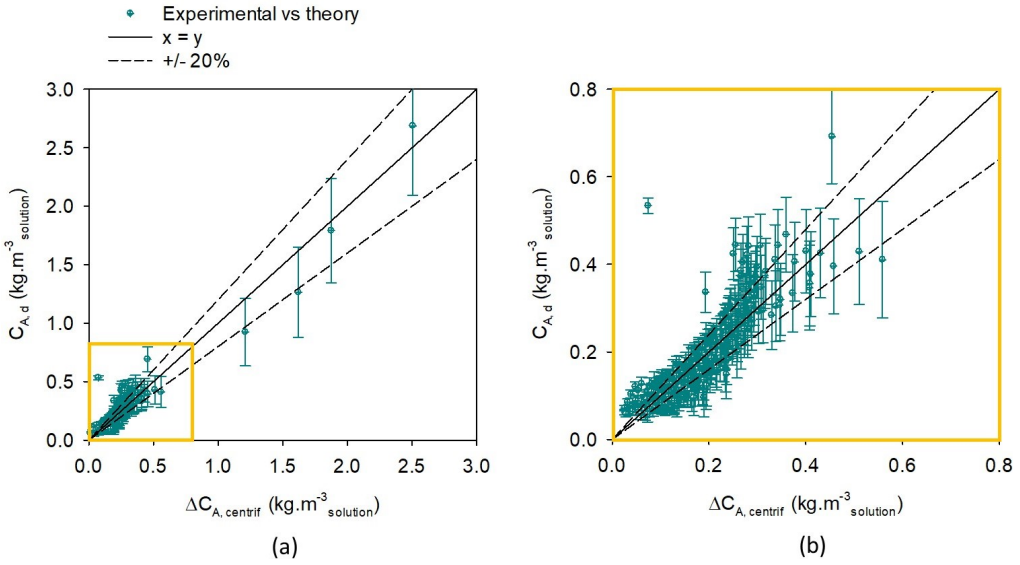

FIGURE 5.24: Scaling analysis of the asphaltene deposition rate as a function of the estimated concentration of generated unstable asphaltenes $\Delta C_{A,centrif}$ at several recorded instants using Equation 5.26

As it can be seen in Figure 5.24, at the exception of a few data points, the comparison between the deposition experimental data and the estimated concentration of primary unstable units provide the expected collapse on an equality line. Despite the many approximations on the experimental measurements as well as the simplistic definition of diffusion coefficient, the present analysis leads to excellent agreements. In this way, the identification of the contributing fraction to the deposition process is supported with statistical experimental evidences and the remainder of our research can assume that the asphaltene deposition is mainly caused by primary unstable units with an average hydrodynamic radius $R_A \sim 7$ nm.
In practice, the limited number of recorded points when increasing the addition rate can perturb the interpretation of experimental data. Therefore, it is usually preferable to add the alkane at a moderated rate in such manner that trends can be exploited from large enough number of data points. However injection of n-heptane at significantly larger addition rates can further help to test the limits of our model. A compromise between increasing the rate of addition of the destabilizing agent and letting enough time for relevant measurements is found for the addition rate equal to 3.5 g.min^{-1}. In this condition, Figure 5.25 shows the evolution of the heptane volume fraction as a function of time.

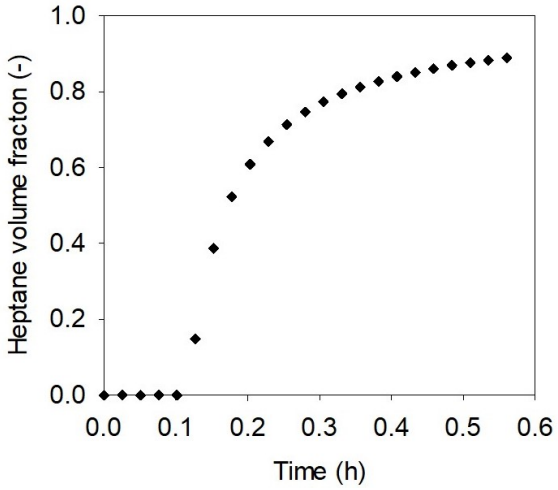

FIGURE 5.25: Volume fraction of *n*-heptane in the oil-heptane mixture against time for the addition rate of 3.5 g.min^{-}1 of *n*-C_7 in 15 g of oil

Comparison of the acquired deposition data with our model is provided in Figure 5.26. The model performs reasonably well with tuned radius of particles in the range of size of asphaltenes nano-aggregates. Note that a peak of deposition seems to occur, which provokes a large instantaneous increase of the deposited mass around 0.22 h. This peak is not captured by our model, it is suspected that this discrepancy might be induced by the model of destabilization kinetics that may not be adjusted with enough experimental measurements at the corresponding mixture composition.

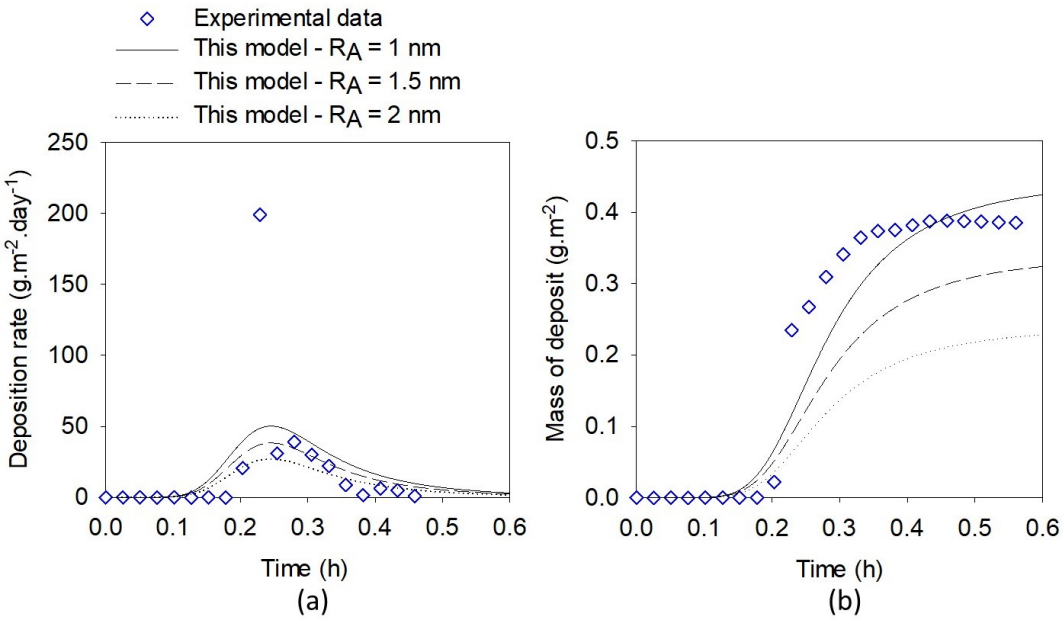

FIGURE 5.26: Volume fraction of *n*-heptane in the oil-heptane mixture against time for the addition rate of 3.5 g.min^{-}1 of *n*-C_7 in 15 g of oil

Assuming that the deposition mechanism is identical for asphaltenes destabilized by different alkanes, the exposed findings of this part upgrade our method to an indirect method of measuring the concentration profile of unstable asphaltenes

C_A as a function of the volume fraction of the added alkane. The proposed assumption is experimentally investigated in the following Chapter of this document.

Effect of superficial fluid velocity

As showed in Figure 5.2 of the introductory part of this Chapter, the theory predicts that for a diffusion-limited surface deposition, the deposition rate $Rate_{dep}$ should scale with the square root of the fluid superficial velocity U_0. Indeed, as the superficial velocity grows, the boundary layer thickness will shorten and aggravate the concentration gradient. The scaled deposition rate J is defined by reorganizing the deposition Equation as follows:

$$J = \frac{Rate_{dep}}{0.664 a_s L^{-1/2} \left(\frac{\rho_{liq}}{\mu_{liq}}\right)^{1/6} C_{A,d}} = D_A^{2/3} U_0^{1/2} \tag{5.27}$$

Thus our deposition model given by Equation 5.22 points that a graphic representation of $\left(\frac{J}{D_A^{2/3}}\right)$ versus the optically measured $\left(U_0^{1/2}\right)$ should superpose the data on a single line. For the graphical representation, deposition rates from multiple experiments at constant stirring speed (or U_0) were averaged to a single point. The error bars were obtained by taking extreme values of diffusivities with hydrodynamic radius of particles of 8 nm +/- 50%. The plot of results in Figure 5.27 serves as a self-consistency verification of the deposition model. First, it verifies the diffusive character of the surface process when the deposition rate is a function of the fluid flow velocity in viscous flow regime. Second, it shows that the proposed simplified approach of the asphaltene deposition mechanism apprehends the physics by considering limited number of tuned parameters.

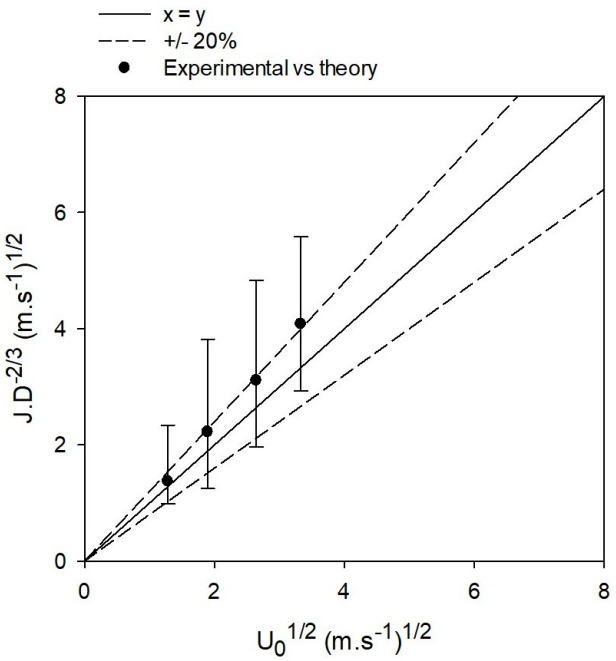

FIGURE 5.27: Scaling analysis of the asphaltene deposition rate as a function of the superficial velocity

5.5 Conclusions

A new laboratory technique was presented to measure the deposition rate of unstable asphaltenes during the continuous titration of *n*-heptane. It consists of a flat resonator disc with an observable parallel flow of the surrounding fluid to the surfaces of the sensor. The deposited mass of asphaltenes is measured as a function of time while heptane is added along the experiments. Deposition rates are then analyzed as a function of the identified relevant variables: the fluid superficial velocity, the generation rate of unstable asphaltenes and the initial presence of large aggregates.
A diffusive deposition model was specifically designed for the geometry of the measuring device. Based on preliminary observations, the proposed model postulates an exclusive deposition of the transforming "stable" clusters into "unstable" units, termed as primary unstable particles. With regards to the size scale of interest, the effects related to the dissociation of aggregates, to the depletion of asphaltenes and to the shear forces at the surface are neglected while the aggregation is assumed instantaneous. Experimental results show the following findings:

- the asphaltene deposition process can be explained by a diffusion-limited deposition of freshly generated particles
- the asphaltene deposition rate scales linearly with the generation rate of unstable asphaltenes ($rate_{dep} \propto C_1 \propto r_1$)
- the average hydrodynamic radius of depositing particles is generally limited to a narrow range varying between 4 and 12 nm
- the initial presence of bulk suspending particles slows down the deposition rate of asphaltenes on the studied surface
- the presupposed fast kinetics of aggregation compared to the destabilization enables an accurate interpretation of the deposition.

This research not only strengthens previous works on the asphaltene diffusion-limited deposition of nanoparticles, it also provides a robust simplified approach to predict the deposition behavior of unstable asphaltenes in continuously changing solutions with limited number of tuning parameters. The proposed method enables to extend our studies to the effect of the nature of the used flocculating agent, i. e. vary the alkane chain length.
Besides, the model can conveniently be extended to multiple geometries, like pipelines, using correlations of the Sherwood number.
Presented principles showed to provide excellent estimations of the deposited mass with incorporating a fraction of trapped solvent. However, although the amounts of trapped liquid are calculated from the typical fractal dimension of unstable asphatenes found in the literature, the morphology of the deposit was not experimentally investigated in our research. Campen et al.[5] first provided insights of the morphological change of the deposit depending on the conditions of asphaltenes destabilization, they suggested that the particles organize in a different way depending on the generation rate of particles. This aspect remains insufficiently documented and requires further investigations that will be of great interest to optimize the cleaning industrial operations.

Bibliography

[1] Asmolov, E. S.
1999. The inertial lift on a spherical particle in a plane poiseuille flow at large channel reynolds number. *Journal of Fluid Mechanics*, 381:63–87.

[2] Barré, L., S. Simon, and T. Palermo
2008. Solution properties of asphaltenes. *Langmuir*, 24(8):3709–3717.

[3] Bennett, C. A.
2012. A theory describing asphaltene adhesion fouling inside heat exchanger tubes. *Heat Transfer Engineering*, 33(15):1246–1250.

[4] Buckley, J. S.
2012. Asphaltene deposition. *Energy & Fuels*, 26(7):4086–4090.

[5] Campen, S., B. Smith, and J. S. Wong
2018. Deposition of asphaltene from destabilized dispersions in heptane-toluene. *Energy & Fuels*.

[6] Chamberlain, A. and P. Little
1981. Transport and capture of particles by vegetation. In *Symposium-British Ecological Society*.

[7] Duran, J., Y. Casas, L. Xiang, L. Zhang, H. Zeng, and H. Yarranton
2018. Nature of asphaltene aggregates. *Energy & Fuels*.

[8] Duran, J., F. Schoeggl, and H. Yarranton
2019. Kinetics of asphaltene precipitation/aggregation from diluted crude oil. *Fuel*, 255:115859.

[9] Eskin, D., O. Mohammadzadeh, K. Akbarzadeh, S. D. Taylor, and J. Ratulowski
2016. Reservoir impairment by asphaltenes: A critical review. *The Canadian Journal of Chemical Engineering*, 94(6):1202–1217.

[10] Eskin, D., J. Ratulowski, K. Akbarzadeh, and S. Andersen
2012. Modeling of asphaltene deposition in a production tubing. *AIChE journal*, 58(9):2936–2948.

[11] Eskin, D., J. Ratulowski, K. Akbarzadeh, and S. Pan
2011. Modelling asphaltene deposition in turbulent pipeline flows. *The Canadian Journal of Chemical Engineering*, 89(3):421–441.

[12] Fávero, C. V. B., T. Maqbool, M. Hoepfner, N. Haji-Akbari, and H. S. Fogler
2017. Revisiting the flocculation kinetics of destabilized asphaltenes. *Advances in colloid and interface science*, 244:267–280.

[13] Fogler, H. S.
2010. *Essentials of Chemical Reaction Engineering: Essenti Chemica Reactio Engi*. Pearson Education.

[14] Freed, D., N. Lisitza, P. Sen, and Y. Song
2009. A study of asphaltene nanoaggregation by nmr. *Energy Fuels*, 23(3):1189–1193.

[15] Gawel, I., D. Bociarska, and P. Biskupski
2005. Effect of asphaltenes on hydroprocessing of heavy oils and residua. *Applied Catalysis A: General*, 295(1):89–94.

[16] Goual, L., M. Sedghi, H. Zeng, F. Mostowfi, R. McFarlane, and O. C. Mullins
2011. On the formation and properties of asphaltene nanoaggregates and clusters by dc-conductivity and centrifugation. *Fuel*, 90(7):2480–2490.

[17] Guan, Q., Y. Yap, A. Goharzadeh, J. Chai, F. Vargas, W. Chapman, and M. Zhang
2017. Integrated one-dimensional modeling of asphaltene deposition in wellbores/pipelines. In *Modeling, Simulation, and Applied Optimization (ICMSAO), 2017 7th International Conference on*, Pp. 1–6. IEEE.

[18] Haji-Akbari, N., P. Masirisuk, M. P. Hoepfner, and H. S. Fogler
2013. A unified model for aggregation of asphaltenes. *Energy & Fuels*, 27(5):2497–2505.

[19] Haji-Akbari, N., P. Teeraphapkul, A. T. Balgoa, and H. S. Fogler
2015. Effect of n-alkane precipitants on aggregation kinetics of asphaltenes. *Energy & Fuels*, 29(4):2190–2196.

[20] Halász, G., B. Gyüre, I. M. Jánosi, K. G. Szabó, and T. Tél
2007. Vortex flow generated by a magnetic stirrer. *American Journal of Physics*, 75(12):1092–1098.

[21] Hashmi, S., M. Loewenberg, and A. Firoozabadi
2015. Colloidal asphaltene deposition in laminar pipe flow: Flow rate and parametric effects. *Physics of Fluids*, 27(8):083302.

[22] Haskett, C. E. and M. Tartera
1965. A practical solution to the problem of asphaltene deposits-hassi messaoud field, algeria. *Journal of petroleum technology*, 17(04):387–391.

[23] Hoepfner, M. P., V. Limsakoune, V. Chuenmeechao, T. Maqbool, and H. S. Fogler
2013a. A fundamental study of asphaltene deposition. *Energy & fuels*, 27(2):725–735.

[24] Hoepfner, M. P., C. Vilas Boas Favero, N. Haji-Akbari, and H. S. Fogler
2013b. The fractal aggregation of asphaltenes. *Langmuir*, 29(28):8799–8808.

[25] Kabir, C., A. Hasan, D. Lin, and X. Wang
2001. An approach to mitigating wellbore solids deposition. In *SPE Annual Technical Conference and Exhibition*. Society of Petroleum Engineers.

[26] Kurup, A. S., F. M. Vargas, J. Wang, J. S. Buckley, J. L. Creek, J. Subramani, Hariprasad, and W. G. Chapman
2011. Development and application of an asphaltene deposition tool (adept) for well bores. *Energy & Fuels*, 25(10):4506–4516.

[27] Leontaritis, K. J. and G. A. Mansoori
1988. Asphaltene deposition: a survey of field experiences and research approaches. *Journal of Petroleum Science and Engineering*, 1(3):229–239.

[28] Lin, Y.-J., P. He, M. Tavakkoli, N. T. Mathew, Y. Y. Fatt, J. C. Chai, A. Goharzadeh, F. M. Vargas, and S. L. Biswal
2016. Examining asphaltene solubility on deposition in model porous media. *Langmuir*, 32(34):8729–8734.

[29] Mansur, C. R., A. R. de Melo, and E. F. Lucas
2012. Determination of asphaltene particle size: influence of flocculant, additive, and temperature. *Energy & Fuels*, 26(8):4988–4994.

[30] Maqbool, T., A. T. Balgoa, and H. S. Fogler
2009. Revisiting asphaltene precipitation from crude oils: A case of neglected kinetic effects. *Energy & Fuels*, 23(7):3681–3686.

[31] Maqbool, T., S. Raha, M. P. , and H. S. Fogler
2011. Modeling the aggregation of asphaltene nanoaggregates in crude oil- precipitant systems. *Energy & Fuels*, 25(4):1585–1596.

[32] McLean, J. D. and P. K. Kilpatrick
1997. Effects of asphaltene solvency on stability of water-in-crude-oil emulsions. *Journal of Colloid and Interface Science*, 189(2):242–253.

[33] Miller, C. C.
1924. The stokes-einstein law for diffusion in solution. *Proceedings of the Royal Society of London. Series A, Containing Papers of a Mathematical and Physical Character*, 106(740):724–749.

[34] Mullins, O. C.
2010. The modified yen model. *Energy & Fuels*, 24(4):2179–2207.

[35] Mullins, O. C.
2011. The asphaltenes. *Annual review of analytical chemistry*, 4:393–418.

[36] Mullins, O. C. and E. Y. Sheu
2013. *Structures and dynamics of asphaltenes*. Springer Science & Business Media.

[37] Nabzar, L. and M. Aguiléra
2008. The colloidal approach. a promising route for asphaltene deposition modelling. *Oil & Gas Science and Technology-Revue de l'IFP*, 63(1):21–35.

[38] Sehmel, G.
1971. Particle diffusivities and deposition velocities over a horizontal smooth surface. *Journal of Colloid and Interface Science*, 37(4):891–906.

[39] Vilas Bôas Fávero, C., A. Hanpan, P. Phichphimok, K. Binabdullah, and H. S. Fogler
2016. Mechanistic investigation of asphaltene deposition. *Energy & Fuels*, 30(11):8915–8921.

[40] Welty, J. R., C. E. Wicks, G. Rorrer, and R. E. Wilson
2009. *Fundamentals of momentum, heat, and mass transfer*. John Wiley & Sons.

[41] Zendehboudi, S., A. Shafiei, A. Bahadori, L. A. James, A. Elkamel, and A. Lohi 2014. Asphaltene precipitation and deposition in oil reservoirs–technical aspects, experimental and hybrid neural network predictive tools. *Chemical Engineering Research and Design*, 92(5):857–875.

Chapter 6

Effect of the nature of *n*-alkanes on asphaltenes

6.1 Introduction

Although asphaltenes are usually named after the *n*-alkane that served to extract them from their native oils, most commonly *n*-pentane or *n*-heptane (e.g. n-C_7 asphaltenes)[52], the effect of the nature of the destabilizing agent on the asphaltenes agglomeration is still a matter of debate. Asphaltenes are a class of polydisperse molecules in petroleum that is composed of hundreds of different molecules with various motifs[6]. The beginning of the 21st century has been marked by a large number of research studies involving the fragmentation and characterization of asphaltene fractions with various techniques[42;22;16;30]. Recent analytical methods enabled to reveal more details on the abundance of specific structures[7]. The immense diversity of asphaltene molecules in crude oils therefore confers to them a strong dependence to the surrounding solvent quality and more specifically to the nature of the destabilizing agent (anti-solvent). Studying the effect of the nature of the anti-solvent on the destabilization, the aggregation and the deposition can help us to better understand the behavior of asphaltenes when volumes of light components expand in the liquid phase during production and transport of crude oils or when relatively light oils are blended to heavier crudes that have larger contents of asphaltenes.

In order to compare asphaltene destabilization results from various type of flocculating agents, many authors have been using a rallying graduated system that applies to all the studied mixtures; the solubility parameter of solutions ($\delta_{solution}$). This scale is equivalent to the degree of interaction between molecules[25] in liquid mixtures. The calculation of these parameters conveniently requires users to know the volume fractions, which can be measured or calculated from equations of state, and the solubility parameters of each constituent that can be derived from other measurable characteristics. The concept of solubility parameters is also interestingly applicable to pressurized conditions with dissolved light molecules in the liquid phase, such as methane or carbon dioxide. $\delta_{solution}$ captures both effects of changes in the solvent; i.e. the density and the interaction attributes of the solution constituents (particularly London dispersion forces). Previous investigations involved mapping of two-dimensional solubility parameters of model oil and crude oil systems[48]. Based on results of a large number of crude oils, authors stated that asphaltenes stability was predominantly governed by Van Der Waals (VdW) interactions. Crude oil systems contain very few permanent dipoles, for this reason generalizing VdW interactions to solely London dispersion interactions is a fair approximation.

In theory, materials with similar solubility parameters will likely dissolve each other, while at the opposite a significant difference in solubility parameters leads solutes

to coagulate out of the solution.
Consequently, one can state as a rule of thumb that asphaltenes that have the largest solubility parameter are expected to be the most subject to agglomeration upon the expansion of light components in crude, which decreases the overall solubility parameter of the carrier oil.

6.1.1 Literature review on the effect of the nature of the anti-solvent

Reported trends

The kinetic behavior related to the appearance of observable flocs of unstable asphaltenes[19;50;31] and their yield at equilibrium[34;40;26] have usually been studied separately. Haji-Akbari et al.[18] related both aspects within a defined range of conditions where the flocculation is not instantaneous. Authors[18] found a linear law between the inverse of the difference in solubility parameters and the logarithm function of the equilibrium concentration of unstable asphaltenes named $C_1(0)$ (recalled C_{A_∞} in this dissertation due to the definition of destabilization kinetics in Chapter 3), the microscopy detection-time of particles $t_{\text{detection}}$ and the viscosity μ of the media.

$$\ln(t_{\text{detection}}\sqrt{C_{A\infty}}/\mu) \propto \frac{1}{\delta_{\text{asph}} - \delta_{\text{solution}}} \tag{6.1}$$

where δ_{asph} is the solubility parameter of asphaltenes and δ_{solution} is the solubility parameter of the mixture solution. This so-called unified model described by equation 6.1 relates the time that unstable asphaltenes take to reach micro-sizes, the number concentration of unstable asphaltenes at equilibrium and the solution properties in a single expression. As showed in Figure 6.1, the proposed model was able to collapse experimental data from various oils and various alkanes into a single master curve.

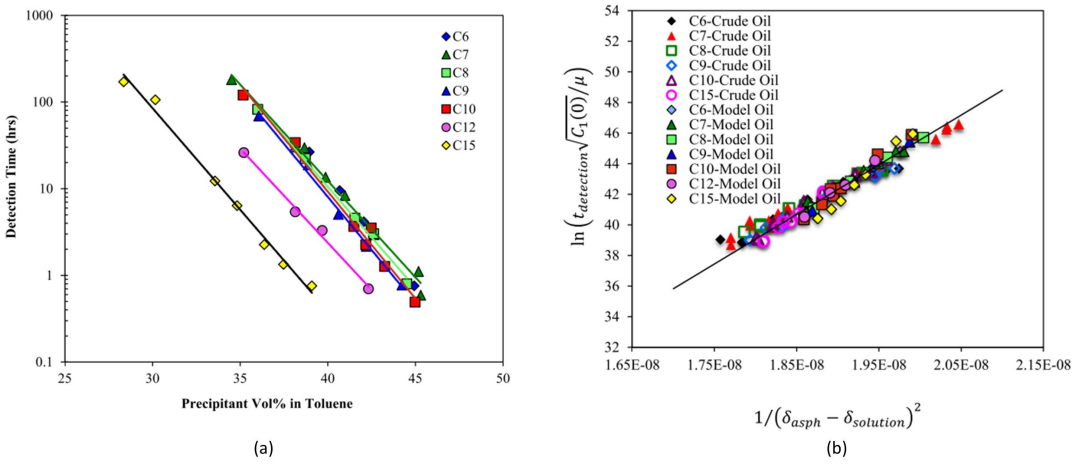

FIGURE 6.1: Reported by Haji-Akbari et al.[18]:
(a) Microscopy detection-time of unstable asphaltenes versus different prepcipitant vol% for several alkanes in model systems made of 1wt% dissolved asphaltenes in toluene
(b) Plots of the unified model results for 6 different alkanes mixed with 2 different oils (crude oil and model system ade of 1 wt% asphaltenes in toluene)

In their data processing, the solubility parameter of asphaltenes was adjusted for each alkane in order to bring data points together on the master curve. Obtained profiles of solubility parameters of the destabilized asphaltenes are replicated in Figure 6.2.

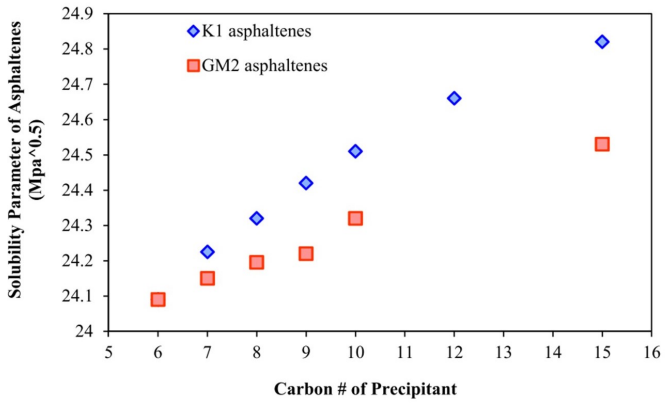

FIGURE 6.2: Reported by Haji-Akbari et al. [18]: Adjusted solubility parameters of unstable asphaltenes as a function of the carbon number of the used non-aromatic solvents

According to the results of Haji-Akbari et al. [18], extracted asphaltenes have lower solubility parameters when destabilized by the addition of relatively shorter n-alkanes. This profile is in agreement with other trends that can be found in the literature showing the increased destabilizing power of shorter alkanes, however this trend has not been experimentally verified with measurements on the properties of extracted fractions. Indeed, this model assumes a critical difference in solubility parameters between the colloidal material and the solution, δ_{asph} is therefore adjusted to keep the difference $(\delta_{\text{asph}} - \delta_{\text{solution}})$ constant.

Mitchell and Speight [26] showed that larger amounts of unstable asphaltenes are collected at high dilution of oil in alkanes (> 90 vol%$_{\text{alkane}}$) as the n-alkane chain is decreased. Complementary to the research of Haji-Akbari et al. [18], the results found by Mitchell and Speight [26] investigate a domain where the flocculation kinetics of asphaltenes are extremely fast upon addition of the bad solvent. The results reprinted from Mitchell and Speight [26] in Figure 6.3 suggests, in agreement with the work of Haji-Akbari et al. [18], that longer chain lengths of n-alkanes are better solvent for asphaltenes compared to shorter ones.

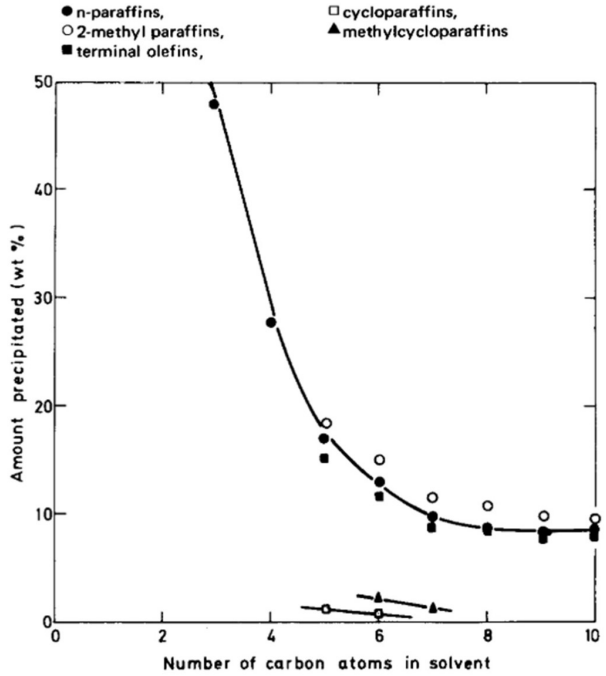

FIGURE 6.3: Reported by Mitchell and Speight[26]: Relation of amount of precipitated asphaltenes to the number of carbon atoms in non-aromatic solvents

Most of the reported investigations on the effect of *n*-alkane carbon numbers added at various concentrations in oils have had the objective to identify the "onset" point of flocculation (or instantaneous detection of unstable asphaltenes). In contrast with the precedent discussed trend, Figure 6.4 shows that volume fractions of alkanes pass through a maximum when varying the alkane's chain for the observation of instantaneous flocculation. This behavior has been referred to as a "paradox" of asphaltenes flocculation by Wiehe et al.[50].

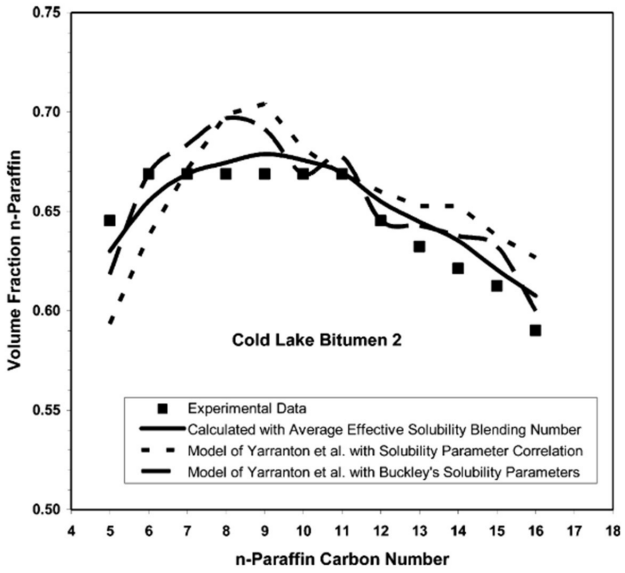

FIGURE 6.4: Reported by Wiehe et al.[50]: "Onset" volume fraction of n-alkanes in oil-alkane mixtures versus the *n*-alkane carbon number

Due to the experimental difficulty of studying the effect of volatile components, the addition of various chains of liquid alkanes at atmospheric conditions are the only ones reported (pentane to hexadecane). Studies involving an associated gas-dissolved at elevated pressures usually intended to predict the point of appearance of unstable asphaltenes or more commonly referred to as the asphaltenes "onset" pressure (AOP) or as the asphaltenes instability threshold[12;31]. Figure 6.5 reprints results of experimental observations using a near-infrared solid detection system and modeling curves with a perturbed chain statistical associating fluid theory (PC-SAFT) equation of state.

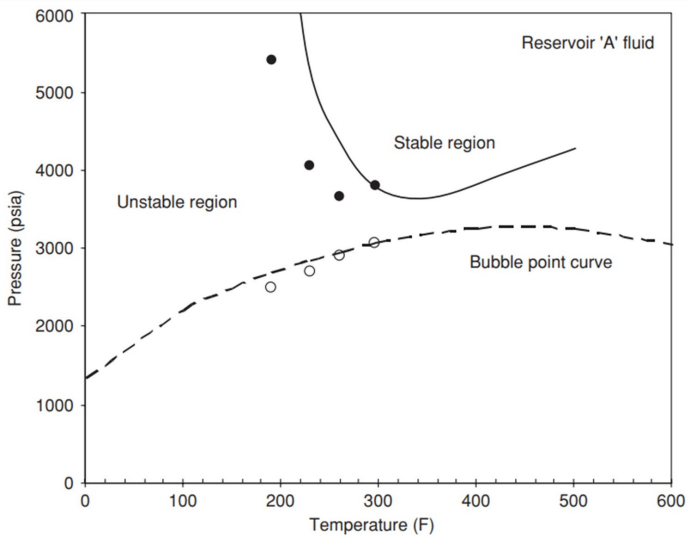

FIGURE 6.5: Reported by Ting et al.[41]: The temperature dependence of the asphaltene instability curve and bubble curve predicted by PC-SAFT and experimental measurements for the reservoir fluid

In this type of pressure vs temperature plot, stable and unstable regions of asphaltenes are commonly defined by authors based on the experimental observations of instantaneous flocculation during depressurization experiments. However, we have seen in previous Chapters that the destabilization and the flocculation processes can be slow with liquid alkanes (*n*-heptane), therefore it is expected that the detection threshold of unstable asphaltenes should also be dependent on the aging time in the case of light dissolved constituents. In the present Chapter, an experimentation investigating this particular point is presented in order to verify that the destabilization and aggregation concepts defined for *n*-heptane still hold for gas-dissolved conditions.

Models and simulation tools

Again because of the cost and the experimental difficulty to perform gas-dissolved tests, efforts have been administered to find predictive techniques of asphaltenes instability curves using simpler laboratory measurements of liquid solvent additions. Under ambient conditions, parameters affecting dispersive forces such as densities[32;33;51;3], molar volumes[47;24;2], volume ratios[50] or refractive indices[4;45;46;5;45] have been subjects of extensive research. For example, Vargas and Chapman[43] related solubility parameters to the density and to the refractive indices of crude oils in order to predict solubility parameters of live-oils.

Volumetric properties of oil-associated light constituents are strongly dependent on the pressure and temperature conditions as showed in Figure 6.6.

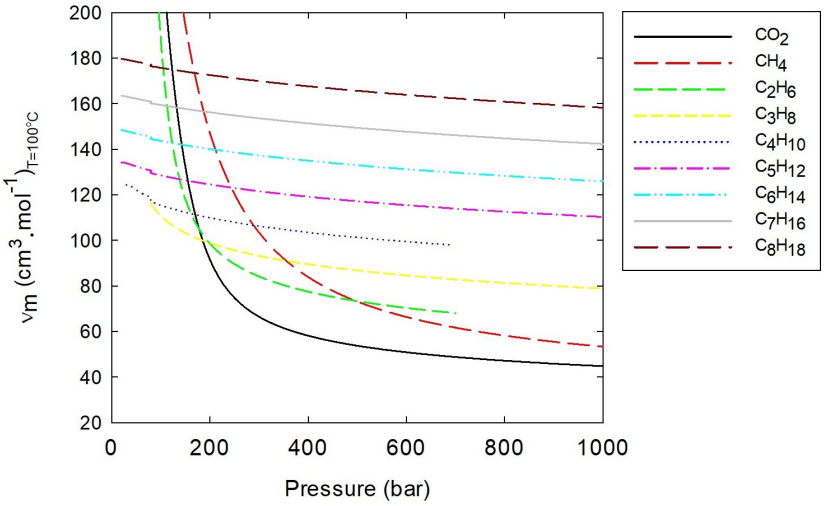

FIGURE 6.6: Comparison of molar volumes of pure fluids as a function of the pressure at constant temperature (100°C) (source: NIST chemical web book)

In other terms, the solubility parameter of light constituents have a strong dependence on pressure and temperature conditions. Consequently, the number of carbons in the alkane chains does not suit as a proper variable to study their effect on the asphaltenes destabilization.
Instead, the molar volume of the expanding components seems to be a more appropriate variable as the ASIST graphic suggests in Figure 6.7. Among the above cited available prediction models, the Asphaltene Instability Trend (ASIST) was developed from concepts mentioned above by New Mexico Institute of Mining and Technology in the frame of DeepStar consortium[4;45]. Thanks to its simple application, the ASIST method is extensively used in the oil & gas industry in order to conduct quick risks evaluations. The experimental approach of ASIST uses instantaneous microscopical detection of unstable asphaltenes with various liquid n-alkanes additions, refractive indices (n_D) measured for the dead oil at a reference condition and routine thermodynamic data. As showed in Figure 6.7, a linear threshold of stability is defined in the diagram of the solubility parameter of solutions $\delta_{solution}$ versus the square root of the molar volume of the precipitant agent $v_p^{1/2}$. The line corresponds to solution compositions at the detection of asphaltenes instability after waiting for a certain time and at a given temperature. The trend is extrapolated to predict the appearance of the least stable asphaltene due to light components expansion during live crude oil transport in wells and pipelines.

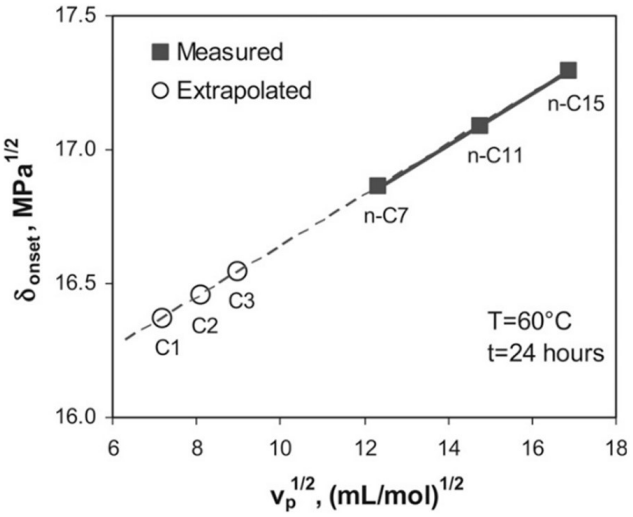

FIGURE 6.7: Reported by Creek et al.[8]: Example of determination of ASIST threshold lines in the diagram of $\delta_{solution}$ vs $v_p^{1/2}$

Authors[4;8;45;46] empirically found the linear relationship, within the range of investigated measurements, between the square rooted partial molar volume of alkanes $v_p^{1/2}$ and the solubility parameter of the solution at "onset" conditions.
The extrapolation of the linear regressions for alkanes ranging between pentane and pentadecane to the entire domain of molar volumes remains questionable. Experimental verification of ASIST predictions conducted by Creek et al.[8] and Dolati et al.[13] showed good agreements when choosing an appropriate aging time of solutions (between 1 and 24h). However trends of ASIST ambiguously go against previous tendencies that reported a larger destabilizing power of light alkanes compared to longer *n*-paraffins. Lines of ASIST counter-intuitively predict that solutions at the detection of unstable asphaltenes, have lower solubility parameters when destabilization is induced by relatively lighter alkanes. To paraphrase what that says; methane is, according to ASIST principles, a better solvent than *n*-heptane to the most unstable fraction of asphaltenes (the ones that first flocculate).
The choice of using different instruments with similar sensitivities can seem reasonable to detect unstable asphaltenes under pressurized conditions of the recombined crude oil compared to the microscope detection at atmospheric pressure. However, solid detection systems (SDS) generally use near-infrared transmittance signals through the oil to indicate if objects of comparable size or larger than the wavelength ($\sim$ 800 nm) are present. Before transcription of experimental results to a single point of "onset" pressure, similarly to piezo-sensors, the recorded signals are first subject to a graphic interpretation as a function of the pressure during constant mass expansion (CME) experiments. The onset is defined as the pressure at which a significant divergence of the signal is observed against the initial slope of the signal at higher pressures. However, as seen in Figure 6.8, the word "significant" in the previous sentence can take various definitions depending on our respective interpretation. The plot of the light transmittance against the pressure shows how difficult it can be to decide of a single diverging point on rounded-shaped curves. We can note the persistence of researchers to define a single point of asphaltenes instability when interpreting the continuous process of destabilization with a smooth record of signals during the continuous change of solution composition. This might lead to unreasonable practice and incorrect conclusions that have implications on the design of

models.

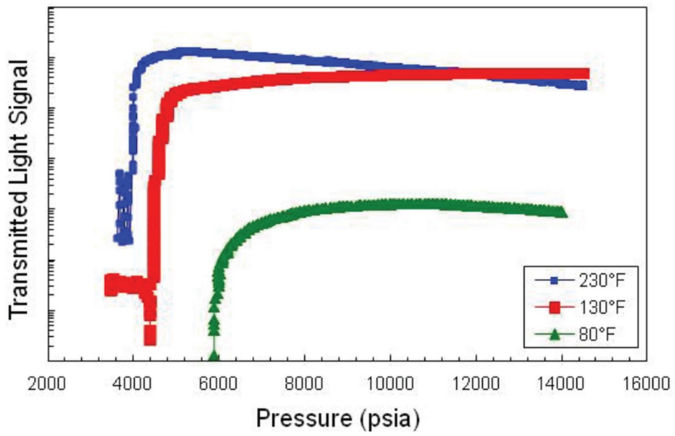

FIGURE 6.8: Reported by Montesi et al.[27]: Various exemples of records of solid detection systems (SDS) signals during CME experiments that are used to determine the asphaltene "onset" pressure (AOP)

Besides ASIST method[8;46] that seeks to predict a threshold of the stability of asphaltenes, other models based on thermodynamic[34;41;37] and colloidal[19;29;40;51] concepts have successfully been applied to calculate the yield of unstable asphaltenes. For example, Figure 6.9 shows modeling results of Akbarzadeh et al.[1] who applied a regular solution based model that fairly compares to the experimental measurement of the unstable asphaltenes yield.

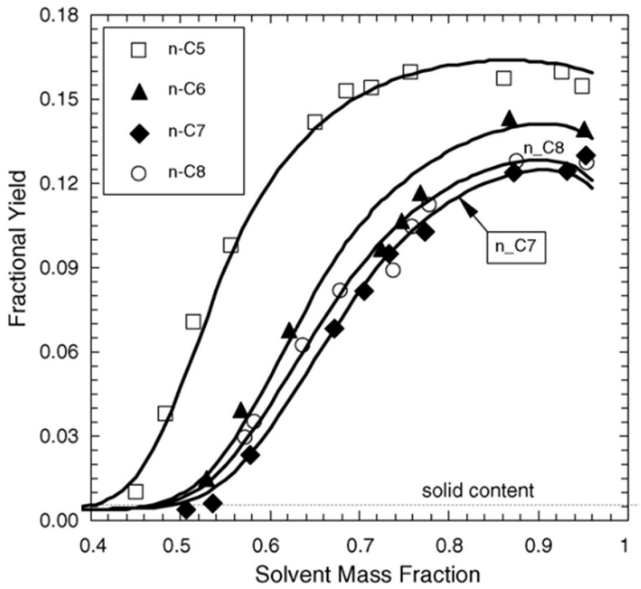

FIGURE 6.9: Reported by Akbarzadeh et al.[1]: Modeled yield of unstable asphaltenes from a bitumen diluted with variable amount and nature of *n*-alkanes at ambient conditions

Although general correlations on the asphaltene properties have been reported[3;43], the use of modeling concepts requires to adjust a certain number of parameters in order to fit curves to the experimental data. Tharanivasan et al.[40] have applied a

similar approach to calculate the yield of unstable asphaltenes as a function of the pressure during a live-oil depressurization. They highlighted the large sensitivity of calculations to adjusting parameters such as the average molecular weight of asphaltenes. Despite the good agreements showed in Figure 6.10; this remark *a priori* prescribes limitations in the predictive capability of the regular solution approach to asphaltenes destabilization from depressurization of live oils.

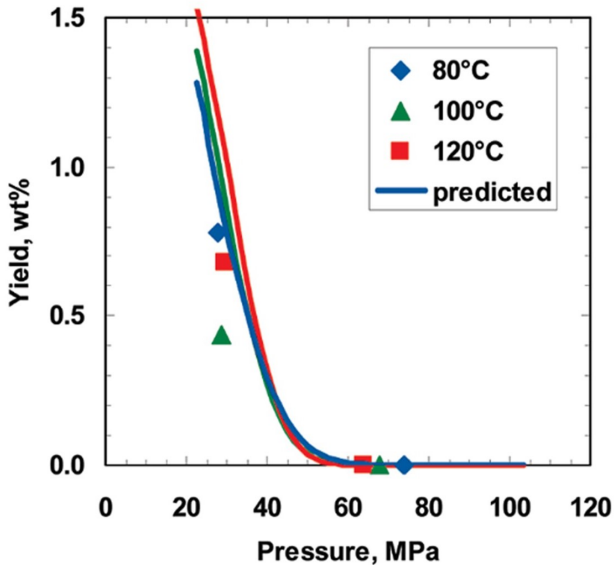

FIGURE 6.10: Reported by Tharanivasan et al.[40]: Modeled yield of unstable asphaltenes from a depressurized live-oil

More detailed summaries of existing modeling tools of asphaltenes destabilization were reported by Wiehe[49] (2012) and Subramanian[36] (2015).

Figure 6.11 shows the comparison between PC-SAFT modeled curves of unstable asphaltenes quantity at equilibrium and experimentally separated asphaltenes after one day of aging. Authors justified the observable difference by the fact that measured data did not reach equilibrium after one day. This result highlights the importance of combining results of our research (Chapter 3) to existing thermodynamic tools.

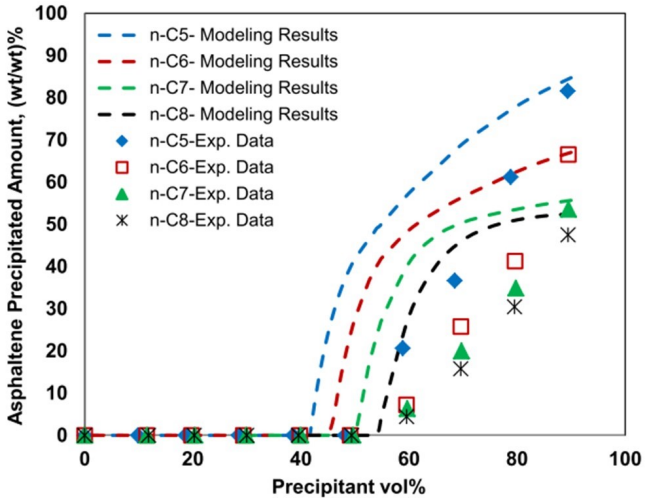

FIGURE 6.11: Reported by Tavakkoli et al.[38]: Modeled yield of unstable asphaltenes by PC-SAFT from a modified oil diluted with variable amount and nature of *n*-alkanes at ambient conditions

Authors[38] then incorporated destabilization kinetics into their model through time-resolved absorbance measurements obtained with additions of several *n*-alkanes. Their method enabled to calculate phase envelopes as a function of the aging time on a pressure versus temperature diagram (Figure 6.12.

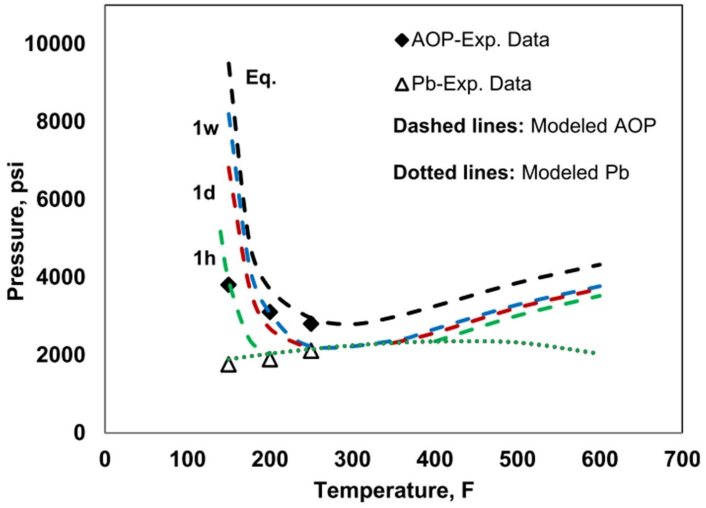

FIGURE 6.12: Reported by Tavakkoli et al.[38]: PC-SAFT modeled phase envelope of unstable asphaltenes as a function of time on a pressure vs temperature diagram for a recombined modified oil with light *n*-alkanes

As seen in the reported figure, authors[38] have reported a theoretical time dependence of such asphaltenes stability diagram, which agrees with our research presented in Chapter 3. However, experimental evidences of such behavior under depressurization of live oils are not showed, indeed only instantaneous "onset" of flocculation was measured in their work.

Available quantitative experimentation to study asphaltenes under gas-dissolved conditions

The concentration of unstable asphaltenes (C_A) is an important input for the developed deposition model in Chapter 5. After additions of liquid solvents at atmospheric pressure C_A is measured by using relatively simple separation techniques (usually filtration or centrifugation). However the experimental measurement of unstable asphaltenes yield, induced by the depressurization of light components in a live-oil, is limited to the sole high pressure filtration method. We should note that large source of uncertainties arise from applying this technique. The deterioration of the amount of unstable asphaltenes is a significant risk during the final depressurization of the system. Even if properly filtrated, nucleation of bubbles in the trapped liquid solution of the cake can break the accumulated solid layer and will promote re-suspension of fractions of asphaltenes in the solution. When the oil is brought back to atmospheric pressure for collection and weighting of the filter, some of the re-dispersed aggregates have eventually stabilized again in the form of nano-scale objects and are not accounted into the mass of unstable material recovered on the filter.
High pressure filtration experiments do not only present the inconvenience of local pressure gradients through the filters, it is also usually complicated to account for asphaltene components that deposited on the inner-walls of the equipment. Collecting the deposits requires to flush the apparatus with a good solvent, like toluene, but the collected amount of wetting and trapped oil during this operation is then difficult to evaluate in the mass balance of the "dry" mass unstable asphaltenes. In addition, such experiments on live-oils are invasive and destructive of the samples after each measurement.
Therefore, according to our knowledge, this is a statement of lacking reliable and non-destructive quantitative measurements of unstable asphaltenes for pressurized systems.
Additionally, the relevance of small unstable aggregates to the deposition was revealed by Hoepfner and Fogler[20 21] and Vilas Bôas Fávero et al.[44]. Indeed, significant accumulations of deposit were experimentally observe while flowing mixtures of *n*-heptane and crude oil for which unstable flocs had not reached a microscope detectable size ($\sim$ 0.5-2μm). In the precedent Chapter, the size of depositing particles was back-calculated from their fitted diffusion coefficients, an average hydrodynamic radius of 7 nm was found to describe depositing particles of unstable asphaltenes. These findings suggest that the size of unstable asphaltenes matters to the main deposition mechanism, smaller aggregates will cause a faster deposition rate under diffusion-limited regime. One should note that the concentration of unstable particles is another significant parameter to such a deposition mechanism.
Consequently a better resolution of the detection of unstable asphaltenes is necessary and methods referred as direct detection ones were judged not sensitive enough according to Tavakkoli et al.[39]. An indirect method of detection was developed by these authors[39] for ambient pressure experiments. The methodology was tested and validated using a model oil, which conveniently has a low viscosity and enables centrifuging out relatively small particles thanks to the good separation efficiency. However, higher viscosities or high pressure recombined oil fluids would still require large flocs of asphaltenes for their separation using the latter technique. At elevated pressures, the wide-spread SDS using NIR light transmittance, the earlier mentioned high pressure filtration or even high pressure microscopy are commonly used[23;17] but their sensitivity is two orders of magnitude larger than the calculated diameters of diffusing particles. The use of those experimental set-ups can lead to risky results that neglect undetectable particles.

In contrary, it can also lead users to push the mixtures to unreasonably severe conditions until flocculated asphaltenes can be seen. For example, a common practice of the oil & gas industry is to inject chemicals downhole to prevent asphaltenes from depositing. Chemical selections are made by comparing their influence on laboratory tests prior to field injections. Therefore, a reference condition of test is usually chosen in such way that asphaltenes are clearly detected without added chemicals. However experimental set-ups that are sensitive to microscopic or macroscopic phenomena will only provide indications on the effect of chemicals on the same length scale.
The sensitivity of immersed quartz resonators has been advantageous to quantitatively study asphaltene destabilization [15;10] and deposition in flow cells under atmospheric pressure as showed in Chapter 5. It has been shown that the fully immersed sensor can probe both liquid/vapor phase transitions and asphaltene destabilization in live crude oils throughout a single experiment [9;11].
This study investigates means of enhancing the analysis of the extracted information from the immersed QCR during the depressurization of live or recombined oils.

6.1.2 Aim of this work

The subordinate objective of precedent Chapters was to relate bulk phenomena to the deposition of asphaltenes on surfaces. Measurements of bulk properties and deposited masses were carried out with a non-destructive device to study the asphaltene deposition at the appropriate length scale (nanometers to micrometers).
At this point of our research, investigations of this dissertation have comprehended the simultaneous kinetics of destabilization, aggregation and deposition of a portion of asphaltenes induced by the (continuous and discontinuous) addition of *n*-heptane in crude oil. Mathematical relationships were derived to link the liquid composition to the concentration of unstable asphaltenes, their aggregation, their deposition and their detection-time by microscopy. Simulated mechanisms showed good agreements against experimental data after additions of *n*-heptane.
Extending the mentioned concepts, that were developed at atmospheric pressure with liquid mixtures of oil and heptane, to pressurized mixtures of oil and light constituents, first requires to verify if the mechanisms in such conditions are identical to those observed at ambient pressure. Therefore the presented results of experimentation will involve high pressure microscopy detection-time of unstable asphaltenes along with deposition measurement with an immersed QCR sensor.
A high pressure compatible vessel is used to study the effect of the molar volume of constituents. Note that due to the difference of geometry between our glass atmospheric pressure vessel (used in Chapter 5 and the high pressure apparatus forces us to repeat tests at atmospheric pressures with liquid anti-solvents in the aparatus that is compatible to high pressures. Indeed, the comparison of obtained data from using various alkanes (including methane) will only hold if using the same conditions of experiments (geometry and fluid superficial velocity).
First, the suggested relation (combining Chapters 4 and 5) between the detection of micron-sized aggregates and the deposition rate of unstable asphaltenes is verified with *n*-heptane (*n*-C_7) and *n*-undecane (*n*-C_{11}) at atmospheric pressure in the PVT cell. Second, the relation that was derived from both liquid alkanes at ambient pressure is used to check its applicability to methane dissolved conditions.

The two different regions of aggregation (slow and immediate) are in turn investigated with methane addition, the initial quantity of injected methane and the pressure variations enable to vary volume fractions as explained in Chapter 2. The presentation of results is divided into two subsections that refer to (i) the region of slow flocculation at which a detection-time curve is constructed and (ii) the region of elevated deposition rates and instantaneous flocculations.
This Chapter implicitly presents an attempt to clarify the above reported and conflicting trends with analyzing experimental data on a single crude oil and various alkanes.
The goal of this research is not to evaluate the accuracy of the existing modeling tools. However thanks to the simplicity of use of the ASIST method, we will take the opportunity to compare its predictions on the detection of unstable asphaltenes to the experimental measurements.
In addition to the verification of theoretical concepts, this work evaluates the capability of our experimental set-up to provide quantitative measurements related to the destabilization and to the deposition of asphaltenes under live-oil conditions.

6.2 Materials and methods

6.2.1 Sample preparation

Liquid solvents (e.g. n-alkanes) and bottles of methane were 99+% purity supplied. For measurements involving addition of *n*-heptane or *n*-undecane, the crude oil was first mixed with an appropriate amount of liquid *n*-alkane. Indeed the volume restrictions of the high pressure vessel would not enable to reach relevant mixture concentrations if not starting with a pre-mixed solution.
The crude oil, the alkanes and vials were all incubated at the temperature of the study until reaching a stable temperature. A known volume of oil was placed into a vial. The pure solvent was added by means of a peristaltic pump at an addition rate of 3 cm^3/min until the desired concentration was obtained (on a mass basis). During the addition, a good agitation was ensured with a magnetic stirrer to minimize localized high concentrations. The solution was then injected in the pressure volume and temperature (PVT) controlled cell. Additional liquid solvent was pumped-in by moving the piston and increasing the total volume of the cell. All the injected alkanes while recording the QCR signal were prepared on a volume measurement basis thanks to the pre-calibrated PVT cell. A schematic of the experimental set-up is showed in Figure 6.13.

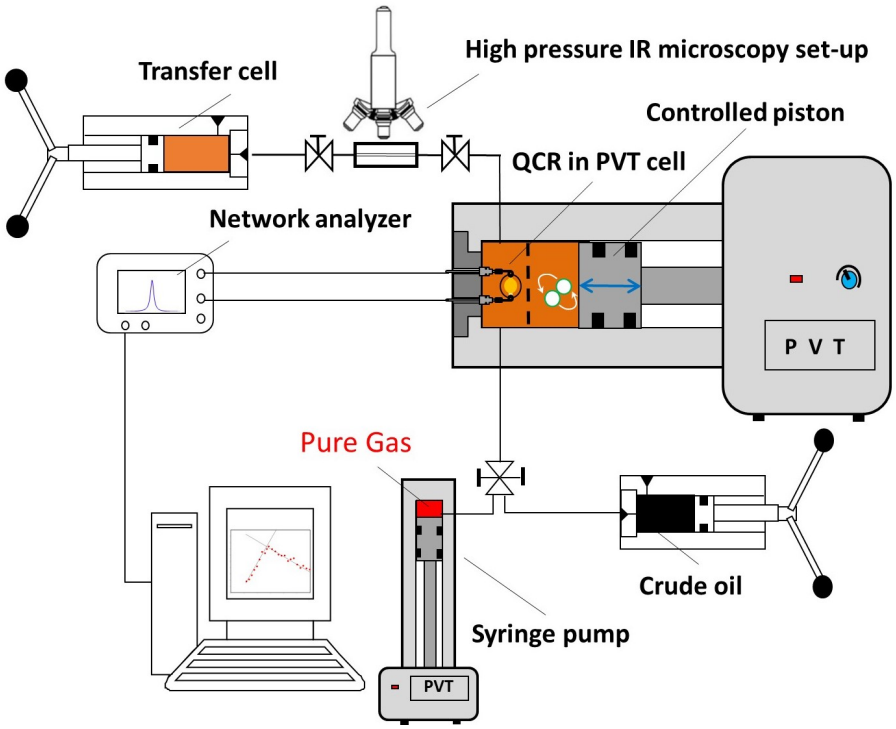

FIGURE 6.13: Schematic of the high pressure compatible apparatus with an immersed QCR

For cases of recombination of the oil with methane, the sample preparation is described in Chapter 2.

6.2.2 Measurements of an immersed QCR in a pressure compatible vessel

We have seen in Chapter 4 that the microscopy detection-time ($t_{detection}$) follows the proportionality:

$$\log\left(\frac{dC_{1_i}}{dt}\right) \propto \log\left(t_{detection}\right) \tag{6.2}$$

where $\left(\frac{dC_{1_i}}{dt}\right)$ is the initial generation rate of primary particles of unstable asphaltenes defined by $r_1(0)$ in Chapter 3. In turn, Chapter 5 advises the relation:

$$\frac{\Delta m}{\Delta t} = rate_{deposition} \propto C_1(t) \tag{6.3}$$

During a given interval of time Δt, a constant deposition rate (linear increase of the deposited mass as a function of time) equates to a constant concentration of primary units over time. The generation rate (showed to be roughly constant within periods of time equivalent to the detection-time) then equals the rate of consumption (aggregation or deposition) of the primary particles. In those circumstances, the concentration of primary particles only depends on the initial conditions and the following implication can be written:

$$\left(\frac{dC_1}{dt}\right) = 0 \implies C_1(t) \propto \left(\frac{dC_{1_i}}{dt}\right) \tag{6.4}$$

Combining equations 6.2, 6.3 and 6.4, one can establish the relation between the microscopy detection-time of particles and the measured deposition rate of unstable

asphaltenes as follows:

$$\log\left(rate_{deposition}\right) \propto \log\left(t_{detection}\right) \tag{6.5}$$

Scanning of a n-alkane expansion can be carried out either continuously or by steps of volume additions. Although the generation rates of unstable asphaltenes are low in the range of compositions corresponding to the detection-time curves, the nano-sensitivity of the immersed QCR lets us measure significant enough deposition rates during successive addition of alkanes in the conditions of interest. The method is first applied with step additions of n-C_7 and n-C_{11} at equivalent concentrations at which the microscopy detection-time curve of asphaltene particles had been observed. In this way, the above proposed relation is verified and the data points will serve as a calibration curve to the interpretation of data with dissolved methane in the same oil, for which the detection-time curve is experimentally more complicated to determine. Figure 6.14 shows the track of the composition of the mixtures over time.

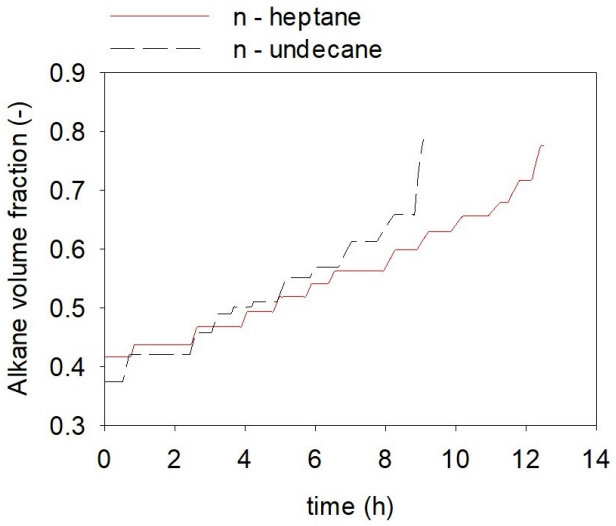

FIGURE 6.14: Tracking records of the mixture composition versus time during step additions of n-heptane and n-undecane

The second part of our work consists of using the QCR records to construct the detection-time curve of flocculated asphaltenes induced by the presence of methane. A pressure scanning, starting from the highest to the lowest pressure, is ran in order to identify conditions at which the deposits significantly accumulate. As observed in the case of n-heptane addition, Figure 6.15 shows that the conditions of the immediate detection of micro-flocs by visual inspection and the departure of the deposition curve roughly coincide.

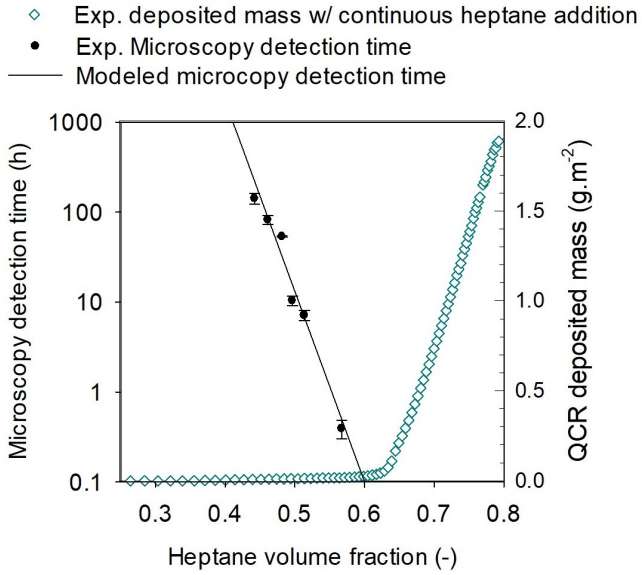

FIGURE 6.15: Comparison of the microscopy detection-time results of individual solutions to the cumulative mass of deposit during the heptane addition as a function of the mixture composition

The first experiment of continuous depressurization is therefore an identification of the conditions at which deposition significantly increase which roughly estimates conditions at which the microscopy detection-time curve should pertain. The experiment is then repeated with making steps of depressurization while taking records of the deposited mass of asphaltenes in the pre-identified region. Figure 6.16 shows the evolution of the composition mixture during this operation.

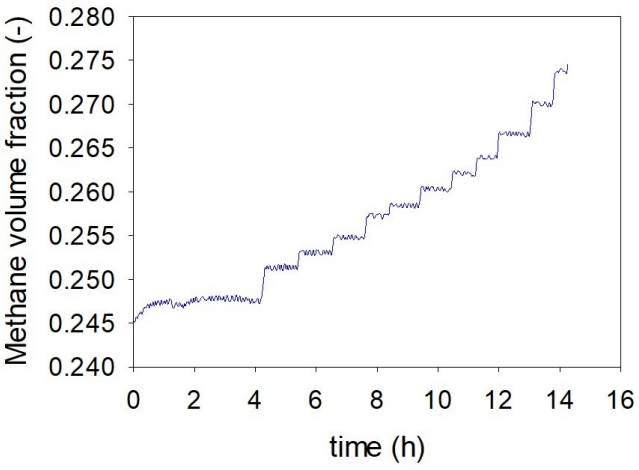

FIGURE 6.16: Tracking records of the mixture composition versus time during steps of depressurization of an oil-methane blend (from P = 950 to 500 bars)

The minor fluctuations occur during each stage due to the pressure adjustments of the apparatus. Indeed, the tracking curve of pressure as a function of time also shows similar fluctuations as seen in Figure 6.17.

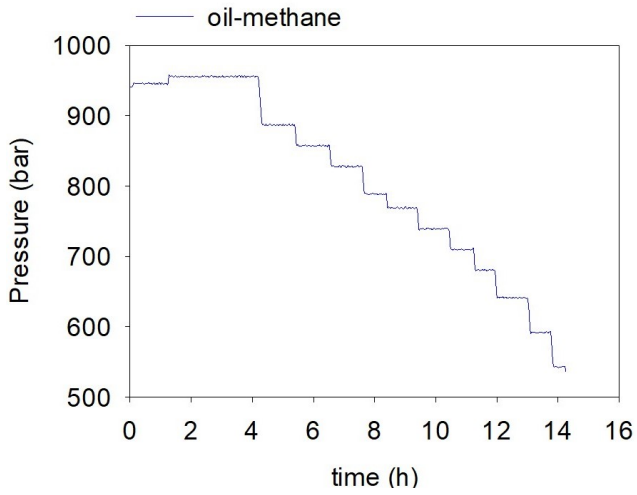

FIGURE 6.17: Tracking records of the pressure versus time during steps of depressurization of an oil-methane blend

The deposition data are then treated through the calibration curve previously arisen from Equation 6.5, in order to estimate the microscopy detection-time curve of unstable asphaltenes from the measured deposition upon stages of methane expansion.
The last part of the pressurized experiments consisted in continuous depressurisation of methane-oil mixtures starting from 900 bar to 100 bar at various depressurization rates (2, 4 and 12 bar.min^{-1}). According to the plot of the volume fraction of methane as a function of pressure, showed in Figure 6.18, a larger volume addition rate of methane is expected as the depressurization rate is increased.

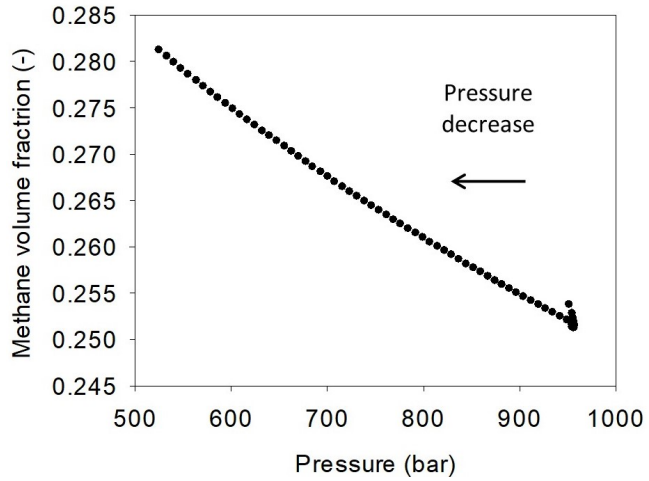

FIGURE 6.18: Composition of the prepared oil-methane mixture as a function of pressure

As shown in Chapter 5, the deposition rate scales with the concentration of primary unstable asphaltenes in the case of *n*-heptane continuous addition. Investigated conditions of deposition are beyond the onset of instantaneous flocculation, therefore the concentration C_1 of primary unstable asphaltenes exclusively depend

on the generation rate of unstable asphaltenes and according to Figure 6.18, the following equation should hold in such conditions:

$$C_1 \propto \frac{dC_1}{dt} \propto \frac{dP}{dt} \tag{6.6}$$

Indeed Chapter 3 advised that during a continuous addition of alkanes in crude oil, the generation rate is controlled by the addition rate of the liquid alkanes. In the studied case, and as illustrated by Figure 6.18, the addition rate of methane is equivalent to the depressurization rate of the recombined oil. The rate of depressurization is expected to be one of the main variable affecting the deposition rate of the studied system. Combining equations 6.3 and 6.6, we get:

$$rate_{deposition} \propto \frac{dP}{dt} \tag{6.7}$$

6.2.3 Microscopy detection of unstable asphaltenes

High pressure microscopy

As discussed in the previous paragraph, predictions of the detection-time curve of unstable asphaltenes is indirectly calculated as function of the methane content using deposition measurements and concepts developed when using *n*-heptane. The applicability of those concepts to different alkanes is uncertain and needs direct experimental verification. Aliquots of pressurized samples cannot be taken, instead the observed fluid has to directly be transferred into a transparent device without altering the pressurized fluid. For this purpose, a custom-made jacketed cell with sapphire windows on both sides of a channel was connected. The distance between both windows is large enough to let micro-objects to flow through ($\sim$ 0.3mm) and narrow enough to enable infrared light to span through a dark sample such that microscope observation are made from the other side. The high pressure experimental set-up presented in Chapter 2 is equipped with the high pressure microscope cell between two different PVT cell (one of them containing the QCR). In this way, pistons on both sides can simultaneously be used to homogenize the fluid without altering the pressure of the sample. This set-up enables to observe an isothermal and isobaric transferred fluid by time-resolved microscopy. Figure 6.19 shows a schematic representation of the high pressure microscope set-up for better visualization of the reader.

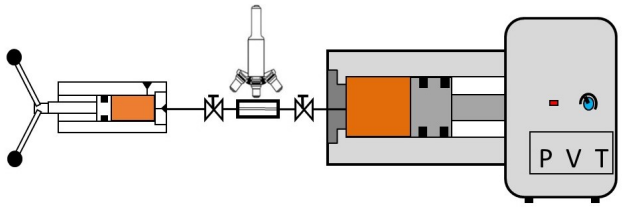

FIGURE 6.19: Schematic of the high pressure microscope set-up

Due to the complexity and the destructive character of experiments performed at different molar compositions, only two data points were collected. Before running each experiment, the mixture is first brought to the highest practical pressure in order to minimize the methane volume fraction and risks of flocculation. After making sure that the signal of the immersed QCR is constant over time (synonym of absence

of detection of unstable asphaltenes), the identifying condition of interest (methane volume fraction or pressure) is reached at a depressurization rate of 20 bar.min^{-1} to minimize the time of this operation. The agitated solution mixture is then left at the pressure of interest and shooting images are taken through the microscope, after manually homogenizing the system in both PVT cells prior to taking a picture.

6.3 Results discussions

6.3.1 Effect of the *n*-alkane chain length on the slow destabilization and aggregation of unstable asphaltenes

detection-time of micro-aggregates in liquid mixtures at atmospheric pressure

The polydisperse distribution of asphaltene molecules that are naturally present in petroleum fluids confers to them a dependence of their dispersion (in forms of nanoaggregates or clusters[28]) on properties of the liquid solution. The concentration and the aggregation rate of destabilized units quantitatively give full account of the effect of solution properties (solubility parameter and viscosity) on the asphaltenes behavior. Their microscopy detection-time represents a combined effect of destabilization and aggregation rates (Chapter 4). Figure 6.20 shows the microscopy measurement for five different liquid *n*-alkanes (*n*-C_7, *n*-C_8, *n*-C_{10}, *n*-C_{11}, *n*-C_{15}) mixed to the crude oil at a temperature of 60°C and at atmospherci pressure. The detection-time of asphaltenes micro-aggregates shown by the studied crude oil system gives similar trends to the results reported by Haji-Akbari et al.[18] showed in Figure 6.1.

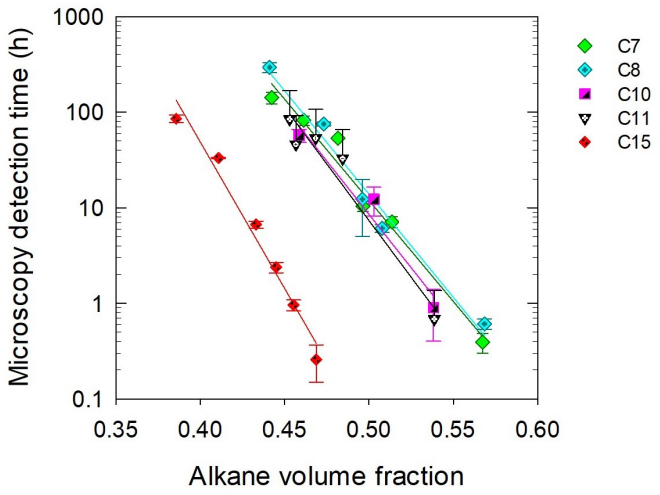

FIGURE 6.20: Microscopy detection-time of unstable asphaltenes as a function of the volume fraction of *n*-alkanes in oil-alkane solutions for five different *n*-alkanes

Despite the higher viscosity and larger solubility parameter of *n*-pentadecane, the destabilizing power of increased carbon numbers of *n*-alkanes compared to *n*-heptane is in agreement with previous observations[18;50]. This unexpected behavior has been attributed to the polydispersity of asphaltenes according to the so-called unified model of Haji-Akbari et al.[18]. They reported that different *n*-alkanes are

expected to destabilize different fractions of asphaltenes solubility class. The fitted trend of δ_{asph} to their model adverts that longer n-alkanes will destabilize asphaltenes that have larger solubility parameters on average, and vice versa (see Figure 6.2). For that, the solubility parameter of mixture solution was introduced as a variable instead of the volume fraction of each alkane. Figure 6.21 reports the measured data plotted in a different manner, i.e. as a function of the solubility parameter of respective solutions with extrapolated regression trends to a range of time between 0.1h ad 1000h.

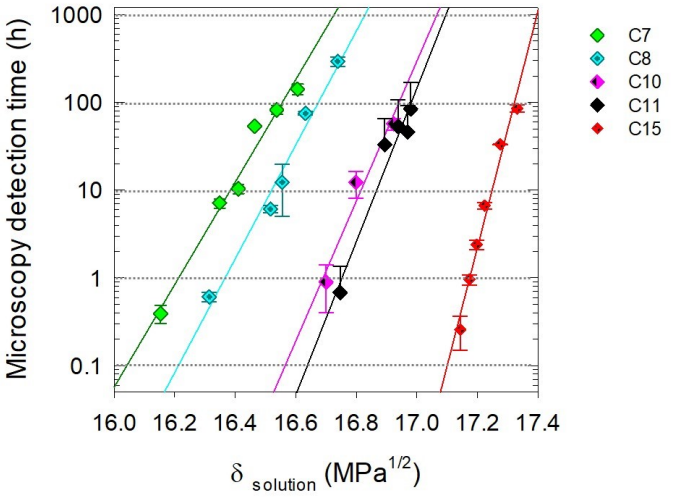

FIGURE 6.21: Microscopy detection-time of unstable asphaltenes as a function of the solubility parameter of oil-alkane solutions for five different n-alkanes at various concentrations

The plot of unstable asphaltenes measurements against of the solubility parameter of solution highlights the strong effect of the nature of the destabilizing solvent. Indeed, equal solubility parameters of solutions (synonym of similar dispersive interaction forces) obtained from adding different alkanes is not able to collapse the microscopy observations in a single line. Trends are rather moved apart when studied with the solubility parameters of mixtures.
We bring the attention of the reader on the fact that no detection-time curves could be simply measured with the same atmospheric pressure set-up for n-alkanes lighter than n-pentane due to their volatility. As predicted by ASIST lines and if the observed trend in Figure 6.21 remains unchanged for lighter solvents; microscopy detection-time curves of asphaltenes destabilized upon addition of light alkanes is expected at a lower solubility parameter than n-C_7.
Figure **??** is the construction of the ASIST plot using Figure 6.21 by reporting each intersection of the regression lines with five chosen aging times represented by graduated dotted lines (0.1h, 1h, 10h, 100h and 1000h). Note that previous verification of ASIST predictions involved the tuning of mixtures aging time up to tens of hours[8]. Consequently, results for multiple ASIST lines corresponding to aging times between 0.1h and 1000h are purposely showed in order to compensate for potential experimental errors. The composed graphic illustrates the above statement of trends mentioned for lighter alkanes.

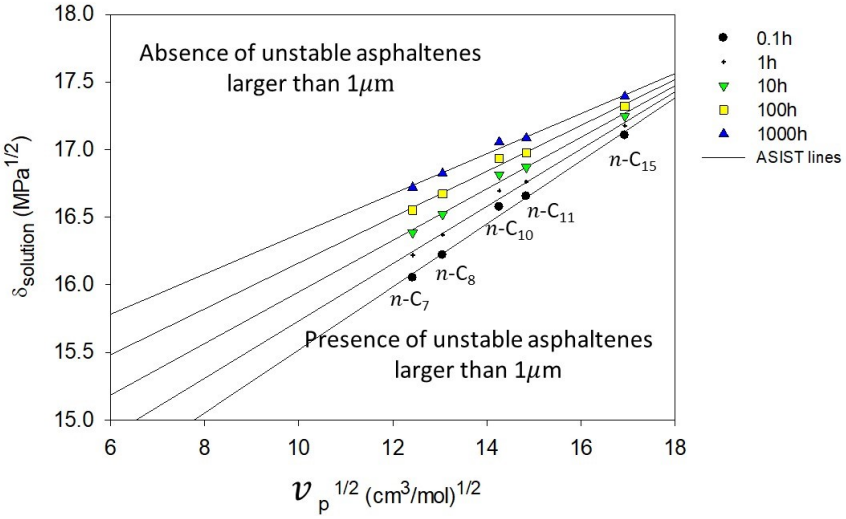

FIGURE 6.22: Solubility parameter of solutions corresponding to the microscope detection of unstable asphaltenes for several aging times and several *n*-alkanes versus the square-root of the partial molar volume of the used *n*-alkane ($v_p^{1/2}$)

ASIST predictions by extrapolations of linear regression trends will later be compared to experimental data obtained for the destabilization of asphaltenes induced by volume expansion of methane ($v_p^{1/2} \sim 6$ - 7 $\left(\mathrm{cm}^3/\mathrm{mol}\right)^{1/2}$).

Relation between the microscopy detection-time of liquid mixtures at atmospheric pressure

Figures 6.23 and 6.24 show results of the record of the deposited mass of unstable asphaltenes on the immersed sensor as a function of time for respective additions of *n*-C_7 and *n*-C_{11}. Successive stages were performed such that let the solution age for 30 minutes or longer between each addition in order to gather enough data points to analyze slopes.

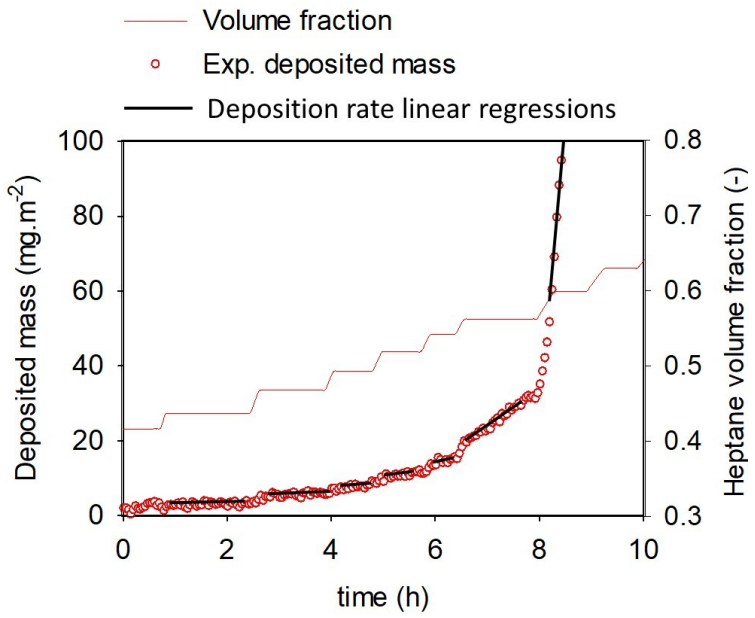

FIGURE 6.23: Records of the deposited mass of unstable asphaltenes as a function of time upon stage additions of n-C_7

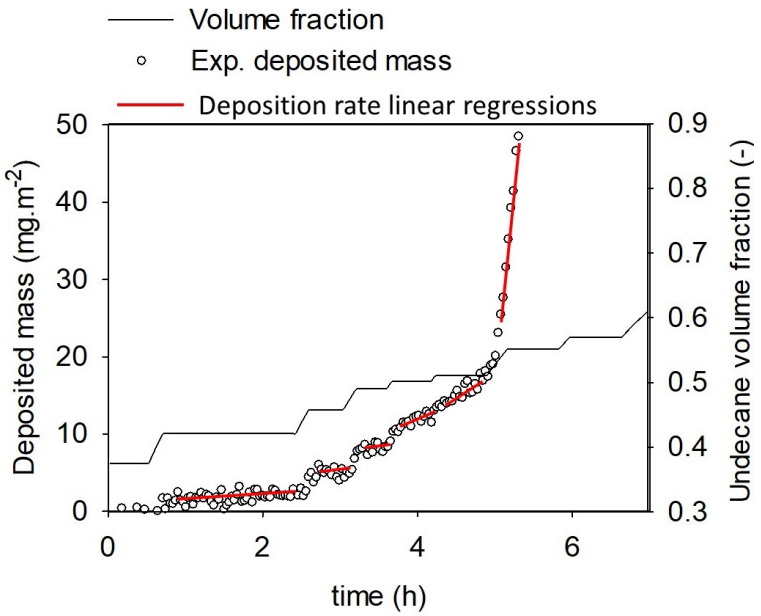

FIGURE 6.24: Records of the deposited mass of unstable asphaltenes as a function of time upon stage additions of n-C_{11}

Two remarkable trends arise from both graphical results of stage records: (i) the deposition rate is significantly augmented by the simultaneous addition of the alkanes compared to time intervals when additions are momentarily stopped and (ii) observed deposition rates (slope) steadily increase with the volume fraction of alkanes and eventually gain significantly larger orders of magnitude when the instantaneous points of flocculation are passed.
According to Equation 6.5 derived from developed models in previous Chapters of

this dissertation; the logarithmic plot of linearized deposition rates $\frac{\Delta_m}{\Delta_t}$ upon successive stage additions of n-C_7 and n-C_{11} against the measured microscope detection-time should result in a line. Figure 6.25 shows the good agreement between the measured data and the expected trend.

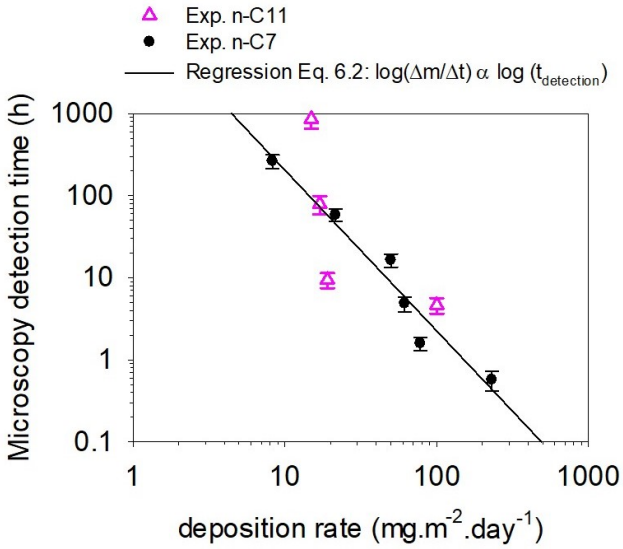

FIGURE 6.25: Logarithmic plot of the observed detection-time of unstable asphaltenes with a microscope against the measured deposition rate

If mechanisms of destabilization, aggregation and deposition are unchanged, the latter trend is theoretically independent of the added alkane to destabilize asphltenes. Its acquisition from experiments using two different alkanes seems to confirm that mechanisms are identical for different alkanes. Note that even if similar mechanisms occur, it does not exclude the sensitivity to the nature of the added alkane and to its concentration in solutions.

Application of the obtained experimental relation to oil-methane mixtures by stages of depressurization

As showed in the previous paragraph, the relation between the microscope appearance of asphaltenes aggregates and their deposition rate seems to be insensitive to the nature of the anti-solvent. Figure 6.26 shows results of the equivalent method of stage measurement of the deposited mass of unstable asphaltenes when applied to an oil-methane system. Steps of volume addition of methane are achieved by means of successive changes of piston positions corresponding to pressure levels.

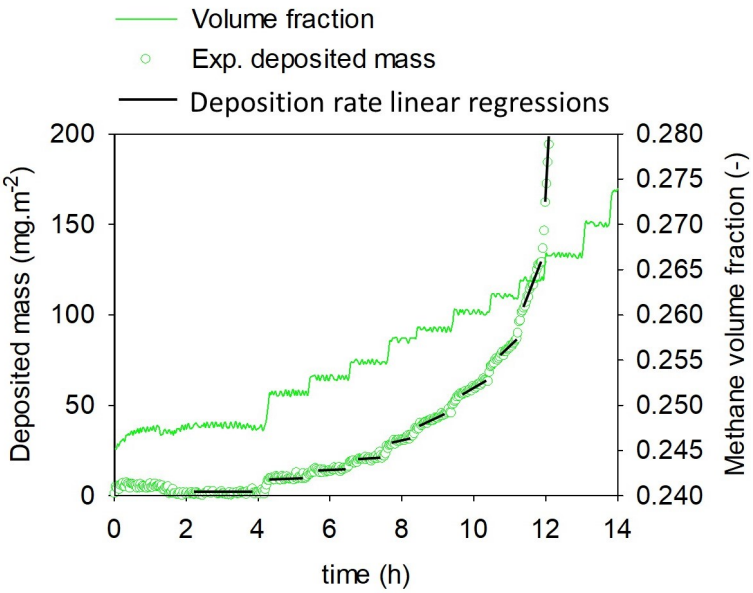

FIGURE 6.26: Records of the deposited mass of unstable asphaltenes as a function of time upon stage additions of CH_4 by steps of depressurization of an oil-methane mixture

The obtained linearized deposition rates are then used to calculate a detection-time curve by microscopy of the pressurized system. The data processing consists of reading the equivalent times corresponding to each measured deposition rate, as illustrated by Figure 6.27.

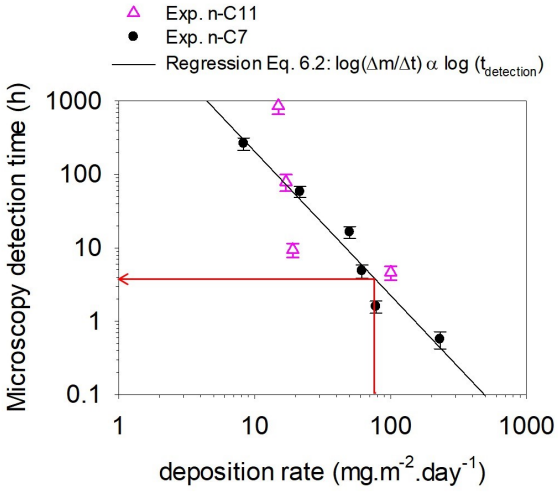

FIGURE 6.27: Data processing of the obtained deposition data of oil-methane mixtures using the previously obtained plot showed in Figure 6.25

The calculated detection-time curve of the unstable asphaltenes upon depressurization of an oil-methane mixture is plotted against the solubility parameter of the solution and the volume fraction of alkanes in Figure 6.28.

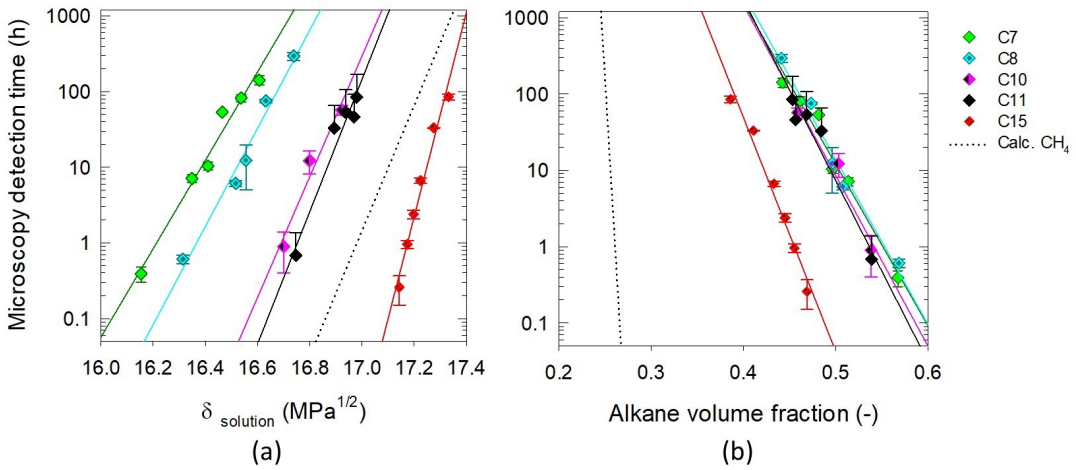

FIGURE 6.28: Calculated microscopy detection-time curve of unstable asphaltenes induced by methane (along with other *n*-alkanes previously showed) as a function of (a) the solubility parameter of oil-alkane solutions and (b) the volume fraction of respective alkanes

As it can be seen, the resulting curve of the applied method goes against the observed trend when only studying the effect of heavier alkanes in previous paragraphs. In the following paragraph, high pressure microscopy results are presented in order to verify that no error arise from the relation between the measured deposition rate of asphaltenes and their detection-time by microscopy.

Verification of the back-calculated detection-time curve of unstable asphaltenes by high pressure microscopy

Figure 6.29 provides examples of images observed during the constant mass expansion and while aging solutions at a fixed compositions (constant pressure). The appearance of opaque material is related to the destabilization of asphaltenes phenomena. Note that more unstable asphaltenes can qualitatively be observed at conditions of instantaneous flocculation than in cases of aging the solution at a higher pressures for hours. This observation is consistent with usual images recorded for flocculation induced by addition of liquid alkanes. It is also worth remarking that the slow growth of unstable asphaltenes appeared as a dynamic process with aggregating and detaching particles from each other at the scale of observation (~ 10 μm). The saturation pressure was clearly observed and despite the lack of experimental measurement of solution properties at pressures lower than the saturation pressure, the asphaltenes were observed to re-disperse very rapidly and could not be observed a few seconds after the saturation pressure was passed.

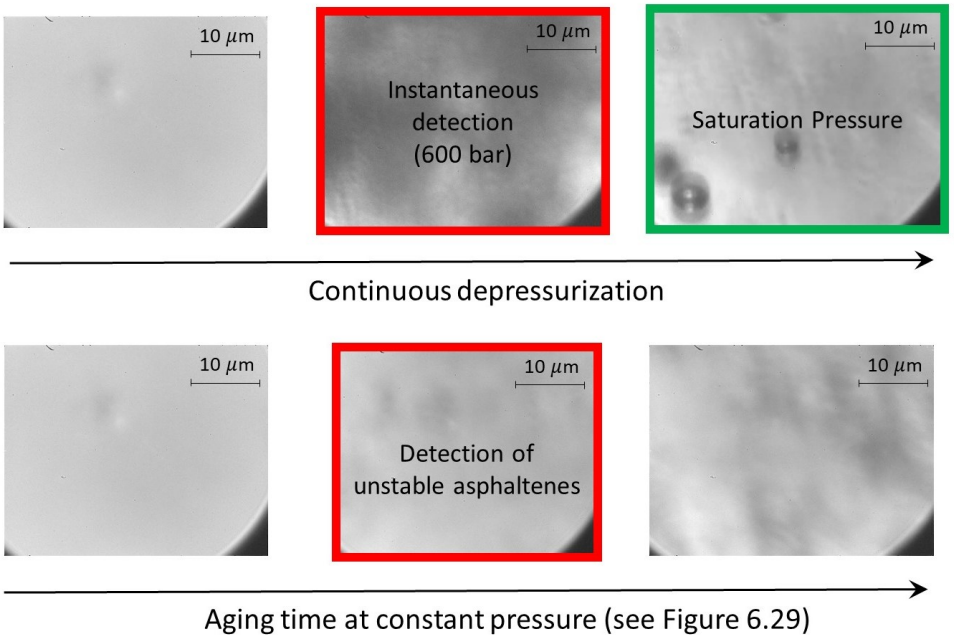

FIGURE 6.29: Example of high pressure microscope shooting images of the crude oil-methane system

The results of the two independently measured data points at different pressures are incorporated to the plot of several alkanes on top of the previously calculated detection-time curve. As seen in Figure 6.30 the experimental measurements and the calculated curve of unstable asphaltees detection by microscopy are in excellent agreement.

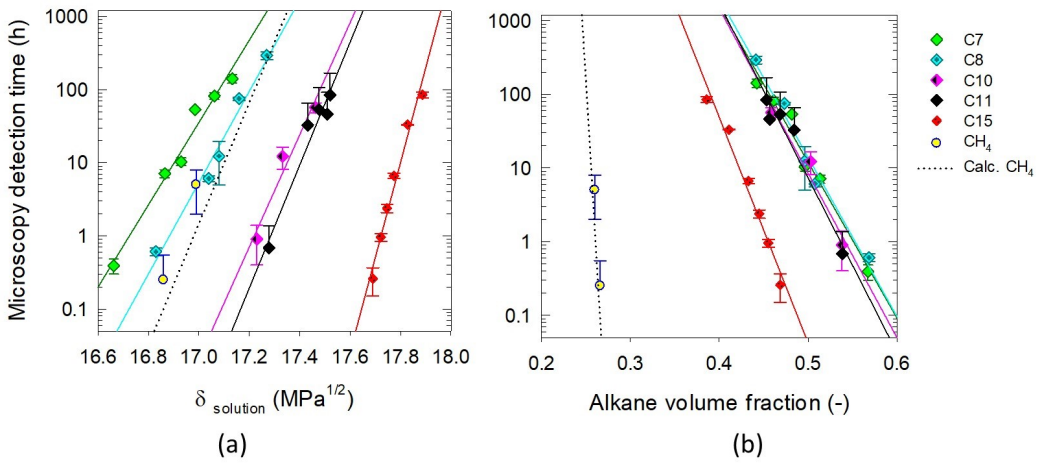

FIGURE 6.30: Measured microscopy detection-time of unstable asphaltenes for six different *n*-alkanes (including methane) at various concentrations as a function of (a) the solubility parameter of oil-alkane solutions and (b) the volume fraction of respective alkanes

Extending our experimental method based on deposition rate measurements enabled us to derive a time-dependent diagram of appearance of unstable asphaltenes

showed in Figure 6.31. Observed results are in agreement with time-resolved modeled asphaltenes instability envelopes reported by Tavakkoli et al. [38].

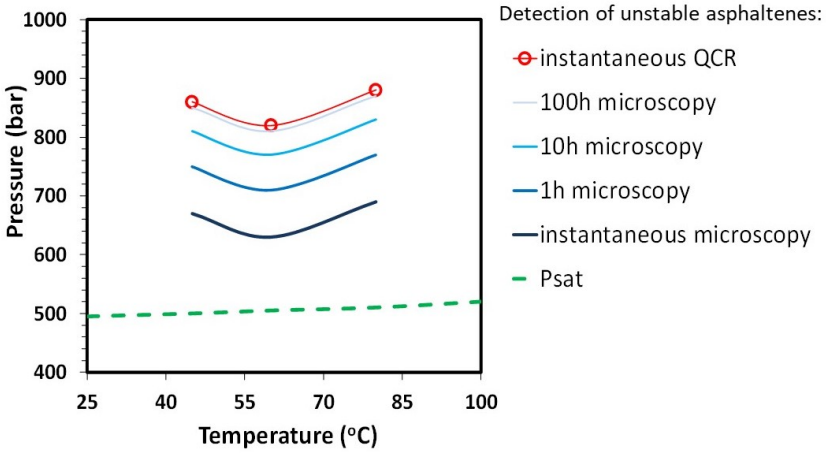

FIGURE 6.31: Time-dependent curves of unstable asphaltenes detection on a pressure versus temperature phase diagram for the studied methane-oil system

ASIST trends can now be evaluated against experimental data obtained with the same observation technique of asphaltenes destabilized by constant mass expansion of oil-methane mixtures. Figure 6.32 shows the complete set of data in comparison to ASIST lines that extrapolate the behavior of data points obtained with liquid components at room pressure and temperature of the study [46;8] (here 60°C). As it can be noticed, CH_4 takes different values of partial molar volume in oil-methane mixtures due to its strong dependence on the pressure (presented in Chapter 2).

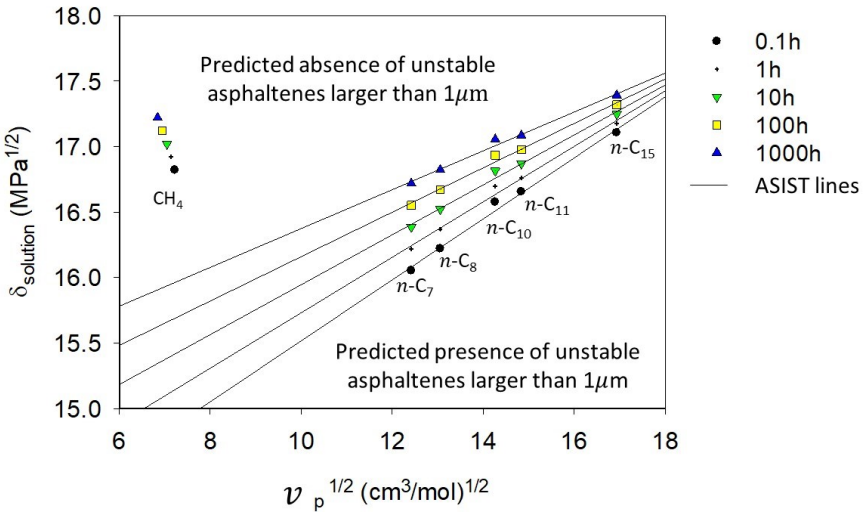

FIGURE 6.32: Predictions of ASIST solubility lines to experimental instability of asphaltenes obtained by constant mass expansion of methane-oil and measured by microscopy for several aging times and several n-alkanes versus the square-root of the partial molar volume of the used n-alkane ($v_p^{1/2}$)

A significant discrepancy is found between the ASIST method and experimental observations. Indeed, the experimental measurement of appearance of the micro-unstable asphaltenes during the methane expansion is found in the predicted zone of "stability" at larger solubility parameters than the ASIST lines. Indeed, despite many reports that seemed to verify the applicability of ASIST extrapolations to alkanes with low molar volumes[8;13;14;35], results showed in Figure 6.32 indicate that ASIST lines under-predict risks of asphaltenes instability in the investigated condition of this Chapter.
Note that refractive indices of gas-dissolved solutions are not measured but calculated following the ASIST method[4]. The calculating is explained in Chapter 2 of this work. Despite assumptions of such calculations, a sensitivity analysis reveals that relative errors of the refractive index calculations should be in the order of $\sim$ 6.5% for ASIST to comply with experimental data. Such relative errors are more than one order of magnitude larger than typical discrepancies found on refractive indices which are very sensitive parameters. Therefore, the discrepancy between ASIST predictions and experimental measurements of asphaltenes instability cannot be explained by the particular calculation of live oils refractive indices of the method.
According to the experimental trends showed in Figure 6.33, solutions in which unstable asphaltenes are detected have similar solubility parameters when induced by additions of n-C_{15} and of CH_4 to the crude oil. However the detection of unstable asphaltenes necessites comparatively lower $\delta_{solution}$ for cases of addition of n-alkanes with intermediate chain lengths.

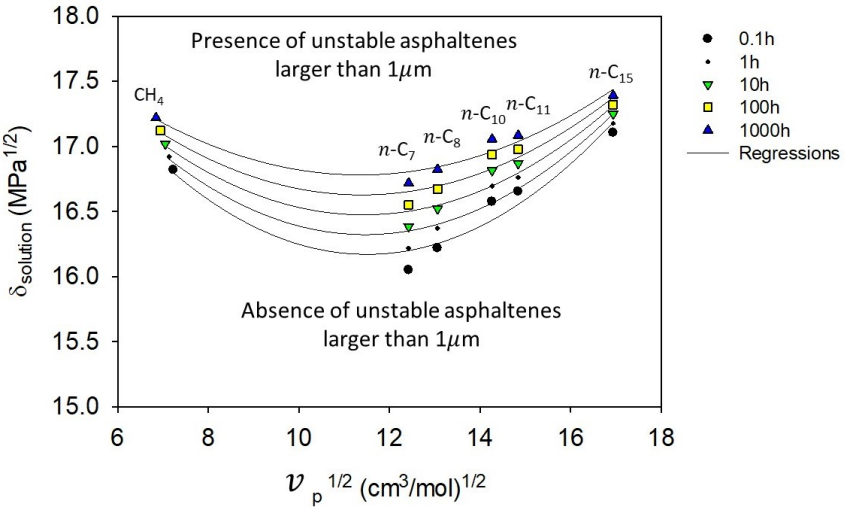

FIGURE 6.33: Trends of time-resolved detection of unstable asphaltenes by microscopy for several several n-alkanes versus the square-root of the partial molar volume of the used n-alkane ($v_p^{1/2}$)

In fact, when plotted in the form of volume fractions of alkanes at detection as a function of $v_p^{1/2}$ (that better represents the more usual carbon number variable for compressible components) the observed trends of this work retrieve the so-called paradox of asphaltenes instability induced by addition of n-hydrocarbons. Figure 6.34 shows that curves pass through a maximum at intermediate chain lengths of the studied alkanes ($\sim$ n-C_7 $-$ n-C_8). Interestingly, the detection kinetics of unstable asphaltenes have a dependent behavior on the nature of the destabilizing agent and

seem to reduce to a single volume content of methane. This behavior could also be noticed by the more vertical detection-time curve of unstable asphaltenes induced by methane compared to other *n*-alkanes in Figure 6.30.

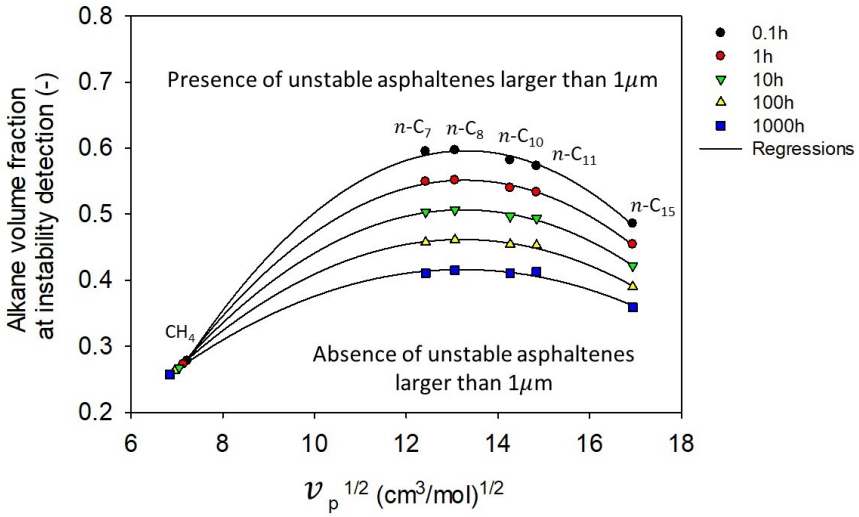

FIGURE 6.34: Trends of volume fractions of *n*-alkanes at time-resolved detection of unstable asphaltenes by microscopy for several several *n*-alkanes versus the square-root of the partial molar volume of the used *n*-alkane ($v_p^{1/2}$)

In comparison to previously reported data found in the literature[50;46], trends are found to have equivalent shapes with similar a specific maximum. Note that volume fractions of the *n*-alkanes have not been reported by Wang and Buckley[46], however the refractive indices of pure oils along with the "precipitation refractive indices" P_{RI} enabled us to back-calculate the volumetric composition at the detection conditions of unstable asphaltenes using the following relation:

$$P_{RI} = \sum \phi_i n_{Di} \tag{6.8}$$

where ϕ_i and n_{Di} are respectively the volume fraction and the refractive index of the pure constituent i (which takes only two states: *n*-alkane or crude oil). For the first time, our measured points complete the wide-spread graphical representation (Figure 6.35) in the region where systems need to be pressurized and expanded in order to observe the volume increase of destabilizing constituents.
It is expected that oils of different origins and that have different compositions and properties require varying amounts of *n*-alkanes for asphaltenes destabilization.

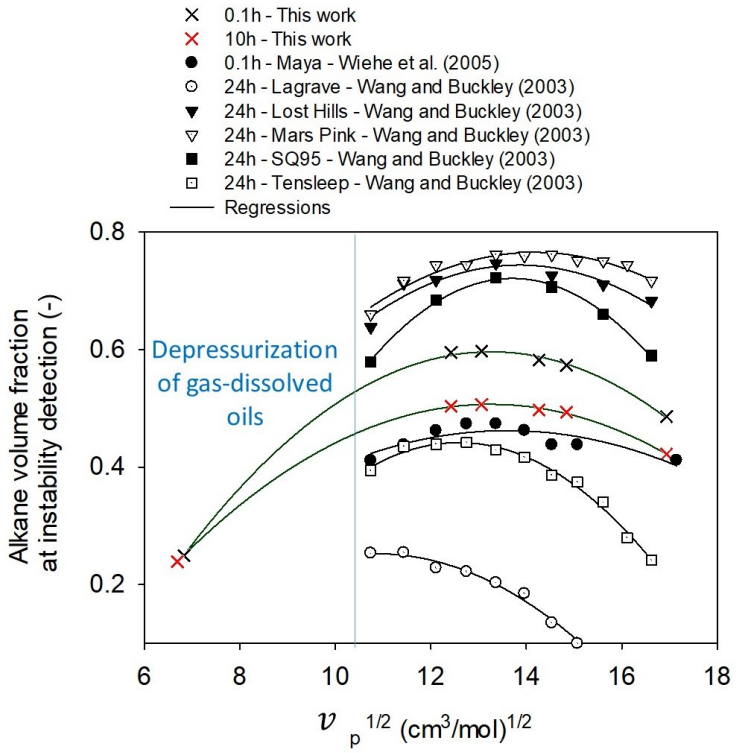

FIGURE 6.35: Literature comparison of trends[50;46] of volume fractions of *n*-alkanes at time-resolved detection of unstable asphaltenes by microscopy for several several *n*-alkanes versus the square-root of the partial molar volume of the used *n*-alkane ($v_p^{1/2}$)

It is important to highlight that the presented results indicates that the pressure is not the definitive variable of interest for the study of asphaltenes instability in live-oils. Instead, future research is suggested to study the effect of the volume fraction of expanded alkanes (which may be induced by decreasing the pressure of the sample).
We should note that despite the oil specific behavior, as showed in the literature review of this Chapter, regular solution based models previously demonstrated excellent capabilities to represent the functions of Figure 6.35 with respect to certain crude oils[51;40;29;19]. Although adjustments of generic parameters might have been a limiting practice to the full prediction of asphaltenes behavior in presence of light alkanes, the incorporation of kinetics of destabilization (Chapter 3) along with the better understanding of asphaltenes polydispersity[18] are promising alternatives for the construction of new thermodynamic predictive tools. Calculations of the amount of unstable asphaltenes as a function of the liquid composition may arise from combining the concepts and requires more research efforts.

6.3.2 Effect of the *n*-alkane chain lengths on asphaltenes deposition rate

Previous results showed that mathematical relations of asphaltenes phenomena in presence of *n*-heptane (destabilization, aggregation and deposition) seem to apply to relatively lighter (CH_4) and heavier alkanes (n-C_{11}). Similar reported trends and modeling practice may enable the improvement of predictive tools. However, limited number of gas-dissolved experiments giving the quantity of unstable asphaltenes

(previous referred to as C_A) are available in such conditions. This part will show the evaluation of the possibility to extract relevant information from measured deposition in the conditions of interest (large deposition rates) during CME experiments.

Evaluation of the effect of the methane expansion rate during live-oil depressurization

As expected, the volume increase of methane destabilizes asphaltenes and enables us to measure their deposition on the immersed sensor. Figure 6.36 is the plot of the measured cumulative deposited mass for several experiments at various depressurization rates (dP/dt). The data are plotted for a range of pressure between 1000 bar (upper limit of utilization of our equipment) and 500 bar (saturation pressure of the studied system).

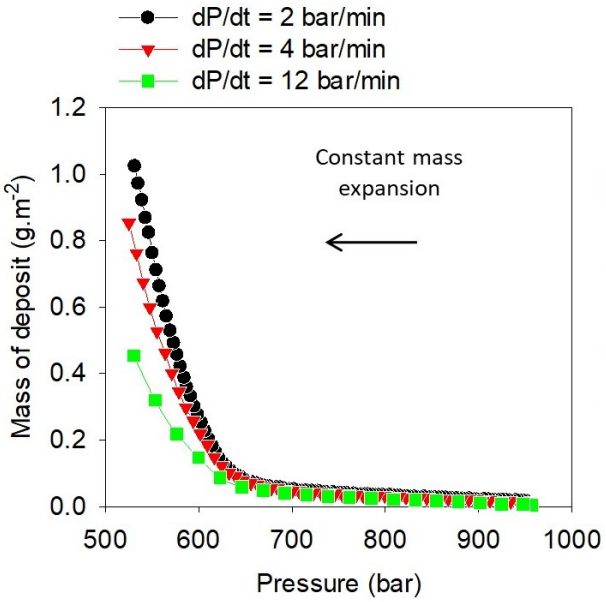

FIGURE 6.36: Measured deposited mass during CME experiment with an immersed QCR of an oil-methane mixture composed of 64%$_{mol}$ of CH_4 at several rates of depressurization as a function of the pressure

As explained, the variable of interest should be referring to solution properties of the liquid solvent instead of the pressure, the volume content of methane in oil is more suitable. Figure 6.37 shows the plot of the same data as a function of the methane volume fraction and is compared to the detection-time curve of micro-aggregates. The graphical interpretation leads us the identical statement compared to the destabilization and deposition trends induced by *n*-heptane (Figure 6.15); the instantaneous (less than 5 min) appearance of large unstable asphaltenes coincides with the significant change of slope of the deposited mass.

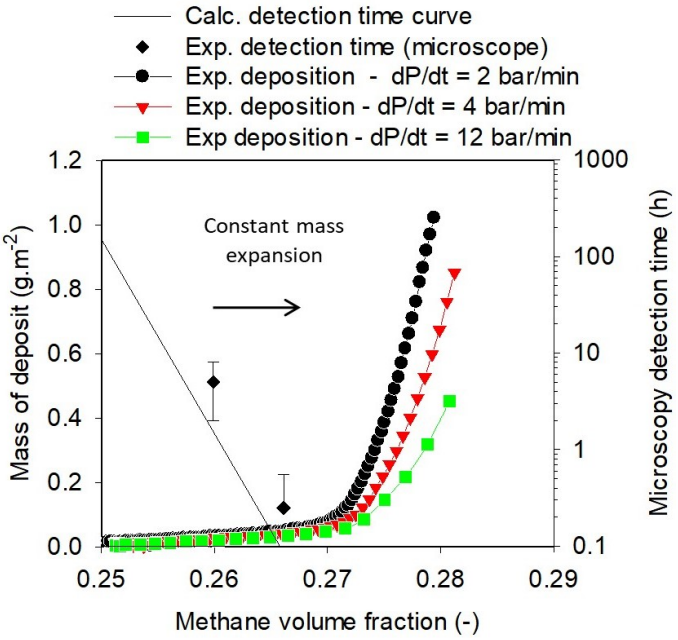

FIGURE 6.37: Measured deposited mass during CME experiment with an immersed QCR of an oil-methane mixture composed of 64%$_{mol}$ of CH_4 at several rates of depressurization as a function of the methane volume fraction

Results indicate that the largest cumulative mass of deposit is recorded for the lowest rate of depressurization. However this graphic does not incorporate the effect of the residence time of the fluid, indeed the variation of the depressurization rate does not permit an equal residence time in the conditions at which significant deposition is observed. As explained in Chapter 5, the data are preferentially plotted in a different manner for direct comparison. Deposition rates are not only more convenient for comparisons on a single chart, the relevance of experimental deposition rates information is easier to interpret industrial implications.

The CME experiment is equivalent to a Lagrangian specification for a flowing fluid along well tubings and pipelines. During petroleum extraction, a given parcel of fluid is driven to flow through channels in response to the pressure gradient. The pressure decrease, itself, incurs an expansion of the light constituents in the composition of the considered parcel of fluid.

The cumulative mass of deposit per unit area in CME experiment corresponds to the mass fraction of asphaltenes that will deposit all along the well. However in practice, localized restrictions that form in short intervals of time are the most problematic and correspond to the equivalent mass of asphaltenes that will accumulate at a given pressure and at a specific rate. It then becomes more appropriate, in the CME data processing, to represent the rate of accumulation at specific conditions of pressure and temperature of the system. Plots of measured deposition rates as a function of pressure and as a function of the equivalent methane volume content in the fluid are presented in Figure 6.38.

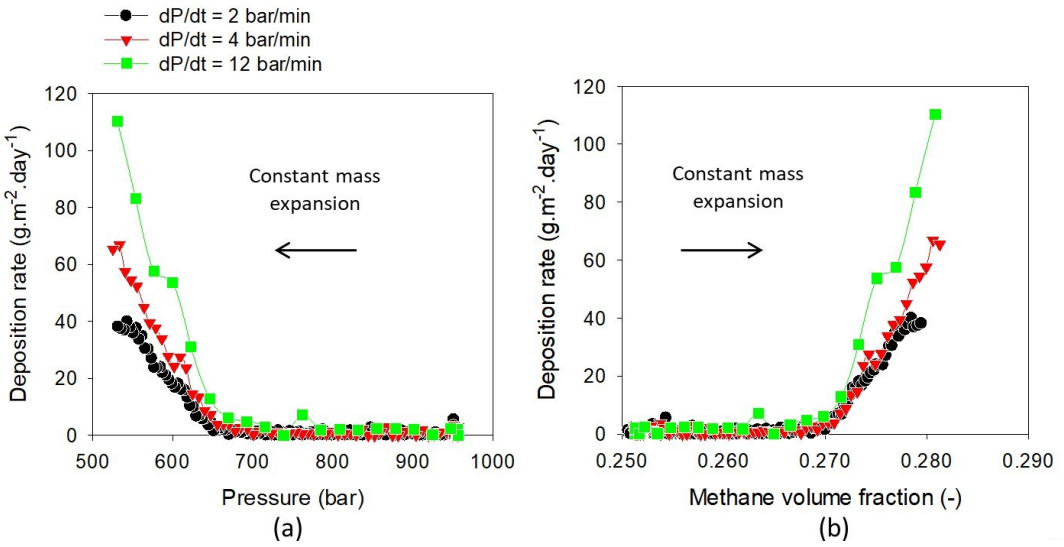

FIGURE 6.38: Measured deposition rates of unstable asphaltenes during CME experiment of an oil-methane mixture composed of 64%$_{mol}$ of CH_4 at several rates of depressurization as a function of (a) pressure and (b) methane volume fraction

As expected from the mechanism described by the dominating deposition of primary units of unstable asphaltenes, larger rates of depressurization will induce more severe destabilization rates. In turn, elevated rates of destabilization will increase the number concentration of primary unstable aggregates in the system and subsequently increase the local deposition rate due to their fast diffusion. This observation further comforts the consensus of identical mechanisms of destabilization, aggregation and deposition of asphaltenes upon increases of volume contents of different alkanes in mixture solvent. This statement does not exclude that the molar volume of alkanes have a strong effect. However it is worth reminding that the purpose of this part is to verify if concepts and equations derived in previous Chapters of this document can be applied several alkanes. Therefore, additional observations are reported in the following paragraph.

Effect of the n-alkane chain length on the deposition rate of unstable asphaltenes

Harmony of the governing mechanisms in both conditions (liquid addition or expansion of dissolved gas components) is further tested by stages of depressurization and records of the deposition rates. Indeed, as seen in the case of step additions of n-heptane or n-undecane (Figure 6.39 and 6.40), the deposition rate of asphaltenes goes through maximum during simultaneous addition of the destabilizing agent. During plateau stages the deposition rate rapidly decreases to significantly lower deposition rates and eventually reaches a null value once the system reaches a local equilibrium (no more generation of unstable asphaltenes). The process is then re-encouraged when the addition of n-alkanes is carried again as predicted by our simplified model that predicts the predominant deposition of primary unstable aggregates.

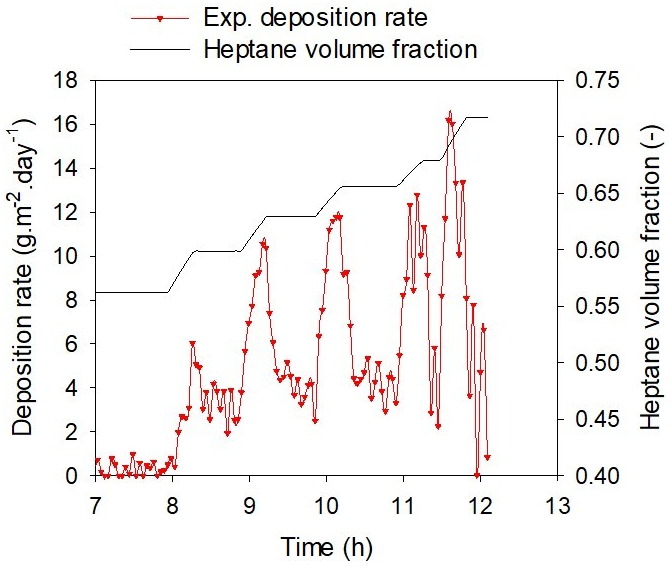

FIGURE 6.39: Observation of peaks of deposition rates upon simultaneous addition of *n*-heptane and minor deposition rates when the addition is stopped as a function of time

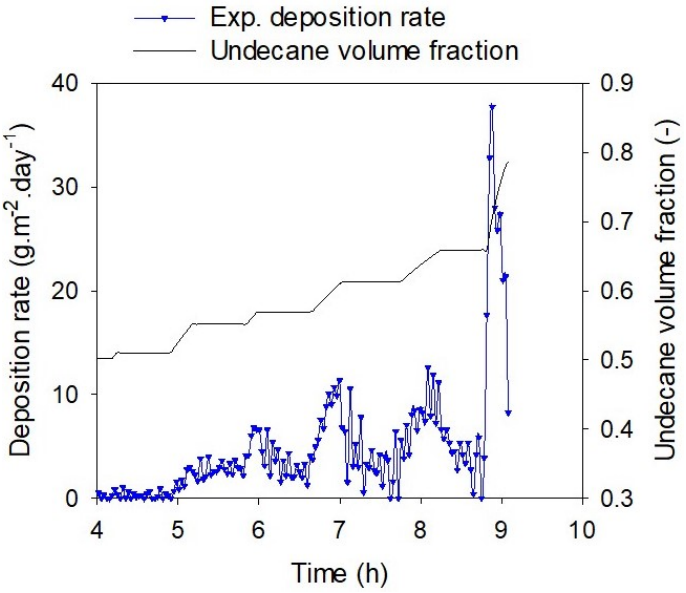

FIGURE 6.40: Observation of peaks of deposition rates upon simultaneous addition of *n*-undecane and minor deposition rates when the addition is stopped as a function of time

Steps of methane volume additions in the mixture of oil-methane were similarly carried by depressurization stages as presented in the previous section. Minor deposition rates (scale in $mg.m^{-2}.day^{-1}$) were observed at low enough volume content of methane compared to the plot showed in Figure 6.41 (scale in $g.m^{-2}.day^{-1}$).

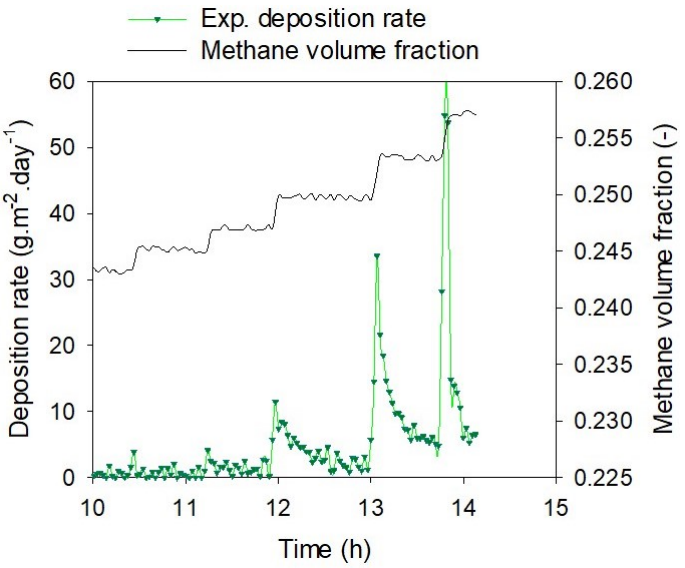

FIGURE 6.41: Observation of peaks of deposition rates upon simultaneous expansion of methane and minor deposition rates when the pressure decrease is stopped as a function of time

The similarities in observations of asphaltenes deposition induced by several conditions of solvent properties further support that mechanisms are identical for the asphaltenes destabilization caused by different n-alkanes. However, the destabilizing power of different n-alkanes non-monotonously varies with their partial molar volumes according to the detection curves of unstable asphaltenes as a function of $v_p^{1/2}$ as precedently showed. Destabilization kinetics are particularly observable in the smooth decay of deposition rates once changes in pressure are stopped.
We have seen in our research that destabilization of asphaltenes is a precursor to the deposition phenomenon and that mainly primary units of unstable asphaltenes contribute to the deposition. Results of depositions induced by continuous addition of n-heptane and by the expansion of methane from a constant mass expansion experiment are compared in Figure 6.42. The power of n-alkanes to cause asphaltenes deposition has, as expected, a comparable behavior to the microscopy detection-time curve. Analogous deposition rates and deposited masses are obtained for both alkanes at different solubility parameters of respective mixture solutions. A lower solubility parameter of the solution needs to be reached for n-C_7 to cause a comparable severity of deposition rates. This behavior indicates that methane has a larger thermodynamic influence than n-heptane on the destabilization rate of asphaltenes. Since larger volumes of n-heptane are required, the deposition rate passes through a maximum due to large dilution effects, while the methane volume content is low enough for this effect to not be predominant.

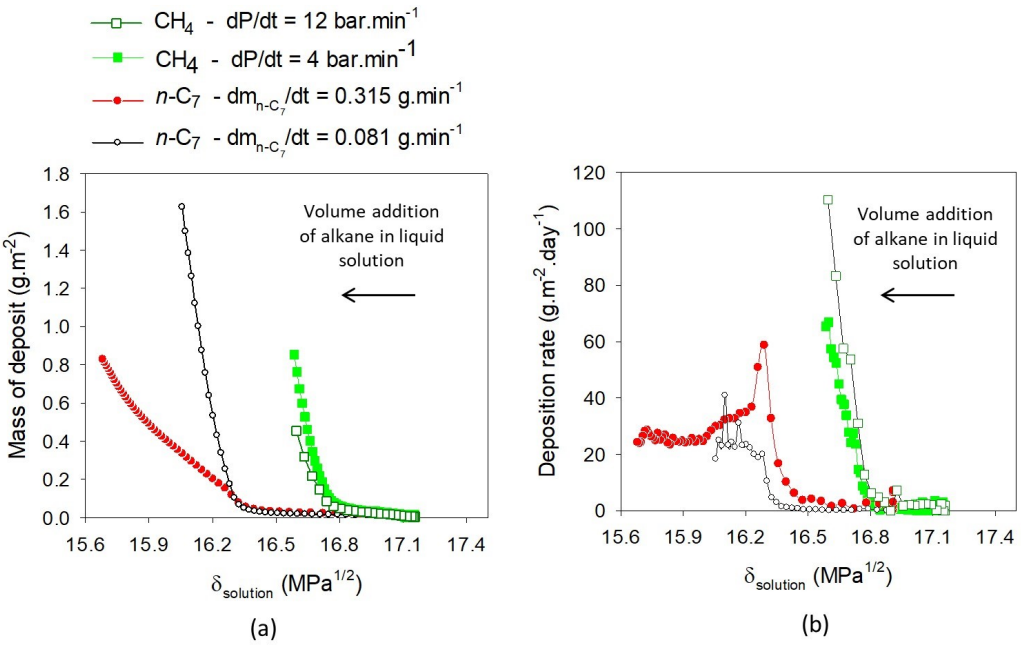

FIGURE 6.42: Comparison of (a) cumulative deposited mass and (b) deposition rates of unstable asphaltenes induced by addition of *n*-heptane and by expansion of methane as a function of the solubility parameter of the solution

We notice in Figure 6.42 that the increase of the depressurization rate of methane recombined fluid has a similar effect compared to the addition rate of *n*-heptane. However both variables are expressed in a different manner. The same graduated scale $\delta_{solution}$ is indeed convenient for the juxtaposition of results obtained with various solvents. Therefore, Figure 6.43 plots the rate of change of the solubility parameter of the solution as a function of $\delta_{solution}$. We can observe that predominant dilution effects of *n*-C_7 are remarkable by the opposite slopes compared to the case of methane increased expansion that causes $\left(\frac{\Delta\delta_{solution}}{\Delta t}\right)$ to increase. As expected, comparatively larger rates of change in solubility parameter of the solution induce larger generation rates of primary unstable asphaltenes particles, directly represented by the proportionality to the deposition rates.

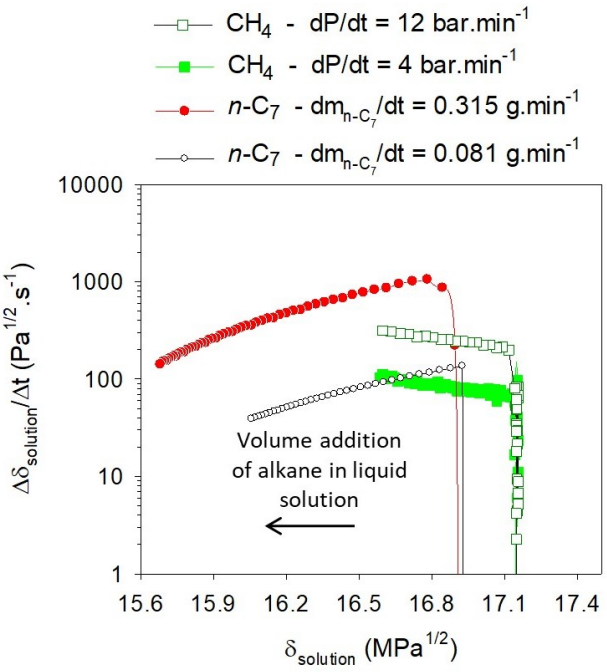

FIGURE 6.43: Comparison of the rate of change of the solubility parameter of the liquid solution upon addition of *n*-heptane and by expansion of methane as a function of the solubility parameter of the solution

Further studies are necessary to understand the fundamental role of the length of *n*-alkanes on asphaltenes destabilization. Results of this study suggest that deposition measurements under several conditions can be rallied to two primary variables: the absolute solubility parameter of solution mixtures and their rate of change upon addition of liquid *n*-alkanes or depressurization of gas recombined systems. Indeed, the rate $\left(\frac{\Delta_{\delta_{solution}}}{\Delta t}\right)$ need to be similar in order to experimentally quantify the effect of different *n*-alkanes on asphaltenes.

6.4 Conclusions

The effect of the carbon number of *n*-alkanes on asphaltenes behavior was studied. Experimental verification were carried with *n*-undecane and with methane to check if mechanisms of asphaltenes phenomena would be sensitive to the alkane nature. The used apparatus is able to monitor both the deposition of an immersed QCR and the appearance of unstable asphaltenes with an infrared microscope at room pressure and at elevated pressures (up to 1000 bar). Non-invasive and non-destructive methods are developed in order to quantify the deposition of asphaltenes gas-dissolved conditions (live oils).

In the first part, investigated conditions were purposely chosen at small thermodynamic driving forces (i.e. at low concentrations of destabilizing agents). A new technique was employed to indirectly measure the detection-time curve of unstable asphaltenes. The technique, which relates the microscopy detection-time to the deposition rate of unstable asphaltenes, showed excellent agreement with the direct microscopy observations. Earlier determined concepts (in this dissertation) revealed to apply to both longer and shorter *n*-alkanes at conditions of slow aggregation. The deposition of unstable asphaltenes under those conditions (range of detection-time

curves) is very limited due to the small number of primary aggregates.
For the first time, methane is treated as another alkane toward the destabilization of asphaltenes (volume fraction as the variable of interest), the pressure is defined as a mean to reach certain mixture composition with compressible constituents, such as methane. In this way, the monotonic trend proposed by the ASIST method of prediction is challenged by non-monotonic experimental observations (that are in agreement with previously reported trends).
In the second part of this Chapter, larger thermodynamic instability of asphaltenes was induced by addition of larger volume fractions of *n*-alkanes. The effect of the rate of expansion of the added solvent is in agreement with the described approaches in our precedent work with *n*-heptane. Indeed, experimental evidences show that primary unstable aggregates (those which are generated while the deposition occurs) dominate in the deposition process. When the generation of units is reduced by keeping constant mixtures, deposition rates tend to negligible values within a few minutes.
The developed experimental methods of this work will enable further quantitative investigations and improvement of models for asphaltene destabilization, aggregation and deposition implied by light constituents only dissolved in the oil at elevated pressures. Further experimental investigations are suggested to be performed with controlling the relevant variables ($\delta_{solution}$ and $\left(\frac{\Delta\delta_{solution}}{\Delta t}\right)$, such that results can directly be compared.

Bibliography

[1] Akbarzadeh, K., H. Alboudwarej, W. Y. Svrcek, and H. W. Yarranton
2005. A generalized regular solution model for asphaltene precipitation from n-alkane diluted heavy oils and bitumens. *Fluid Phase Equilibria*, 232(1-2):159–170.

[2] Alboudwarej, H., K. Akbarzadeh, J. Beck, W. Y. Svrcek, and H. W. Yarranton
2003. Regular solution model for asphaltene precipitation from bitumens and solvents. *AIChE Journal*, 49(11):2948–2956.

[3] Barrera, D., D. Ortiz, and H. Yarranton
2013. Molecular weight and density distributions of asphaltenes from crude oils. *Energy & fuels*, 27(5):2474–2487.

[4] Buckley, J. S., G. Hirasaki, Y. Liu, S. Von Drasek, J. Wang, and B. Gill
1998. Asphaltene precipitation and solvent properties of crude oils. *Petroleum Science and Technology*, 16(3-4):251–285.

[5] Buckley, J. S., J. Wang, and J. L. Creek
2007. Solubility of the least-soluble asphaltenes. *Asphaltenes, Heavy Oils, and Petroleomics*, Pp. 401–437.

[6] Chacon-Patino, M. L., S. M. Rowland, and R. P. Rodgers
2017a. Advances in asphaltene petroleomics. part 1: asphaltenes are composed of abundant island and archipelago structural motifs. *Energy & fuels*, 31(12):13509–13518.

[7] Chacon-Patino, M. L., S. M. Rowland, and R. P. Rodgers
2017b. Advances in asphaltene petroleomics. part 2: selective separation method that reveals fractions enriched in island and archipelago structural motifs by mass spectrometry. *Energy & fuels*, 32(1):314–328.

[8] Creek, J. L., J. Wang, and J. S. Buckley
2009. Verification of asphaltene-instability-trend (asist) predictions for low-molecular-weight alkanes. *SPE Production & Operations*, 24(02):360–368.

[9] Daridon, J.-L. and H. Carrier
2017. Measurement of phase changes in live crude oil using an acoustic wave sensor: Asphaltene instability envelope. *Energy & Fuels*, 31(9):9255–9267.

[10] Daridon, J. L., M. Cassiede, D. Nasri, J. Pauly, and H. Carrier
2013. Probing asphaltene flocculation by a quartz crystal resonator. *Energy & Fuels*, 27(8):4639–4647.

[11] Daridon, J. L., E. Orlandi, and H. Carrier
2016. Measurement of bubble point pressure in crude oils using an acoustic wave sensor. *Fluid Phase Equilibria*, 427:152–160.

[12] David Ting, P., G. J. Hirasaki, and W. G. Chapman
2003. Modeling of asphaltene phase behavior with the saft equation of state. *Petroleum Science and Technology*, 21(3-4):647–661.

[13] Dolati, S., H. Zarei, and R. Kharrat
2015. Asphaltene Instability Trends to Predict Asphaltene Precipitation Onset Pressure: Constrained for Light and Heavy Crude Oils. *Journal of Dispersion Science and Technology*, 36(1):103–110.

[14] Gonzalez, D. L., F. M. Vargas, E. Mahmoodaghdam, F. Lim, and N. Joshi
2012. Asphaltene stability prediction based on dead oil properties: Experimental evaluation. *Energy & fuels*, 26(10):6218–6227.

[15] Goual, L., G. Horváth-Szabó, J. H. Masliyah, and Z. Xu
2005. Adsorption of bituminous components at oil/water interfaces investigated by quartz crystal microbalance: Implications to the stability of water-in-oil emulsions. *Langmuir*, 21(18):8278–8289.

[16] Groenzin, H., O. C. Mullins, S. Eser, J. Mathews, M.-G. Yang, and D. Jones
2003. Molecular size of asphaltene solubility fractions. *Energy & fuels*, 17(2):498–503.

[17] Haghshenas, M., S. Balashanmugam, D. Gonzalez, and M. Pietrobon
2016. Prediction of asphaltene onset pressure from dead oil stability. In *Offshore Technology Conference*. Offshore Technology Conference.

[18] Haji-Akbari, N., P. Teeraphapkul, A. T. Balgoa, and H. S. Fogler
2015. Effect of n-alkane precipitants on aggregation kinetics of asphaltenes. *Energy & Fuels*, 29(4):2190–2196.

[19] Hirschberg, A., L. DeJong, B. Schipper, and J. Meijer
1984. Influence of temperature and pressure on asphaltene flocculation. *Society of Petroleum Engineers Journal*, 24(03):283–293.

[20] Hoepfner, M. P. and H. S. Fogler
2013. Multiscale scattering investigations of asphaltene cluster breakup, nanoaggregate dissociation, and molecular ordering. *Langmuir*, 29(49):15423–15432.

[21] Hoepfner, M. P., V. Limsakoune, V. Chuenmeechao, T. Maqbool, and H. S. Fogler
2013. A fundamental study of asphaltene deposition. *Energy & fuels*, 27(2):725–735.

[22] Kaminski, T. J., H. S. Fogler, N. Wolf, P. Wattana, and A. Mairal
2000. Classification of asphaltenes via fractionation and the effect of heteroatom content on dissolution kinetics. *Energy & Fuels*, 14(1):25–30.

[23] Khaleel, A., M. Abutaqiya, M. Tavakkoli, A. A. Melendez-Alvarez, and F. M. Vargas
2015. On the prediction, prevention and remediation of asphaltene deposition. In *Abu Dhabi International Petroleum Exhibition and Conference*. Society of Petroleum Engineers.

[24] Kraiwattanawong, K., H. S. Fogler, S. G. Gharfeh, P. Singh, W. H. Thomason, and S. Chavadej
2007. Thermodynamic solubility models to predict asphaltene instability in live crude oils. *Energy & fuels*, 21(3):1248–1255.

[25] Lin, H.-M. and R. A. Nash
1993. An experimental method for determining the hildebrand solubility parameter of organic nonelectrolytes. *Journal of pharmaceutical sciences*, 82(10):1018–1026.

[26] Mitchell, D. L. and J. G. Speight
1973. The solubility of asphaltenes in hydrocarbon solvents. *Fuel*, 52(2):149–152.

[27] Montesi, A., R. A. Pinnick, S. Subramanian, J. Wang, and J. L. Creek
2011. Asphaltene management in gom dw subsea development. In *Offshore Technology Conference*. Offshore Technology Conference.

[28] Mullins, O. C.
2011. The asphaltenes. *Annual review of analytical chemistry*, 4:393–418.

[29] Mullins, O. C. and E. Y. Sheu
2013. *Structures and dynamics of asphaltenes*. Springer Science & Business Media.

[30] Östlund, J.-A., P. Wattana, M. Nydén, and H. S. Fogler
2004. Characterization of fractionated asphaltenes by uv–vis and nmr self-diffusion spectroscopy. *Journal of colloid and interface science*, 271(2):372–380.

[31] Panuganti, S. R., F. M. Vargas, D. L. Gonzalez, A. S. Kurup, and W. G. Chapman
2012. Pc-saft characterization of crude oils and modeling of asphaltene phase behavior. *Fuel*, 93:658–669.

[32] Passade-Boupat, N., H. Zhou, and M. Rondon-Gonzalez
2010. Asphaltene Precipitation From Crude Oils : How To Predict It And To Anticipate Treatment? *SPE Middle East Oil and Gas Show and Conference*.

[33] Powers, D., H. Sadeghi, H. Yarranton, and F. Van Den Berg
2016. Regular solution based approach to modeling asphaltene precipitation from native and reacted oils: Part 1, molecular weight, density, and solubility parameter distributions of asphaltenes. *Fuel*, 178:218–233.

[34] Sabbagh, O.; Akbarzadeh, K. B.-Z. A. S. W. Y. Y. H. W.
2006. Applying the pr-eos to asphaltene precipitation from n -alkane diluted heavy oils and bitumens. *Energy Fuels*, 20.

[35] Saidoun, M., T. Palermo, N. Passade-Boupat, J.-P. Gingras, H. Carrier, and J.-L. Daridon
2019. Revisiting asphaltenes instability predictions by probing destabiliztion using a fully immersed quartz crystal resonator. *Fuel*, 251:523–533.

[36] Subramanian, Sreedhar; Simon, S. S.-J.
2015. Asphaltene precipitation models: A review. *Journal of Dispersion Science and Technology*.

[37] Tavakkoli, Mohammad; Chen, A. V.-F. M.
2015. Rethinking the modeling approach for asphaltene precipitation using the pc-saft equation of state. *Fluid Phase Equilibria*.

[38] Tavakkoli, M., A. Chen, and F. M. Vargas
2016. Rethinking the modeling approach for asphaltene precipitation using the pc-saft equation of state. *Fluid Phase Equilibria*, 416:120–129.

[39] Tavakkoli, M., M. R. Grimes, X. Liu, C. K. Garcia, S. C. Correa, Q. J. Cox, and F. M. Vargas
2015. Indirect method: a novel technique for experimental determination of asphaltene precipitation. *Energy & Fuels*, 29(5):2890–2900.

[40] Tharanivasan, A. K., H. W. Yarranton, and S. D. Taylor
2010. Application of a regular solution-based model to asphaltene precipitation from live oils. *Energy & Fuels*, 25(2):528–538.

[41] Ting, P. D., D. L. Gonzalez, G. J. Hirasaki, and W. G. Chapman
2007. Application of the pc-saft equation of state to asphaltene phase behavior. In *Asphaltenes, heavy oils, and petroleomics*, Pp. 301–327. Springer.

[42] Trejo, F., G. Centeno, and J. Ancheyta
2004. Precipitation, fractionation and characterization of asphaltenes from heavy and light crude oils. *Fuel*, 83(16):2169–2175.

[43] Vargas, F. M. and W. G. Chapman
2010. Application of the one-third rule in hydrocarbon and crude oil systems. *Fluid Phase Equilibria*, 290(1-2):103–108.

[44] Vilas Bôas Fávero, C., A. Hanpan, P. Phichphimok, K. Binabdullah, and H. S. Fogler
2016. Mechanistic investigation of asphaltene deposition. *Energy & Fuels*, 30(11):8915–8921.

[45] Wang, J. and J. S. Buckley
2001. A two-component solubility model of the onset of asphaltene flocculation in crude oils. *Energy & Fuels*, 15(5):1004–1012.

[46] Wang, J. and J. S. Buckley
2003. Asphaltene stability in crude oil and aromatic solvents the influence of oil composition. *Energy & fuels*, 17(6):1445–1451.

[47] Wang, J., J. L. Creek, and J. S. Buckley
2006. Screening for potential asphaltene problems. In *SPE Annual Technical Conference and Exhibition*. Society of Petroleum Engineers.

[48] Wiehe, I. A.
1996. Two-dimensional solubility parameter mapping of heavy oils. *Fuel Science and Technology International*, 14(1-2):289–312.

[49] Wiehe, I. A.
2012. Asphaltene solubility and fluid compatibility. *Energy & Fuels*, 26(7):4004–4016.

[50] Wiehe, I. A., H. W. Yarranton, K. Akbarzadeh, P. M. Rahimi, and A. Teclemariam
2005. The paradox of asphaltene precipitation with normal paraffins. *Energy & Fuels*, 19(4):1261–1267.

[51] Yarranton, H., D. Powers, J. Okafor, and F. van den Berg
2018. Regular solution based approach to modeling asphaltene precipitation from native and reacted oils: Part 2, molecular weight, density, and solubility parameter of saturates, aromatics, and resins. *Fuel*, 215:766–777.

[52] Yarranton, H. W., H. Alboudwarej, and R. Jakher
2000. Investigation of asphaltene association with vapor pressure osmometry and interfacial tension measurements. *Industrial & engineering chemistry research*, 39(8):2916–2924.

Chapter 7

Conclusions

Asphaltenes belong to a class of heavy and poly-aromatic molecules usually existing as continuous distributions in crude oils. Those components are originally dispersed in the form of self-associated molecules in good solvents, such as petroleum fluids in equilibrium with geological rock formations.
In general, extraction and treatment facilities of the oil & gas industry are subject to deposition or fouling caused by constituents in flowing mixtures that are in contact with solid surfaces. Driving forces of such economically catastrophic events are related to the change of pressure and temperature or to the mixing of incompatible fluids along the industrial conduits. In fact such thermodynamic variables are only secondary to the phase behavior of asphaltenes which rather results from several primary variables, such as the molar volume of the solvent. The scientifically difficult understanding of asphaltenes then resides in isolating relevant primary affecting variables and respectively explain underlying mechanisms.
Asphaltenes simultaneously undergo destabilization, flocculation and deposition processes upon volume addition of destabilizing agents such as *n*-alkanes. The 3 phenomena are undeniably inter-dependent and are triggered by the change of solution properties. Their respective characteristic times of occurence depend on thermodynamic driving forces of the media (mainly London dispersion interaction component), fluid transport properties and geometrical descriptions of asphaltene structures.
The work presented in this dissertation pursues the objective of comprehending the simultaneous mechanisms by distinguishing them into experimental inquiries. The notion of "stable" or "unstable" asphaltenes is intrinsically related to the time and to the sensitivity of the employed technique for the detection of instability (i.e. aggregates larger than a certain resolution in a minimum concentration). In this work, fully immersed quartz crystal resonators are suitably used to continuously and quantitatively observe the deposition of asphaltenes per unit area of contacted solid surfaces. The presented measurement method is applicable to pressurized systems containing dissolved light components in crude oils. The deposition is induced by continuous changes of the carrier liquid solvencies with limited volumes of oil samples. Time-resolved microscopy observations and experimental separations by centrifuge are used to correlate the deposition, the size and the quantity of bulk flocculating asphaltenes. Main conclusions of this research are presented below and simplifications in modeling the behavior of such complex mixtures arise from our enhanced understanding.

On the kinetics of asphaltenes instability

Past investigations usually interchangeably defined destabilization and aggregation into a single kinetic process. Most of the reported studies assumed immediate availability of equilibrium concentrations of unstable asphaltenes in their models. First

interrogations on this assumption are revealed by the observed absence of deposition while significant amount of bulk unstable asphaltenes are separated at equilibrium of the same conditions.
Chapter 3 explores the possibility to consider distinct kinetic phenomena in oil-heptane mixtures. The transition of "stable" asphaltenes to an "unstable" state is distinguished from the growth of already unstable asphaltenes particles. Based on laboratory inspections, the aggregation is assumed to occur significantly more rapidly than the generation of new primary unstable units. The calculated destabilization rate constant k_N is able to reconcile deposition experiments with theoretical behavior predicted by diffusion-limited transport principles. Consequently, the initial change of solution is found to destabilize a smaller number of asphaltene molecules than the one at equilibrium. The cumulation of unstable asphaltenes conform to an exponential form of mathematical equation based on two parameters that are system dependent; (i) the equilibrium concentration of unstable asphaltenes $C_{A\infty}$ and (ii) the characteristic time τ for equilibration of a given system. Good agreements are found between the modeled and the separated mass of unstable material. In the proposed model, asphaltenes belong to a continuum of molecules in which the number of unstable ones at equilibrium progressively increases as the *n*-heptane content gets large. The time to reach equilibrium decreases as the heptane volume fraction increases.
A final sensitivity analysis of the model identifies the addition rate of *n*-heptane as a key parameter that controls the generation rate of unstable asphaltenes in continuously changing solutions. Destabilization kinetic is identified as a limiting factor to the number of available asphaltenes for the aggregation and for the deposition processes.

Revisiting the aggregation modeling of unstable asphaltenes with incorporation of destabilization kinetics

In Chapter 4 asphaltenes aggregation is investigated at low thermodynamic driving forces. Smoluchowski's coagulation model is revisited with the incorporation of the proposed concepts of destabilization kinetics. Indeed the number of available particle for the aggregation becomes time-dependent and needs to be solved simultaneously along with the aggregation. For simplicity a mono-disperse size of spherical coagulated entities is analytically solved for oil-heptane blends. The aggregation between units of different sizes is theoretically preferred according to the form of Brownian aggregation kernels. Therefore only two radius of particles are assumed to co-exist: freshly generated units (named primary particles) and already aggregated primary particles of unstable asphaltenes. Primary aggregates have geometrical properties equal to "stable" clusters of nano-aggregates that are extensively reported in the literature. The mean size of the aggregated fraction of particles is discretely calculated by time resolution of both analytical solutions. In this way, the track of the average size of aggregates is ensured by calculating the balance of generated unstable asphaltenes entering the system and cumulatively consumed ones by Brownian aggregation. The widely used colloidal stability ratio W is adjusted in order to tune the aggregation rate constant K_{ij}. The calculated aging time for observation of micron-sized particles is in excellent agreement with experimental indications of oil-heptane mixtures in the investigated range.
The notion of critical composition of solution, widely accepted to be represented by ($W = 1$) in the colloidal science, correlates well with the observed instantaneous flocculation by microscopy. In addition, verification are successfully conducted on the

calculation of the practical minimum number concentration of unstable asphaltenes. A correlation is found between the primary particles generation rate dC_1/dt and the detection-time of micro-aggregates $t_{detection}$. Additionally, the deposition of asphaltenes showed to become significant only in conditions of extremely fast aggregation.
Findings further confirm that both kinetics of destabilization and Brownian aggregation control the appearance and growth of unstable asphaltenes at sufficiently low *n*-heptane volume fraction in oil-heptane systems. Beyond the critical conditions of flocculation, aggregation of unstable units is found to be instantaneous due to the dominating attractive forces and to the large concentration of particles.

A simplified model for the deposition of asphaltenes

A closed stirred-batch reactor is introduced to measure asphaltenes deposition during the continuous titration of *n*-heptane in an initial volume of crude oil. The apparatus consists of an immersed sensor in a center-position of the reactor. The fluid superficial velocity to the sensor was measured by visual inspections using a fluorescent dye.
Results of Chapter 5 show that the deposition rate of unstable asphaltenes scales with the square root of the fluid flow velocity. Asphaltenes accumulation on solid surfaces of the sensor can then be explained by a diffusion-limited phenomenon involving nano-particles. The average hydrodynamic radius R_A of depositing units generally ranges between 1 nm and 10 nm. The presence of suspended large flocs is found to slow the deposition process. In those circumstances, the average radius of the depositing aggregates can reach tens of nanometers. With this analysis, primary aggregates of unstable asphaltenes, which are the smallest unstable colloids, are identified to predominantly contribute to the deposition process. Indeed the deposition rate of asphaltenes scales linearly with the calculated concentration of primary particles C_1. The asphaltene deposition rate accordingly develop into a strong dependence on the rate of change of the liquid composition.
Consequently to the fast bulk aggregation previously studied, the proposed simplifications can correlate the generation rate dC_1/dt of unstable asphaltenes and their deposition rate in a proportional relationship. Therefore the method, which is based on the track the deposited mass of asphaltenes can indirectly quantify bulk concentration profiles of unstable asphaltenes.

Effect of the nature of *n*-alkanes on the destabilization, aggregation and deposition of asphaltenes

Industrial asphaltenes deposition caused by the expansion of light constituents during the transport of live oils is diagnosed as the most catastrophic scenario. In Chapter 6, experimental investigations are conducted in a PVT cell for a crude oil mixed with methane, *n*-heptane or *n*-undecane.
The control of the pressure is used as a mean to reach given volume compositions of compressible systems. In those conditions, the deposited mass of asphaltenes per unit area is successfully monitored by correcting for the effect of the hydrostatic pressure on the sensor. In parallel, high pressure infrared microscopy is employed to verify the theoretically expected relation between the deposition of unstable asphaltenes and their detection-time by microscopy. Slow destabilization and aggregation processes are observed at small driving forces (sufficiently low alkane volume fraction). Obtained results questions the accuracy of the so-called ASIST method

that extrapolate measured effects of liquid *n*-alkanes to methane-dissolved conditions. The asphaltenes instability detection follow instead non-monotonous trends as a function of the square root of the molar volume of the destabilizing agent.
The instantaneous micro-flocculation of asphaltenes is jointly found to coincide with significant increases of deposition rates upon *n*-alkanes expansion. At larger liquid volumes of methane, the asphaltenes deposition rate increases with the increase of the light constituent expansion rate. As explained in the precedent Chapter, this is the signature of a diffusive deposition process dominated by primary generated unstable asphaltenes. Along those lines, the developed relationships between rates of destabilization, aggregation and deposition are reinforced. The observed trends suggest that developed models apply to the asphaltenes behavior in presence of various destabilizing constituents.
In order to compare the effect of *n*-alkanes chain length on a single graduated scale of solvent, the solubility parameter of solutions ($\delta_{solution}$) is used. Asphaltenes deposition rate accordingly develop into a strong dependence on the rate of change of the carrier liquid solvency $\left(\frac{\Delta_{\delta_{solution}}}{\Delta_t}\right)$. Measured deposition extents induced by the expansion of *n*-heptane and methane at similar driving forces are compared. Results confirm that methane has significantly more influence on the destabilization rate of asphaltenes.

Provided that mechanisms remain identical, the developed methods of this thesis give room to investigate the effect of the nature of the destabilizing agent on quantitative asphaltenes behavior. For the first time, a non-invasive and non-destructive technique is proposed to experimentally determine quantities of unstable asphaltenes under oil & gas production conditions.

Appendix A

Separation efficiency of centrifuge experiments

The centrifuge separation method of prepared liquid mixtures is used to collect a mass of aggregated asphaltenes that belong to particles larger than a certain size. The cut-off size (smallest separated size of aggregates) is estimated with the separation efficiency S_k of varying sizes of aggregates. The separation efficiency is calculated based on the force balance between the centrifugal and the drag forces exerted on spherical particles in the liquid medium during the centrifuge experiment. Stokes' law is used to estimate the frictional force on particles assuming small enough Reynolds numbers in the viscous fluid. The centrifugal force is calculated based on the classical mechanics with Newton's second law of motion. The effects of Brownian motion and potential collisions between particles that can delay the settling of particles are neglected.

The ability of the centrifuge to separate particles of a given size is depends on the radius of the centrifuge rotor, the angular speed of the rotor ω, the time of centrifugation t, the height of liquid in tubes L, the dynamic liquid viscosity μ_L, the k^{th} particle diameter d_k and the difference of densities $\Delta\rho$ between the fluid and the separated particles.
Densities of oil-alkanes mixtures can be calculated using a simple volume average mixing rule. Viscosities of oil-alkanes mixtures can be estimated applying log-average mixing rule and is given by:

$$\mu_L = 10^{\sum w_i log(\mu_i)} \tag{A.1}$$

where w_i and μ_i are the weight fraction and the dynamic viscosity of the pure i liquid composing the mixture.
The velocity of deported particles increases due to the increase of the centrifugal force as a function of the radial distance from the center of the centrifuge. An acceptable conditions for aggregates to be separated is to reach the bottom of the centrifuge tube.
Consider the k^{th} aggregate that travels from its initial position (x_0) to its the final one (x_f) during the time t. **?** integrated the force balance between both positions and reported the expression of the traveled distance by k^{th} aggregate in time t:

$$\Delta x_i = x_f - x_0 = x_f \left[1 - \exp\left(-\frac{\phi_{solid} d_k^2 \Delta\rho\omega^2 t}{18\mu_L}\right)\right] \tag{A.2}$$

where ϕ_{solid} represents the solid fraction in aggregates composed of solid and trapped solvent. The separation efficiency is the fraction of k^{th} aggregates with a diameter

d_k that get theoretically separated in time t. Assuming that particles are homogeneously distributed in the aliquot, authors[?] defined S_k as:

$$\begin{aligned} S_k &= \frac{\Delta x_k}{L} \text{ for } \Delta x_k \leq L \\ S_k &= 1 \text{ for } \Delta x_k > L \end{aligned} \tag{A.3}$$

For aggregates that travel larger distances Δx_k than the height of liquid L in the tube ($\sim$ length of the tube), their separation efficiency is 1. For smaller aggregates such that $\Delta x_k < L$, their separation efficiency should be less than 1.
Assuming an average density of separated asphaltenes particles equal to 1200 kg.m^{-3}, a sensitivity analysis of the separation efficiency for a typical oil-heptane mixture is shown below. The maximum angular speed of our centrifuge apparatus corresponds to 15000 revolutions per minute (rpm) in a rotor with a radius of 9.7 cm. Parameters related to the liquid are summarized in Table A.1. Results of calculations using

TABLE A.1: Parameters for the calculation of centrifuge separation efficiency of a oil-heptane mixture at 60°C

Parameters	Units	Values
n-C_7 content	wt %	50
Liquid density	$kg.m^{-3}$	762.6
Liquid viscosity	$mPa.s$	1.8
ϕ_{solid}	-	0.63
length of tubes L	cm	3.5

Equations A.2 and A.3 are showed for 4 realistic run-times (10, 20, 30 and 60 min) of the centrifuge experiment. The cut-off size is the smallest size of particles that all get separated ($S_k = 1$).
As shown in Figure A.1 the achieved cut-off size of aggregates is $\sim$ 100 nm for the chosen example.

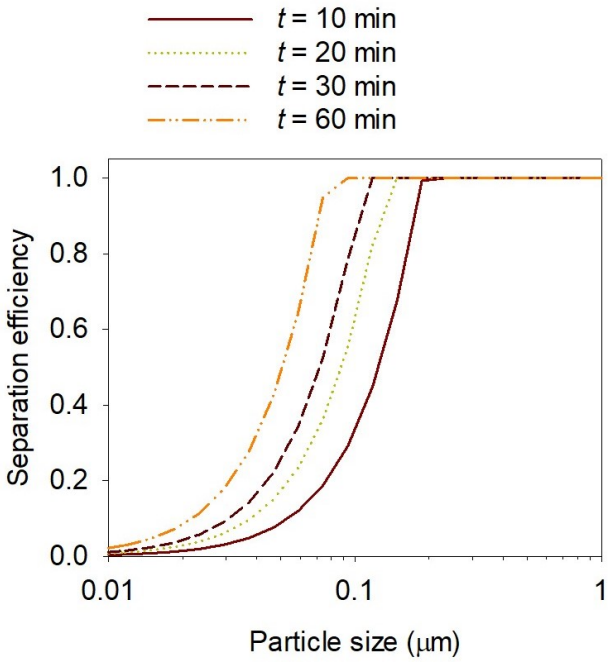

FIGURE A.1: Calculated separation efficiency as a function of the aggregate size for several centrifuge run-times

Note that for particles with smaller diameters than hundreds of nanometer, the Brownian motion becomes significant and the presented calculation in this Appendix does not hold.